THE ROLE AND USE OF HETEROGENEITY IN MICROVASCULAR INSTABILITY

A Dissertation

Presented to faculty of
the School of Engineering and Applied Sciences
in partial fulfillment of the requirements for the degree of

Doctor of Philosophy

---

by Molly Rose Kelly-Goss

March 2018

Department of Biomedical Engineering
University of Virginia

APPROVAL SHEET

This dissertation is in partial fulfillment of the requirements for the degree of
Doctor of Philosophy in Biomedical Engineering

Molly Kelly-Goss
Author

DEDICATION

First and foremost, I would like to dedicate this work to Dr. Shayn Peirce-Cottler. Shayn – your passion for science and enduring intellectual curiosity is both obvious and inspirational to those around you. You gifted me incredible freedom to explore microvascular research and creativity in my experimental design. I was passionate about my science throughout graduate school, even when nothing worked and I was completely lost, because you supported and energized me. Yet, what most inspires me is not your monumental scientific contributions or invaluable insight. Shayn, you use your position as a mentor, educator, and leader to empower those around you. You gave me the tools and encouragement necessary to teach, plan workshops, conduct research in Germany, study for the MCAT, and apply to medical school. Not once did I feel like a cog in the Big Science Machine. You uniquely and holistically treat your trainees as people, each with their own dreams and outside lives. Never did I fear approaching you for help with an outside project; never did I worry that asking you about outside professional development would lead to admonishment for not being focused on my science. You have challenged me as a scientist, author, mentor, educator, and citizen of the workplace. Your patience, openness, and authenticity during my graduate career have made you not only a mentor, but a friend. I have truly appreciated your tutelage during graduate school, and I am confident I will continue to look to you for advice wherever my path takes me next.

To my committee members: I could not imagine a more collaborative and supportive team of scientists to lead me on this journey. Rich – thank you for sharing your appreciation for microvascular fluid mechanics. Often, when talking with you, I was reminded of the initial studies by Y.C. Fung that initially sparked my interest in the microvasculature. You challenged me to

think more deeply about the biomechanics of my project. Even more, you helped me prioritize projects and focus my energy throughout graduate school. Song – thank you for your collaborative spirit and willingness to open your lab to test our hypotheses. Without your team, including Bo and Naidi, a vast proportion of this project could not be completed. Likewise, your insight in intravital imaging was absolutely critical for the development of my own confocal technique. Paul – in addition to introducing me to the wonderful world of ophthalmology, you have supported and encouraged my dream to become a clinician scientist from the very start. You enabled me to attend ARVO – twice! – which exposed me to the incredible work done by clinician scientists. Often, when staying up late studying or staring into the confocal at yet another failed stain, I remembered our talks about your patients and the motivation they bring you. Further, beyond sharing your encyclopedic knowledge of the retina, you encouraged me to pursue a crazy idea to just put a cornea down on the confocal and see what happens next. Thank you. Gary– thank you, first, for making me a more competitive, well-rounded trainee through both your role on my committee and through the Cardiovascular Research Center. Through your rigorous critique, I have been given invaluable training on how to design, write, and test scientific hypotheses. Further, thank you for opening your lab to our ongoing collaboration. Working on the Oct4 project has been a deeply fulfilling project, and I am so excited for our continued collaboration going forward. Finally, thank you for your advice and support as I planned my track to medical school. Your insight was crucial for my approach to applications, and I sincerely appreciate you sharing it with me.

Beyond having an incredible team of mentors on my committee, I had the honor of working with the incredibly talented, humorous, insightful Peirce's Pirates. Anthony, thank you for keeping the ship afloat, and always telling me where that one reagent or material is 'for the very last time.' Your approach to science is truly unique, and that makes you so incredibly smart. To the older

members of the lab – Kyle, Joe, Scott, and Tom – thank you for your incredible wisdom on science, life, and everything in between throughout graduate school. You guys were role models and friends, and it's been an honor training in your footsteps. To Clif, Bruce, Lee, Riley, Michaela, Rachel, and the rest of the Peirce's Pirates – I have appreciated all your help and friendship throughout the years. I am excited to see where you steer the ship, most certainly into exciting, uncharted territories of computational modeling, new disease models and collaborations, and, of course, ice fishees. To Daniel in the Owens lab – thank you for chasing the Oct4 mechanism while I sat on the confocal. You've been a wonderful collaborator, dog park comrade, hiking buddy, and friend.

In truth, there are many other communities – the Cardiovascular Research Center, Heinrich Heine University in Düsseldorf, Jefferson Scholars Foundation – and mentors – Dr. Eckhard Lammert and Dr. Michael Lawrence – who deeply enriched my journey as a doctoral student. I thank them for their role in proving that graduate training at its best focuses on the whole trainee, rather than just the bench researcher. I would be neither the scientist, nor the person, that I am today without their guidance.

Further, I would be remiss to not mention my family who supported me moving across the country to Virginia. Thank you for always providing extra ears for listening to my frustrations, my milestones, my fears, and my successes. Thank you to my father, who inspires me daily to live a balanced live; thank you to my mother, who teaches me that academia should never lose sight of compassion. I love you both. Thank you, also, to my friends who have supported this incredible journey. To my friends across the country, you have kept me company in lab via your texts, phone calls, and FaceTime through all of graduate school's difficulties. To my Charlottesville friends and graduate school friends, thanks for the adventures, and for convincing me to leave the lab. I have

met some of the most incredible people in my life while attending UVa, and I cannot wait to see what their futures hold. I would especially like to thank Allison, Ginger, and Sofia. Allison – our weekly dinners were the sabbath that kept me centered and sane. Without you, I have no idea how I would have survived graduate school. Ginger – your ability to make me laugh is only matched by your beyond-your-years wisdom that I have continued to rely on since our time at Tulane. Also, somehow, even as an intern, you have managed to make medicine still look fun. Sofia – thank you for being my translator, my guide, my collaborator, and my very good friend. Some of my favorite memories in lab were in celebrating our successes or laughing over our mistakes. Never would I have imagined that our research partnership could have left to such a beautiful friendship.

And finally, thank you Ricky Baylis. In the crazy whirlwind that is graduate school, you took the time to sweep me off my feet. Thank you for your enduring support, passionate scientific inquiry, and optimistic love. You taught me to not close doors, just because they were a little more open in the past. You embraced my dream of going to medical school, and started dreaming – no, living – it with me. I can never thank you enough. I love you.

ABSTRACT

Adult angiogenesis offers the potential for functional recovery following injury, whether due to cutaneous wounds, peripheral ischemia, or myocardial infarction. However, clinical interventions to harness this capability have largely failed in their inability to create stable perfused vasculatures. More efficacious therapies require a deeper understanding of vessel stabilization, which is believed to be dependent on recruitment and investment of perivascular cells, including smooth muscle cells and pericytes. Explorations into vessel stabilization have been challenged by the following: First, existing *in vitro* models of angiogenesis cannot fully recapitulate the *in vivo* cross-talk between multiple cells types. Second, *in vivo* angiogenesis models do not permit serial time-lapse analysis at the single-cell resolution needed to understand angiogeneic recruitment. Similarly, current studies are unable to relate cellular biochemical responses to the biomechanical cues from blood flow velocity *in vivo*. Third, both endothelial and perivascular cells are highly heterogeneous populations. Recent evidence suggests that pericytes exhibit pluripotency, which may undermine their stable investment, yet the genetic programs underpinning their differentiation remain unclear. Thus, this thesis makes three primary contributions. First, I have developed a novel dual-modality, high-resolution intravital imaging technique that, when applied to fluorescent-reporting and lineage-tracing mice, is able to uniquely observe angiogenesis at over time in a single network. Using intravital confocal microscopy, I dynamically tracked the maturity of individual endothelial states in a cornea angiogenesis model; then, these images were co-registered with photoacoustic microscopy images to non-invasively quantify shear stress through the vessels. Second, I used intravital confocal imaging in a Myh11-pericyte lineage tracing method to quantify pericyte migration and investment during angiogenesis, with and without pluripotent Oct4 expression. Finally, prior work in our lab demonstrated that adipose-derived stem cells are able to invest the perivascular niche in the diabetic retina to prevent microvascular drop out. In order to extend my considerations of vascular heterogeneity into potential therapies, I studied how diabetes effects the therapeutic potential (*in vitro*) and efficacy (*in vivo*) of adipose-derived stem cells to stabilize the retinal microvessels of diabetic mice. In short, this dissertation provides a deeper understanding of endothelial and pericyte heterogeneity, how these heterogeneities may lead to pathologic angiogenic capabilities and microvascular instability during diabetes.

Table of Contents

LIST OF FIGURES AND TABLES

THE ROLE AND USE OF HETEROGENEITY IN MICROVASCULAR INSTABILITY

By Molly Rose Kelly-Goss

CHAPTER 1

Introduction

Background

Angiogenesis is the growth of new blood vessels from a pre-existing vasculature. In the adult, this process can happen physiologically, to provide oxygen and nutrients to a growing tissue. Angiogenesis may also happen pathologically, such as in disorganized tumor growth. Often, there is a therapeutic need to stimulate angiogenesis into a tissue, such as after injury or ischemia. To date, clinical interventions to harness angiogenesis – either by controlled regression or stable expansion – have largely failed. In order to improve these therapies, ongoing research has focused on understanding the primary components of the vasculature, endothelial cells and their supportive perivascular cells, including pericytes and smooth muscle cells. Given the complex biochemical and biomechanical environment of each cell in the microvasculature, recent research has aimed to understand the complex heterogeneity of both endothelial and perivascular cells. The overarching goal of this thesis was to better understand this heterogeneity of the microvasculature, and how it may be used therapeutically to control angiogenesis.

The second main goal of this thesis was organically inspired while reading the literature and examining images of angiogenic networks. Time and time again, I kept asking myself, "*How? How did these vessels get here? How does this actually happen?"* In the majority of studies on angiogenesis, including many of those presented here, we are presented a series of endpoints. Yet, the microvasculature is highly dynamic, and I wished for a closer study. This curiosity became the foundation of the second goal of this work: to design a confocal imaging protocol to observe an angiogenic network *in vivo,* over time, as it undergoes new vessel growth and vascular remodeling. Indeed, better knowledge of the spatial and temporal dynamics of the vascular networks during angiogenesis may lead to greater success of therapies aimed at the microvasculature.

Anatomy and cellular composition of the blood vasculature

The blood vessels of the cardiovascular system are organized along a hierarchy that dictates their structure and function[1]. The aorta and large arteries transport oxygenated blood away from the heart. Blood then passes through smaller resistance arterioles and into capillaries, where the exchange of nutrients, oxygen, and other gases occurs[1]. Deoxygenated blood exits the tissues through post-capillary venules, which drain into the larger veins. The larger veins convey blood to the inferior and superior vena cava, which return deoxygenated blood to the heart. The expansion of branched capillary networks deep into nearly every tissue of the body occurs in order to permit organismic growth, satisfy the local metabolic demands of tissue during homeostasis, and enable wound healing and regeneration following injury to the tissue.

The vasculature is comprised of many heterogeneous cell types that vary based on their radial location within the vessel wall, as well as their location in the hierarchical network of the blood circulatory system. However, all blood vessels are composed of an inner lining of endothelial cells (or so called "endothelium") surrounding the blood vessel lumen[2]. The endothelium plays an important role in the sensing of mechanical signals, such as blood flow-induced shear stress, due to the fact that the endothelial cells' apical surfaces face the blood stream flowing through the vessel lumen [3-5]. In addition to blood flow-induced shear stress, blood pressure and hydrostatic pressure also represent mechanical stimuli that act on endothelium[6].

Situated in the inner layer of the vessel wall, the vascular endothelium is uniquely positioned to participate in mechanosensing and to transfer mechanical signals to other cells in the vasculature, such as the smooth muscle cells (SMCs) that enwrap the endothelium. In arteries, arterioles, and larger veins, vascular SMCs are responsible for vasodilation (widening of the vessel lumen) and vasoconstriction (narrowing of the vessel lumen). This functionality in the resistance

arterioles (which range from 15-200 microns in diameter) makes vascular SMCs the primary regulators of vascular resistance and major controllers of systemic blood pressure[7]. The endothelium of capillaries is enwrapped by cells, termed 'pericytes', which provide stability and support to capillaries, help to regulate capillary permeability, modulate immune cell trafficking, and, in tissues such as the brain, regulate blood flow via vasoconstriction and vasodilation[8-11].

Microvascular Remodeling

Microvascular remodeling occurs in three different modes throughout an organism's lifespan: vasculogenesis, angiogenesis, and arteriogenesis. In the embryo, the de novo formation of a primary vascular plexus occurs during the process of vasculogenesis via mesoderm differentiation of angioblasts[12]. Primitive vasculature is generated from the non- luminal endothelial networks during network maturation. Quiescent microvasculature is then formed through interactions between endothelial cells and with extracellular matrix, other cells such as smooth muscle cells and pericytes, and other signals such as shear stress and hyperoxia[13]. Interestingly, vasculogenesis – the creation of a new vascular network de novo, without the expansion of a previous network – was suggested to rarely occur in the adult[14]. While the source of cells and their role in adult vascularization are poorly defined, bone marrow derived circulating endothelial progenitor cells have been shown to actively contribute to postnatal vasculogenesis[15].

In vivo blood vessel formation also occurs in the adult through angiogenesis. Angiogenesis is the creation of new blood vessels form a pre-existing network. This process can occur by two different processes – capillary sprouting and capillary splitting – that are discussed in detail below[13]. Finally, as the vasculature begins to stabilize, nascent vessels increase in diameter and obtain a viscoelastic and vasomotor coat of smooth muscle cells[16]. This process is known as arteriogenesis and is important for the consistent perfusion of a tissue. Together, these three processes are required for

healthy tissue function. Understanding the mechanisms and dynamic interplay of the three processes is imperative to the development of angiogenic and anti-angiogenic therapies.

Angiogenesis in the Adult

Sprouting Angiogenesis

Sprouting angiogenesis begins notably early in embryo development and persists throughout adult life. Initially, sprouting angiogenesis is characterized by vasodilation via nitric oxide, in part to increase vascular permeability to vascular endothelial growth factor (VEGF)[17]. VEGF is known to both stimulate and provide direction for sprouting angiogenesis, though much of the other mechanism regarding sprouting directionality and location remains unknown. This process is led by an endothelial tip cell that extends filopodia to guide the direction of sprouting[18]. Degradation of the basement membrane, also termed basal lamina, is mediated by activated endothelial cells after exposure to VEGF and further allows for extension of endothelial cells into extracellular space. Proliferating and migrating endothelial cells then undergo intercalation and fusion to subsequently acquire a lumen[19]. Through this process, new capillary segments are able to grow and mature across their surrounding tissue space until they reach quiescence.

Pericyte recruitment during sprouting angiogenesis

Pericyte recruitment to neovessels is thought to involve chemotactic signals that are secreted from activated endothelial cells, such as platelet derived growth factor-BB (PDGF-BB) and Angiopoietin-1 (Ang1)[4,5]. Endothelial PDGF-BB binds to PC PDGFR- β to induce PC migration and proliferation through the Ras/Rho/Rac pathway[18,19]; elevated Ang1 expression has been shown to enhance PC migration, recruitment, and viability[20-22]. Although these and other chemotactic signals have been studied over the past twenty-plus years in the context of pericyte recruitment[23],

the important question of where new pericytes originate from remains unresolved. It has been speculated that new pericytes may arise from one or more of the following sources: pre-existing smooth muscle cells, pre-existing pericytes, circulating progenitor cells, and/or interstitial tissue-resident cells[24]. Although a few studies have examined pericyte origin in tumor angiogenesis[25], no studies of adult angiogenesis have ruled in or out any endogenous pericyte source. Further, until the work provided in this dissertation, no study has conducted a SMC- or PC-specific genetic knockout during adult angiogenesis.

Intussusceptive Angiogenesis

Intussusceptive angiogenesis, known also as splitting angiogenesis, involves the separation of a whole capillary into two by the extension of a luminal column. Endothelial cells within a vessel will proliferate to produce a lumen wide enough to allow the fusion of the splitting capillary. This "pinching off" of one vessel into two is traditionally only seen in thick-walled vasculature, like that seen in the lung or heart[13]. Intussusception is frequently described in three phases: microvascular growth, arborization, and branch remodeling[20]. During microvascular growth, pillar creation and expansion increases the capillary surface area begins longitudinal division via a central perforation, often aided by local fibroblasts. Arborization encompasses the delineation of generations of feeding and draining vessels to maintain network hierarchy. Merging of septa and horizontal pillar folds create definitive vessel entities that are separated by collagen fibrils. Finally, branch remodeling involves any vascular architectural changes that are done to meet local blood flow demands[20]. Modifications include branch angle adjustment, bifurcation relation, and vessel dilation or pruning. Overall, this process is mediated by VEGF promotion of vessel dilation and expansion. Tie-2 is also implicated with inducing endothelial cell narrowing to begin intussusception[13].

Heterogeneity in the Vasculature

Heterogeneity in Endothelial Cells

In seeking to understand how the endothelium continues to defy therapeutic drug development, studies have long focused on the heterogeneity of the endothelium. Indeed, as stated by Lord Florey in his 1966 publication[21], "Now it is recognized that there are many kinds of endothelial cells which differ from one another substantially in structure, and to some extent in function." While this quote refers to the varying shapes of endothelial cells observed along the vascular lumen, a finding that has been successfully repeated[22], a substantial body of research has added to our understanding of this heterogeneity[23].

One of the most common phenotypes demonstrating endothelial heterogeneity is observed in vessel specification. The endothelium of arteries, veins, and capillaries are all distinct from one another at many levels, including gene expression and cell morphology. During development, varied expression in gene encode differences between arterial and venous endothelium at an early stage. For example, Eph receptor B4, Neuropilin-2, Flt4, and COUP-TFII were shown to be expressed by veins, while ephrin B2, Neuropilin-1, Flt1, and Notch-1, Notch-4, and Notch-5 were shown to be expressed by arteries [24]. Indeed, prior studies have shown that in the absence of one of these vessel specific-factors, COUP-TFII, venous endothelium express genes indicative of arterial endothelial cells, including enphrin B2 and Neuropilin-1, and Notch-1. Further, the endothelium of different vessels is exposed to different biomechanical signaling cues. Arterial endothelial cells observe shear stress levels 10-40 dynes/cm^2, while veins observe shear stress levels 1-4 dynes/cm^2. It is perhaps unsurprising, then, that arterial endothelial cells have increased tight junctions and adherens junctions compared to veins [25]. Though, when compared to arterial and venous endothelial cells, which both retain tight junctions, capillary endothelium can

additionally be highly fenestrated or discontinuous – as in the kidney glomeruli or liver, respectively[26,27] – to permit a higher exchange of gas, nutrients, waste, and circulating cells.

Due to the advent of high-throughput genomic sequencing, recent studies have begun deeply examining the genetic and epigenetic differences between vessel bed-specific endothelial cells. One seminal study pointed to the importance of both the cellular epigenetics and tissue environment in regulating endothelial heterogeneity upon showing that endothelial cells removed from human tonsils lost 50% of their vascular bed-specific genes upon being cultured *in vitro* [28]. Since then, highly detailed genome-wide expression analyses have uncovered unique genetic motifs for capillary endothelial cells in different tissues, including the liver, spleen, brain, heart, muscle, lung, testis, and kidney. These studies have also demonstrated tissue-specific angiocrine responses to injury and irradiation. This further supports the idea that endothelial cells of different vascular beds may require different therapeutic approaches, and that when being isolated for tissue grafting or tissue engineering applications, different endothelial cells may have different therapeutic potential [29].

Finally, in light of our complex understanding of the endothelium, significant research has focused on how to analyze and appreciate these new, rich datasets. Thus, endothelial heterogeneity has seen growing attention from the field of computational modeling. While some studies use a systems engineering approach to grapple with the immense agonist-mediated signaling pathways and their crosstalk[30], others analyze the endothelial phenotypic drift observed in culture[31], mentioned above. Still others use agent-based modeling to tackle the heterogeneity of tip-cell versus phalanx cell specification during the onset of sprouting angiogenesis[32,33]. Finally, complex computational fluid dynamics analysis, linked with growth and remodeling algorithms, are being used to predict the site of abdominal aneurysm by modeling wall shear stress from blood flow, and predicting the

endothelial growth and remodeling response [34]. While this field may still be nascent, by building these models of physiologic endothelial heterogeneity, there exists the ability to leverage complex models to predict endothelial aberrancies and responses during disease.

Heterogeneity in Pericytes

Similar to their neighboring endothelial cells, pericytes vary widely depending on their embryologic origin, location, and disease state. Perhaps the most compelling sign of pericyte heterogeneity is that there does not exist any known cellular marker that can exclusively identity all pericytes[35]. While pericyte heterogeneity, including marker expression, is reviewed in depth in Chapter 4, one can immediately appreciate that this may originate from their stem cell-like character. Indeed, perivascular cells isolated from tissue, including adipose, are able to undergo adipogenesis, osteogenesis, and chondrogenesis in culture, and can elicit substantial regenerative capabilities when injected back *in vivo*[36]. Further, disturbance in endothelial-pericyte interactions has been reported to stimulate osteogenic and adipogenic differentiation of pericytes[31].

This "steminess" that has, in part, motivated extensive studies analyzing the heterogeneity of pericytes. Recent genetic studies have analyzed the transcriptome using RNA-Seq on individual pericytes in the brain[37]. Using this technique, exciting and highly detailed zonation maps have been created for the brain vasculature that show the individual cellular genetic heterogeneity. Further, upon comparing the genomes of individual pericytes in the brain to those in the lung, the authors of this study identified pericyte organotypicity[38]. Specifically, while brain pericytes expressed aminopeptidase N and ATP transporters, lung pericytes did not. This organotypicity is consistent with past research that demonstrates the varied function of pericytes, including phosphate transport in the blood-brain barrier[39,40] and vitamin A metabolism in the liver[41]. However, these findings aren't without their own limitations. The authors did not genetically halt perivascular genetic response

during mechanical and enzymatic digestion. By using an agent to interfere with mRNA synthesis, such as Actinomycin D, the authors could have better-captured the *in vivo* pericyte transcriptome. Indeed, their data suggests that their isolated pericytes were activated in response to being sorted. That said, their work provides great evidence of perivascular organ-specific characteristics and thus echo the idea that vascular therapies may require tissue- or subpopulation-specific targeting[42].

Biomechanical Signaling as a Source of Heterogeneity

While there exists a plethora of biochemical cues that provide heterogeneity, it is worth briefly mentioning the role of biomechanical forces on cell heterogeneity, which is further reviewed at length in Chapter 2. Previous studies have suggested that endothelial maturity, as indicated by Tie2 expression, is affected by changes in blood flow-induced shear [13-16]. Kurniati et al[17], showed that increasing shear stress caused elevations in Tie2 expression in cultured human umbilical vein endothelial cells (HUVECs); also, that HUVECs decreased Tie2 gene expression after being placed in no flow or low flow conditions. They also showed that decreases in blood flow in a murine model of hemorrhagic shock caused a decrease in Tie2 mRNA expression across multiple organs. Moreover, in addition to Tie2, Obi et al.[18] demonstrated a direct relationship between the magnitude of shear stress and the expression of multiple EC markers *in vitro*, including VEGF-R1, VEGF-R2, and VE-Cadherin.

Additionally, few studies have investigated how the onset of (or changes in) blood flow in a neovessel affects pericyte maturity. One study by Naylor et al, demonstrated via muscle overload that shear stress-induced sprouting angiogenesis in skeletal muscle is dependent on pericyte-specific Endosialin and PDGFR-β signaling, but that intussusception, was not[25]. Another study showed that following cessation of blood flow, pericytes maintain their expression of PDGFR-β but decrease their expression of α-SMA, although reinstating blood flow caused pericyte α-SMA

expression levels to recover within 48 hours[26]. These studies support the idea that change in blood flow also contributes to pericyte-specific vascular heterogeneity.

Vascular Heterogeneity during Disease

Aberrant angiogenesis has been implicated as a common denominator in over 70 diseases[1], including heart failure and cancer. For example, hyperactive angiogenesis is observed in tumor metastasis and formation, dysregulated immune-driven angiogenesis is observed in endometriosis[43], inflammation-driven activation of the endothelium leads to thromboembolism[44], and hypoactive angiogenesis leads to ischemic tissues, such as in peripheral arterial disease or cardiac tissue after a myocardial infarction[1]. As of this dissertation, there are over 5,200 studies on angiogenesis reported by the U.S. National Library of Medicine, demonstrating its paramount importance to improving clinical outcomes.

Since Judah Folkman's seminal insight that tumors could not grow beyond 2 mm^3 without microvascular investment[45], many strategies have been developed to curb tumor angiogenesis. These most famously include anti-VEGF agents, such as bevacizumab and aflibercept, as well as mural cell inhibitors[46,47], stromal cell inhibitors[48], leukocyte inhibitors[49], and cytotoxic anti-angiogenic agents[50]. Despite the wide-spread clinical use of these agents, the benefits to date have been considered modest with little-to-moderate improvement in overall survival of various cancers[51]. Underpinning the failure of these therapeutics to work is the innate heterogeneity of the aberrant vascular network. Compared to physiologic vessels, tumorigenic vessels are more dilated, tortuous, permeable, fenestrated, lack a hierarchy, and have chaotic flow patterns and high interstitial fluid pressures[52]. Tumor vascular abnormalities also are present in both the endothelial and perivascular cell populations[53,54]. Tumor endothelial cells are reported to be resistant to serum

starvation, demonstrate aneuploidy, are more proliferative, have increased VEGFR-1, VEGFR-2, and autocrine VEGF expression, and have higher angiogenic Akt phosphorylation levels at baseline[55]. Tumor endothelial cells are also highly mutable depending on their environment; when implanted in different parts of the body, identical tumor types displayed different tumor endothelial phenotypes[56,57]. Similarly, tumor pericytes vary widely in coverage and phenotype. In glioblastoma, pericytes have been shown to upregulate PDGFR-β with increased tumor stage, while also increasing contact-dependent interaction with tumor cells[58]. Another study demonstrated that cancer stem cells can reside in the perivascular niche, assuming a pericyte morphology and location[59]. Similarly, pericytes isolated from human infantile hemangioma, are reported to have decreased contractility, downregulated Ang1, increased proliferation, and increased secretion of pro-angiogenic factors[60], including VEGF-A. These data suggest that pericytes are dynamic and active in tumorigenesis[61]. Indeed, in part due to this heterogeneity, tumors have been able to adapt in the face of anti-angiogenic therapies[62]. Thus, understanding the fundamental mechanisms behind this heterogeneity is believed to be important in furthering anti-angiogenic therapies.

Additionally, in 1963, David Cogan observed that pericytes were absent from capillaries in the diabetic retina[63,64]. The loss of pericytes, as well as smooth muscle cells[65], and later endothelial cells[66], leads to the formation of microaneurysms and eventually sight-compromising disease[67]. Intriguingly, no study has putatively demonstrated the fate of pericytes during diabetic retinopathy[68,69]. While hyperglycemia is known to cause increased oxidative stress and loss of insulin-mediated pro-survival signaling via glycated collagen, the question of which pericytes are susceptible to 'drop out' – and where these pericytes go after vessel dissociation – still remains[70]. This elusivity is reflected in clinical outcomes. Approximately 40% of patients are non-responders to anti-VEGF treatment; even in responsive patients, injections only serve to delay laser

photocoagulation[71], a procedure that compromises peripheral and night vision to spare central vision. Consequently, patients are currently left with treatments that only manage the complications of diabetic retinopathy in the short term[72]. In order to address these limitations, new studies, including those discussed in Chapter 4 and conducted in Chapter 6, are aimed at repairing the damaged tissue via administration of mesenchymal stem cells (MSC) to replace the perivascular niche[73-75]. Indeed, the multipotency of MSCs may be permissive to replacing the heterogeneous perivascular niche in the diabetic retina.

Primary Methods Used to Study Angiogenesis

Angiogenesis and neovessel stabilization are inherently dynamic processes. Consequently, in order to address the multitude of questions that remain, there exist many experimental models that are each uniquely able to test different hypotheses[76].

In vitro

Although *in vitro* techniques do not have immediately applicable physiological relevance, they provide a controlled environment in which to test specific hypotheses. When probing specific molecular and genetic interactions *in vivo* is too laborious or technically challenging, *in vitro* models of angiogenesis are able to test multiple hypotheses quickly for subsequent *in vivo* validation. *In vitro* models also permit high-throughput drug testing, gene candidate searches in response to therapeutic agents, and relatively simple time course imaging and assessment of cellular behavior[77].

In static culture, endothelial cell behavior is tested either alone or in co-culture with multiple other cell types, including fibroblasts, pericytes, tumor cells, monocytes and other immune cells [78-83]. These cultures exist as two-dimensional systems, as well as three-dimensional systems that permit

time course analysis of network and tube formation [84,85]. While *in vitro* assays can readily investigate the proliferative, apoptotic, metabolic, molecular and genetic response to stimuli or environmental changes, they also permit functional analysis of cellular behavior[86,87]. This includes the use of scratch assays and Boyden chambers to assess cell migration and transendothelial transport, respectively[88-90]. Further, *ex vivo* systems, such as the aortic ring assay and mesenteric culture model permit analysis of angiogenic sprouting with a higher degree of physiologic relevance[91-94].

Additional *in vitro* systems also permit extensive study on the role of biomechanics in angiogenesis. The role of static strain, as experienced during circumferential stretch in *in vivo* vascular remodeling, can be tested via tunable stretch chambers; these studies have revealed a role for stretch in endothelial cell proliferation and sprouting-like behavior[95,96]. Further, multiple systems exist in which to study the role of shear stress on endothelial cells and pericyte[97,98]. These systems are highly customizable across a wide range of shear stress ranges, direction[99], and wave profiles[100], in order to test physiologic shear stress experienced across the vasculature and during disease[101], such as the turbulent flow observed in atherosclerosis[102]. Additional systems also allow for analysis of the role of interstitial flow on endothelial sprouting behavior[103-106]. Truly, *in vitro* systems permit highly specific conditions to answer physiologic questions.

In vivo

In addition to *in vitro* models of angiogenesis, there exist a wide range of *in vivo* models of angiogenesis. Invaluable mechanistic insights on developmental angiogenesis have been gained from non-mammalian systems, such as the chick embryo model and zebrafish assay[107,108]. Other developmental insights on VEGFR-1 coordination in mammalian developmental angiogenesis have made use of the mouse embryoid model[109]. While these insights have been invaluable for the

progression of the angiogenesis field, they are limited in application to adult models of angiogenesis, where a pre-existing and quiescent vasculature exists. Likewise, while zebrafish have been used to study angiogenesis in tumorigenic settings, as well as in non-mammalian regeneration, their applicability to human disease is uncertain[110,111].

Adult, mammalian angiogenesis has also been observed through a number of model systems[112]. Rodent mesentery angiogenesis assays[113,114] and hydrogel implant assays[115-119] both permit analysis of sprouting angiogenesis at a single time-point after treatment. The backpack window chamber model has provided insight in angiogenesis and arterialization of microvascular networks over time[120], yet is not permissive for intravital imaging at a single-cellular level. Finally, the cornea angiogenesis assay allows for observation of neovascularization into a previously-avascular tissue over time at a high resolution[121,122]. Corneal angiogenesis may be stimulated via numerous cytokines or tumor placement into a micropocket, placement of sutures, or application of silver nitrate[123-125]. Due, in part, to the accessibility of the cornea, much of the work in this thesis leverages the corneal angiogenesis assay, as presented in Chapter 3 and Chapter 5.

Finally, there exist a number of useful clinical tools that permit study of patient microvascular health. Magnetic resonance angiography of lower extremities is used to quantify collateral vessel health in patients with peripheral artery disease to predict femoral artery plaque area and lowerlimb ischemic risk[126,127]. Additionally, indocyanine green angiography can detect choroidal neovascularization in patients being treated with anti-VEGF bevacizumab for age-related macular degeneration[128,129]. Recent work has used this angiography to predict whether patients are likely to experience recurrent exudation and hemorrhaging during continued “treat-and-extend” protocols of bevacizumab. These studies, while limited in scope, provide insight into how quantitative assessment of angiogenesis during diseases can be used to predict clinical outcomes.

Overview of Thesis

The remaining chapters of this dissertation consider endothelial heterogeneity, perivascular heterogeneity, and one potential therapeutic implication, in that order. Chapter 2 delves into the role of biomechanics in endothelial heterogeneity. Here, the complex mechanisms by which the endothelium senses, responds to, and modifies its environment are outlined. While the chapter focuses healthy physiology, it concludes with clinical considerations for atherosclerosis.

Chapter 3 is the first primary research chapter, in which we present a novel method of intravital confocal microscopy. While developing this technique, we were surprised to observe that the angiogenic endothelium, while perfusion-competent, did not express Tie2. This observation stemmed a collaboration in which we were able to overlay the confocal images with those taken via non-invasive photoacoustic microscopy, which elucidated the blood flow velocity. By combining both techniques, we were able to correlate endothelial Tie2 expression with capillary shear stress in a remodeling network, at the level of a single capillary.

Chapter 4 transitions from the endothelium to pericytes. Here, we discuss the heterogeneity innate to pericytes, including their diverse phenotypic lineage and origin. This chapter also discusses two major questions within the field: (1) are pericytes mesenchymal stem cells? and (2) can we use mesenchymal stem cells to stabilize aberrantly angiogenic vasculature? These questions become foundational for the remaining two primarily research chapters.

Chapter 5 aims to uncover the underpinning mechanism of a pluripotent stem cell gene, Oct4, in pericytes. While the loss of Oct4 exclusively in pericytes seemed to play no role at baseline, it lead to aberrant, leaky angiogenesis in response to corneal alkali burn and hindlimb ischemia. We found significant impairment in perivascular and endothelial cell migration and a substantially decreased pericyte population. Further, RNA-seq and qRT-PCR analysis of cultured

SMC showed that Oct4-KO was associated with dysregulated expression of the migratory signaling cue family, Slit-Robo, including Slit3 downregulation and Slit2 upregulation. Together, these data implied that pericytes to use pluripotent stem cell gene regulation during angiogenesis.

Chapter 6 addresses the second question posed in Chapter 4. Transitioning away from the cornea, we used diabetic Akimba mice in a model of diabetic retinopathy. We built on previous studies that demonstrated that adipose-derived stem cells (ASCs) injected into the vitreous of diabetic mice had a protective effect on the retinal microvasculature. While past studies used stem cells from a healthy source, we investigated the effect of diabetes on the angiogenic potential of ASCs *in vitro*, as well as the vascular protective effect *in vivo*. Indeed, we found that diabetic ASCs have a less active angiogenic secretome and a reduced therapeutic effect.

Chapter 7 provides deeper reflection on the contributions from this thesis. Finally, as no work in science is ever truly complete, I will share some of the exciting new questions we are exploring, as a consequence of this work.

CHAPTER 2

Endothelial Mechanosensitivity as a Source of Heterogeneity

ACKNOWLEDGEMENTS: Sofia Urner[2], Shayn M. Peirce[1,3], and Eckhard Lammert[4]

[1]Institute of Metabolic Physiology, Heinrich Heine University Düsseldorf
[2]Department of Biomedical Engineering, University of Virginia
[3]Institute for Beta Cell Biology, German Diabetes Center, Leibniz Center for Diabetes Research at Heinrich Heine University

The text included in this chapter has been published:
Urner S, Kelly-Goss M, Peirce-Cottler S and Lammert E. Mechanotransduction in vascular and lymphatic development and disease. Advances in Pharmacology, Vol. 81 Vascular Pharmacology: Cytoskeleton and Extracellular Matrix, 2018.

Abstract

The blood and lymphatic vasculatures are hierarchical networks of vessels, which constantly transport fluids and, therefore, are exposed to a variety of mechanical forces. Considering the role of mechanotransduction is key for fully understanding how these vascular systems develop, function, and how vascular pathologies evolve. During embryonic development, for example, initiation of blood flow is essential for early vascular remodeling, and increased interstitial fluid pressure, as well as initiation of lymph flow, is needed for proper development and maturation of the lymphatic vasculature. In this review, we introduce specific mechanical forces that affect both the blood and lymphatic vasculatures, including longitudinal and circumferential stretch, as well as shear stress. In addition, we provide an overview of the role of mechanotransduction during atherosclerosis and secondary lymphedema, which both trigger tissue fibrosis.

Introduction

Two vascular systems exist in the vertebrate body: the blood and the lymphatic vasculatures. The blood vasculature is a closed circulatory system, which transports blood through the body, and is required for exchange of oxygen, nutrients, water, salts, hormones, and waste products between blood and tissues (Figure 2.1). In contrast, the lymphatic vasculature is a blind-ended system responsible for the uptake of interstitial fluid leaking out of the blood vasculature into extracellular spaces (Figure 2.2). The lymphatic vasculature transports this fluid, referred to as lymph, back to the blood circulatory system, thereby maintaining fluid homeostasis in the body. Further, the lymphatic vasculature is involved in the uptake of dietary lipids and in immune surveillance. Both vessel types are found in nearly every tissue in the body, except avascular tissues such as cartilage or the cornea. Strikingly, recent studies discovered functional lymphatic vessels in the brain, previously believed to be lacking lymphatic vasculature[130,131]. Dysfunctions of the blood or lymphatic vasculature are implicated in numerous pathological conditions, including atherosclerosis, myocardial infarction, stroke, lymphedema, chronic inflammation, tumor growth, and diabetic nephropathy and retinopathy.

Biomechanical forces play a critical role during developmental, physiological, and pathological processes, and therefore have gained increasing attention in vascular research [132-137]. In the vasculature, constant fluid transport creates both shear stress by flow along the inner lumen of the vessels and endothelial stretch by exerting pressure on the endothelial cell layer. Several studies demonstrate that these mechanical stimulations critically regulate growth of blood and lymphatic vessels, known as angiogenesis and lymphangiogenesis, respectively. Moreover, extracellular matrix (ECM) receptors, such as those containing the β1 integrin subunit, significantly contribute to mechanotransduction in endothelial cells by translating mechanical stimuli into activation of

Vascular Endothelial Growth Factor Receptor (VEGFR)-2 and -3 [138,139]. These subsequently promote endothelial cell survival, proliferation, and migration [140].

In this review, we aim to discuss the mechanical forces that influence the blood vasculature and introduce relevant molecular players that contribute to responding to these forces. While the lymphatic vasculature was considered in great depth in the initial publication of this review, these sections were removed for the sake of brevity. Here, we further summarize key events of mechanotransduction during the development of the vasculature network. Finally, we briefly describe how mechanotransduction is changed in vascular endothelial cells, and how these changes contribute to atherosclerosis.

Blood transport through veins

- Intrinsic pump
  (phasic contractions of vascular smooth muscle cells)
- Opening and closing of venous valves
  (if present)
- Extrinsic pump
  (contractions created by other tissues)

Mechanical impact on vascular endothelial cells

① Systolic and diastolic blood pressure
(circumferential stretch)
② Hydrostatic pressure
(circumferential stretch)
③ Blood flow
(shear stress, e.g., laminar or oscillatory)

Blood transport through arteries

- Pumping of the heart
- Arteriolar smooth muscle cell contraction and relaxation

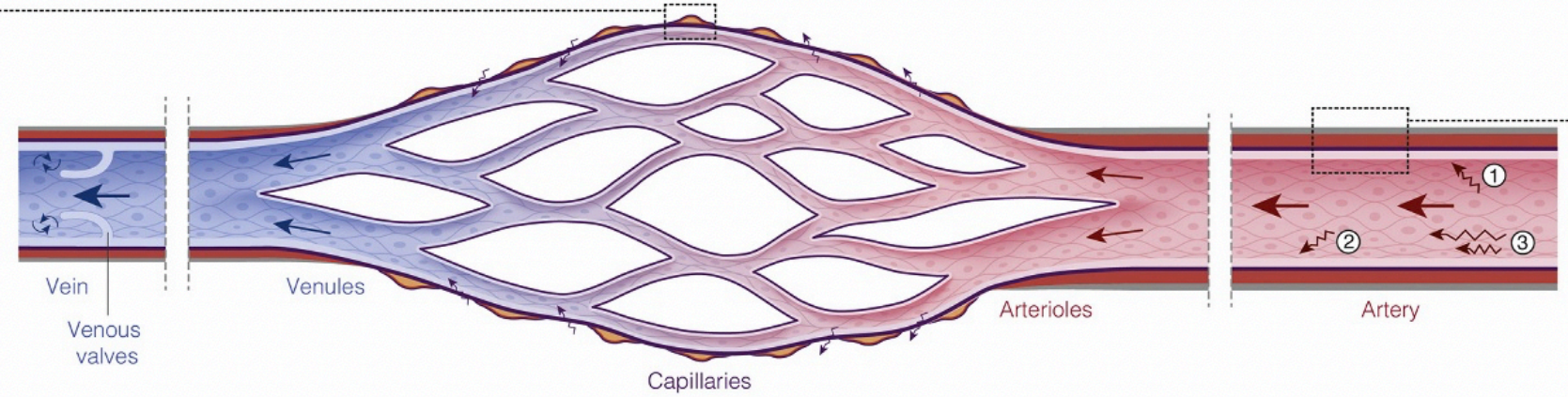

Blood capillaries

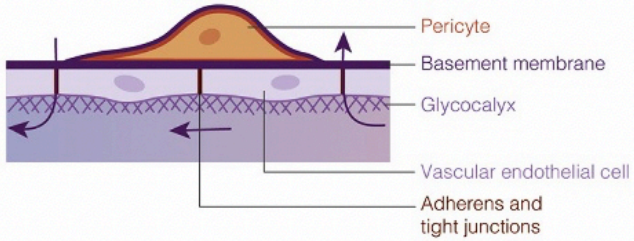

Arteries

↑ Klf2
↑ Nitric oxide
↑ E-selectin
↑ ICAM-1
↑ VCAM-1
↑ PECAM-1
↑ VEGFR1
↑ VEGFR2
↑ Tie2
↑ VE-Cadherin
↑ Integrins
↑ Endoglin

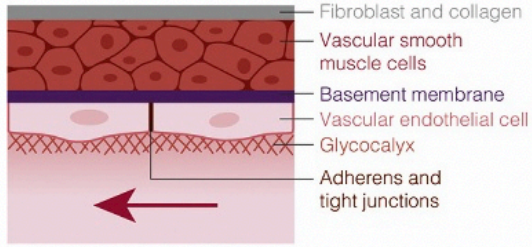

Mechanoresponsive to shear stress

Figure 2.1 Hierarchy of the blood vasculature and physiological role of mechanical forces.

The blood vasculature can be classified into arteries, arterioles, capillaries, venules, and veins. Arteries consist of vascular endothelial cells, which are connected via adherens and/or tight junctions, and are covered by a continuous basement membrane, vascular smooth muscle cells (SMCs), and a layer of fibroblasts and collagen. The apical surface further is covered by a glycocalyx. The main driving force of blood transport through the arteries is the pumping of the heart as well as the arteriolar SMC contraction and relaxation. Blood capillaries allow the exchange of gases and nutrients, and consist of vascular endothelial cells that are covered by a basement membrane and pericytes. The endothelial cells are also connected via adherens and/or tight junctions, and face a glycocalyx on the apical surface. The arterial part of a capillary bed allows fluid to escape from the capillaries, while the venous part allows uptake of fluid back into the blood circulation. Veins show a similar morphology to arteries, but generally exhibit a thinner vascular SMC layer, and additionally can contain venous valves. Blood transport through veins is mainly driven by phasic contractions of vascular SMCs that act as an intrinsic pump, opening and closing of venous valves, and contractions created by other tissues that serve as an extrinsic pump. In general, vascular endothelial cells of the blood vasculature experience circumferential stretch created by systolic and diastolic blood pressure (1) and hydrostatic pressure (2) as well as shear stress created by blood flow (3). Several molecules are involved in the transient endothelial response to increased shear stress.

Interstitial fluid uptake

- Pressure gradient

High interstitial fluid pressure (e.g., generated by capillary fluid leakage) vs. Low intraluminal pressure (e.g., generated by lymphatic valves further downstream)

Mechanical impact on lymphatic endothelial cells

① Systolic and diastolic lymph pressure
(circumferential stretch)
② Hydrostatic pressure
(circumferential stretch)
③ Lymph flow
(shear stress, e.g., laminar or oscillatory)

Lymph transport

- Intrinsic pump
(phasic contractions of lymphatic smooth muscle cells)
- Opening and closing of lymphatic valves
- Extrinsic pump
(contractions created by surrounding tissues)

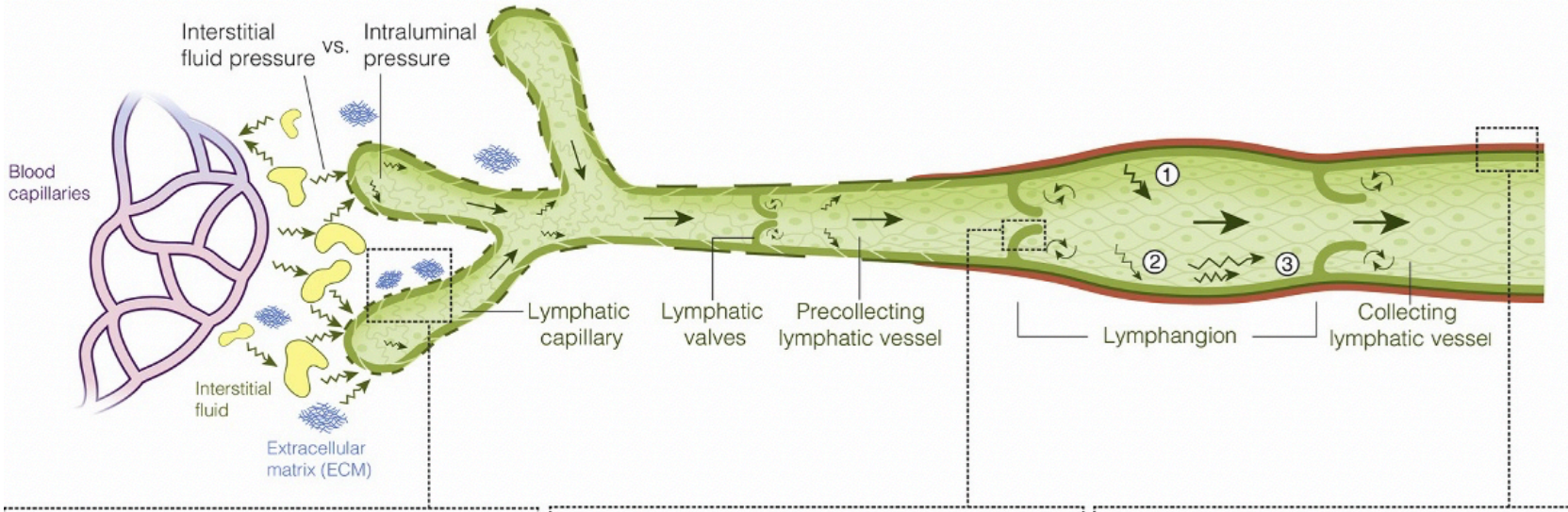

Lymphatic capillaries

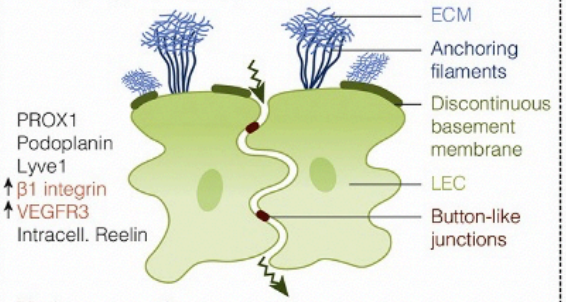

Mechanoresponsive

Lymphatic valves

↑PROX1
Podoplanin
↓Lyve1
↑Neuropilin-1
↑VEGFR3
↑FOXC2
↑GATA2
↑Laminin-α5
↑FN-EIIIa
↑EMILIN1
↑Integrin-α9
↑Connexin-37,-43,-47

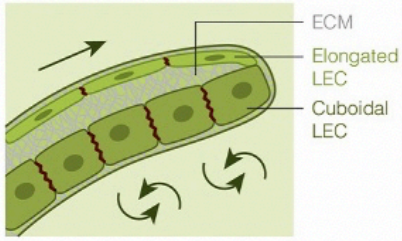

Mechanoresponsive

Collecting lymphatic vessels

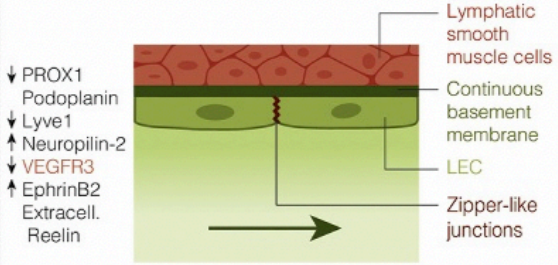

Mechanoresponsive

Figure 2.2 Hierarchy of the lymphatic vasculature and physiological role of mechanical forces.

The lymphatic vasculature can be classified into lymphatic capillaries, and pre-collecting and collecting lymphatic vessels. The lymphatic capillaries are responsible for the uptake of interstitial fluid. The main driving force for fluid uptake is a pressure gradient between the high interstitial fluid pressure and low intraluminal pressure within lymphatic capillaries. The special morphology of lymphatic capillaries contributes to the uptake of fluid, as they are covered by a discontinuous basement membrane. Moreover, they are tightly connected to the extracellular matrix (ECM) via anchoring filaments and focal adhesions, and lymphatic endothelial cells (LECs) are connected via discontinuous button-like junctions. In contrast, collecting lymphatic vessels are responsible for the lymph transport. They exhibit a continuous basement membrane, are surrounded by lymphatic smooth muscle cells (SMCs), and their LECs are connected via zipper-like junctions. Lymph propulsion is mainly driven by phasic contractions of lymphatic SMCs that act as an intrinsic pump, opening and closing of lymphatic valves, as well as by contractions created by surrounding tissues that serve as an extrinsic pump. The LECs in lymphatic valves that are exposed to linear lymph flow are elongated, whereas the LECs exposed to the recirculating lymph flow are cuboidal shaped but can also be elongated. In general, LECs experience circumferential stretch created by lymph pressure (1) and hydrostatic pressure (2) as well as shear stress created by lymph flow (3). The expression of different mechanoresponsive molecules like VEGFR3, FOXC2, or GATA2 by LECs varies depending on the hierarchical lymphatic vessel type.

Mechanical forces in blood vessels and molecular players essential for mechanotransduction

Since the 1890s, studies of the vascular endothelium have demonstrated that blood flow is actively controlled by vascular responses throughout the circulatory tree [141], and recent decades of research have demonstrated how mechanical forces imparted by blood flow dynamically affect the vasculature. The most widely studied mechanical influences on vascular responses in the blood circulation are circumferential stretch (or stress), longitudinal stretch, hydrostatic pressure, and blood flow-induced shear stress [142] (Figure 1). For example, in response to increased or decreased blood flow, the inner diameter of an arteriole will expand or narrow, respectively, to normalize the amount of shear stress to which the endothelium is exposed [143]. Likewise, in response to increased or decreased blood pressure, the vessel wall will thicken or thin, respectively, in order to accommodate the mechanical force applied in the direction perpendicular to the vessel wall by circumferential stretch. In these examples, the temporary changes in vessel wall thickness are imparted via vascular SMC contraction or dilation. Alternatively, larger, more permanent increases in vessel wall thickness (for example, resulting from long-term hypertension) require SMC hypertrophy and/or hyperplasia, as well as endothelial cell remodeling and/or proliferation [16,144-146]. Furthermore, changes in hydrostatic pressure can lead to new capillary growth (angiogenesis), possibly caused by increases in local inflammatory signaling molecules, such as interleukin-1β (IL-1β) and tumor necrotic factor-α (TNF-α) [147-149].

In the following sub-sections, we will briefly discuss the biomechanics of the cardiovascular system as a whole, including the propulsion of blood from the heart to the systemic circulation, pre-capillary regulation of the blood flow in the resistance arterioles, and post-capillary regulation of blood flow via the venous valves. Then, we will summarize the most well-studied molecular

components that are known to participate in sensing of and transduction of mechanical forces, emphasizing how these molecular components differ as a result of cell heterogeneities across the blood circulation.

Mechanical forces during blood propulsion and transport

Two opposing forces control the movement of blood through the vasculature: the propulsion of blood from the left ventricle via pumping of the heart versus regulation of blood flow in the resistance arterioles of the peripheral circulation via SMC contraction (resulting in vessel constriction) and relaxation (resulting in vessel dilation) (Figure 2.1). Hence, arterial blood pressure is related to both cardiac output (defined as heart rate times stroke volume) and total peripheral vascular resistance [150,151]. This balance between arterial relaxation and arterial constriction is dynamically maintained through a number of biochemical pathways, including peroxisome proliferator-activated receptor-γ (PPARγ), chloride (Cl^-) channels, nitric oxide (NO) synthase, arginase, and the renin-angiotensin system, all of which are known to enact their effects in both endothelial and smooth muscle cells [152-155]. Imbalance in these signals can lead to pathologically increased blood pressure, which, in turn, can cause inflammation-inducing turbulent flow [156,157].

Mechanosensors of blood flow-induced shear stress

"Mechanosensors", or molecular signals that are responsive to changes in mechanical forces, have been identified in both the developing and adult endothelium. However, to date, a comprehensive understanding of the molecular mechanisms that relate mechanosensation (i.e. sensing of mechanical signals), mechanotransduction (i.e. conversion of mechanical signals to downstream effectors), and downstream cellular accommodation (i.e. alterations in cell morphology, size, or behaviors) has remained elusive. Nonetheless, numerous prior studies have described multiple mechanisms by which endothelial cells can sense a change in shear stress, as reflected by

alterations in vascular architecture and endothelial cell gene expression. Some of these studies are reviewed below.

Cell-Cell Junctions: When considering shear stress across a confluent layer of vascular endothelial cells (such as endothelial cells on a culture plate or along the wall of a blood vessel segment), endothelial cells will redistribute the force experienced along the cell wall to minimize the tension in the membrane. Classic biomechanics studies have used mathematical modeling approaches to demonstrate that the location of highest membrane tension is at the upstream cell-cell junction (i.e., the cell-cell junction nearest to the aorta, on the arterial side of the cell), while the lowest membrane tension is on the downstream cell-cell junction (i.e., closest to the venous side of the vascular network) [158]. Recent empirical studies have identified that the gradient in membrane tension is maintained by cytoskeletal remodeling dependent on a mechanosensory complex that is primarily located at the endothelial junction upstream the direction of flow [159-161]. This complex consists of three subunits: platelet endothelial cell adhesion molecule 1 (PECAM-1, also referred to as CD31), VE-Cadherin, and VEGFR2. PECAM-1 serves as the transmitter of the force across the cellular membrane; VE-Cadherin recruits VEGFR2 and serves as its adaptor to PECAM-1; VEGFR2 is then phosphorylated to activate various downstream intracellular signaling pathways, such as Akt, mitogen-activated protein (MAP) kinases, NO production, and actin polymerization [162-167]. Together, they translate mechanical force into biochemical activity. Live fluorescence resonance energy transfer (FRET) imaging of endothelial cells has demonstrated that flow induces PECAM-1 attachment to vimentin at endothelial-endothelial cell junctions upstream to the direction of flow [97]. Additionally, VE-Cadherin was shown *in vitro* to mediate the transfer of actomyosin bundles from endothelial-endothelial junctions to focal adhesion junctions [168-172]. *In vivo*, this might suggest that VE-Cadherin responds to healthy, physiologic shear stress by decreasing

vascular permeability and leukocyte extravasation by increasing the endothelial actin cytoskeleton around cell-cell junctions [173-176]. Consistent with this hypothesis, studies using *ex vivo* imaging of human vascular segments found a distinct upregulation of F-actin cytoskeleton in arteries compared to veins. Likewise, HUVECs cultured on coverslips coated with arterial ECM (versus venous) had more positive immunostaining for VE-Cadherin and F-actin bundles [177,178].

G-Proteins: Fluid shear stress has also been shown to activate G-protein coupled receptors (GPCR) in a ligand independent manner. Specifically, endothelial cells exposed to shear stress conditions revealed ligand-independent activation of the bradykinin B2 GPCR using a combination of fluorescence and FRET microscopy [179]. In addition, shear-induced GPCR signaling has also been suggested to increase platelet-derived growth factor (PDGF) gene expression by triggering protein kinase C (PKC) activation [180]. Additional studies demonstrated that small G protein Ras is rapidly activated in response to fluid flow in dose-dependent manner [181]. Additional historic reviews have thoroughly outlined challenges in the field to de-couple the many hypothesized G-protein linked signaling mechanisms to understand their relative contributions to mechanosensing and mechanotransduction in vascular endothelial cells [182,183].

Primary Cilia: Primary cilia are organelles that extrude from the cell membrane into the interstitial space, composed of microtubules that communicate with the extracellular environment [184]. As demonstrated in renal epithelia, apical fluid flow bends primary cilia and induces an intracellular signaling cascade, including opening of calcium (Ca^{2+}) channels as a shear stress-induced response [185-188]. Prior work done *in vitro* demonstrated that endothelial cells with genes knocked out for the proteins polycystin-1 and polycystin-2, which strongly localize in primary cilia, were unable to generate NO and had lower intracellular Ca^{2+} [189-191].

Caveolae: Caveolae are flask-shaped invaginations (~50-100 nm) in the cell surface that are rich in glycosphingolipids and have recently been implicated in endothelial mechanosensing [192]. They are locally enriched with the membrane protein caveolin-1 (Cav-1), which has been demonstrated to be necessary for vascular stability *in vivo* [193-195]. *Cav-1* knockout mice demonstrated an impaired vasomotor response to ligation of the left external carotid artery; compared to arteries in wild type and caveolin-1 reconstituted mice, decreased blood flow in KO mice did not lead to a decrease in lumen diameter [196]. However, the authors did report an increased vessel wall thickness and cellular proliferation. This, along with dual *endothelial NO synthase (eNOS)* and *Cav-1* knockout studies, suggests that eNOS vasoreacitivity (i.e. flow-mediated dilation) requires Cav-1 localization to sense changes in shear stress [192,197].

Integrins: Integrins significantly contribute to mechanosensing by translating stresses within the intracellular cytoskeleton and ECM to receptor tyrosine kinase (RTK) or ion channels [198-200]. Previous studies have rigorously demonstrated the role of multiple integrins that integrate with both ECM and cytoplasmic kinases [138,201]. Integrins assist in translating various mechanical stimuli into signaling events, including shear stress, ECM stiffness, and compression of the cell membrane [160,162,199,202-212]. In the vasculature, these integrin-mediated responses are not limited to the endothelium, as they also include sensing of shear stress and cyclic stretch by vascular SMCs and fibroblasts in the adventitia of large blood vessels [213-215]. Integrin sensing of mechanical forces primarily occurs through focal adhesion kinase (FAK), although multiple other pathways have been reported, including Rho small GTPase family signaling (RhoA, Cdc42, and Rac), focal adhesion kinase, c-Src PI3K, myosin light chain kinase, Akt kinase, IxB kinases, nd receptor tyrosine kinase Flk-1 [204,216-219].

Glycocalyx: The endothelial glycocalyx is a 500 nm thick, gel-like mesh of membrane-bound glycoproteins and proteoglycans on the apical or luminal surface of the endothelium (Figure 1). It serves as a nest for soluble molecules sourced from both the endothelium and plasma [220,221]. Initial studies observed that the glycocalyx bends in the direction of blood flow, influencing the direction of cytoskeletal remodeling through the direct connection between syndecans and actin filaments [222]. Specifically, the heparin sulfate fraction of the glycocalyx is responsible for short-term responses to change in endothelial shear stress, as its movement will either expose or hide the membrane-bound syndecans [223-225]. Additional *in vivo* studies have further described the role of the apical glycocalyx in regulating endothelial NO production through modulation of heparin sulfate [226,227]. While the exact mechanism is unclear, ongoing fluorescence imaging studies suggest that the movement of the glycocalyx might lead to mechanical disruption of eNOS-loaded caveolae [226,227].

Ion Channels: Flow-activated ion channels mediate fast-acting responses to changes in endothelial shear stress that have been thoroughly reviewed in prior works [228-231]. Briefly, inwardly-rectifying potassium (IRK) channels primarily govern endothelial resting membrane potential [232]. Endothelial Cl^- channels are opened at low levels of shear stress (0.3 dyne/cm^2 – 3.5 dyne/cm^2), remain open during nonreversing pulsatile flow, and directly correlate with Akt phosphorylation. However, oscillatory flow fails to either open Cl^- channels or induce subsequent Akt phosphorylation [233]. Flow-responsive Ca^{2+} channels are also activated through two primary mechanisms. Transient Receptor Potential Cation Channels (TRPV4) open directly in response to shear stress, while P2X4 ATP-operated channels open after shear stress-induced increase in intracellular ATP [234]. Additionally, endothelial cells are mechanosensitive to stretch-activated Ca^{2+} channels, a finding that has also been reported in vascular SMCs [235,236].

Intermediate Filaments: In addition to signaling induced by integrins, G-protein coupled receptors, and ion channels, membrane signal transduction through intermediate filaments modulates intracellular responses to shear stress. Live imaging studies performed on endothelial cells *in vitro* have demonstrated significant remodeling of vimentin intermediate filaments only three minutes after a change in shear stress, suggesting that the dynamics of intermediate filament shear stress sensing are relatively rapid [237,238]. However, greater mechanistic studies analyzing the signaling that causes this change are required.

Actin Cytoskeleton: While the actin cytoskeleton polymerization responds to changes in shear stress within minutes, it has been reported that endothelial cells require 24 hours of exposure to fluid flow to obtain full alignment [239]. Prior work also has demonstrated that after flow stimulation, the initial response to shear stress is cytoskeletal depolymerization in order to permit enhanced cellular remodeling. However, this change in cytoskeletal remodeling is translated into changes in endothelial cell shape to improve barrier integrity, rather than migration [240].

Nucleus: In addition to cytoskeletal remodeling, cell nuclei are purported to participate in mechanosensing and signaling. *In vitro* work has reported elongated nuclei after exposure to physiologic shear stress, most likely due to a change in compression of the nucleus along the direction of flow. Interestingly, this change in nucleus length was preserved after they were isolated from the cells, suggesting an inherent increase in nuclei stiffness and elastic modulus [241]. Additional work *in vitro* suggests that this change in nucleus shape following shear stress allows the cell to determine the direction of flow [242].

Time Scale of Blood Flow-Induced Shear Stress Responses

Given the varied molecular mediators described above that are capable of sensing alterations in shear stress, it is not surprising that there exists a range of timescales during which sensing and transduction by each of these types of mediators occurs. Many signaling pathways are activated in seconds in response to blood flow-induced shear stress. For example, changes in ion signaling through Cl^- and potassium (K^+) channels are widely observed [243-245]. Phosphorylation events, such as phosphorylation of PECAM-1, are also seen as early as 30 seconds, as well as release of NO from endothelial cells [246,247]. On the time scale of minutes, in response to activation of eNOS, endothelial VEGFR2 phosphorylation is upregulated [248]. Additionally, the Src protein family kinases (SFKs) are activated within 1-10 minutes of shear stress exposure [249]. Many endothelial intracellular signaling pathways are also upregulated on the order of minutes, including MAP Kinases, Rho/Rac GTPases, nuclear factor-κB (NF-κB) and c-Jun N-terminal kinase (JNK) phosphorylation [250-255]. Integrins, cytoskeletal remodeling, and focal adhesion remodeling are also activated in this timeframe [256-258]. On the scale of hours to days, much more comprehensive changes in intracellular signaling and cellular structures have been measured. For example, *in vitro* studies found that the Tie2-Angiopoietin signaling complex, which is required for the maturation of endothelial progenitor cells, has a ~48 hour delay when responding to changes in shear stress [259]. Tie2 is a receptor tyrosine kinase whose phosphorylation during quiescence is induced by pericyte-derived angiopoietin-1[260]; this interaction is destabilized in response to stimuli, including hypoxia and inflammation, by the endothelial-dervied competitive antagonist, angiopoietin-2[261].

Endothelial Heterogeneity in Blood Flow-Induced Shear Stress Responses

Spatial and temporal endothelial cell heterogeneities have long been observed in vascular biology. Given the vast number of chemical and mechanical cues happening in the microenvironment of each cell, this heterogeneity might be a reason for the difficulty in designing therapies that target the vascular endothelium [262]. In light of these difficulties, perhaps it is not surprising that even well-established vascular endothelial markers, such as Tie2 and PECAM-1, demonstrate great heterogeneity in the face of mechanotransduction [159,259,263].

Given the vast heterogeneity in the magnitude of fluid-induced shear stress throughout the circulatory tree (from 70 dyn/cm^2 in arteries to 1 dyn/cm2 in venules), it is important to consider how these mechanical signals promote and sustain endothelial cell heterogeneities across the variety of vessel sizes in the systemic circulation. Indeed, expression of VEGFR1, VEGFR2, VE-Cadherin, Tie2, vascular cell adhesion molecule 1 (VCAM-1), Integrin α_v/β_3, and E-Selectin increase in a dose-dependent manner when HUVECs are exposed to increasing shear stress *in vitro* [259] (Figure 1). Additional work demonstrated the inverse relationship by placing endothelial cells in static conditions after being exposed to flow [264]. Moreover, increased PECAM-1 signaling under shear stress has been linked to downstream increased ERK signaling, β1 integrin activation, eNOS activation, VE-Cadherin and VEGFR2 phosphorylation [159,265-267]. These examples highlight the fact that the proteins that have long been used to study the endothelium are tightly and transiently regulated by fluid-induced shear stress.

One significant limitation in the field, however, is that the majority of studies that have examined how temporal changes in flow-induced shear stress affect vascular genotype and phenotype have been performed *in vitro*. To date, few if any studies have been able to measure subtle changes in

blood flow-induced shear stress in small vessels; fewer still have paired these measurements with biochemical read-outs of gene expression, such as those gathered via gene-driven green fluorescent protein (GFP) expression in individual cells. In order to address this limitation in the field, current studies exist to probe vessel hemodynamics and Tie2-driven GFP-expression in the same vessel segments dynamically over time. By coupling photoacoustic microscopy with intravital confocal microscopy to image the same vessel segments across angiogenic microvascular beds in the murine cornea, some of us have reported spatial and temporal data on endothelial Tie2 expression in capillary segments, as well as shear stress measurements at multiple time points during both angiogenesis and microvascular network hemodynamic remodeling.

Mechanical forces at venous valves

Due to their pivotal role in mediating peripheral vascular resistance, the arterioles have received the most attention for their ability to sense and respond to mechanical cues. However, the venous endothelium also experiences dynamic mechanical cues that affect their function. While the blood velocity in large, central veins (e.g., jugular vein) is thought to be sufficient to provide unidirectional flow, small veins that act against gravity (e.g., saphenous vein and its tributaries in the calf), require valves and skeletal muscle pumping to prevent blood stasis or turbulent flow [268,269] (Figure 2.1). Interestingly, recent reports have also observed venous valves in central veins, including the jugular vein and jugular lymph sac during development, implying their role in the regulating venous fluid mechanics may be more extensive than originally thought[270,271]. The anatomical and geometric complexities of venous valves, in particular, create spatially heterogeneous levels of mechanical shear stress, to which the venous endothelium has been shown to be highly sensitive.

Venous valves begin developing as ridges on endothelial cells; these ridges protrude from the endothelium and extend as long, thin flaps, termed 'cusps' (Figure 2.1). These cusps consist of two layers of endothelial cells that surround a core rich with laminin-α5 and fibronectin [269,272]. Venous valves are typically bicuspid, though unicuspid and tricuspid veins are also rarely observed. These valves ensure directional flow through a four-step valve-cycle [273]. The cycle begins with an opening phase, during which the two previously-closed valve cusps separate to permit blood flow. Once they open, they reach the second phase: the equilibrium phase. During the equilibrium phase, blood flows through the opening created by cusps of the valve. Then, while the primary stream of blood flow continues along the vessel, smaller streams of the blood flow circulate along and around the valve cusps, into pockets created between the cusps and the vessel wall. This creates a vortex between the vessel wall and the cusp that acts as a pressure to begin the third closing phase, during which the valve cusps close. Finally, the valve reaches the fourth phase, the closed phase, where there is no observed flow through the vein.

The endothelium in veins and venules is hypothesized to possess many of the same mechanosensitive signaling mechanisms that are present in arteriolar endothelial cells, including ion channels, GPCRs, the glyocalyx, and integrins [274]. Additionally, multiple integrins known to participate in mechanical force-sensing in arterioles, such as α_2, α_5, β_1, and $\alpha_5\beta_3$, have also been identified in saphenous vein SMCs [275]. These (and other) biochemical signaling molecules that are known to be involved in mechanotransduction will be described in more detail in the subsequent sections. Finally, longitudinal stretch, or mechanical stretch along the length of vessel wall in the direction of blood flow, is another type of mechanical stimuli in large veins, (e.g., human saphenous vein) that triggers matrix metalloproteinase (MMP)-driven vessel wall thickening via integrin α_v [276].

Blood vascular development, cardiac development, and role of mechanotransduction

The development of the vascular circulation has been described in depth by multiple reviews [12,13,17,277]. In brief, vasculogenesis begins by the creation of a primary plexus of precursors to endothelial cells in the yolk sac as well as formation of two dorsal aortae in the embryo [14,278]. After the formation of the primary plexus or dorsal aortae, mechanisms of angiogenesis (including endothelial sprouting, intussusception, regression, and fusion, as well as mural cell recruitment) remodel the network to obtain the endothelial and blood vessel heterogeneity that characterizes the hierarchical circulatory network.

Recent, sophisticated experimental methods have permitted time-lapse movies of mammalian blood vessel development to further probe the relationship between vascular morphogenesis and endothelial VEGFR1 signaling [109]. Live imaging has also been leveraged to demonstrate the sensitivity of endothelial cells to changes in blood flow during vascular remodeling [279]. These, as well as other studies, have shown that blood flow regulates endothelial cell migration, vessel segment fusion, and branch formation [280].

Notably, changes in shear stress appear to be relatively unimportant in driving the initial stages of angiogenesis. Studies in zebrafish have successfully monitored morphologically normal vessel formation in the absence of a heart beat and blood flow until 14 days post-fertilization [281]. Thus, while tissues still require oxygen to be viable, the initial stages of angiogenesis do not necessitate blood flow-induced shear stress [281]. However, in mammalian development, tissues require blood flow during plexus remodeling at a much earlier time point in order to prevent hypoxia [282]. Additionally, multiple genes in both zebrafish and mammalian vascular development require shear stress, including *activin receptor-like kinase 1(alk1)* and *endoglin 1 (edn1)*, which are predicted to

limit arterial diameter at the onset of flow during development [283-287]. Interestingly, while arteriogenesis does not traditionally occur during embryonic development, vascular endothelium in the developing embryo is capable of undergoing NO-mediated vessel dilation, endothelial activation, and increased proliferation due to either changes in embryonic hemodynamic forces or *alk1* expression in zebrafish [288-290]. Finally, valvulogenesis is yet another process in the vascular tree that is hemodynamically-dependent, as demonstrated by studies on flow-through-induced expression of *miR-21* [291].

Perhaps the most well-described transcription factor in fluid shear stress activation is Krüppel-like Factor (Klf) 2, an essential regulator of cardiovascular responses to fluid shear stress [292-298]. Other detailed studies showed that endothelial expression of *Klf2* mirrors the rise and fall of fluid shear stress during murine development [297]. Embryonically lethal, *Klf2* knockout mice die without any structural vascular defects, despite experiencing cardiac defects indicative of heart failure caused by increased cardiac output in response to decreased vessel tone. Moreover, heart failure was rescued by phenylephrine, which targets the α1 adrenergic receptor on vascular SMCs and increased vessel tone without improving myocardial performance [299].

The development of both the heart's endocardium and vascular endothelium are reliant on many overlapping biomolecular responses to similar mechanical stimuli. Much like the vasculature, endocardial development occurs in response to mechanical cues sensed by primary cilia [300,301]. Also, *Klf2* signaling is reported to be important in cardiac valve development [296,302]. During cardiac development, retrograde blood flow is reported to act through *Klf2a* in order to ensure normal valvulogenesis in the developing heart [303]. As reviewed previously, cardiac development also involves numerous wall shear stress-mediated steps, including cardiac 'looping,' chamber

ballooning, trabeculation, valve formation, and conduction through hemodynamically-driven differentiation of cardiomyocytes [295,304-306].

Mechanotransduction in blood vessels during atherosclerosis

The leading cause of death worldwide is atherosclerotic cardiovascular disease [307]. Therefore, there exists a critical need to better understand the underlying molecular mechanisms behind inflammatory endothelial activation, ischemia, and systemic atherosclerosis.

Mechanistic studies of atherosclerosis have long focused on the role of mechanotransduction during the onset of disease. For nearly fifty years, atherosclerotic plaques have been reported to develop at points of low or disturbed wall shear stress [308,309] (Figure 2.3). Later studies reported that lesions under low shear stress were larger, contained fewer SMCs and lipid deposits, and showed more regions of outward vascular remodeling [310]. Additionally, lesions in regions of lower shear stress exhibited increased inflammatory mediators (VCAM-1, intercellular adhesion molecule 1 (ICAM-1), C-reactive protein, IL-6, and VEGF), angiotensin-II-induced hemorrhaging, and MMP activity [310] (Figure 3). Studies employing a partial carotid ligation to disturb blood flow *in vivo* replicated these results, while also showing a decrease in the expression of *Klf2* and eNOS, which are reported to be anti-atherogenic [311-313]. Recent studies have also reported that endothelial gene expression, including *Klf3*, is regulated by flow-dependent DNA methylation in atherosclerosis [314]. More recently, mechanistic studies have begun to focus on the integrin-YAP/TAZ cascade as a mediator of endothelial responses to changes in blood flow-induced shear stress [315,316]. Specifically, normal physiologic, unidirectional shear stress might activate integrin to suppress YAP and down-regulate pro-inflammatory gene expression, as well as monocyte attachment and infiltration.

Consistent with these results, YAP/TAZ overexpression increases plaque formation, while its inhibition decreases formation, in ApoE knockout mice [315,316].

As plaque rupture is the leading cause of myocardial infarction and stroke, many studies have also examined the role of ECM remodeling in atherosclerosis [317,318]. For example, several studies showed that a reduction in arterial fibronectin causes a decrease in atherosclerotic plaque size and fibrous cap formation [319,320]. As a potentially mechanism, PECAM-1 was recently purported to induce fibronectin assembly via β1 integrin and RhoA activation in response to disturbed shear stress [321]. Additionally, studies focused on SMC collagen deposition in response to stretch magnitude, frequency, and duration [322-325]. Multiple studies have shown that cyclic stretch of vascular SMCs in culture causes a strain-dependent increase in collagen I, collagen III, and elastin, as well as an increase in angiotensin II and transforming growth factor-β (TGF-β) signaling [326-328]. Thus, increased strain during cyclic stretch increases ECM stiffness and expression of inflammatory signaling molecules involved in atherogenesis as well as atherosclerotic plaque composition and stability.

Blood flow at branching points and regions of high curvature

- Reduced blood flow velocity
- Decrease in shear stress as well as circumferential stretch
- Reciprocating flow
- Changes in VEC alignment and shape (endothelial activation)
- Recruitment of leukocytes

Molecular response:

- ↑ C-reactive protein
- ↑ ICAM-1
- ↑ IL-6
- ↑ VCAM-1
- ↑ Angiotensin II
- ↑ MMP activity
- ↓ Klf2
- ↓ eNOS

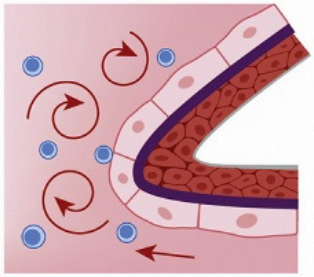

Arterial tree

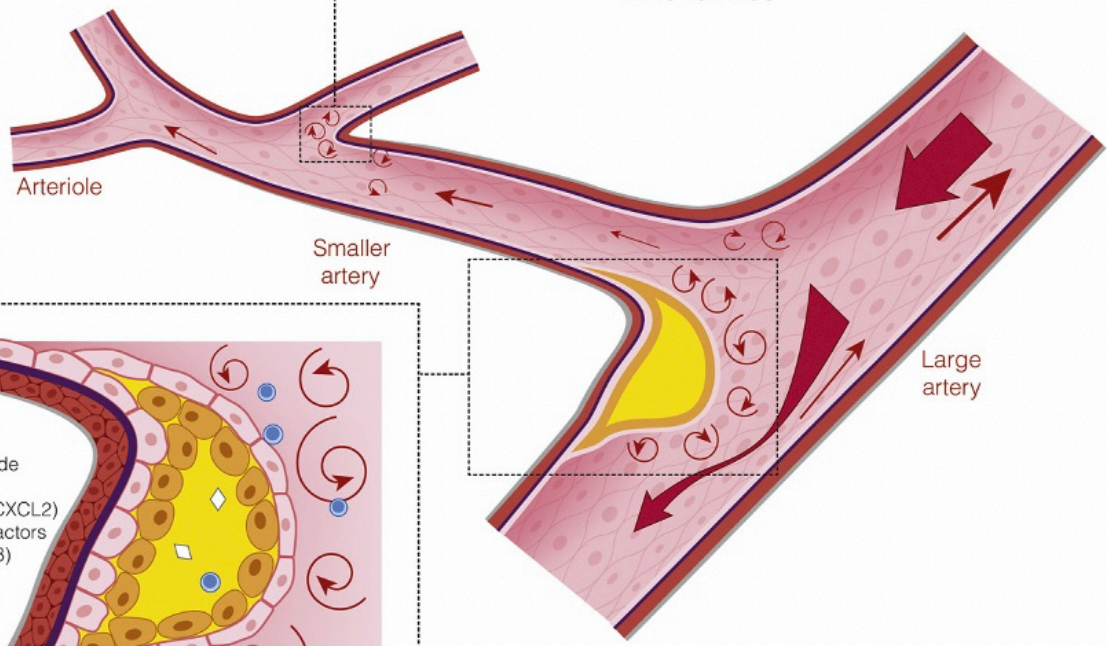

Plaque formation

- Blood flow turbulence/ disturbed blood flow
- Accumulation of lipids, foam cells, leukocytes, cholesterol crystals
- Smooth muscle cell migration
- Calcification
- Development of necrotic core

Molecular response:

- ↑ NADPH oxidase and ROS
- ↑ Macrophage response (superoxide and hydrogen peroxide)
- ↑ oxLDL deposition (MCP-1, IL-8, CXCL2)
- ↑ Inflammatory cytokines, growth factors (IFN-γ, IL-1α, IL-1β, TNF-α, TGF-β)
- ↑ Fibrinogen
- ↑ Fibronectin
- ↓ NO

Figure 2.3 Role of mechanical forces during atherosclerosis progression.

In contrast to the unidirectional blood flow and laminar shear stress found at linear parts of the arterial tree, branching points and regions of high curvature are characterized by reciprocating blood flow, reduced blood flow velocity, and decreased shear stress, as well as decreased circumferential stretch. This goes along with changes in vascular endothelial cell alignment and shape as well as leukocyte recruitment. The molecular response in regions with reciprocating blood flow differs from regions with laminar flow. On the long term, disturbed flow patterns can contribute to plaque formation. Plaques are surrounded by turbulent blood flow and characterized by smooth muscle cell migration, accumulation of lipids, foam cells, leukocytes, and cholesterol crystals. Eventually, calcification and development of a necrotic core follow. On the molecular level, changes like increased production of inflammatory cytokines can be observed.

Conclusion

Irrespective of the type and location of the vessels, mechanical cues constantly affect the blood and lymphatic vasculature. Endothelial and mural cells of any given tissue are uniquely affected by fluid flow, hydrostatic pressure, and longitudinal and circumferential stretch. These mechanical stimuli differ depending on the stage of development, disease, and diurnal and hormonal cycles as well as physical activities. Consequently, as presented in this review, a vast number of heterogeneous components of mechanotransduction have been identified in both the blood and lymphatic vasculatures. These signaling domains are extracellular or transmembrane (i.e., glycocalyx, integrins, ion channels or primary cilia) and intracellular (i.e., cytoskeletal remodeling, nuclear stiffness), and induce a variety of biochemical responses in the cell, such as transcription factor expression, kinase activation or NO production).

In addition to the many ways the vasculature detects qualitative and quantitative changes in mechanical stimuli, both blood and lymphatic vessels have an armamentarium of mechanisms ready to react to these stimuli. Vascular growth and expansion, vessel wall thickening, valve formation, plaque formation, vessel pruning, and angiogenesis are only a few of the mechanisms by which vessels react. Continuous cycle of mechanical stimulation and biochemical signaling on the one hand, and vascular adaptation on the other hand, add to the incredible complexity of this system. Better understanding the mechanotransduction pathways operating in the cells of the vasculature in health and disease will likely assist in developing effective therapies to treat many different human diseases, including lymphedema, atherosclerosis, and myocardial infarction.

CHAPTER 3

DYNAMIC, HETEROGENEOUS ENDOTHELIAL TIE2 EXPRESSION AND CAPILLARY BLOOD FLOW DURING MICROVASCULAR REMODELING

ACKNOWLEDGEMENTS: Bo Ning PhD[1], Anthony C. Bruce[1], Daniel N. Tavakol[1], David Yi[2], Song Hu PhD[1], Paul A. Yates MD PhD[2], and Shayn M. Peirce PhD[1,2].

[1]Department of Biomedical Engineering, University of Virginia, Charlottesville, VA, USA
[2]Department of Ophthalmology, University of Virginia, Charlottesville, VA, USA

The text included in this chapter has been published:
Kelly-Goss M, Ning B, Bruce A, Tavakol D, Yates P, Hu S, Peirce S. Dynamic, heterogeneous endothelial Tie2 expression and capillary blood flow during microvascular remodeling. Scientific Reports, 2017.

Abstract

Microvascular endothelial cell heterogeneity and its relationship to hemodynamics remains poorly understood due to a lack of sufficient methods to examine these parameters *in vivo* at high resolution throughout an angiogenic network. The availability of surrogate markers for functional vascular proteins, such as green fluorescent protein, enables expression in individual cells to be followed over time using confocal microscopy, while photoacoustic microscopy enables dynamic measurement of blood flow across the network with capillary-level resolution. We combined these two non-invasive imaging modalities in order to spatially and temporally analyze biochemical and biomechanical drivers of angiogenesis in murine corneal neovessels. By stimulating corneal angiogenesis with an alkali burn in Tie2-GFP fluorescent-reporter mice, we evaluated how onset of blood flow and surgically-altered blood flow affects Tie2-GFP expression. Our study establishes a novel platform for analyzing heterogeneous blood flow and fluorescent reporter protein expression across a dynamic microvascular network in an adult mammal.

Introduction

Angiogenesis involves network level coordination of individual cellular behaviors accomplished through alterations in biochemical and biomechanical signals in the local environment[12,109,329]. These signaling mechanisms are driven by the initial onset of, and subsequent changes in, blood flow and oxygenation throughout the angiogenic vascular network[277]. At any point in time, the combination of biomechanical and biochemical signals varies across the vasculature, and may potentially give rise to endothelial heterogeneities[23,262,330]. While these combined inputs have been evaluated in both cultured endothelial cells and in large vessels, they have not yet been studied in the context of cell heterogeneity in small blood vessels. We developed a novel *in vivo* platform to quantify changes in blood flow across individual capillaries throughout a microvascular network and in the same microvessels where changes in endothelial gene expression were also recorded non-invasively over time. Our platform makes use of photoacoustic microscopy (PAM) and intravital confocal microscopy (ICM) to image the well-established murine cornea angiogenesis assay[121], wherein networks of neovessels can be dynamically observed.

Using this platform, we found that endothelial Tie2 expression is heterogeneous across the newly-established microvascular network of the cornea. Tie2 is a receptor tyrosine kinase whose phosphorylation is induced by angiopoietin-1, which activates the Ras/MAP kinase pathway and has been shown to affect endothelial cell adhesion, differentiation, and/or survival, as well as pericyte-endothelial interactions and neovessel maturation[331-335]. There is a substantial body of literature that describes hemodynamic control over endothelial cell protein expression in large vessel endothleium[257,298,336-340], and compelling data from *in vitro* studies on cultured endothelial cells has suggested that shear stress is a regulator of Tie2 signaling and vascular quiescence[259,263]. However, this relationship has never before been corroborated by *in vivo* studies, despite the

ongoing clinical evaluation of a drug, VE-PTP, intended to constitutively block this pathway's inhibitor. Additionally, multiple groups have leveraged complicated computational modeling techniques to investigate endothelial heterogeneity, without the detailed spatial and temporal data on Tie2 gene modulation in tandem with hemodynamic readouts[19,32,33,257,341-343]. Given that blood flow is dynamic and highly variable from vessel to vessel[28], we hypothesized that heterogeneity in endothelial cell Tie2-driven green fluorescent protein (GFP) expression during growth and remodeling of the microvascular network may, in part, result from changes in blood flow-induced wall shear stress (WSS) during angiogenesis[344-346].

To test this hypothesis, we employed ICM to visualize GFP expression in adult transgenic Tie2-GFP fluorescent reporter mice and PAM to quantify blood flow and WSS in the angiogenic network over time, as well as before and after surgically redistributing blood flow in the network. Our experimental platform enables the first *in vivo* investigation into correlated heterogeneities in endothelial protein expression and microvessel hemodynamics throughout a microvascular network. As we executed our study in the murine cornea, Table 3.1 conveys the advantages of our platform over other experimental approaches and demonstrates how broadly generalizable our method is to other model systems of angiogenesis, such as tumor vascularization and hydrogel scaffold compatibility assays[121,347-357]. Further, our platform has broader applicability to elucidate the pathogenesis of microvascular disease, such as that associated with diabetes and obesity, where the interplay between hemodynamics and gene expression heterogeneities during pathologic vascular processes may also underlie the success or failure of potential therapeutic treatments.

Experimental Model	Investigation focus	Intravital imaging modality*	Vascular network architectur	Single-cell resolution	Protein expressio n	Serial imagin g	Blood velocit y	sO_2	Depth of vascular bed	Citation
Micropocket (tumor)	Tumor vascularization	Bright field microscopy	✓			✓				351, 352
Micropocket (growth factor)	Evaluation of angiogenic growth factors in mice	Slit lamp microscopy	✓			✓				353
Micropocket (pancreatic islet)	Pancreatic islet vascularization; β-cell function and rate of death	Confocal microscopy	✓	✓	✓					354
Micropocket (ASCs)	ASCs in HLA scaffolds; corneal regeneration	Bright field microscopy			✓					355
Micropocket (hydrogel scaffold)	Live imaging of biomaterial compatibility	Confocal microscopy	✓	✓		✓	✓			356
Topical (anti-VEGF)	Anti-angiogenic therapy (human)	Bright field microscopy	✓			✓				357
Suture	Lymph-angiogenesis	Confocal microscopy	✓	✓	✓	✓				333
Chemical burn	Detect vessels in cornea with PAM	Photoacoustic microscopy	✓						✓	358
Chemical burn	EC Tie2 expression	Photoacoustic and confocal microscopy	✓	✓	✓	✓	✓	✓	✓	Present study

Table 3.1 In vivo models of cornea angiogenesis. (*Used at the highest resolution)

Methods

Experimental Animals

All surgical procedures were approved by the Institutional Animal Care and Use Committee at the University of Virginia. We used transgenic Tie2-GFP mice from The Jackson Laboratory (Stock Tg(TIE2GFP)287Sato/J, Stock Number 003658, Bar Harbor, ME). The number of mice per figure is reported in each figure caption. All mice were 8-24 weeks of age at time of manipulation, with treatment and control groups age-matched within each experiment.

Cornea Alkali Burn

The corneal alkali burn model was adapted from Suvarnamani C et al[358]. Briefly, animals were anesthetized with an intraperitoneal injection of ketamine/xylazine/atropine (60/4/0.2 mg/kg body weight). A drop of sterile 0.5% Proparacaine Hydrochloride Ophthalmic Solution (Henry Schein Inc; Melville, NY) was added as a topical anesthetic to numb the eye before treatment. The right eye was chemically cauterized by pressing applicator sticks coated with 75% $AgNO_3$/25% KNO_3 to the cornea (SnyptStix by Grafco; Atlanta, GA) for five seconds while the animals were anesthetized. Excess silver nitrate was removed by rinsing corneas with 0.9% NaCl saline solution (Healthmark Services, Montreal, Quebec, Canada). An additional drop of Proparacaine was applied to each cornea post-treatment as a topical anesthesia. All treatments were conducted while the mouse was on a heat source to maintain constant body temperature. At the terminal end point, mice were humanely euthanized by carbon dioxide asphyxiation.

Blood Flow Intervention

Blood flow was dynamically altered throughout the corneal neovascular networks by cauterizing of a primary feeder arteriole, thus preventing flow through this vessel. Cauterization was accomplished using a Bovie Fine Tip Cautery knife (Aaron Medical, Clearwater, FL), with one or more of the multiple small, feeder arterioles being sealed with diathermy.

Intravital Cornea Imaging

Intravital corneal microscopy was accomplished through modification of the technique described by Di Girolamo et al[359]. Briefly, animals were anesthetized with an intraperitoneal injection of ketamine/xylazine/atropine (60/4/0.2 mg/kg body weight)(Zoetis; Kalamazoo, MI / West-Ward; Eatontown, NJ / Lloyd Laboratories; Shenandoah, IA). A drop of sterile 0.5% Proparacaine Hydrochloride Ophthalmic Solution was added as a topical anesthetic to numb the eye before imaging. To allow visualization of vascular endothelium, anesthetized mice were administered a retro-orbital injection of labeled isolectin[73] (IB4-Alexa647; Life Technologies, Carlsbad, CA) 10 minutes before imaging began. Digital images of the corneal neovasculature were acquired using confocal microscopy (Nikon Instruments Incorporated, Melville, NY; Model TE200-E2; 10X, 20X,and 60X objectives). Three to four fields of view per cornea were imaged at each time point, and full-thickness Z-stack (2-5 μm step cells) volume renders were used to capture the entire thickness of the corneal neovascular network in each field of view. Genteal gel was applied to the eye during imaging to prevent drying. Mice were placed on a microscope stage that contained a warming pad to maintain a constant body temperature of 37°C, eyelashes and whiskers were gently pushed back with ophthalmic lubricant Genteal gel (Alcon; Forth Worth, TX), and the snout was

gently restrained with a nosecone. During imaging, the eye was placed against a coverslip that rested on the stage of the inverted confocal microscope.

Corneas were imaged prior to the burn injury, 2 days after the burn injury, and 7 days after the burn injury. In the subset of mice that received a subsequent cautery-induced blood flow redistribution, fine needle tip diathermy was performed 7 days after initial burn injury and corneas were imaged 48 hours and also 4 days following cauterization. Validation of GFP signal and separation from background autofluorescence was determined by imaging both uninjured contralateral cornea, as well as imaging of corneal burns performed in C57Bl6 WT non-GFP expressing mice (not shown).

Bright Field Imaging

Bright field images of corneas under 4X magnification were obtained using a Nikon Digital Sight DS-L2 Camera Controller (Nikon Instruments Inc, Melville, NY; Model 214602) to assess the network-wide hierarchy of neovessels and determine the presence or absence of blood flow in individual vessel segments. For each mouse, multiple fields of view were taken encompassing the entire circumference of the eye.

Photoacoustic Microscopy

Optical-resolution, multi-parametric photoacoustic microscopic (PAM) images of the angiogenic corneal networks were acquired as thoroughly described in our previous literature[360,361]. This technique enabled simultaneous quantification of microvascular diameter, oxygen saturation of hemoglobin (sO_2), and blood flow within individual vessel segments[74]. In particular, a temporal decorrelation approach has been developed and optimized for quantifying blood flow by both our

group and others[360,362]. Prior work establishing PAM has demonstrated that we can correctly measures blood flow speeds within the range of 0.18–21 mm/s[360], which well covers the reported murine physiologic capillary flow velocity of 0.75–6.75 mm/s[363].

Consistent with prior work, in this study we acquired images using two laser wavelengths, 532 nm and 559 nm. The applied laser pulse energies at the corneal surface were 50 nJ and 30 nJ at 532 nm and 559 nm, respectively. The laser beams were through a doublet onto the cornea with a beam diameter of 2.7 μm. Two-dimensional raster scans were performed over the regions of interest; scans of the entire cornea took approximately 30 minutes. It is worth noting that the temporal decorrelation method is primarily sensitive to the blood flow in capillaries that are perpendicular to the optical axis (i.e. transverse blood flow). Fortunately, the corneal vascular network is a very planar structure that has few penetrating capillaries. Therefore, the approximate angle between the measured capillaries and the optical axis of the PAM system was 90 degrees. To ensure the correct orientation of the vessel bed, the network was carefully pre-imaged and aligned to be perpendicular to the optical axis before we conducted obtained measurements for quantification. Throughout the experiment, the mouse was maintained under anesthesia with 2.0% vaporized isoflurane and the body temperature was kept at 37 °C.

After obtaining the measurements using a single scan, our system could provide the same spatial resolution for all the measurements, which is ~2.7 μm, as tested in our previous study outlining the PAM system[360]. After we acquired the measured value in each pixels, a 10 μm × 10 μm averaging window, which is close to the average diameter of the capillaries, was used to suppress the fluctuation in the measurements. No additional image processing or repeated measurements were utilized.

For corneas undergoing burn injury, PAM and ICM was performed 2 days, and 5-7 days after burn injury. For corneas that underwent burn injury and subsequent vessel cauterization, PAM and ICM were performed prior to the cautery-induced blood flow redistribution, one hour after intervention, and 48 hours after intervention.

RT-PCR

In order to determine if regulation of Tie2 is observed at the gene level, we enucleated the eyes to harvest the cornea for RT-PCR analysis (n = 5 mice). We harvested corneas for analysis prior to cautery-induced blood flow redistribution and two days after performing cautery-induced blood flow redistribution. In an attempt to maximize the extent of blood flow redistribution, we cauterized every major arteriole feeding the corneal neovascular network. RNA extraction was conducted with the PureLink RNA Micro Scale Kit, followed by CDNA generation with a SuperScript cDNA Synthesis Kit and RT-PCR using SensiMix II Probe (Bioline; Taunton, MA). PCR was run on a Bio-Rad CFX96 Detection System. We measured Tie2 gene expression [Primer 1 – 5'-GCCTCCTAAGCTAACAATCTCC-3'; Primer 2 – 5'-GATGGCAATCGAATCACTGAAC-3'] normalized to constitutively-expressed Flk1 [Primer 1 – 5'-GGATCTTGAGTTCAGACATGAGG-3'; Primer 2 – 5'-GGAATTGACAAGACAGCGACT-3'] to control to the number of endothelial cells within the tissue and also assess the general health of the network in the event that cauterization induced excessive endothelial cell dysfunction[259]. We also utilized the housekeeping gene, PPIA [Primer 1 – 5'-TTCACCTTCCCAAAGACCAC-3'; Primer 2 – 5'-CAAACACAAACGGTTCCCAG-3'] as control[364] (all primers and probe were purchased from Integrated DNA Technologies, Coralville,

IA) Calculations for comparing the expression levels of two genes from the same cell samples were performed as previously described[365,366].

Quantification of Microvascular Outgrowth, Tie2-GFP Expression, and Shear Stress

ImageJ (NIH, Bethesda, MD) imaging software was used to quantify vessel lengths, vessel segment area, vascular network areas, and mean pixel intensities in both confocal and bright field images. PT Gui (New House Internet Services BV; Rotterdam, The Netherlands) software was used to overlay the ICM image onto PAM image, providing good alignment between Tie2 fluorescence and corresponding flow velocity maps in the same vessel segment through use of manually specified control points. When analyzing vessel segments imaged via ICM and PAM, we analyzed at least two fields of view with at least ten candidate vessels per cornea at 2 days after burn injury, 7 days after burn injury, 2 days after cautery-induced blood flow redistribution, and 7 days after cautery-induced blood flow redistribution.

GFP was imaged using an excitation wavelength of 488 nm, and perfused lectin was imaged using an excitation wavelength of 647 nm. Gain settings on the confocal microscope were held constant throughout the experiment. Vessel segments were outlined using the draw tool in ImageJ, and both the mean and raw GFP fluorescence intensity were measured, as well as the vessel area and vessel length. Background auto fluorescence of the cornea was determined by measuring and averaging fluorescence intensity in three regions absent of vessels. Then, this value was subtracted from the fluorescence intensity density for each vessel segment.

Neocapillary segments chosen for analysis were in focus in both imaging modalities, aligned with the PAM image plane (i.e., ran perpendicular to the optical axis), exhibited blood flow in PAM and lectin perfusion in ICM, and were fully contained in regions of interest for both imaging

modalities. Ten vessel segments per cornea, sampled from different locations throughout the corneal neovascular networks, from 4 different mice were identified in both PAM and ICM images and analyzed using a custom analysis algorithm run within Matlab based on previously established algorithms to calculate WSS[81]. Briefly WSS within each vessel segment was calculated according to the measured diameter and flow from PAM using the general formula $shear\ stress = 8 \cdot \mu \cdot \frac{v}{d}$ (Equation 1), where v indicates the blood velocity, d indicates the vessel diameter, and μ indicates the blood viscosity (assumed to be 10 cP)[367].

Average GFP expression intensity density over the vessel segment versus WSS in the same vessel segment was plotted for each analyzed vessel segment. Plots indicate at which time point the data were collected. In networks where measurements of blood flow were obtained pre- and post intervention, the change in Tie2-GFP expression was plotted against the change in WSS, and the R^2 value was reported.

Statistical Analysis

Correlation between WSS and Tie2 gene expression was calculated by a goodness-of-fit linear regression and reported as the co-efficient of determination (R^2). RT-PCR data was compared using Student's t-test. Significance was asserted at $p < 0.05$, and data are presented as mean +/- standard error.

Results

Imaging of capillary hemodynamics and endothelial cell protein expression

By combining PAM and ICM, we can obtain concurrent information about hemodynamics in capillary segments and protein expression at the cellular level throughout an *in vivo*, mammalian angiogenic network. To demonstrate this, we applied a focal silver nitrate alkali burn to the central cornea to stimulate angiogenesis from the limbal vessels of 8-week-old Tie2-GFP mice (Figure 3.1A). Angiogenesis occurred over seven days, and the new vascular network was imaged using multiple imaging modalities. Standard bright field microscopy (BFM) enabled macroscopic analysis of the developing vascular network. ICM enabled us to visualize GFP expression in endothelial cells (Figure 3.1B). PAM provided structural details of the developing vasculature with higher spatial resolution than BFM, as well as functional details of blood flow including relative hemoglobin concentration (C_{Hb}), oxygen saturation (sO_2), and blood velocity.

Further, PAM enables visualization of individual capillaries throughout both the corneal and iris vasculatures due to its ability to image with high-resolution in the x, y, and z directions (Figure 3.1C). By analyzing individual cross-sectional images (Figure 3.1C, right panel), we separated the iris (green) and corneal (red) vessels to distinguish between the two vascular beds (Figure 1C, left panel). Using an image processing algorithm developed in MATLAB, we pseudo-colored iris vessels in grey and corneal vessels using a colormetric scale to indicate hemodynamic parameters (Figure 3.1D). Specifically, hemoglobin content, oxygen saturation, and blood velocity in individual vessel segments throughout the entire neovascular network were plotted using a colormetric scale (Figure 3.1D). PAM provided numerous advantages over BFM (Figure 3.1D, right panel), including improved contrast, removal of surface reflections, and the ability to delineate corneal neovessels from iris vessels.

Using ICM, we imaged Tie2-GFP fluorescence intensity in the same corneal neovessel segments that were also imaged using PAM (Figure 1E, first and second panels from left). The ICM image was manually overlayed onto the blood flow velocity map provided by PAM by visually aligning vessel segments (Figure 1E, third panel from the left). Additionally, automated projection of PAM onto ICM images using PT Gui software (see Methods) was achieved by generating overlapping alignment pair control points in the two images at locations where vessels branched, in a manner that permitted adjustment of the orientation (roll, pitch, and yaw) and the field of view in the two imaging modalities (Figure 3.1E, right-most panel). Individual neovessel segments were manually selected in the PAM image (Figure 3.1F), and the fluorescence intensity of Tie2-GFP (indicative of endothelial cell Tie2 expression levels[41]) within those neovessel segments was then quantified. Blood flow velocity in the selected neovessel segments, as measured with PAM, was converted to blood flow-induced WSS according to Eq. 1 (Methods). Plotting Tie2-GFP fluorescence intensity versus blood flow-induced WSS for individual corneal neo-vessel segments revealed a direct linear correlation between Tie2-GFP and WSS (Figure 1G, $R^2 = 0.73$, n = 15 individual neovessel segments from 4 mice). In order to consider the variance across segments, we calculated the ratio of Tie2-GFP expression to WSS at each data point to determine that the overall variance in this ratio was 8.5% across the network (Tie2-GFP/WSS = 336.9 ± 28.78 a.u., mean ± standard error).

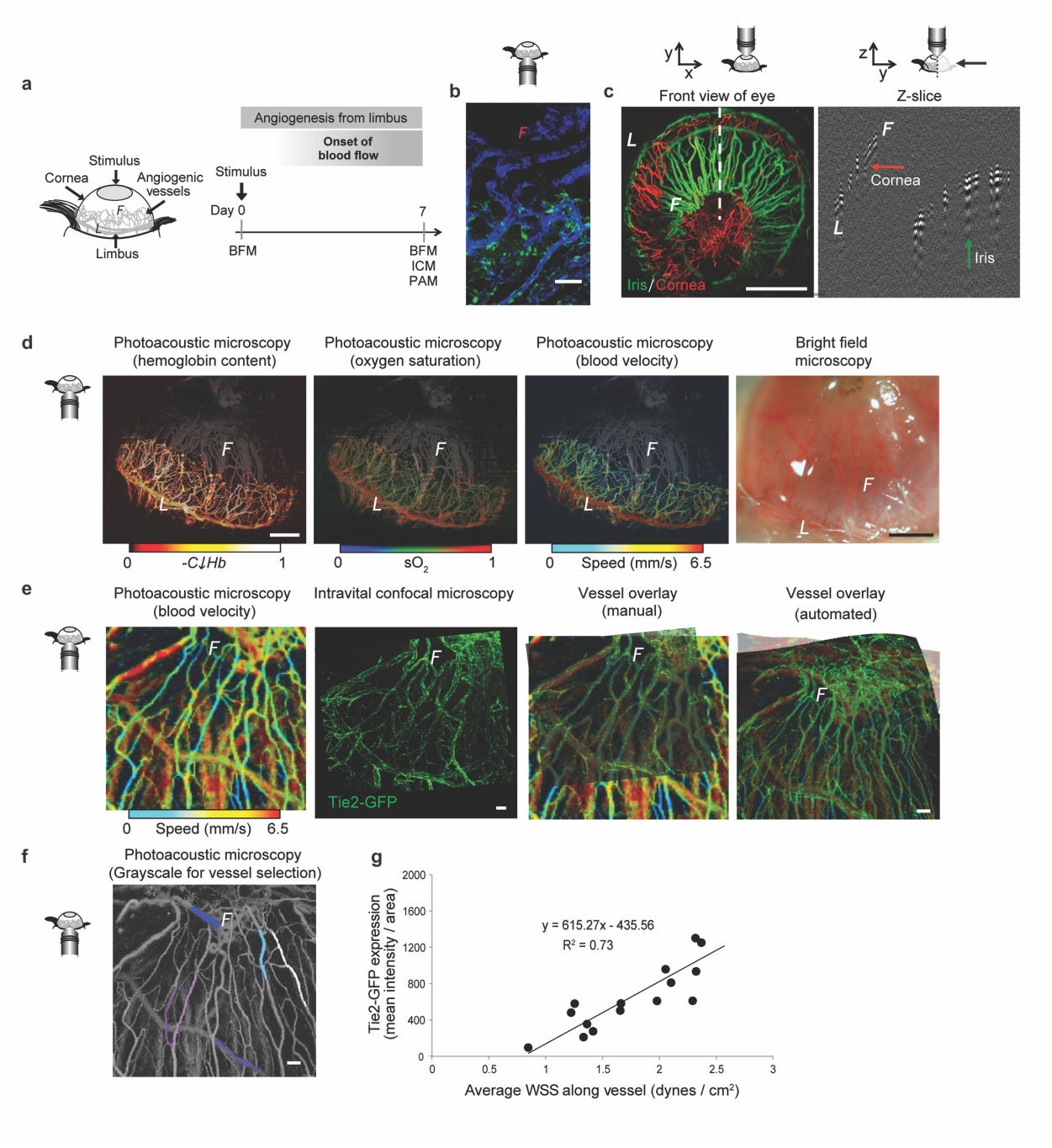

Figure 3.1 Functional imaging of vascular and cellular activity.

(A) Schematic of corneal angiogenesis assay in which blood vessels grow from the limbus ("*L*") into the avascular cornea, creating an angiogenic front ("*F*") as they develop toward an angiogenic stimulus (gray oval). **(B)** Fluorescence intensity of Tie2-GFP (green) along vessels (perfused with

IB4-lectin-647, blue) throughout the network (day 7 shown). **(C)** PAM distinguishes between the iris (green) and corneal (red) vasculatures, due to their different depths. Green arrow points toward iris vessels; red arrow toward corneal neovessels in the Z-slice. **(D)** Unlike BFM, PAM permits functional imaging of relative hemoglobin content ("C_{Hb}"), sO_2 saturation, and blood velocity in the angiogenic corneal network (day 7 shown). The iris vasculature, pseudo-colored in gray based on vessel depth, is visible in the background of each image. **(E)** Overlayed images of the same field of view acquired at day 7 using PAM (blood flow velocity) and ICM (GFP fluorescence intensity), done both manually and with automated software (PT Gui) enables correlation between blood flow-induced wall shear stress (WSS) and GFP fluorescence intensity. **(F)** Grayscale image of same PAM field of view as shown in "d" to facilitate vessel identification. Pseudo-coloring of vessels (white, dark blue, light blue, pink, purple, fuchsia) to exemplify those that were quantified for evaluation in the study. **(G)** Tie2-GFP fluorescence intensity in individual vessels versus average WSS in those vessels calculated using blood velocity maps obtained with PAM, such as those shown in "d". $R^2 = 0.73$ for comparison of 18 vessel segments from four mice. Small schematics next to each microscopy image indicate the direction of the objective relative to the cornea during imaging. Scale bars indicate (c, d) 1 mm, (b, e, f) 50 μm.

Imaging of capillary hemodynamics and endothelial cell protein expression after surgical redistribution of blood flow

Previous studies of corneal angiogenesis, using a variety of techniques to induce neovessel growth, have measured either protein expression or capillary hemodynamics (Table 3.1). However, no study to date has measured changes in capillary hemodynamics alongside changes in protein expression at the level of a single vessel segment or over time. To fill this void, we modified an established vessel ligation technique[353,356] to alter blood flow in limbal vessels, and we applied this technique to the corneal neovasculature to demonstrate the ability to measure changes in capillary hemodynamics and endothelial cell protein expression in individual neovessel segments across sequential time points (Figure 3.2A).

By applying a surgical cautery knife to one of the arterioles feeding into the corneal network, we were able to surgically induce a redistribution of blood flow throughout the neovessel network (Figure 3.2a, light blue 'x'). Blood flow redistribution was evidenced by the change in hemoglobin content in the neovessels (Figure 3.2B, vessels with higher hemoglobin content ("-$C{\downarrow}Hb$") are depicted by lighter colors, according to the scale beneath each image). For example, one hour after intervention, corneal capillaries at the angiogenic front (below the "F") demonstrated an increase in oxygenated hemoglobin, consistent with redistribution of blood flow through collateral arterioles in the network.

Over the first four days following cauterization, changes in blood flow occurred throughout the neovessel network (Figure 2C). For example, in the vessel indicated in the inset (Figure 2C, white arrow), the flow speed was diminished 48 hours after cauterization but returned to pre-intervention levels by 96 hours after cauterization. Over this time course, endothelial cell Tie2-GFP fluorescence intensity increased in some vessel segments (Figure 3.2D, white arrow and vessel

outlined in white in zoomed image below) following blood flow redistribution but decreased in other segments (Figure 3.2D, orange arrow and vessel outlined in orange in zoomed image below). A comparison of Tie2-GFP fluorescence intensity with WSS in individual neovessel segments (acquired by ICM and PAM, respectively), both prior to the surgically-induced blood flow redistribution ("Pre-intervention", circles) and four days later ("Post-intervention", squares) revealed a significant linear correlation between Tie2-GFP fluorescence intensity and WSS (R^2 = 0.74), as confirmed by a parallel lines statistical test (Figure 3.2E).

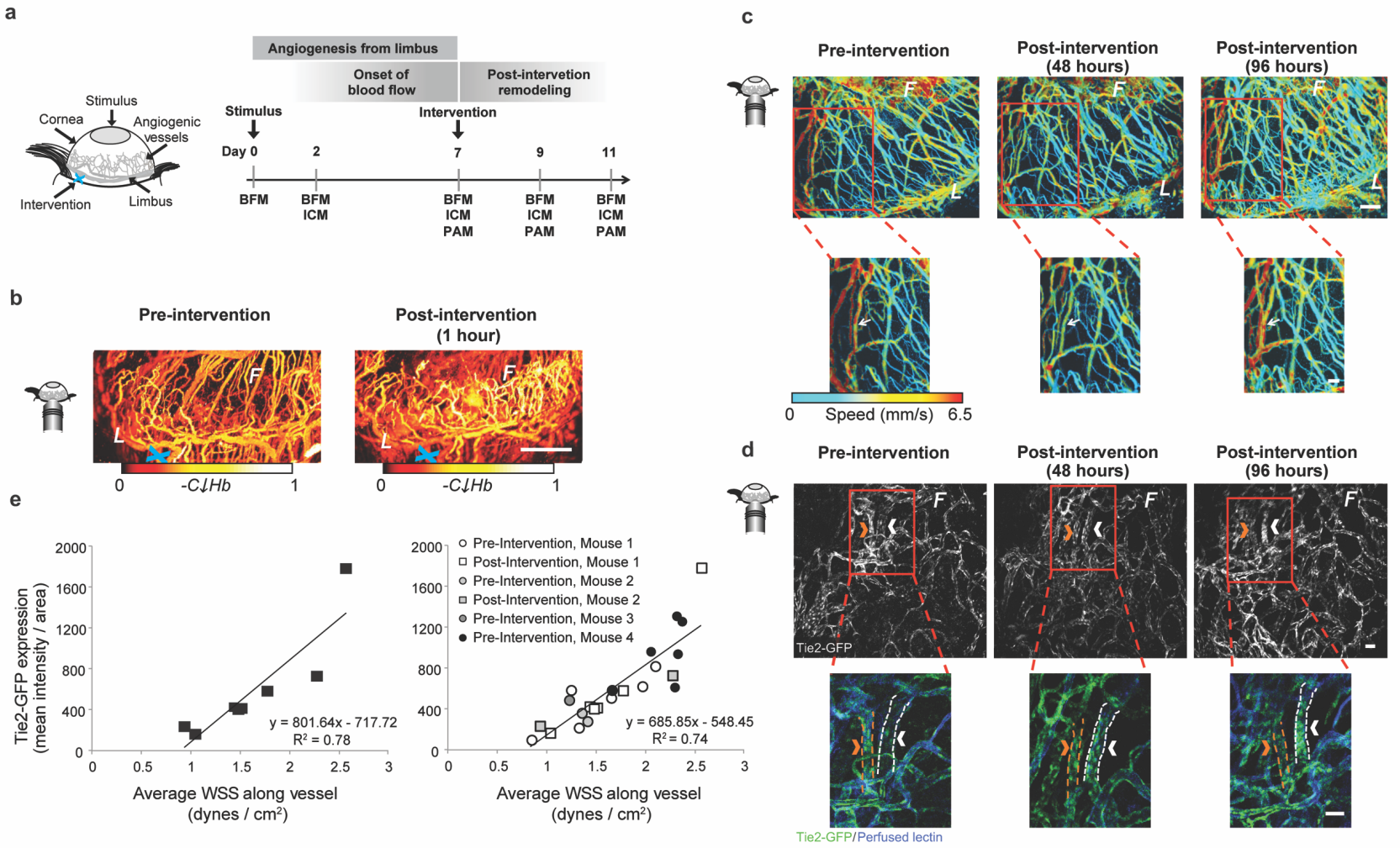
a
Angiogenesis from limbus
Onset of blood flow
Post-intervetion remodeling
Stimulus
Cornea
Angiogenic vessels
Intervention
Limbus
Stimulus
Intervention
Day 0
2
7
9
11
BFM
BFM ICM
BFM ICM PAM
BFM ICM PAM
BFM ICM PAM
b
Pre-intervention
Post-intervention (1 hour)
F
L
0
-CΔHb
1
c
Pre-intervention
Post-intervention (48 hours)
Post-intervention (96 hours)
F
L
0
Speed (mm/s)
6.5
d
Pre-intervention
Post-intervention (48 hours)
Post-intervention (96 hours)
Tie2-GFP
Tie2-GFP/Perfused lectin
e
Tie2-GFP expression (mean intensity / area)
Average WSS along vessel (dynes / cm²)
y = 801.64x - 717.72
R² = 0.78
y = 685.85x - 548.45
R² = 0.74
Pre-Intervention, Mouse 1
Post-Intervention, Mouse 1
Pre-Intervention, Mouse 2
Post-Intervention, Mouse 2
Pre-Intervention, Mouse 3
Pre-Intervention, Mouse 4

Figure 3.2 Surgical intervention caused a redistribution in blood flow that resulted in a quantifiable change in blood velocity, flow distribution, and Tie2-GFP fluorescence intensity over time throughout the network.

(A) Schematic represents the corneal angiogenesis assay in which blood vessels grow from the limbus ("*L*") into the avascular cornea, creating an angiogenic front ("*F*"). Surgical "intervention" (blue "x") was performed by applying thermal cautery to an arteriole that feeds into from the limbus. **(B)** PAM images showing relative hemoglobin content ("C_{Hb}") of corneal vessels pre-intervention and one hour post-intervention. **(C)** Dynamic changes in blood flow were visible using PAM in single capillary segments. Bottom row shows a magnified view of the regions boxed in red above. Changes in blood flow velocity (mm/s) are evident in individual vessel segments; white arrow indicates to one segment where flow speed was initially reduced and then returned to pre-intervention levels by 96 hours post-intervention. **(D)** Tie2-GFP fluorescence captured with ICM in single capillary segments over time. Bottom row shows a magnified view of the regions boxed in red above. Changes in Tie2-GFP fluorescence intensity within individual vessel segments are evident between time points. Arrows indicate the same vessel at each time point. Orange arrow indicates a vessel with decreased GFP fluorescence intensity at 96 hours post-intervention; white arrow indicates vessel with increased GFP fluorescence intensity 96 hours post intervention. In the bottom row, Tie2-GFP is green, and perfused IB4-isolectin is blue. **(E)** Vessels with higher WSS exhibited increased Tie2-GFP fluorescence intensity post-intervention. Data in graph on left are from vessels from two mice post-ligation (slope and R^2 indicated); data in the graph on the right are from vessels assessed both pre- and post-ligation (slope and R^2 indicated) from multiple mice. White scale bar indicates (B) 1 mm, (C,D) 50 μm. = 4.

Imaging of capillary hemodynamics and endothelial cell protein expression in individual neovessel segments before and after surgical redistribution of blood flow

After confirming that the linear correlation between Tie2-GFP fluorescence intensity and WSS in neovessel segments throughout the corneal network was preserved following surgical redistribution of blood flow, we sought to determine if the change in WSS in a given individual neovessel segment (resulting from the surgical redistribution of blood flow) was correlated with the change in Tie2-GFP fluorescence intensity in that same neovessel segment. Using the experimental protocol outlined in Figure 2A and described above, we imaged the neovascular network of a stimulated (chemically burned) cornea in the Tie2-GFP mouse using BFM, ICM, and PAM seven days after applying the chemical burn. We then induced a surgical redistribution of blood flow ("intervention") by cauterizing an arteriole feeding into the neovascular network. Two days after intervention, we re-imaged (using BFM, ICM, and PAM) the same field of view in order to visualize the same vessel segments.

As highlighted by colored arrows (first and third panels in Figure 3.3A) and vessel outlines (second panel in Figure 3A), the same individual vessel segments could be identified with both ICM and PAM before ("Pre-intervention", top) and two days after ("Post-intervention", bottom) surgical redistribution of blood flow (Figure 3.3A, blood velocity is shown in first panel, with gray scale images of blood velocity shown in second panel). Tie2-GFP fluorescence intensity in individual neovessel segments within this corneal network correlated linearly with WSS, both before and two days after surgical redistribution of blood flow (Figure 3.3B top, $R^2 = 0.79$). Moreover, the change in blood flow-induced WSS in individual corneal neovessels after two days was directly proportional to the change in Tie2-GFP expression levels in those same neovessels (Figure 3.3B bottom, $R^2 = 0.92$). Specifically, when WSS in a given vessel segment decreased as a result of the

surgical redistribution of blood flow, Tie2-GFP expression also decreased in that segment (e.g. blue square in Figure 3.3B bottom). Conversely, when WSS in a vessel segment increased as a result of the surgical redistribution of blood flow, Tie2-GFP expression also increased in that segment (e.g. red square in Figure 3B bottom). Data points in the upper-right quadrant indicate vessels that experienced a decrease in both WSS and Tie2-GFP fluorescence intensity. Data points in the bottom-left quadrant indicate vessels that experienced an increase in both WSS and Tie2-GFP fluorescence intensity.

Further confirmation of the correlation between Tie2-GFP expression and blood flow/WSS was obtained by more extensively reducing blood flow via cauterization of all visible feeder arterioles within the corneal angiogenic network. BFM images confirmed significantly diminished blood flow immediately following surgical intervention (Figure 3C left). A network-wide decrease in Tie2-GFP fluorescence intensity was observed by ICM 48 hours later ($p < 0.01$, $n = 5$ corneas), and Tie2 mRNA levels in harvested corneas as measured by RT-PCR were also significantly diminished ($p < 0.02$, $n = 5$ corneas) at this time-point (Figure 3.3C middle). The maintenance of constitutive Flk1 expression following this intervention implies that the reduction in Tie2-GFP was not due to loss of or general poor health of endothelial cells (Figure 3.3C right). PPIA was used as housekeeping gene.

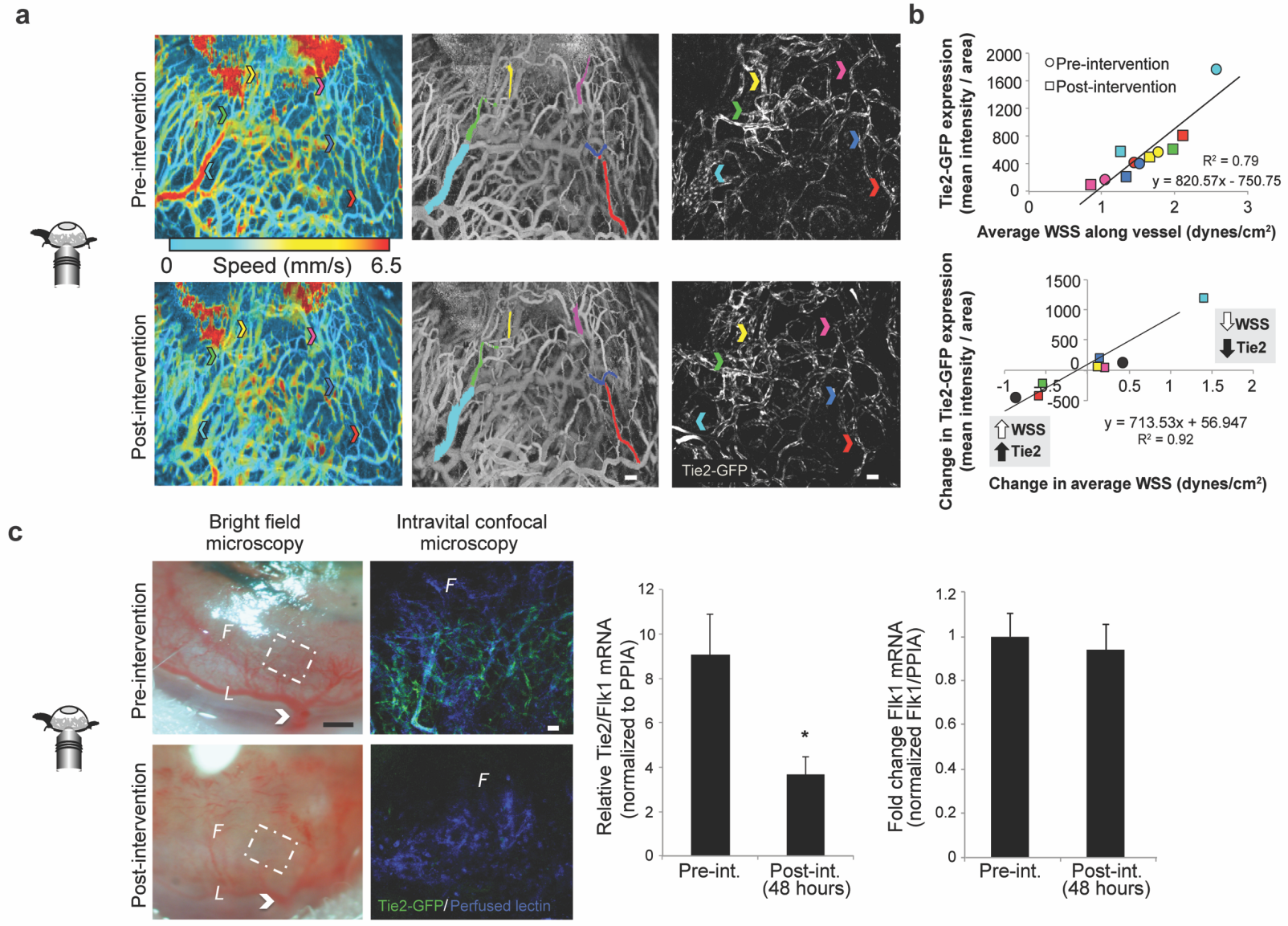
a
Pre-intervention
Post-intervention
0
Speed (mm/s)
6.5
Tie2-GFP
b
Tie2-GFP expression (mean intensity / area)
Pre-intervention
Post-intervention
R² = 0.79
y = 820.57x - 750.75
Average WSS along vessel (dynes/cm²)
Change in Tie2-GFP expression (mean intensity / area)
WSS
Tie2
WSS
Tie2
y = 713.53x + 56.947
R² = 0.92
Change in average WSS (dynes/cm²)
c
Bright field microscopy
Intravital confocal microscopy
Pre-intervention
Post-intervention
F
L
Tie2-GFP/Perfused lectin
Relative Tie2/Flk1 mRNA (normalized to PPIA)
Pre-int.
Post-int. (48 hours)
*
Fold change Flk1 mRNA (normalized Flk1/PPIA)
Pre-int.
Post-int. (48 hours)

Figure 3.3 Representative example murine cornea analyzed using the dual imaging method demonstrates that endothelial cell Tie2-GFP fluorescence intensity was directly correlated with blood flow-induced WSS.

(A) Changes in average WSS were correlated with changes in Tie2-GFP fluorescence intensity. Arrows indicate the color-matched vessel segments between PAM (center) and ICM (right). (**B**) The top graph shows the quantification of Tie2-GFP fluorescence intensity (mean intensity/pixel^2) obtained using ICM versus blood flow-induced WSS (dynes per cm^2) obtained using PAM. Measurements obtained pre-intervention are plotted as circles, measurements obtained post-intervention are plotted as squares, and each vessel segment that was analyzed is represented by the color that corresponds to the vessel segment highlighted in (A). The bottom graph reports the change in Tie2-GFP fluorescence intensity obtained using ICM versus the change in WSS obtained using PAM (both measurements are pre-ligated minus post-ligated values). **(C)** Bright field images of a representative cornea pre-intervention (top left) and 48 hours post-intervention (bottom left) show that blood flow is decreased throughout the network following an extensive surgical intervention. Right panel shows ICM images of the magnified vascular networks that are outlined by the white, dashed line boxes in the bright field images to the left, both pre- and 48 hours post-intervention. White arrow indicates the location of an arteriole branching off the limbus that was cauterized. Tie2 mRNA normalized to Flk1+ mRNA (left graph, n = 5 mice, $p < 0.01$) demonstrates a significant decrease in corneal Tie2 gene expression 48 hours after network-wide decrease in blood flow. In the same corneas, however, endothelial cell Flk1 mRNA (right graph, n = 5, $p = 0.4$) was unchanged. White scale bar indicates (A,C) 50 μm. Black scale bar indicates (C) 500 μm.

Discussion

Heterogeneities in endothelial gene and protein expression have been observed at multiple levels of spatial scale throughout the blood circulation. These cell-to-cell[357] and vessel-to-vessel[368] differences have profound implications for the design of therapeutics that target the vasculature[369] and for drugs that aim to ameliorate pathological vascular adaptations[370]. Although the topic of endothelial heterogeneity is an emerging focus of research[371], the control systems that establish and maintain endothelial heterogeneities *in vivo,* and particularly in the microcirculation, have not yet been determined. Studies conducted in large vessels and in cultured monolayers of endothelial cells have demonstrated that endothelial cells are highly mechanosensitive, with fluid flow-induced shear stress serving as a regulator of endothelial cell gene expression[372]. Our novel observation of heterogeneous endothelial cell Tie2-GFP expression in murine corneal microvessels during angiogenesis motivated us to determine whether vessel-to-vessel differences in Tie2-GFP expression were dynamically coupled with differences in blood flow-induced shear stress. This required us to develop a new experimental platform for quantifying both vascular hemodynamics and endothelial cell protein expression in the same individual vessel segments throughout an *in vivo* microvascular network and across sequential time points. Employing dual-modality PAM and ICM imaging in an *in vivo* model of adult mammalian angiogenesis yielded two novel findings: 1) endothelial cell Tie2-GFP expression in an angiogenic network is linearly correlated with shear stress, and 2) local changes in shear stress are directly proportional to changes in endothelial cell Tie2-GFP expression in individual neovessel segments. To our knowledge, our study is the first to relate changes in endothelial cell protein expression within individual microvessel segments to changes in blood flow *in vivo*. Together, these findings implicate variable

blood flow-induced shear stress levels throughout an angiogenic microvascular network as a dynamic driver of endothelial cell heterogeneity.

To our knowledge, our study is the first to use PAM to analyze functional hemodynamic changes in microvessels over time during adult corneal angiogenesis. The cornea permits detailed study of mechanisms of adult angiogenesis because it provides an avascular space that generates a reproducible angiogenic response in which each neovessel segment is formed de novo and easily visualized using optical imaging approaches[121,123]. The superficial location and largely planar growth of this angiogenic network makes it highly amenable to multi-modality imaging. In particular, the shallow depth of field allows high resolution imaging of dynamic changes in vessel structure at cellular resolution. In contrast, high resolution study of angiogenesis in other end-organ systems, such as the heart, can be particularly challenging given tissue depth and complex three-dimensional structure rendering them less amenable to ICM and PAM, which has a penetration depth of 1.2 mm[373]. Furthermore, PAM provides functional measurements of the microvasculature that supplement traditional metrics of vascular architecture, including blood flow velocity, hemoglobin content, and sO_2. The use of PAM has allowed us to demonstrate that blood flow and hemoglobin content throughout the corneal angiogenic network is altered following limbal vessel cauterization**.** Vascular occlusions in the retina induce similar shunting of flow from the superior to inferior retinal circulation through pre-existing, but normally unperfused, collaterals[374,375]. We believe this to be the first report of shunting of blood flow through collateral vessels within a corneal angiogenic network, a finding that should enable further study of the mechanisms that drive collateral recruitment. In addition to these acute flow changes, we also report for the first time secondary transitory flow changes seen over larger time courses, with alterations in flow occurring by 48 hours and taking up to 7 days to return to baseline. The prolonged timeline for

these events should allow high resolution *in vivo* study of the compensatory response of endothelial cell and mural support cells to alterations in flow, also providing insight into how these accumulated changes can restore flow to baseline levels over time.

Prior studies of angiogenesis or vasculogenesis using intravital imaging have focused primarily on embryological development, predominantly using BFM and ICM. In the embryoid body model[376,377] and in the zebra fish[378], for example, studies have elucidated events occurring a few hours or days after the initiation of blood flow[379,380]. Our combined imaging technique should, in principle, be well suited for studying these early events because ICM and PAM are both compatible with the tissue thickness and required depth of field in these model systems. We further anticipate that the combination of ICM and PAM will be useful in studying microvascular adaptations that occur throughout adulthood and during the aging process, potentially providing time-lapse images of the same vessel or set of vessel segments within an expansive whole network over long time durations. While our study employed a GFP reporter mouse, additional applications could include fluorescently-tagged beads, therapeutic microspheres, DiI (1,1'-dioctadecyl-3,3,3'3'-tetramethylindocarbocyanine perchlorate) lipophilic membrane stain-labeled cells, and other lineage-tracing or reporter mice.

By demonstrating a dynamic and linear relationship between endothelial protein expression and blood flow-induced shear stress *in vivo*, our study serves as critical validation for published *in vitro* observations in cultured Human Umbilical Vascular Endothelial Cells (HUVECs) that link endothelial cell Tie2 expression to blood flow-induced WSS levels[259,264,381,382]. Further, our findings are consistent with the notion that endothelial cells throughout the circulation exhibit a spectrum of maturation states[383,384] since endothelial cell Tie2 expression signifies phenotypic maturity[385]. Beyond validating previous *in vitro* observations, the data and imaging tools we present in this study may

be leveraged by researchers who seek to build quantitative computational models of microvascular adaptations. Previous studies have demonstrated the dynamic, spatially-heterogeneous remodeling of collateral vessels after acute vessel ligation[386]. However, these data have not yet been coupled with genetic reporting, and our study provides unique and potentially valuable approach for parameterizing and validating computational models that are focused on evaluating mechanisms linking hemodynamics with gene expression in the microvasculature[19,341-343,387,388].

One caveat of our study is that we used relative GFP expression under the control of the Tie2-promoter as a surrogate for endothelial cell Tie2 expression. This assumption has been previously validated using an inducible GFP reporter in single cells where GFP fluorescence was shown to be directly proportional to GFP gene copy number and GFP mRNA expression. ICM can provide a sensitive and quantitative measure of endothelial cell protein expression over at least a 1,000 fold range[389]. However, it should be noted a lack of GFP signal may potentially reflect a fluorescence signal below the limits of ICM detection or a bias in photomultiplier threshold calibrated to higher expression levels, rather than a complete absence of Tie2 expression[389]. Furthermore, the strong positive correlation that we observed between endothelial cell Tie2-GFP and WSS in vessel segments does not prove that changes in WSS are sufficient to induce changes in endothelial cell Tie2-GFP expression. Indeed, there are likely a multitude of spatially and temporally altered regulators of Tie2 during angiogenesis, such as growth factors and the presence of hypoxia or inflammation in the tissue, that dynamically affect Tie2 expression[331,390]. Therefore, future work is needed to determine whether changes in WSS cause changes in endothelial cell Tie2 expression, and if so, via what molecular mechanisms.

Tie2 has a known functional role in mural cell recruitment via Angiopoietin 1 (Ang1) signaling[15,391,392]. Therefore, one implication of our study is that changes in WSS during angiogenesis

are correlated with the dynamics of mural cell recruitment through Tie2 expression and activation. However, it remains to be determined to what extent endothelial cell Tie2 expression levels relate to other structural and functional indicators of endothelial cell maturity, such as mural cell recruitment and vessel permeability alterations[331,332,391-394], and to what extent those characteristics correlate with WSS levels. Moreover, studies performed on cultured endothelial cells have demonstrated that other signaling molecules implicated in angiogenesis and vessel maturation, including VEGF-R1, VEGF-R2, and VE-Cadherin, are also affected by WSS levels[259,264]. Therefore, it would be interesting to apply the combination of PAM and ICM to other *in vivo* model systems where it is possible to visualize endothelial cell expression of these (and other) relevant genes and proteins. Nonetheless, the study of Tie2-Ang signaling in endothelial cells has inspired both pre-clinical and clinical studies[344-346] designed to evaluate a drug, VE-PTP, which increases phosphorylation of Tie2 even in the presence of high Angiopoetin 2 (Ang2) levels. However, the impact of this drug on the endothelium's ability to respond to signals associated with injury and disease, including blood flow shunting or hemodynamic alterations during angiogenesis, has not yet been examined. Indeed, no study to date has attempted to ascertain the efficacy of VE-PTP given the endothelial heterogeneity that we have demonstrated with respect to Tie2 expression and its relationship to biomechanical cues. Our experimental platform would enable this and other similarly informative studies to be completed in *in vivo* disease models.

In conclusion, we have presented a new experimental platform that uniquely combines PAM and ICM to obtain quantitative, high-resolution information about both hemodynamic parameters and protein expression levels in individual capillary segments during adult mammalian angiogenesis. Understanding how biomechanical and biochemical stimuli integrate with one another to drive the dynamic, multi-cell process of angiogenesis and vessel maturation is key to developing effective

therapies for controlling these processes, which are essential to tissue function, healing, and regeneration. We envision that this approach will be most useful for placing cell-level changes in the context of local hemodynamic alterations, which will facilitate discoveries of how spatial and temporal phenotypic heterogeneities arise and persist *in vivo* during vascular remodeling and disease.

CHAPTER 4

TARGETING PERICYTES FOR ANGIOGENIC THERAPIES

ACKNOWLEDGEMENTS: Rick S. Sweat[2], Peter C. Stapor[2], Shayn M. Peirce[1], Walter L. Murfee[2]

[1]Department of Biomedical Engineering, University of Virginia
[2]Department of Biomedical Engineering, Tulane University

The text included in this chapter has been published:
Kelly-Goss M, Sweat R, Stapor P, Peirce S, Murfee W. Targeting Pericytes for Angiogenic Therapies. Microcirculation, 2014.

Abstract

In pathological scenarios, such as tumor growth, and diabetic retinopathy, blocking angiogenesis would be beneficial. In others, such as myocardial infarction and hypertension, promoting angiogenesis might be desirable. Due to their putative influence on endothelial cells, vascular pericytes have become a topic of growing interest and are increasingly being evaluated as a potential target for angioregulatory therapies. For example, the strategy of manipulating pericyte recruitment of endothelial cells to influence capillary stability could result in anti- or pro-angiogenic effects. However, our current understanding of pericytes is limited by knowledge gaps regarding pericyte identity and lineage. To use a music analogy, this review is a "mash-up" that attempts to integrate what we know about pericyte functionality and expression with what is beginning to be elucidated regarding pericyte phenotypic plasticity and regenerative potential. In this review, we explore the lingering questions regarding pericyte phenotypic identity and lineage that both complicate and add to our understanding of this apparently plastic cell type. The expression of different pericyte markers (e.g., SMA, Desmin, NG2 and PDGFR-β) varies for different pericyte subpopulations and tissues. Previous use of these markers to identify pericytes has suggested potential phenotypic overlaps and possible plasticity toward other cell phenotypes. Our review chronicles the state of the literature, identifies critical unanswered questions, and motivates future research aimed at understanding this intriguing cell type and harnessing its therapeutic potential.

Introduction

Pericytes are elongated mural support cells that extend along endothelial cells[18,395]. First identified by French physiologist and anatomist Charles–Marie–Benjamin Rouget in 1873 and termed "Rouget cells," pericytes are present in every vascularized tissue in the body[396]. Although it has been suggested that pericytes may reside in large vessels[397], pericytes are most commonly associated with the microvasculature. At the capillary level, pericytes regulate vessel permeability, vessel diameter, and endothelial cell proliferation through both paracrine signaling[398-400] and direct contact with endothelial cells[18,401]. Through cell-matrix and cell-cell interactions, pericytes play an essential role in contractile force transmission[402-404], vessel diameter regulation[405], vessel stabilization[18], and endothelial cell survival[406]. Pericytes can even directly control capillary diameter, as their presence has been shown to be necessary for constriction[405]. The functional effects of pericyte-endothelial cell signaling have previously been highlighted by comprehensive reviews[407,408]. Pericytes are considered "angioregulators" in that they can both stabilize and promote angiogenesis. Their importance in angiogenesis is evident when considering the case of diabetic retinopathy and tumor growth, in which pericyte loosening from the endothelium is associated with uncontrollable angiogenesis[407,409]. But importantly, their function can be dependent on the type of stimulus. For example, angiogenesis in skeletal muscle has been correlated with both the withdrawal of pericytes and an increase in pericyte number[396,410]. In recent years, new and intriguing roles have emerged for the pericyte. These include mediating leukocyte trafficking[411,412], contributing to fibrosis[413], and functioning as a tissue-resident stem or progenitor cell[368,414]. The multi-faceted role for pericytes emphasizes the need to both carefully identify their structural alterations during different pathological scenarios and better understand how their specific phenotypes relate to their functions. Meanwhile, pericytes have been convincingly established as critical players in

angiogenesis and as potential therapeutic targets in inflammation and tissue regeneration. In addition to serving as putative drug targets, pericytes have been implicated as tools for cell-based therapies due to their angioregulatory capabilities.

As pericytes receive increasing attention from a wider array of research domains, it has become even more apparent that advancing our knowledge about pericytes and our ability to therapeutically manipulate their function will require answering fundamental questions about pericyte ancestry, progeny, and phenotypic differentiation capacity that have confounded studies since Rouget's time. Even within the field of pericyte biology, varying terminology has created confusion[415]. The perplexity of pericyte identity can be attributed to pericyte phenotypes being cell and tissue specific and is best exemplified by considering Ito cells in the liver. Ito cells, also known as hepatic stellate cells, are thought to be mesenchymally derived and display smooth muscle-like, pericyte-like characteristics[416]. Ito cells, like pericytes, can exist in a quiescent or activated state depending on the local environment[416,417]. Ito cells interact with the sinusoid endothelium and control blood flow. They also can express multiple pericyte markers and participate in fibrogenesis. Based on the similarities to pericytes, Ito cells are, unsurprisingly, classified as the pericytes of the liver[418]. In this review we further identify sources of potential confusion regarding pericyte phenotypes based on their overlaps with other cell types. Then, we focus on the plastic relationships between pericytes and mesenchymal stem cells and the potential for therapeutically using stem cells to play the roles of pericytes. Pericytes represent a scientifically intriguing and therapeutically exciting cell type, but there are far more questions than answers. We approach some of these questions by convolving some of the basic science understanding about pericyte form and function with emerging evidence that suggest multipotency and points to their application as a cell-based therapy.

Pericyte Dynamics

Much of what constitutes our understanding about a cell population, and more importantly, the "identity" of a given cell population, are the behaviors and functionality that cells and their environment impart on one another. This is particularly true for pericytes, for which no cell type-specific expression markers exist. Even more informative than their behaviors during homeostasis is their behavior during dynamic processes. In the case of pericytes, the dynamic process of reference is angiogenesis, defined as the sprouting of new capillaries off of existing vessels. The role of pericytes in regulating angiogenesis has been reviewed extensively[402,419], so we briefly summarize some of the landmark findings that have shaped the field's understanding about pericyte function during this dynamic process.

Pericyte dynamics during angiogenesis have been shown to include alterations in cell-to-cell contacts with endothelial cells, migration, growth factor presentation, proliferation, and extracellular matrix modulation (Figure 4.1)[18,420]. Pericytes are present along capillary sprouts and have been shown to both lag and lead endothelial cells at the sprout tip[421,422]. In some cases, pericytes can even bridge the gaps between two sprouting endothelial cell segments[423]. Subsequently, the integration of pericyte dynamics during capillary sprouting logically can be linked to endothelial cell guidance. While the full scope of communication between pericytes and endothelial cells remains to be elucidated, work in this area has established that the pericyte-endothelial cell interactions during angiogenesis are regulated in part by Ang-1/Tie2, TGF-β and PDGFB/PDGFR-β signaling[424].

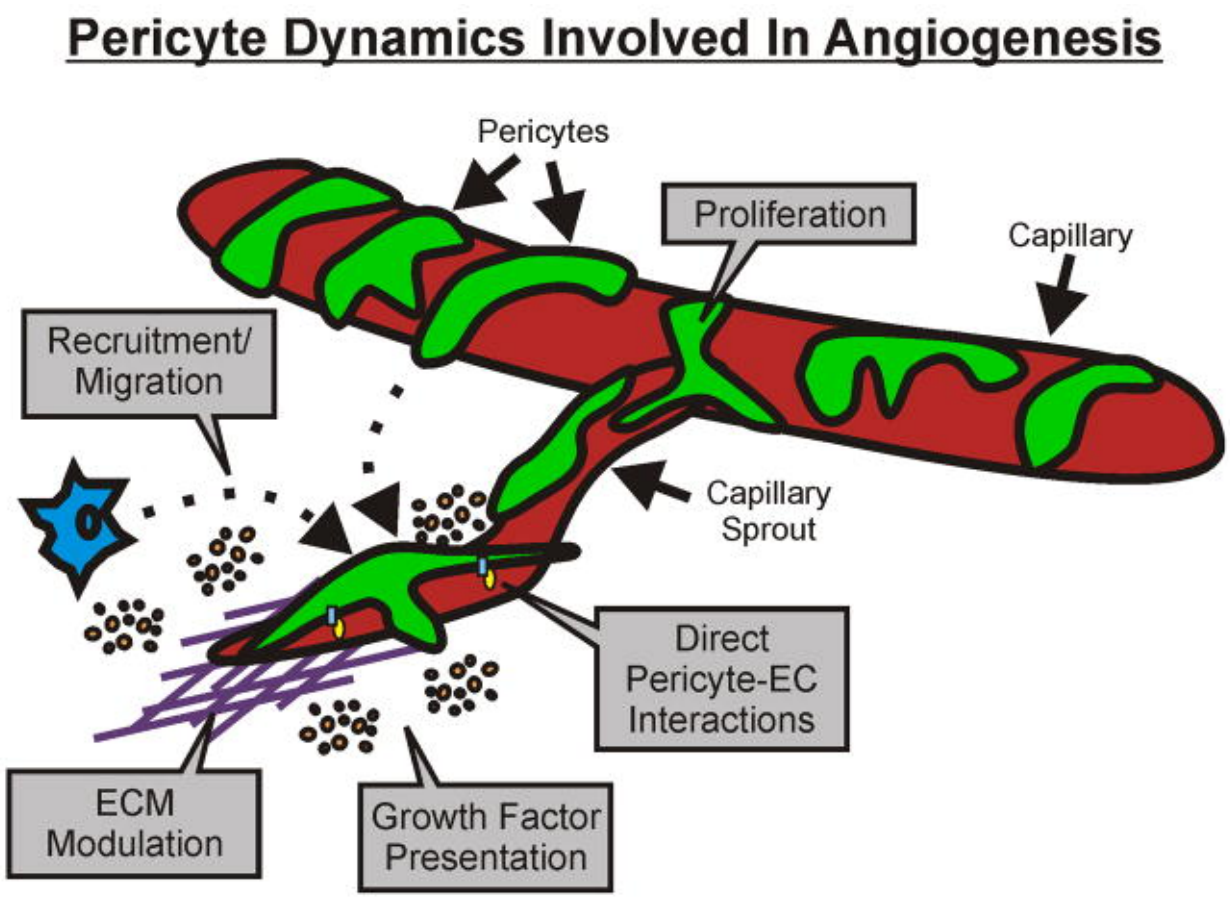

Figure 4.1 Pericyte dynamics involved in angiogenesis.

The main dynamics include cell-to-cell contacts with endothelial cells, migration, growth factor presentation, and extracellular matrix modulation. In some cases, pericyte proliferation has also been implicated. Each cellular interaction represents a target to manipulate capillary sprouting.

Perhaps the most convincing evidence for a requirement of endothelial cell-pericyte dynamic interaction during angiogenesis has been shown through work with PDGFB and PDGFR-β[398-400,425]. Manipulating proper pericyte investment by altering recruitment to the endothelium through PDGFB-PDGFR-β signaling can cause lethal microvascular dysfunction, affect vascular

patterning during development, and affect the formation of new vessels during physiological and pathological angiogenesis[18]. Indeed, tremendous research efforts using transgenic mice and co-culture *in vitro* assays have generated a molecularly detailed picture of the proteins that regulate pericyte dynamics during angiogenesis[403].

These and other landmark studies are foundational to the field's current understanding of what pericytes are and the how they function during angiogenesis. Advancing our knowledge requires identifying how and when pericyte behaviors change during the transition from quiescent to angiogenic states. This entails not only a description of their spatial and temporal dynamics, but also a prospective method for identifying pericytes and potential specific subpopulation cell types. As we explore in the next section, this has proven to be a challenge that has created insights, as well as some degree of confusion, about pericyte lineage and plasticity. Indeed, the scope of pericyte dynamics broadened upon considering the potential of transdifferentiation of pericytes into or from other cell types[426-428]. The putative links between interstitial cell populations (including macrophages, fibroblasts, and progenitor cells), pericytes, and SMCs necessitates discussion of how cell phenotypes, rather than cell nomenclature *per se*, relate to specific functions.

A case of mistaken identity?

As researchers recognize the importance and therapeutic potential for vascular pericytes, more questions than answers have been generated. Reflection on the literature reveals some historical confusion about pericytes – confusion propagated by a lack of cell type-specific markers, potential for transdifferentiation, and visualization in histological cross-sectional views that may obscure their true identity.

Pericyte Morphology

Cell types by are typically identified by their morphology and expression of certain genes and/or proteins. A quintessential hallmark of pericyte identity has long been the characteristic wrapping of cell processes, or filopodia, around capillary endothelium. Another morphological trait is the sharing of a common basal lamina with the endothelium[429,430]. Pericytes are most convincingly identified by their morphology when using electron microscopy of sectioned tissues[431] or confocal microscopy of whole-mounted tissues[432,433]. However, in most cases pericytes are identified using lower resolution techniques, which limits the classification to their general localization next to an endothelial cell. At low magnification (e.g., 20x or lower), it is impossible to determine where the ablumenal membrane of the endothelium ends and where the pericyte membrane starts, creating the possibility for one to mistake an extravasating monocyte, a proliferating endothelial cell, or any number of other cell types in the niche for a pericyte. Moreover, other cell types that can occupy space in the perivascular niche (e.g. macrophages, fibroblasts) may also express the same cell surface marker(s) being used to denote a pericyte phenotype. While morphology alone may be insufficient for ascribing a pericyte identity to an

observed cell, marker expression is similarly inadequate for distinguishing pericytes from other cell types.

Pericyte Phenotypic Markers

Unlike some cell types, such as the endothelial cell, that are classically and specifically identified by their expression of cell type-specific genes or proteins (e.g. VE-cadherin and PECAM-1), a cell-type specific marker for pericytes has yet to be identified. Pericytes are known to express a battery of different proteins that can be visualized using off-the-shelf antibodies, but expression is shared by other cells, many of which occupy similar locations in tissues, further exacerbating the challenge of distinguishing pericytes from non-pericytes. Although this has the potential to create uncertainty, this challenge is an opportunity to gain new insights into pericyte lineage and identity.

Commonly used pericyte markers include SMA, Desmin, NG2 and PDGFR-β[18]; however, their expression patterns are not pericyte-specific and differ depending on species, tissue, and even developmental stage[18,420]. The question remains: How do we unequivocally identify a pericyte? The use of the above-mentioned markers and morphological characteristics provide a partial solution, but as Table 4.1 highlights, the "marker equals phenotype" approach can create confusion. Table 4.1, which lists the various pericyte markers that have been used by investigators interested in identifying pericytes, also raises the question whether the combination of different pericyte markers can be used to identify different pericyte subpopulations. As seen in Figure 4.2, the expression of known markers (NG2, Desmin, SMA) can identify two neighboring cells. Expression differences highlight what we still do not know regarding how local cues might regulate pericyte phenotypes. We postulate that observations like these implicate a possibility of

pericyte phenotype specialization and motivate a new area of research that might be analogous to tip-cell versus stalk-cell sub-classifications for endothelial cells along a capillary sprout.

Table 4.1: Expression Markers Used for Pericyte Identification

Cell Surface Markers	Physiological Location	Detection Method	Citation
Aminopeptidace N, Aminopeptidase A, Nestin	Adult Mouse Brain	IHC	Alliot, et al. J. Neurosci Res. 1999. (1)
Endosialin, Mayer's Hemalaun	Human Primary Pericytes	IHC, RT-PCR, Western Blot	Christian, et al. Am J Pathol. 2008. (20)
NG2	Rat Mesentery	IHC	Murfee, et al. Microcirculation. 2006. (64)
NG2	Mouse Retina	IHC	Taylor, et al. Microvasc Res. 2010. (95)
NG2, Alkaline Phosphatase	Human Skeletal Muscle	IHC, RT-PCR	Dellavalle, et al. Nat Cell Bio. 2007. (26)
NG2, Class III β-Tubulin	Rat Mesentery	IHC	Stapor, Murfee. Microvasc Res. 2012. (88)
NG2, PDGFRβ, CD29, CD90, CD146	Mouse Femoral Artery	IHC	Tigges, Stallcup. J Vasc Res. 2012. (96)
NG2, PDGFRβ, RGS5	Mouse Brain, Lung, Gut, Kidney, Artery, Vein	IHC, RNA Microarray, *in situ* Hybridization	Bondjers, et al. Am J Pathol. 2003. (14+D20)
NG2, SMA	Rat Mesentery, Spinotrapezius, Dorsal Subcutaneous Tissue	IHC	Taylor, et al. Microciruation. 2007. (94)
NG2, SMA, 3G5	Bovine Retina	IHC	Kutcher, et al. Am J Pathol. 2007. (56)
NG2, SMA, Desmin	Mouse Choroid	IHC	Condren, et al. PLOS ONE. 2013. (22)
NG2, SMA, PDGFRβ	Mouse Kidney Interstitium	IHC	Schrimpf, Duffield. Curr Opin Nephrol Hypertens. 2011. (84)
NG2, SMA, PDGFRβ, Calponin I, smMHC	Murine Infantile Hemangioma	IHC, qRT-PCR, Western Blot	Boscolo, et al. Arterioscler Thromb Vasc Biol. 2011. (15)
NG2, SMA, PDGFRβ, Nestin	Rat Aorta	IHC, RT-PCR	Howson, el al. Am J Physiol Cell Physiol. 2005. (44)
NG2, SMA, TLR2, TLR4, FPR2, TNFR1, NLRP3, ICAM-1	Human Placental Pericytes	IHC, RT-PCR	Stark, et al. Nat Immunol. 2012. (89)
SMA, 3G5	Human Neonatal Foreskin	IHC, Phase-Contrast Microscopy, Magnetic Bead Isolation, FACS	Helmbold, et al. Microvasc Res. 2001. (41)

Table 4.1 Expression markers used for pericyte identification. *Citations listed from publication.*

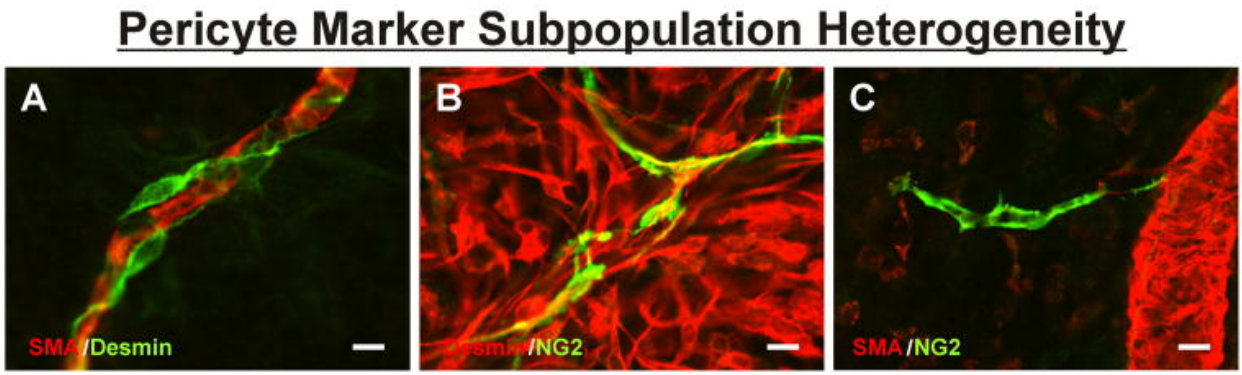

Figure 4.2 Pericyte marker subpopulation heterogeneity between neighboring cells in adult rat mesenteric microvascular networks.

(**A**) Example of Desmin-positive cells wrapping around a SMA covered capillary in a quiescent scenario. (**B**) Example of NG2-positive pericytes along capillaries that co-localize to a sub-population of Desmin-positive cells during a wound healing response. (**C**) Example of an NG2-positive pericyte apparently along a capillary sprout off a SMA-covered venule. Scale bar=10 μm.

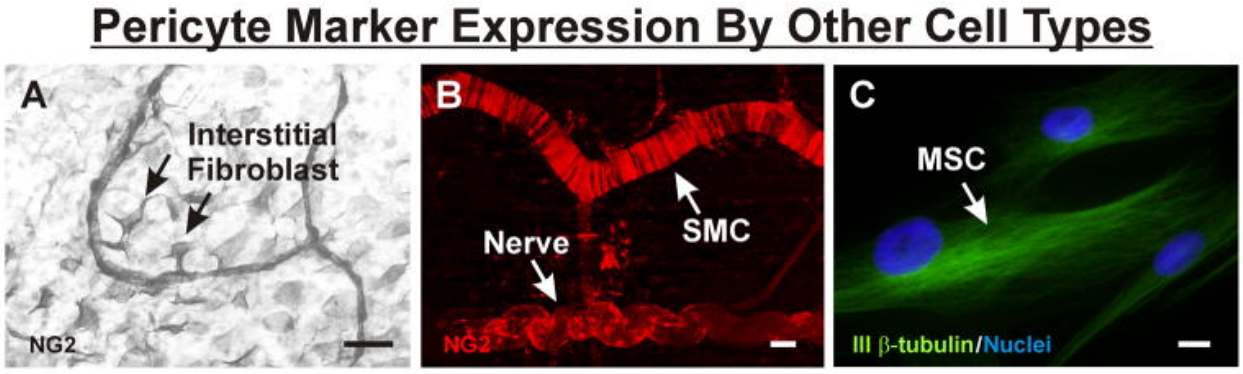

Figure 4.3 Pericyte marker expression by other cell types.

(**A**) Example of NG2 identification of interstitial fibroblasts in remodeling adult rat mesenteric networks. The fibroblasts apparently interact with NG2-positive pericytes along capillaries. (**B**) Example of NG2 identification of tightly wrapped SMCs along an arteriole and a nerve in unstimulated mouse spinotrapezius muscle. (**C**) Example of class III β-tubulin identification of MSCs *in vitro*. Scale bars = 50 μm (A), 20 μm (B), and 10 μm (C).

Pericyte Marker Overlap with Other Cell Types

As mentioned above, a pericyte-specific marker has not been identified by current research. Consequently, we must resort to identifying pericytes using a combination of markers, each of which is expressed by a multitude of other cell types that can occupy the perivascular niche (Figure 4.3). Recognition of labeling overlaps offers a potential opportunity to gain fundamental insight into both the lineage and plasticity of pericytes. Although the shared expression of one or more markers does not confirm that two different cells share the same lineage, it may suggest the possibility of a common lineage and should not be ruled out without further investigation. The idea that pericytes and other cell types resident in the perivascular-niche share a common lineage, which is evidenced by overlapping marker expression, is provocative.

For example, SMA is expressed by pericytes, immature SMCs, which express SMA but not smMHC, and mature SMCs, which express both contractile proteins[412,426,434,435]. Myofibroblasts, which can also reside in the perivascular niche, also can express SMA. For example, SMA expression identifies myofibroblasts in scenarios of wound healing and fibrosis[436]. Recent studies have further suggested that SMA-positive myofibroblasts in the kidney originate from pericytes[437], lending support to the idea that coincident expression of the same marker in pericytes and other cell types may, in fact, signify a common lineage. Desmin and PDGFR- β are also expressed by mature SMCs and interstitial fibroblasts[427].

Perhaps the most common marker used to identify pericytes in recent years has been neuron-glia antigen 2, or, more commonly, NG2[423,438]. We have demonstrated that NG2 is dramatically upregulated along venules during capillary sprouting, implicating its involvement and potential as an angiogenic specific marker[439]. But like other pericyte markers, NG2 is not pericyte specific. During development, NG2 is expressed by oligodendrocyte progenitor cells, immature

chondroblasts, skeletal myoblasts, and cardiomyocytes[440]. NG2-positive cells in the CNS have been referred to as O2A cells because they can be differentiated into either oligodendrocytes or another type of glial cell *in vitro*. In the adult, NG2-positive cell populations increase following CNS injury, in part due to upregulation of NG2 by glial cells and macrophages[440]. NG2 expressing cells also include Schwann cells, at least in mouse, and can be found near the nodes of Ranvier in the peripheral nervous system. This suggests a role for NG2-positive cells in regulation of myelination[440]. NG2 was also found to be the same as HMP, previously associated with tumor cells, further confirming the concept that NG2 is expressed by highly active cell types[441]. As mentioned above, NG2 is expressed by pericytes throughout the microvasculature in most, if not all, quiescent tissues. This above evidence suggests that pericyte NG2 expression pattern in the microvasculature mimics that in the nervous system, wherein NG2 expression contributes to both homeostasis and regeneration. Indeed, NG2-positive pericytes acquired from the central nervous system and exposed to bFGF in culture can acquire phenotypes that overlap with glial cell lineages[442]. The common use of NG2 as a pericyte marker and its analogous expression pattern – and possibly function -- in neural and vascular support cells raises the question of whether other neural phenotypic markers also identify pericytes during angiogenesis.

Class III β-tubulin, which like NG2 has been identified as a marker of neural progenitor cells in the CNS and peripheral nerves in the adult, is another candidate pericyte marker. In contrast to other markers, class III β-tubulin might offer a temporal and spatial marker of angiogenic pericytes *in vivo*[443]. In unstimulated adult rat mesenteric networks, class III β-tubulin is nerve specific and absent along arterioles, venules, and capillaries. After the networks are stimulated to undergo angiogenesis, class III β-tubulin is upregulated by pericytes along these vessel types and is subsequently down regulated to unstimulated levels after capillary sprouting[443]. Class III β-

tubulin is one of seven β-tubulin isotypes that forms α/β-tubulin heterodimers with six β-tubulin isotypes during microtubule assembly and is most commonly used as a marker of neural phenotypes[444]. Much like NG2, during development in the central nervous system class III β -tubulin is transiently expressed by glial precursor cells; in the adult it is expressed by peripheral nerves[444]. Outside the nervous system, class III β -tubulin expression by tumor cells correlates with increased metastasis and resistance to tubulin binding agents[445,446]. The positive expression of class III β -tubulin by tumor cells and human pericytes *in vitro* (unpublished data) highlights a potential issue with using class III β -tubulin expression to indicate a neural phenotype. For example, stem cell differentiation into nerves has been confirmed, in part, based on class III β -tubulin expression[447,448]. However, data from our laboratories, suggests that class III β -tubulin can be expressed by pericytes and is not nerve specific. We have also confirmed that human placenta-derived pericytes, human mesenchymal stem cells (Figure 4.3), and mouse embryonic stem cells also express class III β -tubulin *in vitro* (data not shown). Since mesenchymal stem cells might be a source of vascular pericytes in adult tissues[449] and, vice versa, vascular pericytes can be induced to exhibit multipotent stem cell activity[442], we speculate that the transient class III β-tubulin *in vivo* identifies a precursor cell population.

Both NG2 and class III β -tubulin expression by pericytes and neural cells highlight an emerging area of microvascular research focused on the link between neural and vascular patterning[450-452]. This link is supported at the molecular level when considering growth inhibitors in the CNS such as ephrins, semaphorins, NG2, and Nogo[453], and is commonly presented in the context of either endothelial cell tip cells or arterial/venous identity. The overlap between neural and vascular patterning offers an exciting new perspective on the study of adult microvascular

remodeling. The shared expression of NG2 and class III β -tubulin by pericytes and neural cells motivates the need to understand if and how perineural cells and pericytes are related.

Indeed, these findings motivate an even broader question: are pericytes able to differentiate into other cell types? Emerging evidence suggests the answer is "yes," and a putative mechanism is via a bridging cell type that has well known multipotent differentiation capabilities: the MSC. For example, G. Paul et al.[454], recently isolated, purified and characterized a progenitor cell population from the ventricular wall and the neocortex in the adult human brain. They confirmed that these cells co-express markers for MSCs and pericytes *in vivo* and *in vitro and have* multilineage potential towards both mesodermal and neuroectodermal phenotypes. As discussed above, it is intriguing that the brain harbors a cell population with the ability to both modulate angiogenesis as pericytes and regenerate neural tissues as neural progenitor cells. Evidence from other tissues corroborates this interesting finding in the brain, and in the following section we use recent reports to conceptualize the putative linkage between pericytes and MSCs (Figure 4.4).

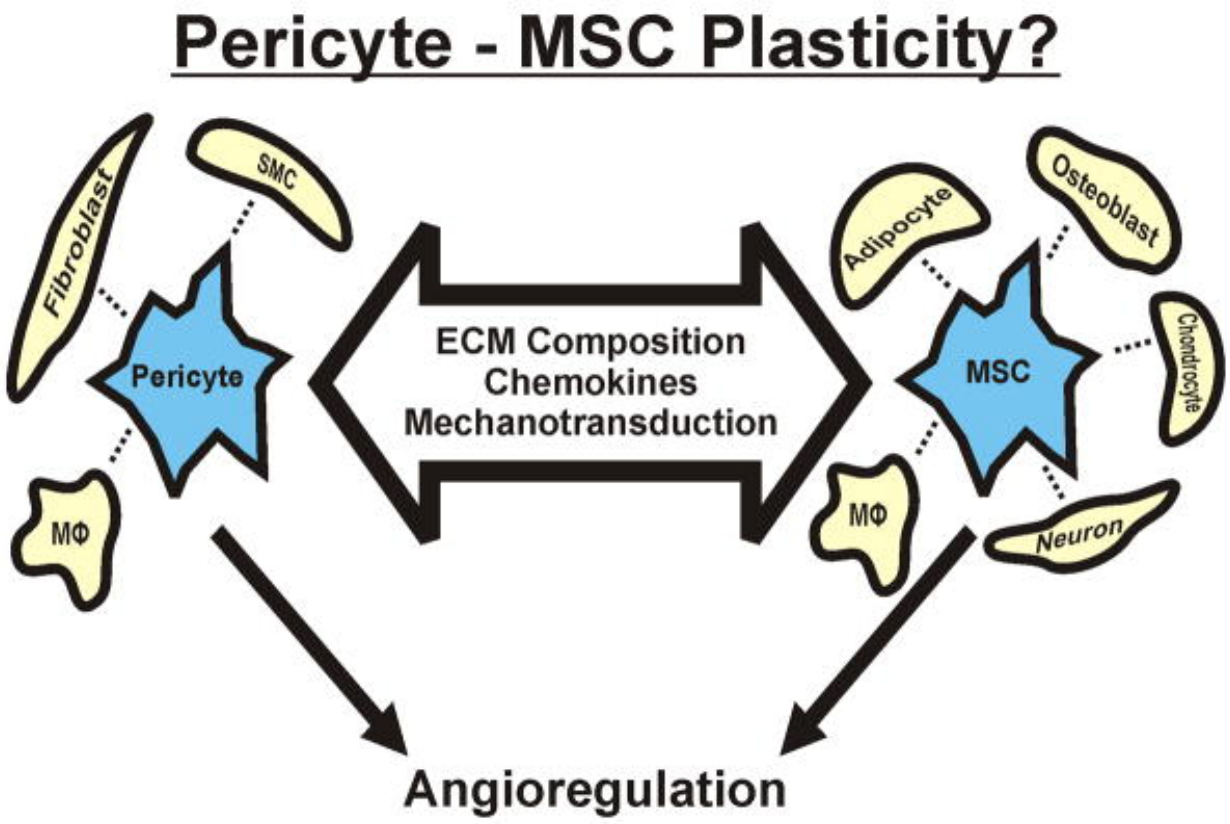

Figure 4.4 Pericyte and MSC phenotypic plasticity.

Recent studies have suggested that pericytes (or a subset therein) and MSCs share a common lineage and possess phenotypic plasticity that can be modulated by different environmental factors (large arrow). A functional intersection between the different phenotypes is their potential to participate in angioregulation by either stimulating angiogenesis or stabilizing new vessel formation.

Pericytes or Mesenchymal Stem Cells (or Both)?

Within the past ten years, a number of studies have demonstrated that MSCs and pericytes co-localize within the perivascular niche and express many of the same cell surface markers. Implying that the perivascular niche may serve as a systemic reservoir of tissue-resident stem cells[455,456], these findings have generated a number of provocative questions around the topic of MSC and pericyte identity and lineage, and their possible overlap (Figure 4.4). In this section we will briefly review the literature in this area with respect to two fundamental questions that have yet to be completely answered: 1) are pericytes MSCs? and 2) do MSCs give rise to pericytes?

Are pericytes MSCs?

Initially isolated from the bone marrow, MSCs have been defined by the International Society for Cellular Therapy as a population of cells that, upon removal from tissue depots, is adherent to plastic, expresses a panel of defined surface markers (CD73, CD90, and CD105, and lack of CD11b or CD14, CD19 or CD79, CD45, and HLA-DR), and have the ability to differentiate into adipocytes, chondrocytes, and osteoblasts[457]. Emerging evidence confirms the presence of MSCs within the perivascular niche in a wide array of tissues throughout the body, including fat, muscle, bone, and brain[458-462]. Indeed, several studies have suggested that blood vessels throughout the circulation contain multi-lineage precursors and contribute to tissue repair/regeneration[463,464]. Dr. Bruno Péault and colleagues[36] were the first to identify, purify, and characterize distinct populations of MSCs from the vasculature of multiple human organs[456,465]. MSCs in the perivascular niche have been classified into subsets that include pericytes[36], adventitial cells[466,467], and myogenic endothelial cells[468]. Each subset is able undergo adipogenesis, osteogenesis, and chondrogenesis in culture, and can elicit substantial regenerative capabilities when injected back *in vivo*. The regenerative

capacity of multipotent pericytes, isolated by flow cytometry selection of CD34–/CD146+/CD45–/CD56– cells from adipose and other tissues, has been evaluated in skeletal muscle[469], lung[470], dermal[471], and nervous tissues[472]. The lack of CD34 expression (CD34–) is thought to be a hallmark of multipotent pericytes in most tissues[36], but a rare CD34+/CD146+/CD45–/CD31– population of adipose-derived pericytes has also been identified in adipose tissue[473-478] using stringent rare-event strategies for its detection and isolation by flow cytometry [476,479]. So in many ways, detection of a multipotent subpopulation of pericytes, as is the case for pericyte identification in general, is still invariably elusive using the currently available techniques, such as flow cytometry and immunohistochemistry[458].

The extent to which pericytes share a common identity or lineage with MSCs may differ from tissue to tissue and depend on how quiescent or stimulated the tissue may be[480]. There are likely a number of different mechanisms that control the endogenous phenotype of a pericyte at any given point in time (Figure 4.4). An alteration in chemical cues—either diffusible or matrix bound, is likely a key contributor to pericyte-MSC differentiation *in situ*. The source of these chemical cues is likely variable but attributable to cells in and around the perivascular niche, like endothelial cells, fibroblasts, and macrophages. Lee et al.[481] found that IL-1β –activated macrophages promote differentiation of perivascular-resident MSCs in adipose tissue to vascular SMCs through a prostaglandin F2α –mediated paracrine mechanism. It is also likely that changes in the extracellular matrix composition itself are candidates for regulators of MSC and pericyte differentiation[482]. Mechanical stiffness of the underlying substrate has also been shown to influence de-activation of stem cells and myofibroblasts[483], so there are likely mechanical cues, in addition to chemical cues, that guide pericyte differentiation in situ. A disturbance in the endothelial-pericyte interaction has also been proposed as a driver for osteogenic and adipogenic differentiation of

pericytes. In settings where endothelial-pericyte interactions are disrupted, like heterotopic ossification and atherosclerosis, pathological bone mineralization and adipogenesis has been observed, suggesting that disruption of endothelial-pericyte interactions may be another key driver of pericyte/MSC differentiation[423,469].

Do MSCs differentiate into pericytes?

The relevance of this perivascular stem cell niche to tissue homeostasis and regeneration is only beginning to be explored, but one of its more obvious implications is as a sustainable source for new pericytes *in vivo*. As an example, MSCs derived from excised bone marrow and co-cultured with endothelial cells have been shown to differentiate into pericytes that can support engineered vessels in three-dimensional collagen gels implanted *in vivo* for more than 130 days[484]. In another study where MSCs derived from the bone marrow of GFP transgenic mice were intravenously injected into mice that had received cutaneous wounds, GFP-positive bone marrow cells in the wound expressed pericyte markers[485].

Support for MSC differentiation into vascular pericytes is also provided by bone marrow lineage studies. Ozerdem et al. showed that NG2-expressing pericytes were recruited from the bone marrow when the mouse cornea was treated with bFGF to induce angiogenesis[486]. Over ninety percent of these pericytes expressed CD45 or CD11b, indicating their hematopoietic origin and mesenchymal lineage overlap. Similar findings were presented by Rajnate et al. during tumor and VEGF induced angiogenesis. Song et al., also demonstrated that PDGFR-β expressing pericyte progenitors from the bone marrow reside in the tumor interstitium and are capable of differentiating into NG2, Desmin, and SMA-positive pericytes. Jung et al. identified what they

termed “multipotent pericyte-like cells” [487]in the circulating blood based on fluorescence or magnetic activated cell sorting with anti-PDGFR-β antibody.

While compelling evidence seems to support that pericytes can be derived from MSCs and contribute to vascular growth and remodeling, the dynamics of this process remain an open avenue for discovery. Whether or not MSCs are derived from the bone marrow and circulate systemically to tissues throughout the body, or if they self-renew within tissue-resident perivascular niches, or both, have yet to be determined and will likely require some of the tools presented in the final section of this review.

Stem Cell Applications for Pericyte-targeted Angiogenic Therapies

Clearly, confusion remains: do pericytes and MSCs belong in the same pool, or are they distinct populations that share no such common lineage? Regardless of the answer, the fields of tissue engineering and regenerative medicine have continued to move forward, focusing on isolating and injecting these cells, despite their uncertain lineage, for therapeutic gain. While the mechanisms influencing their recruitment out of the circulation, differentiation, and dominant function are undefined, their application and our developing ability to manipulate their multifaceted role during angiogenesis offers promising potential for future therapies. This section will overview just a small sampling of the many studies (pre-clinical and clinical) that have explored cell-based angioregulation therapies where a pericyte-like role has either been explicitly mentioned or indirectly implicated (Figure 4.5; Table 4.2).

As mentioned above, it has been suggested that MSCs can be derived from multiple tissue sources, including circulating blood. Our group was among the first to attribute a pericyte-like role to MSCs harvested from adipose tissue (Figure 4.6). Passaged MSCs from adipose tissue (also known as hASCs) were injected I.P. into Nude mice that had been stimulated by Compound 48/80 to invoke angiogenesis in the mesenteric tissues[488]. Ten days later, the injected cells exhibited pericyte-like morphologies, expressed NG2 and SMA, and significantly increased vascular density. These effects persisted out to sixty days, suggesting that the injected MSCs may have differentiated into vessel-stabilizing pericytes. In the setting of diabetic retinopathy, Mendel el al.[74] also very recently demonstrated that MSCs obtained from human and mouse adipose tissue, operating in a pericyte-like capacity, stabilized the compromised vasculature in different murine models of retinal vasculopathies, including oxygen-induced retinopathy and Akimba diabetic mice. The authors showed that injected MSCs integrated alongside host endothelial cells in a

vasculoprotective mechanism that was strengthened with TGF-β1 treatment, across all three murine models of disease.

Cardiac and peripheral ischemic diseases also represent potential uses for MSC-pericytes. Katare et al.[489] evaluated the effects of BMSC pericyte progenitor cells in an infarcted heart model and concluded that the delivered cells worked through a paracrine mechanism to reduce myocardial scaring, apoptosis, and fibrosis, while increasing vascular stability and attenuating permeability. In the setting of peripheral ischemic disease, Rehman et al.[413] reported that MSCs from adipose tissue increased endothelial cell growth and reduced endothelial apoptosis in a pericyte-like manner. In a model of hindlimb ischemia, perfusion recovery was accelerated when MSCs from adipose tissue were injected.

Another promising application of MSCs is in cutaneous wound healing. Kim et al.[490] demonstrated that topical transplantation of allogeneic MSCs in canine cutaneous wounds increased the rate of wound closure and degree of collagen production, cell proliferation, and angiogenesis primarily through paracrine effects on the local cell population. Using a model of delayed diabetic wound healing, Amos et al.[491] demonstrated that topically applied MSCs from adipose tissue also increased rate of wound closure through the production of extracellular matrix proteins and soluble factors. Similar results were obtained in a clinical trial by Vojtassak et al.[452] using autologous MSCs derived from bone marrow. In this study, a chronic non-healing diabetic ulcer was treated with BMSCs and autologous skin fibroblasts delivered in a collagen membrane. The ulcer experienced increased vascularity and dermis thickness, as well as significant wound closure over the 29 days of treatment. While pericytes were not explicitly monitored in any of these wound healing studies, each reported increases in vascularity, which is consistent with pericyte contributions.

Future studies like the examples detailed above will serve to transcend our understanding of MSC and pericyte functionality, especially in a therapeutic context. Whether or not MSCs and pericytes share a common lineage, the ease of culture expansion and transplantation make MSCs an attractive cell source for therapeutic angioregulation in different disease settings.

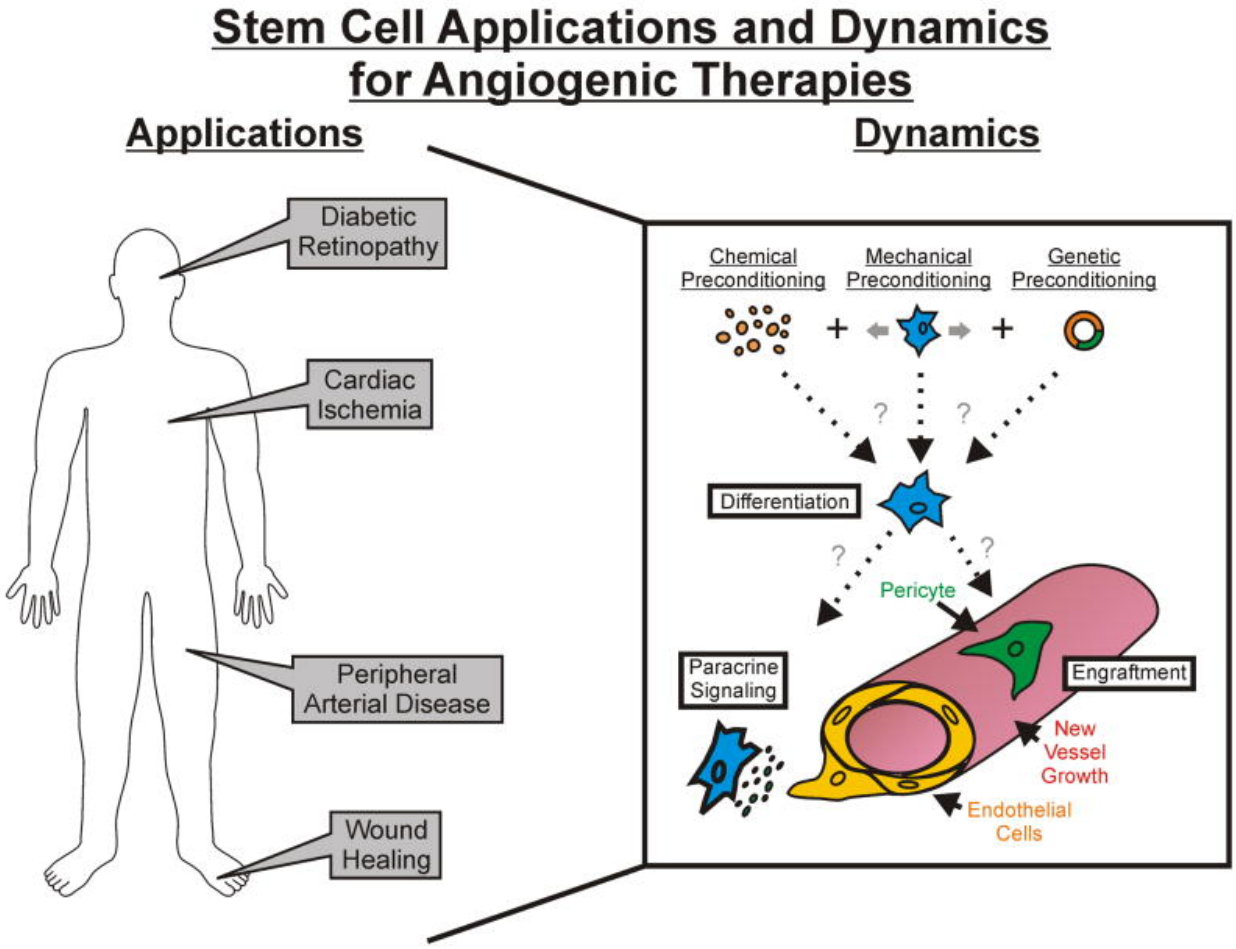

Figure 4.5 The application of MSCs in cell-based therapies to manipulate angiogenesis.

The integrated schematic highlights the wide range of disease scenarios that can be targeted and the approaches to influence MSC fate and function for capillary sprouting. We hypothesize that optimal therapies will result from a combination of chemical, mechanical, and genetic preconditioning modalities. The embedded Table 2 details the pathology and delivery method for recent examples of stem cell therapeutic use.

Table 4.2: MSC / Pericyte Therapeutic Uses			
Pathology	**Delivery Method**	**Fate / Function**	**Citation**
Infantile Hemangioma	Subcutaneous Matrigel	Pervascular Niche / Endothelial Cell Contact Mediated Vessel Formation	Boscolo, et al. Arterioscler Thromb Vasc Biol. 2011. (15)
Diabetic Retinopathy	Intravitreal Injection	Perivascular Niche / Vessel Stabilization	Mendel, et al. PLOS ONE. 2013. (61)
Myocardial Infarction	Intracardiac Injection	Perivascular Niche / Paracrine Signaling	Katare, et al. Circ Res. 2011. (49)
Bone Defects	Ectopic Intramusclar Implant	Osteoblast / Vascularized Bone Regeneration	Askarinam, et al. Tissue Eng Part A. 2013. (7)
Multiple Sclerosis	Intravenous Injection	Undetermined / CNS Inflammation Reduction	Cohen. Neurology. 2012. (21)
Malignant Gliomas	Intravenous Injection	Perivascular Niche / Tumor-Directed Migration	Bexell. Mol Ther. 2009. (13)
Bronchopulmonary Dysplasia	Intratracheal Injection	Perivascular Niche / Paracrine Signaling	Pierro, et al. Thorax. 2013. (75)

Table 4.2 Therapeutic uses for mesenchymal stem cells and pericytes. *Citations from publication*.

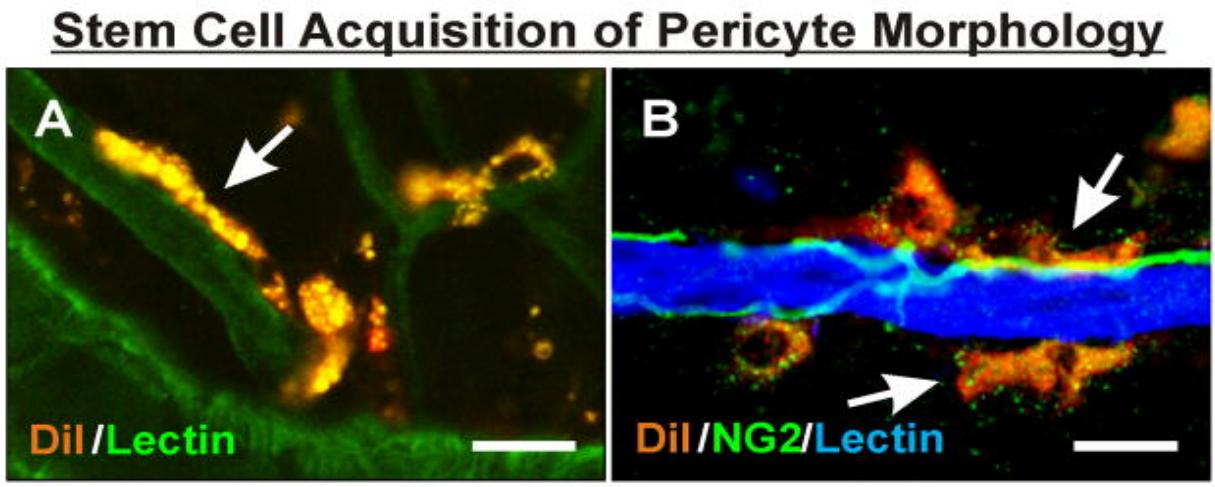

Figure 4.6 MSCs from adipose tissue adopt a pericyte fate *in vivo* after therapeutic delivery. DiI-labeled MSCs from human adipose tissue were injected intraperitoneally and identified in the inflamed Nude rat mesentery (**A**; (4)) or injected intravenously and identified in the ischemic spinotrapezius muscle of NOD-SCID mice (**B**). In both tissues, injected MSCs (arrows) were observed aligning along BSI-Lectin-positive capillaries in a manner similar to native pericytes and exhibited morphologies similar to that of native pericytes. NG2 labeling in (**B**) also identifies nerves. Scale bar = 10 μm.

Future Perspective

Pericytes have recently attracted a lot of attention from the research community at large. Moving forward, new model systems and imaging approaches will greatly advance our understanding of their dynamics, functionality, and phenotypic flexibility. The ability to monitor and track endogenously-labeled pericytes *in vivo* using confocal imaging and other high-resolution intravital imaging approaches enables us to observe the dynamic behaviors of cells in tissues, such as the ear[401]. *Ex vivo* explant systems where pericytes can be labeled and dynamically visualized will also help us learn how they interact with the microvasculature and other cell types throughout the tissue space and over time[47]. Using these and other new tools will help us learn more about pericyte identity and lineage, which in turn will help us leverage our understanding of this unique cell population for therapeutic means. Meanwhile, fundamental questions remain to be answered regarding where pericytes come from, where they go, what they do, and what they can become.

CHAPTER 5

THE LOSS OF PERICYTE-SPECIFIC STEM CELL PLURIPOTENCY GENE OCT4 INHIBITS ANGIOGENESIS

ACKNOWLEDGEMENTS: Daniel L. Hess[1,2], Olga A. Cherepanova[1,4], Anh T. Nguyen[1], Brian H. Annex[1,5], Shayn M. Peirce[1,3], and Gary K. Owens[1,4]

[1] Robert M. Berne Cardiovascular Research Center, University of Virginia, VA, USA
[2] Department of Biochemistry and Molecular Genetics, University of Virginia, VA, USA
[3] Department of Biomedical Engineering, University of Virginia, VA, USA
[4] Department of Molecular Physiology and Biological Physics, University of Virginia, VA, USA
[5] Department of Medicine, Cardiovascular Medicine, University of Virginia, VA, USA

The text included in this chapter has been submitted for publication:
Hess D and Kelly-Goss M (co-first author), Cherepanova O, Nguyen A, Annex B, Peirce S, Owens G. Perivascular cell-specific knockout of the stem cell pluripotency gene Oct4 inhibits angiogenesis in part by attenuating perivascular and endothelial cell migration.

Abstract

Angiogenesis requires coordinated migration of endothelial cells and perivascular cells, including smooth muscle cells and pericytes (together, SMC-P). EC-specific loss-of-function studies have provided key insights into mechanisms whereby EC form nascent vascular tubes and recruit SMC-P. However, far less is known regarding SMC-P specific mechanisms that are critical for stable vascular network formation. Therefore, we used Myh11-CreER^{T2} eYFP lineage-tracing, combined with SMC-P specific knockout of the pluripotency gene Oct4, to test the hypothesis that SMC-P specific Oct4 regulates perivascular cell migration and recruitment necessary for angiogenesis. SMC-P-specific tamoxifen-inducible Oct4 wildtype and knockout Myh11-CreER^{T2} eYFP mice were subjected to corneal alkali burn or hindlimb ischemia (HLI). SMC-P Oct4 knockout mice had decreased eYFP+ SMC-P cell density, impaired eYFP+ and CD31+ EC migration, and increased vascular leak following corneal alkali burn. SMC-P Oct4 knockout mice had impaired perfusion recovery and decreased eYFP+ and EC density following HLI. SLIT3 was expressed in eYFP+ vessels in cornea and hindlimb muscle and was decreased *in vivo* following SMC-P Oct4 knockout. RNA-seq and qRT-PCR analysis of cultured SMC showed that loss of Oct4 was associated with dysregulated expression of multiple Slit-Robo family members, including downregulation of *Slit3*, but upregulation of *Slit2*. SLIT3 increased, whereas SLIT2 decreased, EC migration *in vitro* suggesting that the impaired EC migration in SMC-P Oct4 KO mice may be due in part to decreased Slit3 and increased Slit2 expression by perivascular cells. Thus, we believe SMC-P specific Oct4 is essential for angiogenesis following both corneal alkali burn and HLI. SMC-P Oct4 knockout was associated with impaired migration of both SMC and EC, which we postulate was due in part to dysregulation of Slit-Robo signaling and EC-SMC-P crosstalk.

Introduction

Angiogenesis, the growth of new blood vessels from a pre-existing vasculature, is critical for supply of blood and nutrients to tissues during development and throughout adult life, both under physiologic and pathophysiologic conditions. Lack of a robust angiogenic response in the setting of ischemic diseases such as peripheral arterial disease (PAD) contributes to worse patient outcomes. Conversely, excessive or aberrant (e.g. inadequate perivascular cell investment) angiogenesis is a hallmark of numerous pathologies, including cancer and ocular diseases, such as wet macular degeneration and diabetic retinopathy.[492-494] Angiogenesis requires coordinated movement of the two major cell types of the blood vessel wall: 1) endothelial cells (EC), which line the inner lumen, and 2) perivascular cells [smooth muscle cells (SMC) and pericytes], which enwrap EC. In general, SMC concentrically wrap arteries, arterioles, veins, and venules which have diameters >10μm, while pericytes extend longitudinally along capillaries <10μm in diameter. Despite these distinct anatomical differences, SMC and pericytes often express many common proteins including ACTA2, MYH11, and PDGFR-β, which vary in expression across different vascular beds under both normal and pathologic conditions.[420] Indeed, no marker or set of markers known to date is able to unequivocally distinguish between SMC and pericytes.[420]

During angiogenesis, EC and SMC-pericyte (SMC-P) communication is essential for new blood vessel formation.[495] Global genetic knockout (KO) studies have identified a number of pathways critical in EC-SMC-P cross-talk, including PDGF-B/PDGF-Rβ, ANG/TIE2, TGFβ, S1P, and Notch, among others[419,495-497]. In general, knockout of genes in these pathways results in improper EC and SMC-P function, including their decreased association with one another,[498-502] often leading to increased vascular leak and hemorrhaging.[503,504] Therefore, perivascular cell investment of EC tubes is critical for normal function and stability of vascular networks. [503,504] [398] However, to

determine which cell type(s) and gene(s) drive specific phenotypes, cell-specific loss-of-function studies involving candidate genes are required.

EC-specific deletion of genes, such as *Pdgfb*[66,505], *Notch*[506-508], and others[509-511] result in impaired angiogenesis, demonstrating that EC play a critical role in regulating angiogenesis. Extensive insight into VEGF-induced EC filopodia guidance[18] and DLL4-NOTCH specification of EC tip cell migration and stalk cell proliferation[425] provide further evidence that EC can drive angiogenesis, and in turn recruit SMC-P to invest newly formed EC tubes.[492,493] However, to our knowledge, comparable SMC-P specific conditional loss-of-function studies have not been performed. Several studies have shown that genetic loss or mutations of PDGF-Rβ[496] or *Pdgfrb-Cre* mediated knockout of genes such as *Ephrin-B2*[512] or *CD146*[513] resulted in impaired angiogenesis, including defective SMC-P investment of EC tubes and increased vascular leak. However, PDGF-Rβ was deleted throughout development and is expressed in multiple cell types, including fibroblasts, myofibroblasts, macrophages, and neurons.[420] A recent study demonstrated that inducible *Pdgfrb-Cre* mediated ablation of pericytes or deletion of *flt1* results in impaired retinal angiogenesis, including defective endothelial cell sprouting.[514] These studies suggest that PDGF-Rβ+ SMC-P play a critical role during normal developmental and postnatal angiogenesis. However, to our knowledge, no studies to date have examined whether SMC-P play a direct role during angiogenesis following injury. Indeed, a widely held belief in the field is that, although SMC-P are critical for angiogenesis, they play a more passive role, mostly responding to signaling initiated by EC and subject to modulation by factors secreted by macrophages as well as other mesenchymal cells.[492,493] Taken together, studies underscore the fact that, in spite of overwhelming evidence that investment of nascent endothelial tubes with perivascular cells is critical in formation

of stable and functional vascular networks, there is as yet little evidence that perivascular cells play a direct regulatory role in this process.

Recently, our lab demonstrated that the stem cell pluripotency gene *Oct4* (also known as *POU5F1*), previously thought to be permanently epigenetically silenced in all somatic cells, is reactivated in SMC in the setting of atherosclerotic disease.[515] Moreover, we showed that SMC-specific conditional knockout of Oct4 resulted in marked exacerbation of atherosclerosis due to impaired migration and investment of SMC-derived cells into the lesion and the failure to form a SMC-rich protective fibrous cap. However, Oct4-dependent migration clearly did not evolve as a response to atherosclerosis, a disease whose clinical manifestations occur well after our reproductive years. Rather, herein we hypothesize that SMC-P derived Oct4 is essential for SMC-P migration and investment of blood vessels during angiogenesis following injury. We demonstrate that SMC-P specific conditional deletion of the stem cell pluripotency factor Oct4 results in markedly impaired angiogenesis in both corneal burn and hindlimb ischemia (HLI) models. We also present evidence showing that knockout of Oct4 results in numerous downstream changes including dysregulated expression of multiple members of the Slit-Robo pathway, which may have contributed to impaired SMC-P and EC migration and cell-cell communication. To our knowledge, this is the first direct evidence that conditional loss of a single gene in SMC-P can impact angiogenesis following injury.

Material and Methods

Mice

Myh11-CreER^{T2} ROSA floxed STOP eYFP Oct4$^{FL/WT}$ mice were generated as previously described.[515] Briefly, we first bred Oct4$^{FL/FL}$ (Pou5f1^{tm1Scho}) mice with Myh11-CreER^{T2} (Tg(Myh11-cre/ERT2)1Soff)[3] mice to generate Oct4$^{FL/WT}$Myh11-CreER^{T2} mice. The Myh11-CreER^{T2} transgene is on the Y chromosome, precluding the use of Cre-negative mice as controls. We then bred Myh11-CreER^{T2} Oct4$^{FL/WT}$ males with Oct4$^{FL/WT}$ females to generate Myh11-CreER^{T2} Oct4$^{FL/FL}$ and Myh11-CreER^{T2} Oct4$^{WT/WT}$ male littermates. We then crossed ROSA26-STOP^{flox}YFP$^{+/+}$ mice (B6.129X1-Gt(ROSA)26Sortm1(eYFP);Cos/J) with Myh11-CreER^{T2} mice to yield Myh11-CreER^{T2} ROSA26-STOP^{flox}YFP$^{+/+}$ mice using the same strategy described above. We then crossed Oct4$^{FL/FL}$;Myh11-CreER^{T2} male mice with Myh11-CreERT2 ROSA26-STOP^{flox}YFP$^{+/+}$ mice to generate Oct4$^{FL/WT}$ Myh11-CreER^{T2} ROSA floxed STOP eYFP males and Oct4$^{FL/WT}$ROSA floxed STOP eYFP female mice. To generate mice on a congenic C57BL/6 background, we backcrossed these mice to C57BL/6 mice (Jackson Labs; Bar Harbor, ME) for nine generations. We then used these mice as breeders to generate Myh11-CreER^{T2} ROSA floxed STOP eYFP Oct4$^{WT/WT}$and Myh11-CreER^{T2} ROSA floxed STOP eYFP Oct4$^{FL/FL}$ male littermate mice which were genetically identical other than containing WT versus floxed Oct4 alleles. We achieved Cre-mediated recombination via ten daily intraperitoneal injections of tamoxifen (Sigma-Aldrich; St. Louis, MO) (1mg in 100 µl of peanut oil (Sigma-Aldrich; St. Louis, MO)) between 6-8 weeks of age. All experimental mice received identical amounts of tamoxifen. We only used male progeny for experiments, since the Myh11-CreER^{T2} transgene is located on the Y chromosome. Upon tamoxifen treatment, there is simultaneous activation of eYFP and excision of the floxed Oct4 alleles, generating Myh11-CreER^{T2} ROSA eYFP Oct4$^{WT/WT}$and Myh11-CreER^{T2} ROSA eYFP Oct4$^{\Delta/\Delta}$ mice. Henceforth, we refer

to them as Oct4$^{SMC\text{-}P\ WT/WT}$ and Oct4$^{SMC\text{-}P\ \Delta/\Delta}$, for simplicity. At 12-16 weeks of age, mice were used for experiments. We also crossed our Myh11-CreER^{T2} ROSA floxed STOP eYFP mice with NG2-DsRED (Tg(Cspg4-DsRed.T1)1Akik/J) (Jackson Labs; Bar Harbor, ME) mice to generate NG2-DsRED Myh11-CreER^{T2} ROSA floxed STOP eYFP mice. We treated these mice with the same tamoxifen protocol outlined above to generate NG2-DsRED Myh11-CreER^{T2} ROSA eYFP mice. Protocols for experiments involving mice were approved by and done in accordance with the University of Virginia Animal Care and Use Committee.

Blood pressure telemetry

Blood pressure and heart rate were measured using radiotelemetry units (Data Sciences International; St. Paul, MN). The catheter of a radiotelemetry unit was inserted into the left carotid artery and the radiotransmitter was placed in a subcutaneous pouch on the right flank. Blood pressure was recorded for 5 minutes per hour for 2 days on, then five days off, for a total of 10 days of recording. Recordings were limited to weekend days to minimize noise and stress-related fluctuations in blood pressure.

Corneal alkali burn model

Corneal alkali burn surgery was performed as previously described.[516,517] At 12-16 weeks of age, mice were anesthetized with isofluorane (2% isofluorane, 200 ml/min flow rate). A drop of sterile 0.5% Proparacaine Hydrochloride Ophthalmic Solution was added as a topical anesthetic to numb the eye two minutes prior to burn and another drop applied immediately prior to burn. Corneal alkali burn was induced by applying applicator sticks coated with 75% $AgNO_3$/25% KNO_3 (SnypStix by Grafco; Atlanta, GA) to the center of the right cornea for 10 seconds. An additional

drop of Proparacaine was applied to the right cornea immediately post-burn, and mice received post-operative analgesic (buprenorphine 0.1-0.2 mg/kg subcutaneous). For each experimental mouse, the contralateral eye remained unburned and untreated.

Intravital confocal microscopy

Intravital confocal microscopy of the cornea was performed as previously described.[4] Briefly, animals were anesthetized with an intraperitoneal injection of ketamine/xylazine/atropine (60/4/0.2 mg/kg body weight) (Zoetis; Kalamazoo, MI/West-Ward; Eatontown, NJ/Lloyd Laboratories; Shenandoah, IA). A drop of sterile 0.5% Proparacaine Hydrochloride Ophthalmic Solution was added as a topical anesthetic to numb the eye before imaging. Ophthalmic lubricant Genteal gel (Alcon; Fort Worth, TX) was applied to the eye during imaging to prevent drying. Mice were placed on a microscope stage that contained a warming pad to maintain a constant body temperature of 37°C, eyelashes and whiskers were gently pushed back with ophthalmic lubricant Genteal gel, and the snout was gently restrained with a nosecone. Mice were imaged immediately (within ten minutes) prior to injury (day 0), and then at days 3, 7, and 21 post-injury on a confocal microscope (Nikon Instruments Incorporated, Melville, NY; Model TE200-E2; 10X, 20X, and 60X objectives optimized for 3 channels-laser excitation wavelengths at 488, 543, and 632). Immediately prior to each round of imaging, mice were perfused with isolectin GS-IB4 (lectin) or rhodamine-dextran (MW 70 kDa, Sigma-Aldrich) via retro-orbital injection into the contralateral eye to visualize perfusion-competent vasculature. During imaging, the right eye was placed against a coverslip that rested on the stage of the inverted confocal microscope. The entire portion of the eye that rested on the stage, or approximately one quarter of the entire corneal circumference, was imaged on 20x or 60x magnification by taking multiple fields of view (FOV) using Z-stack

imaging through the entire cornea thickness. Each FOV was then compressed into a maximum intensity projection. All FOV from each eye were stitched together into montages using Adobe Illustrator and then analyzed as described below. Researchers were blinded to the genotype of the animals until the end of analysis.

Quantification of intravital confocal microscopy images

To rigorously quantify the number of eYFP+ cells within each montage, the corneal vascular networks were divided into distinct regions, numbers of eYFP+ cells counted within each of those regions, and then that number divided by the area of the respective region to account for differences in area between each mouse. The number of cells on the arteriole-venule (A-V) pair was counted to determine the number of eYFP+ cells per A-V pair. To quantify number of eYFP+ cells beyond the A-V pair in the direction of the center of the cornea, we divided the vascular network into 50 μm regions, where 50 μm was measured from the A-V pair towards the cornea center along the entire length of the montaged image. The number of eYFP+ cells in each of these regions was counted and normalized as described above. Following corneal burn, the total vascular area extending beyond the A-V pair is referred to as the neovascular area. The neovascular area plus the A-V pair is referred to as the network area. Researchers were blinded to the genotype of the animals until the end of analysis.

Bright Field Microscopy

Bright field images of corneas under 4X magnification were obtained using a Nikon Digital Sight DS-L2 Camera Controller (Nikon Instruments Inc, Melville, NY; Model 214602) to assess the

network-wide hierarchy of neovessels and determine the macrostructural health of the tissue. For each mouse, multiple fields of view were taken encompassing the entire circumference of the eye.

Quantification of hemorrhaging in bright field microscopy images

Corneal hemorrhaging in bright field montages was graded on a scaled score from 0-7, adapted from Kisucka et al.[518] In our scoring system, 0 = no hemorrhages; 1 = 1 hemorrhage; 2 = 2-3 hemorrhages, healthy corneal tissue; 3 = 2-3 hemorrhages, disrupted corneal tissue; 4 = continuous hemorrhage, healthy corneal tissue; 5 = 3 – 4 hemorrhages, torn corneal tissue; 6 = continuous hemorrhaging, torn corneal tissue; 7 = completely ruptured cornea, lens ruptured from tissue. Researchers were blinded to the genotype of the animals until the end of analysis.

Rhodamine dextran injections and quantification

Following anesthetization with ketamine/xylazine/atropine, mice were administered a retro-orbital injection of 70kDa rhodamine-dextran (Sigma-Aldrich) immediately prior to imaging, such that movie recording started < 5 minutes post-injection. Digital images of the vascular networks were acquired using a NikonTE200-E2 confocal microscope, as described above. One field of view per cornea was imaged with full-thickness Z-stacks (25-30 slices at 3 μm between each slice) on repetition for 90 minutes. Volume renders of z-stacks, using the maximum intensity projection, were used to capture the entire corneal vascular network in the field of view. Movie files were analyzed in ImageJ, where we measured the mean pixel intensity in three equal-size regions of interest (ROIs) that were evenly distributed across three different areas in the field of view (above limbus, in vascular loops within the limbus, and below the A-V pair defining the start of the limbus), for a total of nine ROIs being analyzed per frame. The three ROIs within a given area

were then averaged for each frame and recorded as a single value. These values were then plotted against time. Finally, we quantified the Area Under the Curve to capture the total leak of dextran from the mouse over time. Mice were imaged at day 3 post corneal-burn.

Whole Mount Cornea Immunostaining and Quantification

Mice were euthanized by CO_2 asphyxiation and then whole corneas, including the limbus, were removed and washed 3x10 min in phosphate-buffered saline (PBS; Life Technologies; Carlsbad, CA) in 0.5 ml Eppendorf tubes. Corneas were then fixed in 1% paraformaldehyde (PFA; Electron Microscopy Sciences; Hatfield, PA) for 45 min, followed by blocking for 1 hour in blocking buffer containing 2% Bovine serum albumin (BSA; Roche; Indianapolis, IN), 10% horse serum, and 0.2% saponin in PBS. Primary anti-GFP antibody (Abcam ab6673, 1:100) was added overnight at 4°C in blocking buffer. Corneas were then washed in PBS+0.2% saponin and stained for 1.5 hours in blocking buffer with CD31 (Dianova 310, 1:250) and/or Slit3 (Sigma SAB2104337, 1:50). Corneas were then washed in PBS+0.2% saponin, followed by staining with appropriate secondary antibodies (Alexafluor, 1:250) for 1.5 hours in blocking buffer. Corneas were washed in PBS+0.2% saponin, stained with DAPI (1:100) for 10 min, washed with PBS, and then flat-mounted on slides using 50/50 PBS/Glycerol. Images were acquired at 10x magnification on a Zeiss LSM700 scanning confocal microscope using full-thickness Z stacks (approximately 15-20 slices at 5μm between each slice). For each cornea, 2-3 FOV from different leaflets were used for analysis. Individual slices were then collapsed into maximum intensity projections for pixel analysis using Image-Pro Plus. Researchers were blinded to the genotype of the animals until the end of analysis.

Whole Mount Retina Imaging

Thirty minutes prior to sacrifice, isolectin (IB4-Alexa647; Life Technologies; Carlsbad, CA) was injected into the mouse tail vein. Mice were euthanized by CO_2 asphyxiation and then whole retinas were removed and flat-mounted on slides to image isolectin plus endogenous NG2-dsRED and eYFP fluorescence. Images were taken on a Zeiss LSM700 scanning confocal microscope on 20x magnification.

Hindlimb ischemia model

Hindlimb ischemia surgery was performed as previously described.[519] At 12-16 weeks of age, mice were anesthetized with ketamine (90 mg/kg) and xylazine (10 mg/kg) and then subjected to unilateral femoral artery ligation and resection. Blood flow in the plantar soles was monitored with a laser Doppler perfusion imaging system (Perimed, Inc, Ardmore, PA) immediately after surgery (day 0) and then at days 3, 7, 14, and 21 post-surgery. Mice were placed on a warming pad during surgery and during laser doppler image acquisition to maintain a constant body temperature of 37ºC. Perfusion was expressed as the ratio of the left (ischemic) to right (nonischemic) hindlimb. The right hindlimb served as an internal control for each mouse. Animals received buprenorphine (intraperitoneal) immediately after surgery and every 8-12 hours thereafter until 48 hours post-surgery.

Harvesting of hindlimb tissue

Mice were euthanized by CO_2 asphyxiation and then perfused through the left ventricle with 5 ml of PBS, followed by 10 ml of 4% Periodate-Lysine-Paraformaldehyde (PLP), followed by 5 ml of PBS. Calf muscle (containing gastrocnemius and soleus muscles) and medial thigh muscle

(containing adductor magnus semimembranosus, semitendinosus, and gracilis muscles) were harvested and fixed for an additional 2 hours in 4% PLP. Tissues were then transferred to 7.5% sucrose in PBS overnight, followed by 15% sucrose in PBS for 4 hours, followed by 30% sucrose in PBS for 2 hours. Tissues were then embedded in OCT compound, frozen in liquid nitrogen, and stored at -80°C until sectioning.

Analysis of hindlimb tissue

Hindlimb muscles were serially sectioned at 5 (calf) or 10 (thigh) μm thickness on a cryostat. For immunohistochemical staining, slides were blocked for 1 hour in blocking buffer containing 10% horse serum + 0.6% fish skin gelatin in PBS. Primary antibodies were added overnight in blocking buffer at 4°C and then washed 2x with PBS-Tween (0.1%). Secondary antibodies were added for 1 hour at room temperature in blocking buffer, washed 2x with PBS-Tween (0.1%), counterstained with DAPI, and cover slipped using Prolong Gold mounting medium. Slides were stained using combinations of the following primary antibodies: GFP (Abcam ab6673, 1:250), CD31 (Dianova 310; 1:250), NG2 Chondroitin Sulfate Proteoglycan (Millipore AB5320, 1:500), PDGFRβ (abcam ab32570, 1:500), and Slit3 (Sigma SAB2104337, 1:50). DAPI (1:100) was used to label nuclei and Alexafluor 555 Phalloidin (1:1000) was used to label muscle fibers. Isotype-matched IgG antibodies were used as a negative control in all instances. All secondary antibodies were Alexafluor and used at 1:250 concentration. Images were acquired using a Zeiss LSM700 scanning confocal microscope. Depending on specific analysis, 3-6 fields of view (FOV) on 10-20x magnification from 1-2 sections/muscle were used for analysis. High-resolution Z-stack analysis was performed using Zen 2009 Light Edition Software to ensure staining was limited to a single cell. For pixelation analysis, Z-stack slices were collapsed into maximum intensity projections and

analyzed using Image-Pro Plus. Researchers were blinded to the genotype of the animals until the end of analysis.

Cell Culture

$Oct4^{+/+}$ and $Oct4^{\Delta\Delta}$ mouse aortic SMC were isolated and cultured as previously described.[1] Cells were maintained in 10% serum-containing media (DMEM/F12 (Gibco), Fetal bovine serum (FBS; GE Healthcare Bio-Sciences; Pittsburgh, PA), 100 U/ml penicillin/streptomycin (Gibco), 1.6 mM/L L-glutamine (Gibco)). For experiments, cells were grown to 80-90% confluency and then switched to serum-free media (SFM). After culturing in SFM for 2 days, passages 5-13 of mouse aortic SMCs were harvested for qRT-PCR analysis. Mouse aortic EC were purchased from Cell Biologics (C57-6052) and maintained in complete mouse endothelial cell medium plus kit (M1168).

RNA isolation, cDNA preparation, and qRT-PCR

Total RNA was harvested using phenol-chloroform extraction (TRIzol, Life Technologies, Grand Island, NY). 0.5-1 μg of RNA was reverse-transcribed with iScript cDNA synthesis kit (Bio-Rad). Real-time qRT-PCR was performed on a C1000 Thermal Cycler CFX96 (Bio-Rad) using SensiFAST SYBR NO-ROX mix (Bioline) and primers specific for mouse *Robo1*, *Robo2*, *Slit2*, *Slit3*, and *B2M*. Expression of genes was normalized to B2M.

Scratch wound assays

Scratch wound assays were performed in 6 well plates. Once cells were 100% confluent, cells were washed 2x with 1xPBS and placed in SFM for 24 hours. A scratch down the middle of each well

was made using a p200 pipet tip and then media was immediately replaced with SFM containing 1nmol/L SLIT2 (MyBioSource.com, MBS2031306), 1nmol/L SLIT3 (MyBioSource.com, MBS2010323), or Vehicle (PBS). Images were taken immediately after scratch and every 24 hours thereafter for up to 72 hours post-scratch on 4x magnification using an inverted microscope. Prior to cell plating, horizontal lines were made on the underside of each well at 12 mm, 20 mm, and 28 mm from the bottom of each well to ensure the same FOV was imaged at each time point. Numbers of cells that migrated into the scratch were counted in each FOV using ImageJ analysis software. Counts were then averaged together across 9 FOV per condition (3 wells with 3 FOV each).

Statistical Analysis

Statistical analysis was performed using GraphPad Prism Version 7 software. Normality of the data was determined using a Kolmogorov-Smirnov test. For comparison of two groups with normal distribution, an unpaired two-tailed *t*-test was used. For comparison of two groups with non-normal distribution, a Mann-Whitney test was used. For analysis of three or more groups with normal distribution, a two-way ANOVA was used. All results are presented as mean ± SEM. $p < 0.05$ was considered significant. Specific statistical tests and number of mice used for each *in vivo* analysis are reported in the figure legends.

Results

Myh11-CreER^{T2} eYFP efficiently labeled SMC and pericytes in multiple tissues, thus allowing for perivascular cell-specific gene knockout studies

We previously developed a Myh11-CreER^{T2} ROSA floxed STOP eYFP inducible lineage tracing mouse that specifically labels >95% of SMC within large conduit arteries with eYFP following two weeks of tamoxifen injection.[520] Recently, using this mouse, we demonstrated that a subset of eYFP+ cells in the pre-metastatic lungs express the pericyte markers NG2 and PDGFR-β.[521] To determine whether Myh11 efficiently labels pericytes in a number of different microvascular beds, we crossed our Myh11-CreER^{T2} ROSA floxed STOP eYFP mice to NG2-DsRED reporter mice and injected with tamoxifen to generate Myh11-CreER^{T2} ROSA eYFP NG2-DsRED mice (Figure 5.1A). We examined whole mounts of the retina, which has the highest pericyte density in the body,[495] and observed eYFP+ cells surrounding isolectin+ EC tubes, including those of capillary size diameter (Figure 5.1B). There was near complete co-localization of eYFP and NG2-DsRed in pericytes surrounding isolectin+ EC tubes, demonstrating eYFP efficiently labels NG2+ pericytes in the retina (Figure 5.1C). We then examined the limbal vasculature of the cornea and again observed labeling of NG2-DsRED+ cells with eYFP (Figure 5.1D). We next used our Myh11-CreER^{T2} ROSA eYFP lineage-tracing mice (Figure 5.1E) to quantify efficiency of eYFP labeling of pericytes in calf muscle vasculature. We found that approximately 80% of eYFP+ cells surrounding CD31+ capillaries express multiple pericyte markers, including NG2 and PDGFR-β (Figure 5.1F through 1H). Over 90% of NG2+ cells express eYFP and 80% of PDGFR-β+ cells express eYFP (Figure 5.1I), consistent with the fact that other cells in muscle e.g. interstitial fibroblasts can also express PDGFR-β.[419] Taken together, our results demonstrate that Myh11 labels both SMC[520] and a large subset of pericytes within

multiple tissues. Using Myh11-driven CreER^{T2}, we can therefore conditionally delete genes of interest in both SMC and pericytes to test their functional role in these cell types.

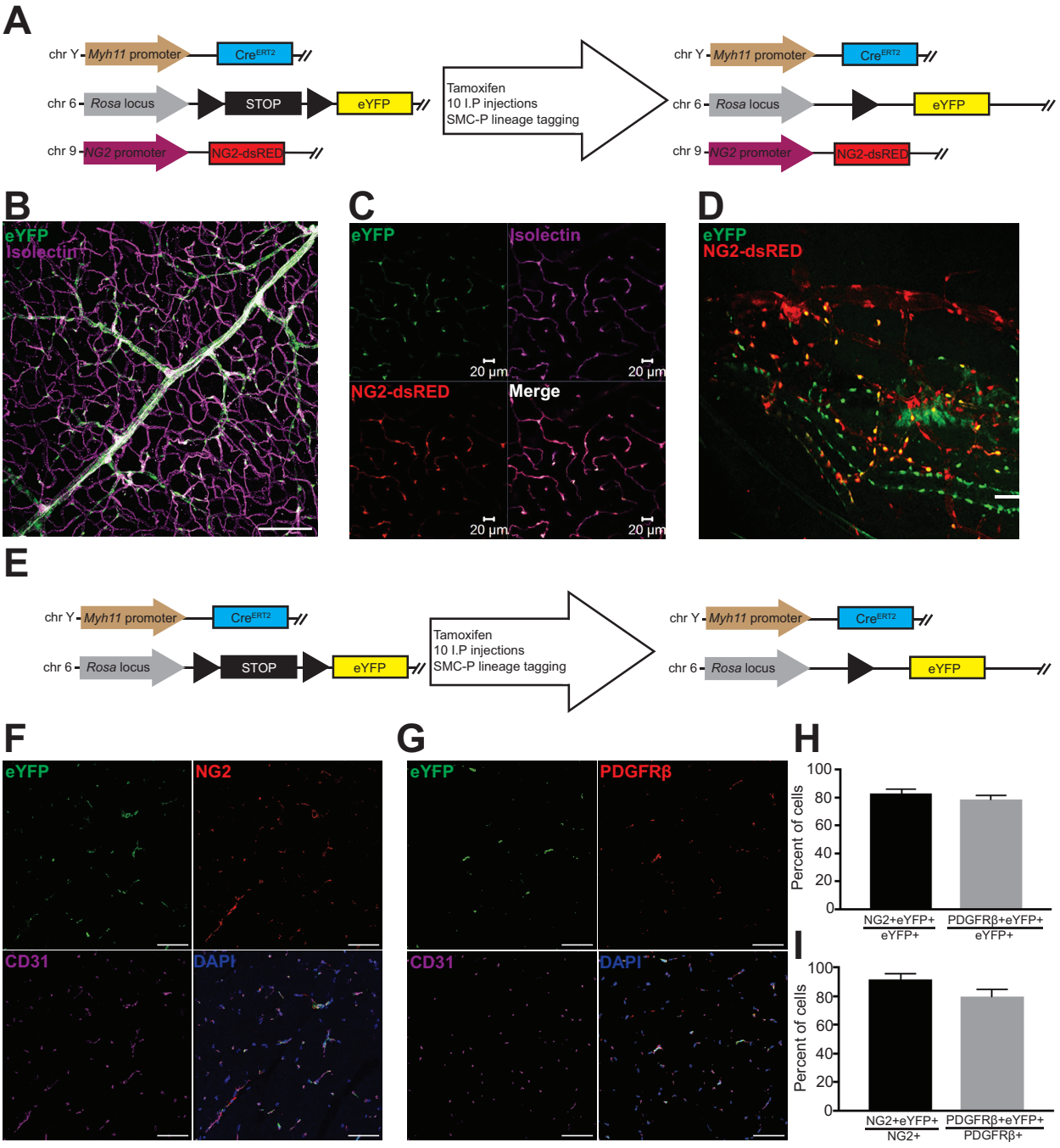

Figure 5.1 Myh11-CreER^{T2} ROSA eYFP efficiently labeled SMC and a large subset of pericytes in multiple microvascular tissue beds.

(**A**) Schematic showing crossing of Myh11-CreER^{T2} ROSA floxed STOP eYFP mice with NG2-DsRED mice plus tamoxifen injection to generate NG2-DsRED Myh11-CreER^{T2} ROSA eYFP

mice. (**B-C**), Imaging of retina whole mounts for eYFP, NG2-DsRED, and isolectin. Scale bar in B = 100 μm. Scale bar in C = 2 μm. (**D**), Intravital microscopy of cornea limbal vasculature for eYFP and NG2-DsRED. (**E**), Schematic showing Myh11-CreER^{T2} ROSA eYFP mice. (**F-G**), Co-staining of uninjured calf muscle cross sections from Oct4$^{SMC\text{-}P\ WT/WT}$ mice for DAPI, eYFP, and NG2 (F) or PDGFR-β (G). Scale bars = 50μm (**H-I**), Quantification of percentages of dual positive cells within calf muscle (n=4 mice).

SMC-P specific knockout of the stem cell pluripotency gene Oct4 resulted in impaired angiogenesis following corneal burn, including impaired migration of SMC-P and EC and increased vascular leakage

To knock out *Oct4* and determine its role in Myh11-expressing SMC-P, we injected Myh11-CreER^{T2} ROSA floxed STOP eYFP Oct4$^{WT/WT}$ and Myh11-CreER^{T2} ROSA floxed STOP eYFP Oct4$^{FL/FL}$ male littermate mice with tamoxifen from 6-8 weeks of age, as previously described.[515] This induces lineage tagging of Myh11-expressing cells, without and with *Oct4* knockout respectively, to generate Myh11-CreER^{T2} ROSA eYFP Oct4$^{WT/WT}$ and Myh11-CreER^{T2} ROSA eYFP Oct4$^{\Delta/\Delta}$ mice (Figure 5.2A through 2B). Henceforth, for simplicity, we refer to them as Oct4$^{SMC\text{-}P\ WT/WT}$ and Oct4$^{SMC\text{-}P\ \Delta/\Delta}$, respectively. We previously showed that Oct4 is reactivated in diseased blood vessels and that, following tamoxifen injection, Oct4 knockout recombination efficiency is greater than 95% in SMC-P.[515]

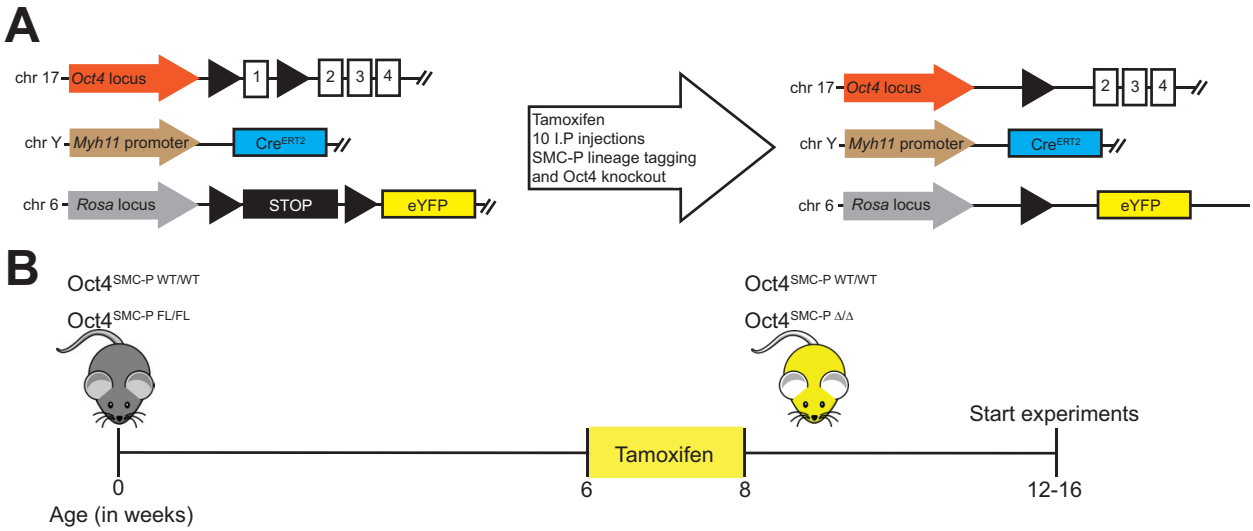

Figure 5.2: Mice with zero or two Oct4 floxed alleles were injected with tamoxifen to allow simultaneous SMC-P lineage tagging and Oct4 KO.

(**A**), Myh11-CreER^{T2} ROSA floxed STOP eYFP Oct4$^{WT/WT}$ and Myh11-CreER^{T2} ROSA floxed STOP eYFP Oct4$^{FL/FL}$ male littermate mice were injected with tamoxifen (10 intraperitoneal injections) from 6-8 weeks of age to induce simultaneous lineage tagging, without or with Oct4 KO, respectively. For simplicity, we refer to them henceforth as Oct4$^{SMC\text{-}P\ WT/WT}$ and Oct4$^{SMC\text{-}P\ \Delta/\Delta}$, respectively. (**B**), At 12-16 weeks of age, mice were used for the start of experiments.

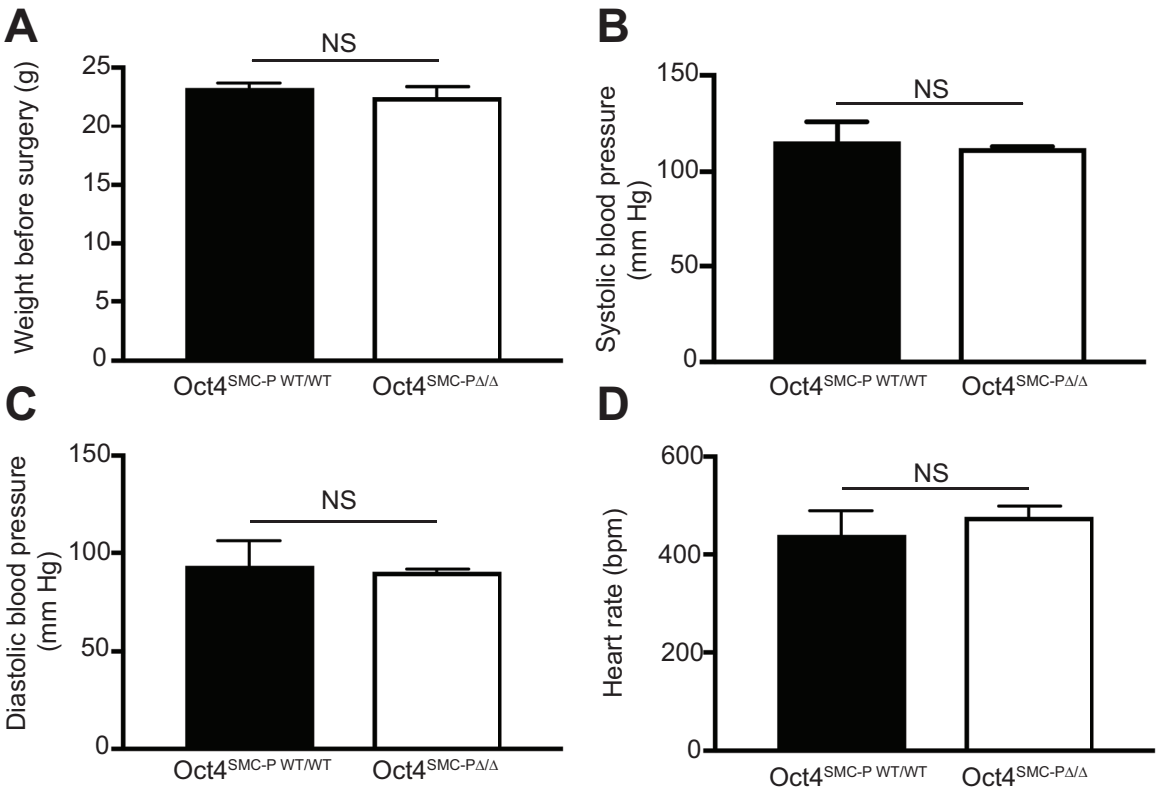

Figure 5.3 There were no baseline differences in weight, blood pressure, or heart rate following SMC-P specific Oct4 KO.

(A), Weight of mice (g) immediately prior to surgery (n=8WT, 8 KO). **(B-D)**, A catheter-based radiotelemetry system was used to monitor systolic blood pressure (B), diastolic blood pressure (C), and heart rate (D) (N=4 WT, 5 KO). Values = mean ± SEM. *P* = NS using unpaired *t*-test (A) or Mann-Whitney (B-D).

We first determined whether loss of *Oct4* in Myh11-expressing SMC-P results in any effects prior to injury. Twelve-sixteen week old $Oct4^{SMC\text{-}P\ \Delta/\Delta}$ mice did not show any significant changes in total body weight, blood pressure, or heart rate, compared to littermate controls (Figure 5.3A through 3D). To test whether SMC-P-specific Oct4 plays a functional role during angiogenesis, we subjected 12-16 week old $Oct4^{SMC\text{-}P\ WT/WT}$ and $Oct4^{SMC\text{-}P\ \Delta/\Delta}$ mice to corneal alkali burn injury (Figure 5.4A), as previously described.[517] Prior to burn, there is limbal vasculature encircling the cornea circumference, including an arteriole-venule (A-V) pair as well as a vascular network that extends approximately 200 μm away from the main A-V pair towards the center of the cornea (Figure 5.5). Following corneal burn, the limbal vasculature gives rise to angiogenic sprouts that extend towards the alkali burn in the center of the cornea (Figure 5.6) We used intravital confocal microscopy to visualize eYFP+ cells prior to corneal burn (day 0) and during angiogenesis towards the burn site at days 3, 7, and 21 post-corneal burn. We administered Alexaflour-647-labeled isolectin GS-IB4 (lectin) via retro-orbital injection ten minutes prior to imaging in order to label EC and to visualize perfusion-competent vasculature.

Figure 5.4 *(Next page)* SMC-P specific conditional knockout of *Oct4* resulted in reduced density and impaired migration of SMC-P eYFP+ cells throughout the network following corneal burn.

(**A**), Schematic outlining experimental design. (**B**), Representative intravital confocal microscopy images for eYFP (green) and isolectin GS-IB4 (lectin, blue) at days 0, 3, 7, and 21 post-corneal burn. Scale bar = 50 μm (**C-F**), Quantification of the number of eYFP+ cells per area at days 0, 3, 7, and 21 post-burn [n = 8 (C, D); 6 (E); 4 (F) per genotype]. Areas quantified are described in Supplemental Figures 4 and 5. Values = mean ± SEM. ****$P < 0.0001$ using two-way ANOVA.

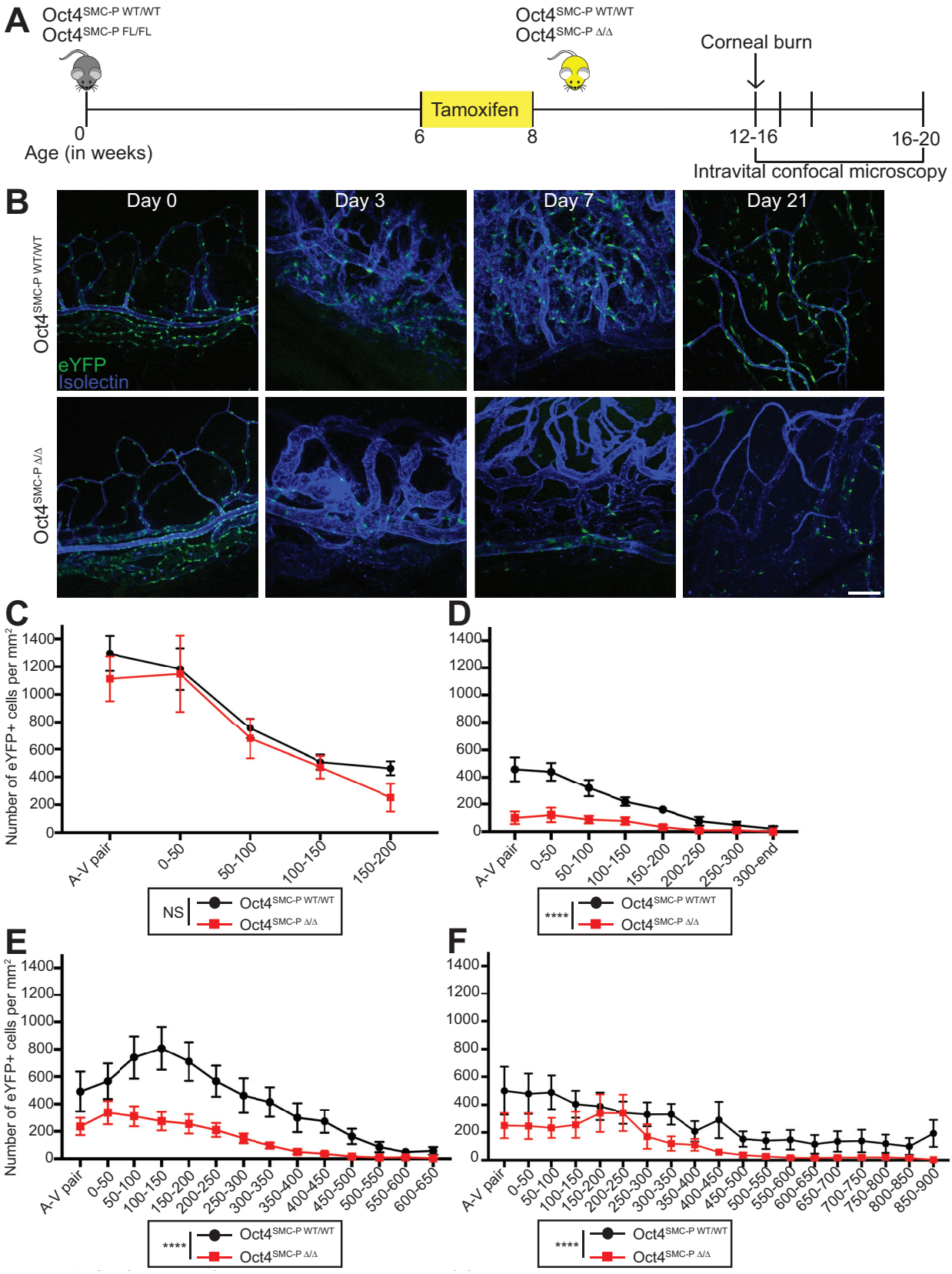

Figure legend on previous page.

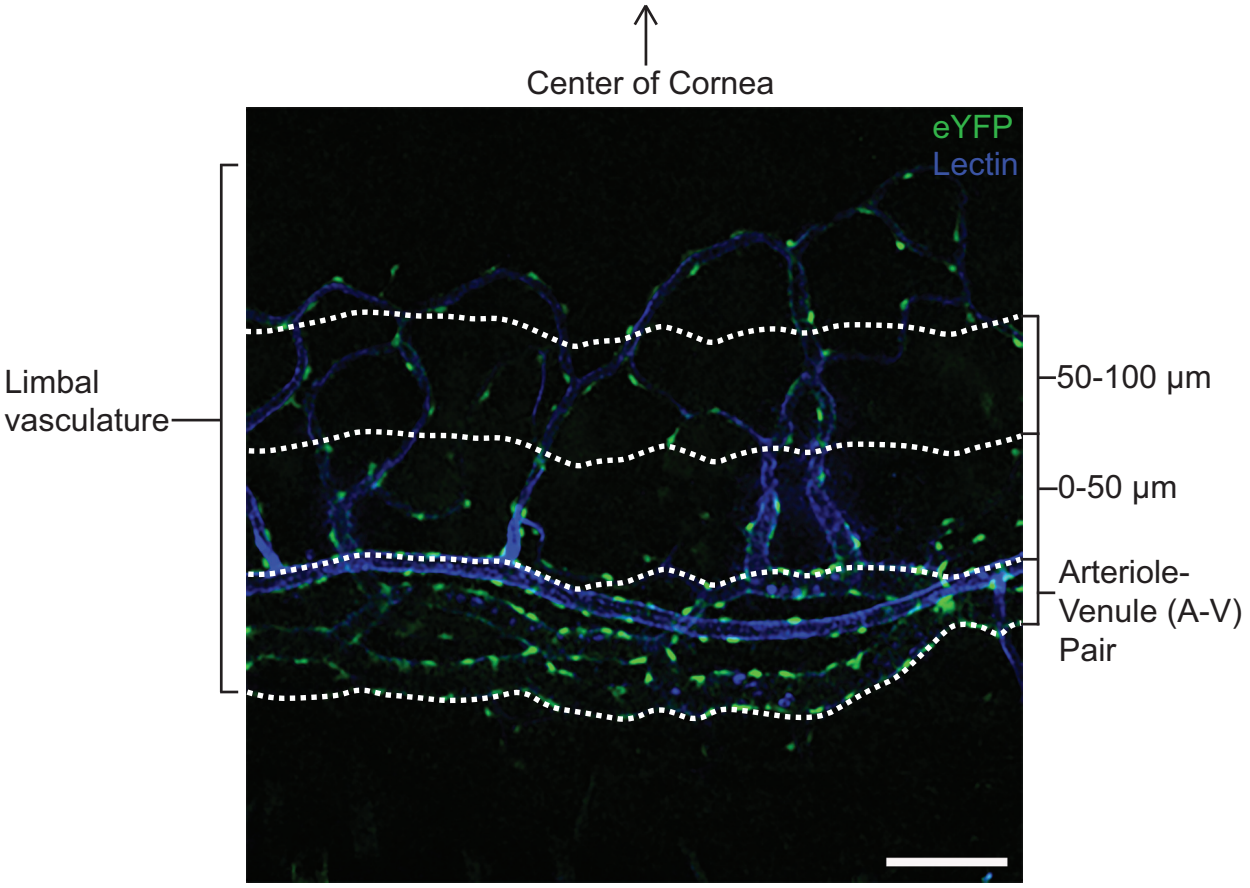

Figure 5.5 Intravital microscopy of baseline limbal vasculature, which consists of an arteriole-venule (A-V) pair and a vascular network that extends approximately 200 μm beyond.

At baseline (prior to injury), there is limbal vasculature consisting of a main arteriole-venule (A-V) pair at the base of the vascular network as well as vessels extending approximately 200 µm away from the A-V pair toward the center of the cornea. To more rigorously quantify number of cells in the limbal vasculature, we divided this region in to 50 μm regions, where 50 μm was measured from the edge of the A-V pair towards the center of the cornea along the total width of the montaged image. eYFP is in green and perfused isolectin is in blue. Scale bar = 50 µm.

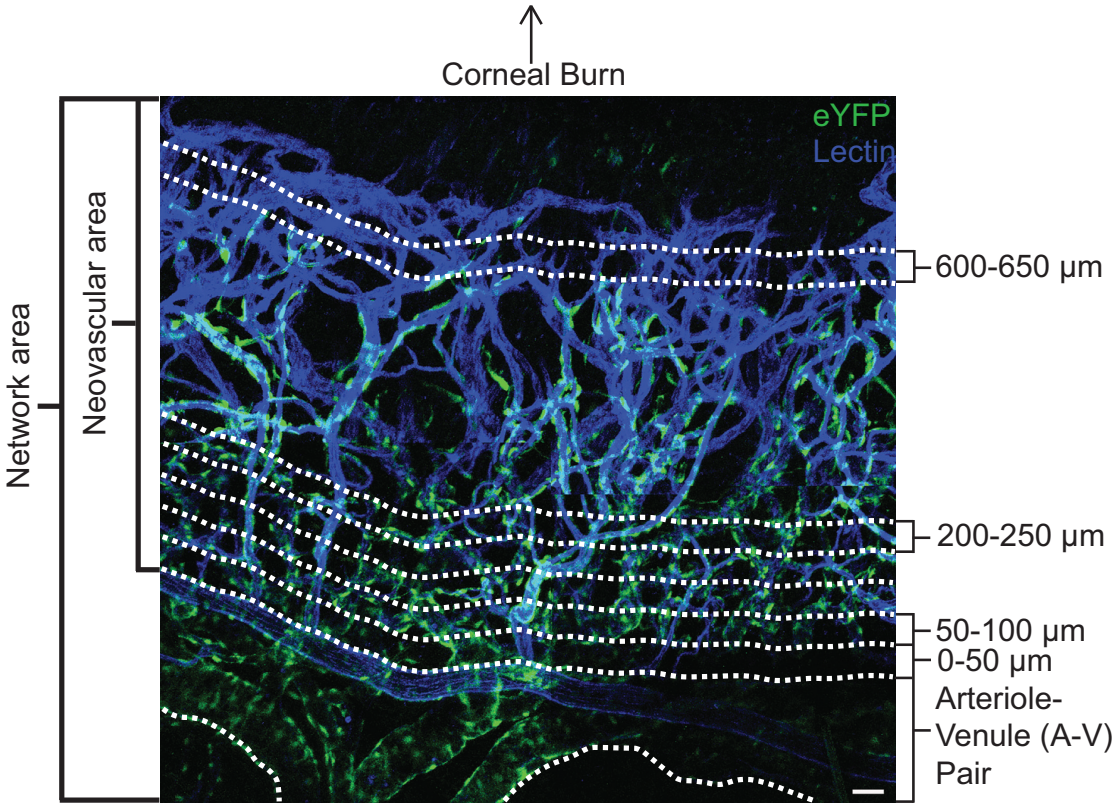

Figure 5.6 Intravital microscopy following corneal burn captures a robust angiogenic response as lectin+ and eYFP+ cells form new vasculature.

The area of new growth is further divided into 50 μm regions for rigorous quantification of eYFP+ cell density. The vasculature beyond the A-V pair is now termed the neovascular area. The neovascular area plus the A-V pair is referred to as the network area. Shown is a representative image of a Oct4$^{SMC\text{-}P\ WT/WT}$ cornea at day 7 post-corneal burn. Scale bar = 50 μm.

Consistent with the lack of a detectable cardiovascular phenotype at baseline, there was no difference in eYFP+ cell density or distribution throughout the limbal vasculature between Oct4$^{SMC\text{-}P\ WT/WT}$ and Oct4$^{SMC\text{-}P\ \Delta/\Delta}$ corneas at day 0 (Figure 5.4B through 5.4C; Figure 5.5). At days 3, 7, and 21 post-corneal burn, however, there were dramatic reductions in eYFP+ cell density in Oct4$^{SMC\text{-}P\ \Delta/\Delta}$ corneas as compared to Oct4$^{SMC\text{-}P\ WT/WT}$ controls (Figure 5.4B through 5.4F), consistent with increased eYFP+ apoptosis (and phagocytic clearance) and/or shedding of these cells into tears following SMC-P *Oct4* knockout.

In addition to decreased eYFP+ cell density throughout the network, Oct4$^{SMC\text{-}P\ \Delta/\Delta}$ corneas also had remarkable changes in the distribution of eYFP+ cells throughout the network. Specifically, in Oct4$^{SMC\text{-}P\ WT/WT}$ corneas at day 7 post-burn, eYFP+ cells migrated away from the limbal vasculature to form a dense neovascular area extending approximately 600 μm away from the limbal A-V pair (Figure 5.4E; Figure 5.6). In Oct4$^{SMC\text{-}P\ \Delta/\Delta}$ corneas, however, there were very few eYFP+ cells >350 μm away from the limbal A-V pair, indicative of impaired eYFP+ migration following SMC-P *Oct4* knockout. Similarly, in Oct4$^{SMC\text{-}P\ WT/WT}$ corneas at day 21 post-corneal burn, numerous eYFP+ cells migrated out to 900 μm away from the A-V pair. In contrast, in Oct4$^{SMC\text{-}P\ \Delta/\Delta}$ corneas at day 21 post-corneal burn, there were very few eYFP+ cells that had migrated >450 μm away from the limbus, indicative of impaired migration. Therefore, following corneal burn, SMC-P specific knockout of *Oct4* resulted in reduced eYFP+ cell density, impaired eYFP+ cell migration, and diminished eYFP+ cell participation in angiogenesis.

We then tested if these changes due to SMC-P specific knockout of *Oct4* were associated with increased vascular leakage and incidence of hemorrhage. To assess vascular leakage, we administered a retro-orbital injection of 70 kDa rhodamine-dextran into the mouse's contralateral eye immediately prior to live confocal imaging at day 3 post-corneal burn. We observed very little

dextran leak in Oct4$^{SMC\text{-}P\ WT/WT}$ corneas (Figure 5.7A, video not shown). However, in Oct4$^{SMC\text{-}P\ \Delta/\Delta}$ corneas, there was extensive accumulation of 70 kDa rhodamine-dextran in the tissue parenchyma, indicative of marked vascular leakage (Figure 2A, video not shown). Indeed, when we quantified fluorescence intensity of dextran in regions outside the vasculature, vascular leak was increased more than four-fold in Oct4$^{SMC\text{-}P\ \Delta/\Delta}$corneas compared to Oct4$^{SMC\text{-}P\ WT/WT}$corneas (Figure 5.7B).

To evaluate the extent of hemorrhaging in Oct4$^{SMC\text{-}P\ \Delta/\Delta}$corneas, we took bright field images of Oct4$^{SMC\text{-}P\ WT/WT}$ and Oct4$^{SMC\text{-}P\ \Delta/\Delta}$ corneas at days 0, 3, 7, and 21 post-corneal burn and quantified the number of hemorrhages, or areas of blood not confined to the vasculature, using a semi-quantitative scoring system (Figure 5.7C). The scoring also took into consideration the health of the corneal tissue, i.e. whether it was healthy, torn, or ruptured, which directly correlated with the extent of hemorrhaging. We observed increased hemorrhaging in Oct4$^{SMC\text{-}P\ \Delta/\Delta}$ mice, indicative of increased vascular leak, consistent with reduced eYFP+ cell density and migration (Figure 5.7D).

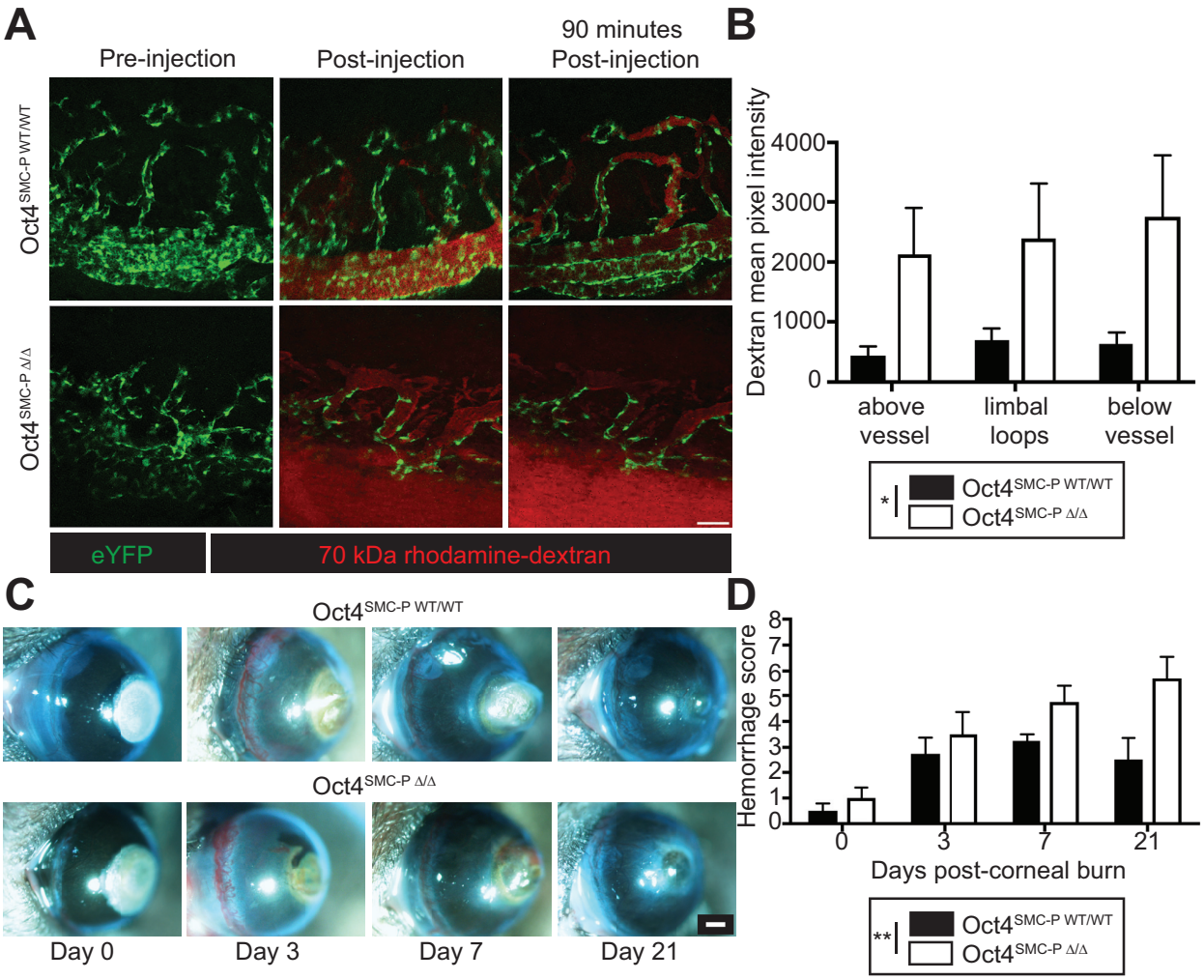

Figure 5.7 SMC-P specific conditional knockout of *Oct4* resulted in increased vascular leak and hemorrhaging following corneal burn.

(A), Representative still-frame images of $Oct4^{SMC\text{-}P\ WT/WT}$ and $Oct4^{SMC\text{-}P\ \Delta/\Delta}$ corneas pre-injection, immediately post-injection, and 90 minutes post-injection of 70kDa rhodamine-dextran (red). **(B)**, Quantification of dextran mean pixel intensity of defined regions throughout the vascular network (n=3 WT, 5 KO). **(C)**, Representative bright field images of corneas at days 0, 3, 7, and 21 post-corneal burn. Scale bar = 500 μm **(D)**, Quantification, using a scaled score, of hemorrhaging and

cornea integrity at each time point post-corneal burn (n=4 WT, 4 KO). Values = mean ± SEM. *$P < 0.05$ and **$P < 0.01$ using two-way ANOVA.

Although we specifically deleted Oct4 in *Myh11*-expressing SMC-P, we asked whether SMC-P *Oct4* knockout results in downstream changes in EC, possibly due to disruption of Oct4-dependent signaling networks. To assess changes in EC, we performed whole mount immunostaining of post-burn corneas for the EC marker CD31. In $Oct4^{SMC\text{-}P\,\Delta/\Delta}$ corneas, there was a significant decrease in CD31+ neovascular area, defined as the CD31+ pixel area extending beyond the A-V pair (Figure 5.8A; Figure 5.6). There was also a decrease in the distance that CD31+ vessels extended away from the limbal A-V pair, indicative of impaired EC migration (Figure 5.8B). However, there was no significant change in CD31+ vascular density, as measured by dividing the CD31+ pixelation by the CD31+ neovascular area (Figure 5.8C through 5.8D). Therefore, following SMC-P Oct4 knockout, EC migrate a shorter distance away from the limbus and spread out over a smaller area, but CD31+ vascular density within that area is preserved. These results indicate that loss of *Oct4* within perivascular cells is associated with impaired EC migration.

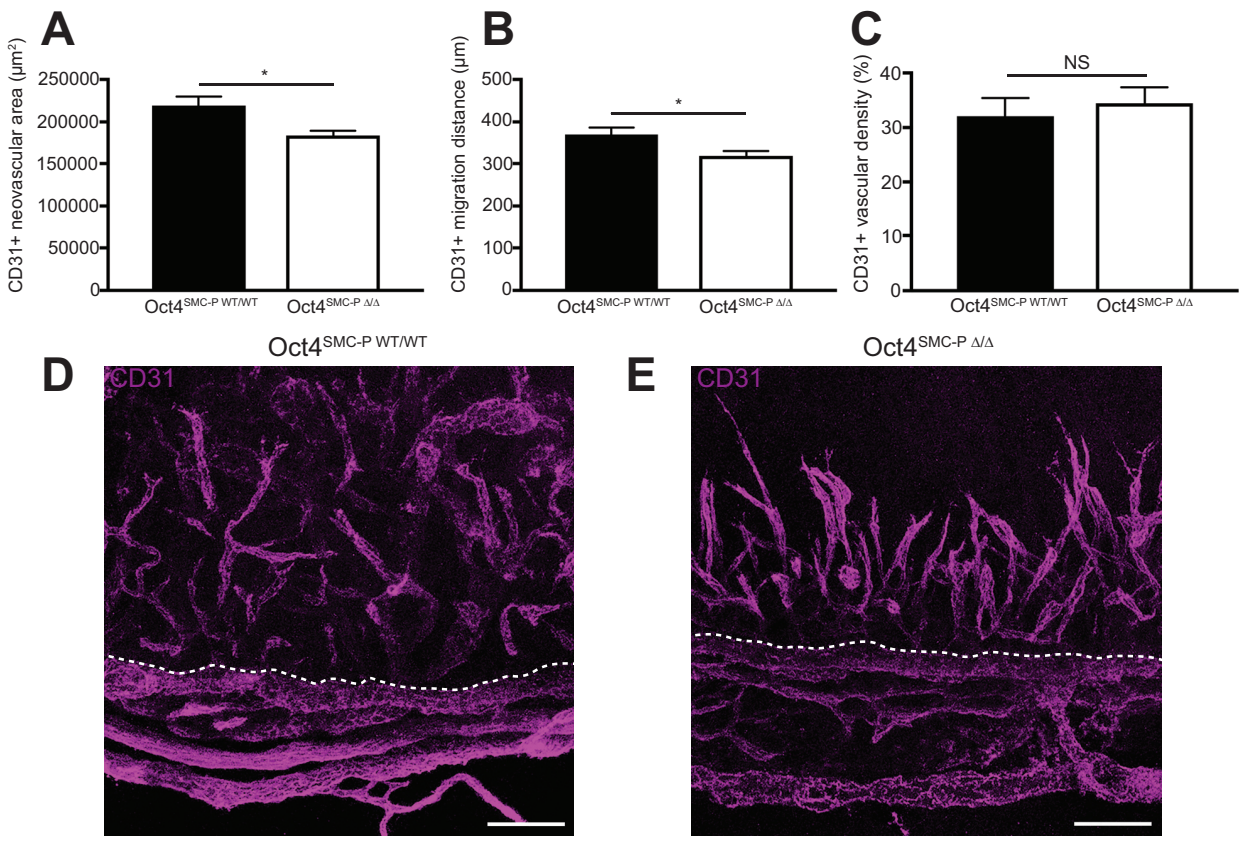

Figure 5.8 SMC-P *Oct4* knockout resulted in decreased CD31+ neovascular area and distance away from limbus, but preserved CD31+ vascular density, following corneal burn.

(**A**), Quantification, at day 3 post-corneal burn, of the CD31+ neovascular area, defined as the CD31+ area (in µm²) beyond the A-V pair of the corneal limbus. (**B**), Quantification of the distance of the three furthest EC away (in µm) from the A-V pair of the corneal limbus. (**C**), Quantification of CD31+ vascular density, defined as CD31+ pixelation per neovascular area (n=6 WT, 6 KO). (**D**), Representative CD31 (magenta) staining of whole mount corneas from Oct4$^{SMC\text{-}P\ WT/WT}$ and Oct4$^{SMC\text{-}P\ \Delta/\Delta}$ mice. Dashed lines delineate the end of the limbal A-V pair. Scale bar = 100 µm Values = mean ± SEM. *$P < 0.05$ or using Mann-Whitney (A and B) or unpaired two-tailed *t*-test (C).

SMC-P Oct4 knockout resulted in impaired angiogenesis and decreased perfusion recovery following hindlimb ischemia

Next, we sought to determine whether the dramatically impaired angiogenesis resulting from SMC-P specific *Oct4* knockout extended to other models of angiogenesis in addition to corneal alkali burn. We performed femoral artery ligation and resection (hindlimb ischemia (HLI)) surgery, a well-established mouse model of PAD, on $Oct4^{SMC\text{-}P\ WT/WT}$ and $Oct4^{SMC\text{-}P\ \Delta/\Delta}$ mice and monitored blood flow recovery over the course of 21 days post-HLI (Figure 5.9A), as previously described.[522] There was no significant difference in perfusion recovery as assessed by Laser Doppler imaging at days 0 (immediately post-injury), 3, and 7 post-HLI. However, $Oct4^{SMC\text{-}P\ \Delta/\Delta}$ mice had significantly impaired perfusion recovery at days 14 and 21 post-HLI, compared to $Oct4^{SMC\text{-}P\ WT/WT}$ littermate controls (Figure 5.9B through C). We then measured vascular density in the calf muscle via immunostaining. At days 0 and 7 post-HLI, there was no significant difference in capillary density, measured by counting the number of CD31+ cells per muscle fiber, between $Oct4^{SMC\text{-}P\ WT/WT}$ and $Oct4^{SMC\text{-}P\ \Delta/\Delta}$ mice (Figure 5.9D, Figure 5.10A). At day 21 post-HLI, there was significantly impaired capillary density in SMC-P Oct4 KO calf muscle compared to control muscle, mirroring the perfusion deficit detected by Laser Doppler (Figure 5.9D through 5.9E). There was also a significant decrease in both CD31+ and eYFP+ pixelation but no change in the ratio of eYFP to CD31 following SMC-P Oct4 KO (Figure 5.9F through H). Decreases in arteriogenesis, or collateral vessel remodeling, could potentially contribute to the impaired perfusion recovery we observed following HLI. Therefore, we measured arteriogenesis by staining thigh muscle for eYFP and counting the number of vessels with a diameter >10μm. We did not detect any significant differences in arteriogenesis between $Oct4^{SMC\text{-}P\ WT/WT}$ and $Oct4^{SMC\text{-}P\ \Delta/\Delta}$ mice at baseline (Figure 5.10B) or

following HLI (Figure 5.11). Therefore, SMC-P derived Oct4 plays a major role in angiogenesis, but not arteriogenesis, in mouse hindlimb muscle.

Taken together, our results demonstrate that loss of the stem cell pluripotency gene Oct4 specifically in SMC-P results in marked impairment of angiogenesis in two distinct mouse models, corneal alkali burn and hindlimb ischemia. Results show that impaired angiogenesis is at least partially due to altered migration of both eYFP+ cells and CD31+ cells following SMC-P *Oct4* knockout.

Figure 5.9 *(Next page)* SMC-P specific conditional knockout of *Oct4* resulted in impaired perfusion recovery and angiogenesis at day 21 post-HLI.

(A), Schematic outlining experimental design. **(B)**, Perfusion recovery of $Oct4^{SMC\text{-}P\ WT/WT}$ and $Oct4^{SMC\text{-}P\ \Delta/\Delta}$ mice as assessed by Laser Doppler perfusion and expressed as left (ligated) over right (unligated) perfusion ratio of the plantar sole (n=11 WT, 10 KO). **(C)**, Representative images of perfusion to the plantar soles at days 0, 7, and 21 post-HLI. **(D)**, Quantification of number of CD31+ cells per muscle fiber at days 0, 7, and 21 post-HLI. For each mouse, data was normalized to the number of CD31+ cells per muscle fiber of the corresponding unligated muscle [n = 14 WT, 14 KO (D0); 8 WT, 7 KO (D7); 6 WT, 7 KO (D21)]. **(E)**, Representative images of calf muscle cross-sections at day 21 post-HLI stained for DAPI, eYFP, CD31, and Phalloidin. Scale bar = 50 μm. **(F-G)**, Quantification of pixelation in calf muscle for CD31 (F) or eYFP (G) (n=6 WT, 6 KO). **(H)**, Percentage of eYFP to CD31 pixelation as measured in F-G (n=6 WT, 6 KO). Values = mean ± SEM. $*P < 0.05$ and $****P < 0.0001$ using two-way ANOVA with Sidak's multiple comparisons test (B) and unpaired two-tailed *t*-test (D, F-H).

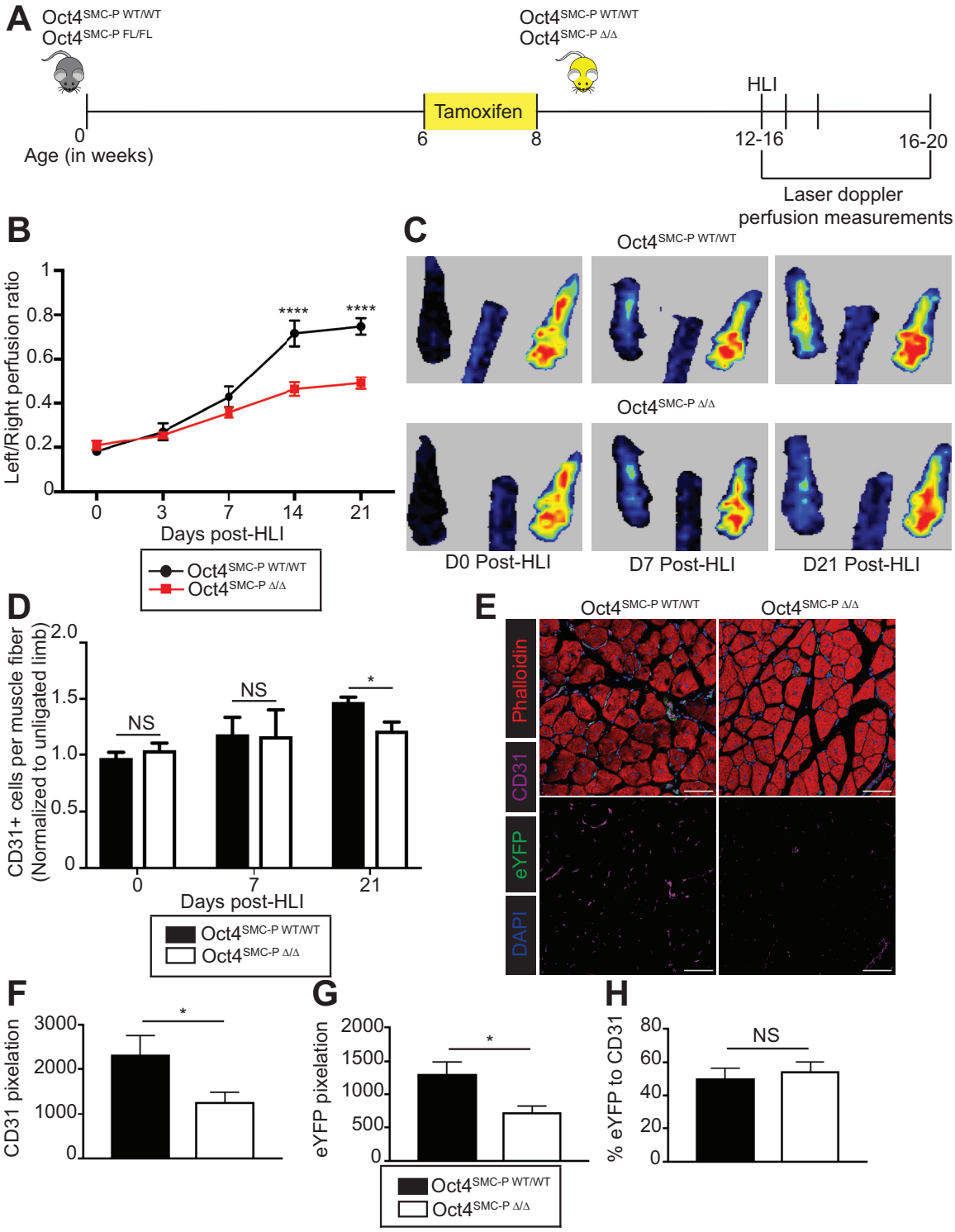

Figure legend on previous page.

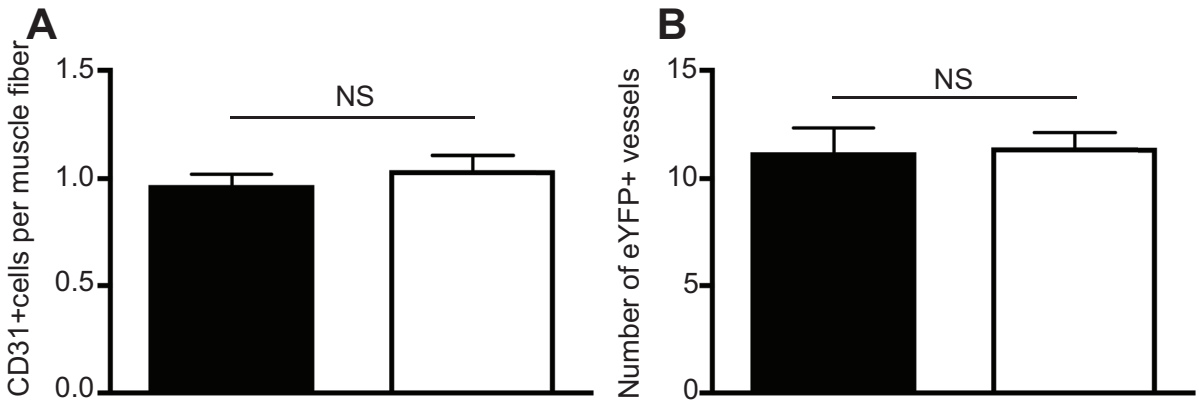

Figure 5.10 There were no baseline differences in hindlimb vasculature resulting from SMC-P specific conditional KO of Oct4.

(A), Quantification of number of CD31+ cells per muscle fiber in unligated calf muscle (n=14 WT, 14 KO). **(B)**, Quantification of the number of eYFP+ vessels >10 μm in diameter in unligated thigh muscle (n=5 WT, 7 KO). Values = mean ± SEM. *P* = NS, unpaired two-tailed *t*-test.

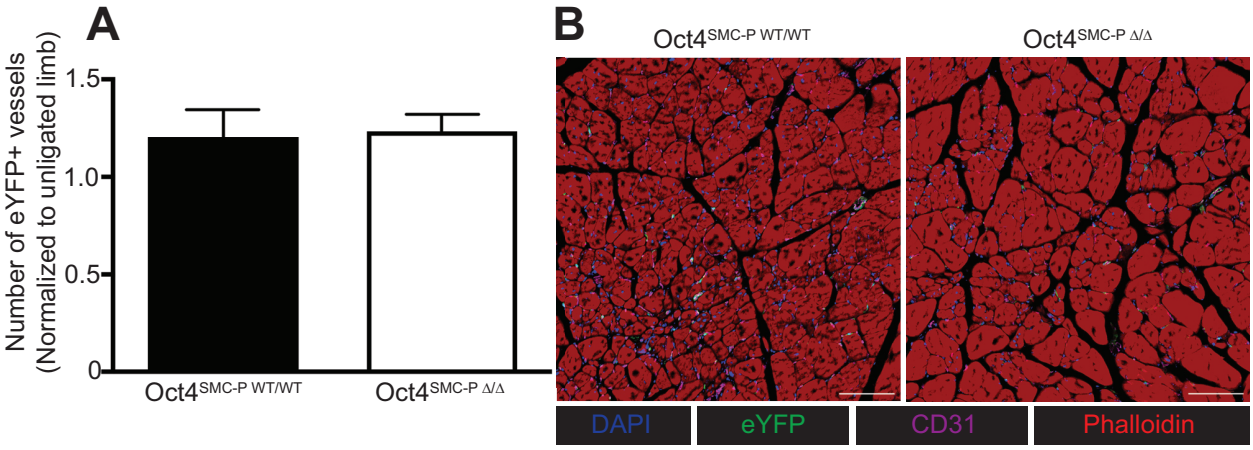

Figure 5.11 SMC-P specific conditional KO of Oct4 did not affect arteriogenesis following HLI.

(A), Quantification of the number of eYFP+ vessels >10 μm in diameter in ligated (left) thigh muscle at day 21 post-HLI normalized to the same parameter in the corresponding unligated (right) thigh muscle (n=5 WT, 7 KO). **(B)**, Representative images of thigh muscle cross-sections stained

for DAPI, CD31, eYFP, and Phalloidin. Scale bar = 100 μm. Values = mean ± SEM. *P* = NS using unpaired two-tailed *t*-test.

SMC-P Oct4 knockout was associated with altered expression of multiple members of the Slit-Robo pathway

We previously identified a number of Oct4-dependent genes implicated in regulation of cell migration and homing.[515] Of these, Slit3 was particularly interesting given its previously reported role in regulating EC migration *in vitro* and angiogenesis in several *in vivo* models.[523-525] To determine whether Slit3 is expressed by SMC-P derived eYFP+ cells within the microvasculature, we performed Slit3 immunostaining and detected SLIT3+eYFP+ cells following both corneal burn and HLI (Figure 5.12A through B). SLIT3 protein was expressed in eYFP+ cells of corneal blood vessels measuring approximately 10-20 μm in diameter (Figure 5.12A). In ischemic hindlimb, SLIT3 was expressed by many eYFP+ vessels, including small arterioles, venules, and capillaries (Figure 5.12B). Total SLIT3 levels were decreased in $Oct4^{SMC\text{-}P\ \Delta/\Delta}$ muscle compared to $Oct4^{SMC\text{-}P\ WT/WT}$ muscle following HLI (Figure 5.12C through 5.12D). However, since SLIT3 is produced and secreted by a number of different cell types *in vivo*, it is not possible to measure SLIT3 production exclusively by SMC-P *in vivo*. Therefore, to determine whether SLIT3 expression is altered specifically in SMC-P, we compared *Slit3* expression in $Oct4^{+/+}$ versus $Oct4^{\Delta\Delta}$ cultured SMC by qRT-PCR. Results showed that *Slit3* was decreased in *Oct4* knockout SMC relative to WT, thus providing additional evidence that expression of *Slit3* within SMC-P is Oct4-dependent (Figure 5.13A).

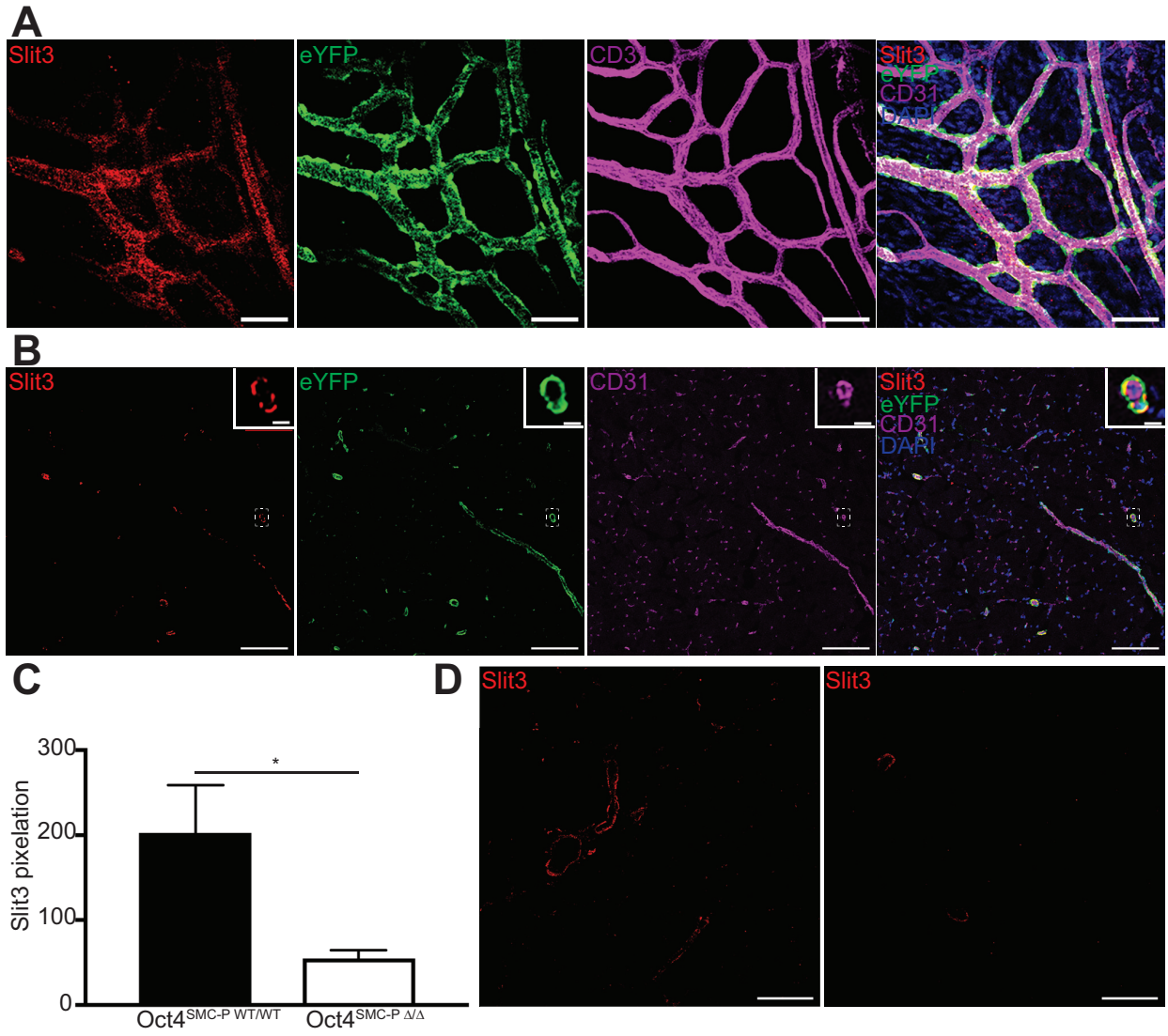

Figure 5.12 SLIT3 was expressed in SMC-P eYFP+ cells within injured cornea and gastrocnemius muscle and was decreased following SMC-P *Oct4* knockout.

(**A**), Immunostaining of whole mount cornea at day 3 post-corneal burn for CD31, eYFP, and SLIT3. Scale bar = 50 μm. (**B**), Immunostaining of ischemic calf muscle at day 7 post-HLI for DAPI, CD31, eYFP, and SLIT3. Scale bar=100 μm. Zoom scale bar=10 µm. (**C**), Quantification of SLIT3 pixelation in ischemic calf muscle at day 21 post-HLI (n=6 WT,KO). (**D**), Representative images of staining for DAPI, SLIT3, eYFP, and CD31 in $Oct4^{SMC\text{-}P\ WT/WT}$ and $Oct4^{SMC\text{-}P\ \Delta/\Delta}$ ischemic hindlimb muscle. Scale bar=50 µm. Values = mean ± SEM. *$P < 0.05$, unpaired two-tailed *t*-test.

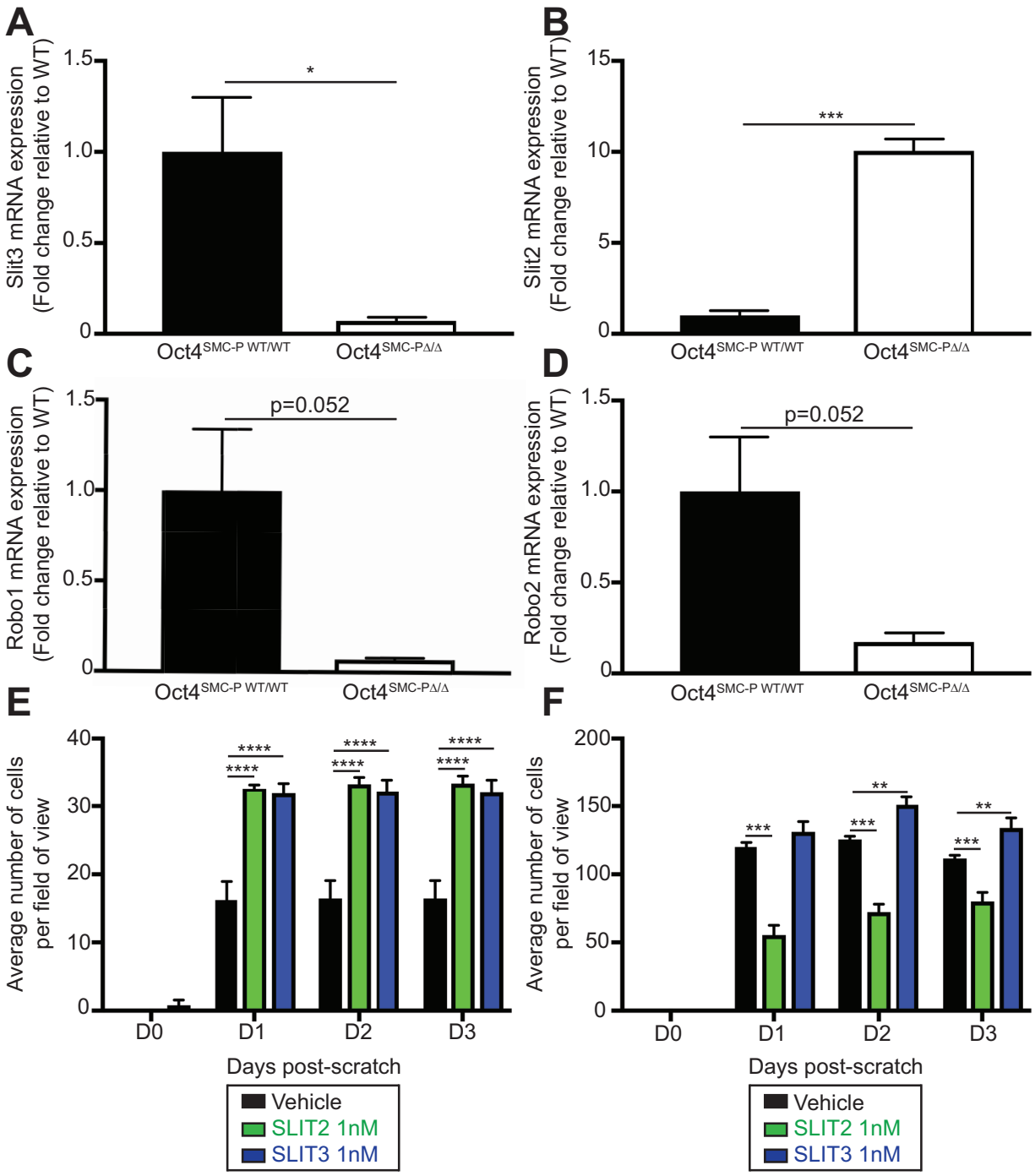

Figure 5.13 *Oct4* knockout led to dysregulation of the Slit-Robo family of guidance genes, which affected both SMC-P and EC migration.

(A-D), qRT-PCR of Oct4$^{+/+}$ and Oct4$^{\Delta/\Delta}$ cultured aortic SMC for expression of *Slit3* (A), *Slit2* (B), *Robo1* (C), and *Robo2* (D). Data is expressed as fold change relative to wild type (WT).

Experiments were performed in triplicate. (**E-F**), *In vitro* scratch wound assays showing effects of SLIT2 and SLIT3 on SMC (E) and EC (F) wound closure. Data shown is representative of three independent experiments. Values = mean ± SEM. *$P < 0.05$, **$P < 0.01$, ***$P < 0.001$, ****$P < 0.0001$ versus vehicle analyzed by unpaired two-tailed *t*-test (**A-D**) or two-way ANOVA with Dunnett's multiple comparisons test (**E-F**).

Gene	Log2 Fold Change (KO/WT)
Slit1	0.34
Slit2	2.60
Slit3	-5.13
Robo1	-4.24
Robo2	-6.40
Robo3	-0.35
Robo4	-0.09

Table 5.1 RNA-seq analysis showed downregulation of *Slit3*, *Robo1*, and *Robo2* and upregulation of *Slit2*.

Table showing Log_2 Fold Change (KO vs. WT) of all 7 members of the Slit-Robo family. Asterisks indicate expression of that member of the family is significantly changed with Oct4 KO. Positive numbers in blue indicate upregulation with Oct4 KO. Negative numbers in red indicate downregulation with Oct4 KO. Numbers in black indicate those genes were not significantly changed with Oct4 KO.

We then determined whether other members of Slit-Robo were altered with Oct4 knockout. Slit3 is one of seven members of the Slit-Robo family of guidance genes, which consists of the secreted ligands Slit1-3 and their receptors Robo1-4.[526] We found that *Slit2* (Figure 5.13B) was upregulated, and the receptors *Robo1* and *Robo2* were downregulated (Figure 5.13C, D), in cultured $Oct4^{\Delta/\Delta}$ SMC relative to $Oct4^{+/+}$ SMC via qRT-PCR. Our comparative RNA-seq data sets also showed that $Oct4^{\Delta/\Delta}$ SMC had decreased expression of *Slit3*, *Robo1*, and *Robo2* and increased expression of *Slit2* but no significant change in *Slit1*, *Robo3*, or *Robo4* (Table 5.1).

Slit-Robo signaling is known to affect migration of various cell types including EC [511,523,524,527] and SMC-P,[528,529] with both pro- and anti-migratory effects reported. Therefore, we tested the effects of SLIT2 and SLIT3 on migration of EC and SMC-P using *in vitro* scratch wound assays. SLIT2 or SLIT3 treatment of SMC resulted in increased migration (Figure 5.13E). In contrast, SLIT3 increased, whereas SLIT2 decreased, EC migration (Figure 5.13F). Taken together, results suggest that knockout of Oct4 within SMC-P results in alterations in Slit-Robo signaling important in regulating angiogenesis (Figure 5.14).

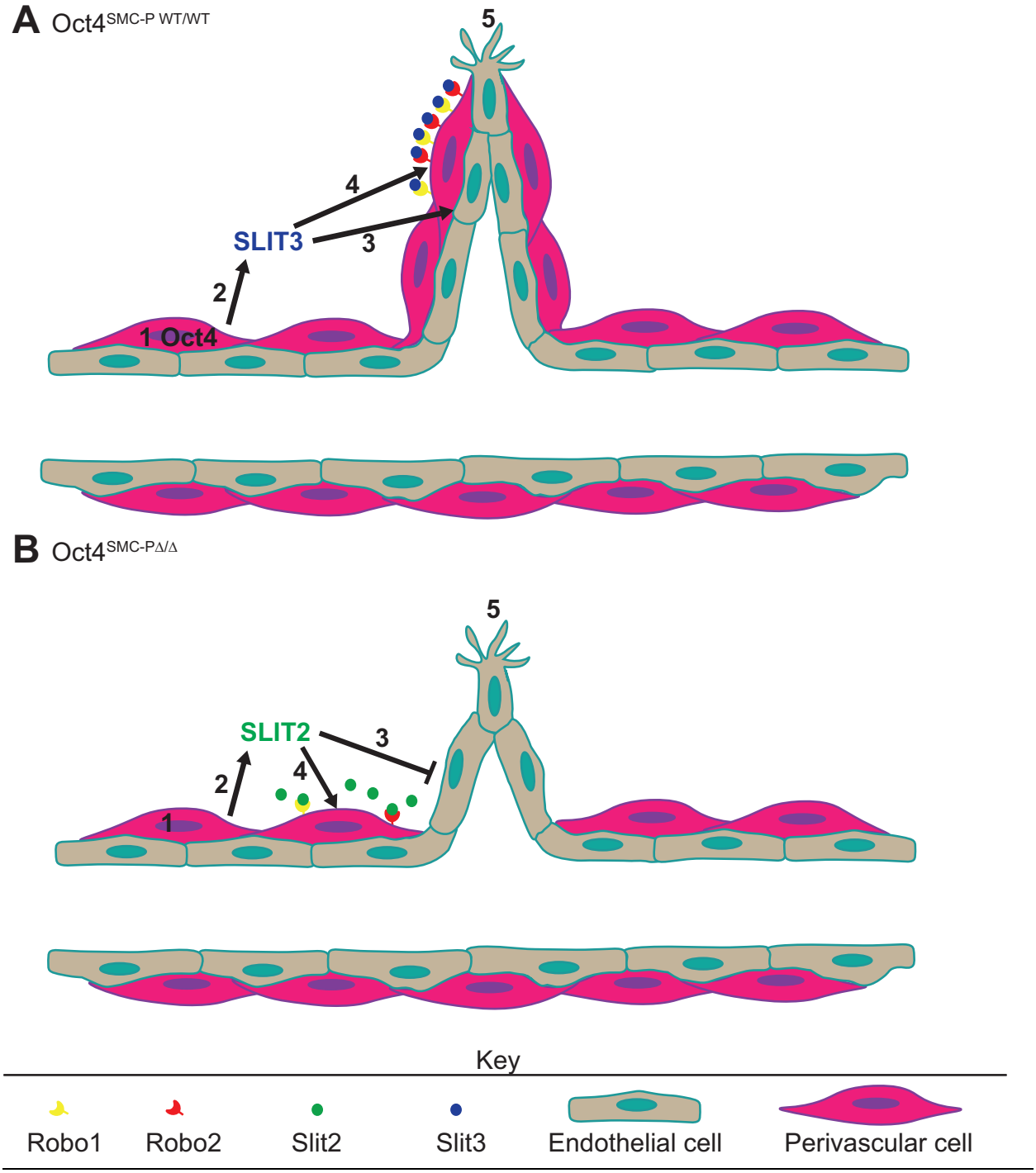
A Oct4SMC-P WT/WT
5
4
SLIT3
3
2
1 Oct4
B Oct4SMC-PΔ/Δ
5
SLIT2
3
2
4
1
Key
Robo1
Robo2
Slit2
Slit3
Endothelial cell
Perivascular cell

Figure 5.14 We postulate that SMC-P specific knockout of *Oct4* results in dysregulated expression of Slit2, Slit3, Robo1, and Robo2 in SMC-P, leading to impaired SMC-P-EC communication, migration, and angiogenesis.

(**A**), **1.** Following vascular injury, Oct4 is activated in SMC-P, leading to a number of downstream changes. **2.** This includes SLIT3 production and release into the tissue parenchyma. **3.** SLIT3 acts on nearby EC, resulting in EC migration. **4.** SLIT3 also acts on nearby SMC-P expressing ROBO1 and ROBO2 receptors, resulting in SMC-P migration. **5.** EC and SMC-P migration leads to the formation of SMC-P invested blood vessels with high perfusion capacity and appropriate EC barrier functions. (**B**), **1.** The preceding processes appear to be dependent on expression of Oct4 in SMC-P in that its knockout results in impaired migration of both SMC-P and EC in response to angiogenic stimuli, likely due to loss of multiple Oct4-dependent downstream changes including numerous genes important for SMC-P and EC migration and/or guidance. **2.** This includes decreased SLIT3 and increased SLIT2 production and release into tissue parenchyma. **3.** SLIT2 acts on nearby EC, resulting in impaired EC migration. **4.** In addition, in the absence of Oct4, SMC-P have reduced levels of ROBO1 and ROBO2, leading to impaired SMC-P migration. **5.** Importantly, these defects compound one another with the net effect that loss of Oct4 in SMC-P results in profound overall impairment of angiogenesis.

Discussion

In the present study, we addressed whether Oct4 in Myh11-expressing perivascular cells is required for angiogenesis following injury. We found that SMC-P KO of Oct4 resulted in impaired angiogenesis in two models: corneal alkali burn and HLI. Prior to this study, the long-standing hypothesis in the angiogenesis field was that EC tip and stalk cells drive angiogenesis[492,493] and once new endothelial tubes form, SMC-P are recruited via EC and SMC-P derived cytokines such as PDGF-B and ANG1.[495,496] This endothelial-centric view arose primarily due to numerous EC-specific loss-of-function studies that showed impaired angiogenesis.[508,509] However, similar SMC-P specific loss-of-function studies had not been performed. In this study, we specifically knocked out a single gene in perivascular cells and show that this, too, profoundly impairs angiogenesis. While it has been well-appreciated that proper communication between EC and SMC-P is critical for the formation of stable networks,[496] herein we provide the first direct evidence that SMC-P dependent signaling plays a key role in regulating angiogenesis following injury, including having a major influence on migration and distribution of SMC-P and EC. Prior to our study, there was evidence demonstrating that SMC-P number correlated with EC number and function. Specifically, global *Pdgfrβ*$^{+/-}$ mice show reduced pericyte coverage, which correlates with decreased CD31+ and lectin+ microvessel density and length in the adult central nervous system.[530] *Pdgfrb-Cre* mediated cell ablation and/or deletion of VEGFR1 leads to altered EC sprouting during postnatal retinal angiogenesis.[29] Further, perivascular cell investment of EC tubes has been shown to regulate EC proliferation rates, basement membrane deposition, and tube diameter.[462,531,532] However, through conditional SMC-P specific deletion of a single gene, Oct4, we now definitively and directly demonstrate that changes in SMC-P can drive changes in SMC-P and EC that are required for angiogenesis following injury. Taken together, we posit a revised model of angiogenesis in which

gene networks activated in both EC as well as SMC-P initiate signaling cascades that act on both cell types in a manner that is critical for angiogenesis and formation of non-leaky functional vascular networks.

One of these signaling cascades is initiated in SMC-P by Oct4, a stem cell pluripotency transcription factor that was, until last year, believed to be permanently epigenetically silenced in all somatic cells.[515,533] In Cherepanova et al, *Nature Medicine*, 2016,[515] we demonstrated that Oct4 is reactivated in SMC through hydroxymethylation of the Oct4 promoter-enhancer via HIF-1α and KLF4-dependent mechanisms. For the first time, we showed Oct4 played a functional role in somatic cells, specifically in regulating migration of SMC during atherosclerosis development.[534] However, a functional role for Oct4 in SMC did not evolve during the development of atherosclerosis, a disease with no selective pressure, as it typically manifests in individuals well after their reproductive years. Herein, we present evidence that Oct4 reactivation likely evolved to play a normal, physiologic role in perivascular cells to enable them to participate in angiogenesis following injury. This raises the possibility that Oct4 reactivation might participate in other processes including tumor growth and metastasis as well as microvascular dysfunction associated with metabolic disease.

Reactivation of the pluripotency factor Oct4 might be expected to lead to a multitude of downstream changes, similar to its role as a master transcription factor in embryonic stem (ES) cells.[534] Indeed, our previous *in vitro* and *in vivo* RNA-seq analyses identified thousands of Oct4-dependent genes in SMC.[515] In addition, we previously showed that Oct4 knockout resulted in impaired migration of SMC in culture and ex vivo in aortic medial explants.[515] Moreover we presented evidence suggesting that this occurs through Oct4-dependent regulation of numerous genes critical for cell migration including matrix metalloproteinases 3 and 13, multiple collagens,

and osteopontin.[535,536] In the present study, we showed that loss of Oct4 in perivascular cells resulted in a dramatically altered distribution of SMC-P and EC, demonstrating impaired migration of both cell types during angiogenesis. We also showed reduced numbers of eYFP+ cells throughout the vascular network, indicative of increased cell death and/or decreased cell proliferation. The mechanisms responsible for relatively rapid loss of perivascular cells in SMC-P Oct4 knockout mice following corneal burn injury are unclear. However, one possibility is that eYFP+ cells attempt to leave the vessel wall but are incapable of migrating due to the loss of Oct4, and subsequently undergo cell death. Consistent with this possibility, eYFP+ cells of Oct4$^{SMC\text{-}P\ \Delta/\Delta}$ corneas at day 3 post-burn appeared unhealthy, often with retracted processes (data not shown). A second possibility is that Oct4 plays an anti-apoptotic role in SMC-P, similar to what has previously been reported in ES cells. .[535,536] A third possibility is that SMC-P Oct4 knockout results in increased sloughing off of these cells from the corneal surface and removal in tears. Consistent with this idea, our genomic analyses identified multiple Oct4-dependent genes associated with cell adhesion and cytoskeletal remodeling. [515]

The role of Oct4 in SMC-P is clearly complex and is likely a product of the combinatorial effects of a multitude of Oct4-dependent genes that in aggregate result in the observed phenotype. However, of major interest, our previous genomic analyses identified the Slit-Robo family of guidance-migration cues as putative Oct4 regulated genes, thus raising the possibility that impaired SMC-P and EC migration in our studies may be due in part to dysregulation of Slit-Robo signaling and SMC-P-EC cross talk. [515] Consistent with this possibility we showed that the receptors Robo1 and Robo2 were downregulated in SMC-P following Oct4 KO, which may have contributed to impaired SMC-P migration.[526] We also demonstrated that Oct4 KO resulted in decreased expression of Slit3 and increased expression of Slit2 (Figure 5.14). Since Slits are secreted glycoproteins, they

participate in autocrine and paracrine signaling and can modulate migration of any nearby cell expressing ROBO receptors.[526] Indeed, numerous studies have previously shown that cell types critical for angiogenesis, including SMC-P[528,529] and EC,[511,527,537,538] express ROBO receptors. Moreover, a variety of other cell types that are known to impact angiogenesis, including macrophages[539-541] and nerve cells,[542] have also been shown to express members of the Slit-Robo family.

Taken together, our results suggest that dysregulation of both Robo and Slit expression in SMC-P following Oct4 KO likely contributed to the impaired migration of both SMC-P and EC observed in our studies. Because SMC-P and EC communicate extensively during angiogenesis, and both cell types are critical for stable network formation, altered migration of one cell type will likely affect downstream function of the other cell type, leading to further dysregulation of angiogenesis including not only failed SMC-P investment of nascent EC tubes but also impaired outgrowth and migration of EC in a reciprocal fashion. This ultimately contributes to profoundly impaired angiogenesis including decreased vascular density, decreased perfusion, and increased vascular leak. The complexity of the Slit-Robo family, the numerous cell types that express them, and observations that decreases in expression of one Slit member is associated with compensatory changes in other family members,[511,543] highlight how extraordinarily difficult it will be to clearly resolve exact mechanisms as to how these factors work. However, our data indicate that Oct4-dependent regulation of this gene family in perivascular cells is critical for a normal angiogenic response following injury.

In conclusion, this study provides multiple lines of evidence that SMC-P Oct4 is critical for angiogenesis following either corneal alkali burn or HLI. We present a revised model of angiogenesis that considers a more active role for SMC-P through Oct4-dependent changes in SMC-P and EC, including Slit-Robo. The vast majority of clinical trials for diseases such as PAD,

heart failure, and stroke have sought to augment angiogenesis through administration of growth factors to promote EC proliferation and migration (e.g. VEGF and bFGF).[544-547] However, these studies have failed to meet primary endpoints, which appears at least partially due to uncontrolled EC growth without coordinated SMC-P migration and investment.[548] Our study suggests that future trials could benefit from targeting both SMC-P and EC in order to enhance the angiogenic response, not only through direct effects on investment and migration but also through promoting appropriate SMC-P and EC communication.

CHAPTER 6

ADIPOSE-DERIVED STEM CELLS FROM DIABETIC MICE SHOW IMPAIRED VASCULAR STABILIZATION IN DIABETIC RETINOPATHY

ACKNOWLEDGEMENTS: Stephen M. Cronk[1], H. Clifton Ray[1], Thomas A. Mendel[2], Kyle L. Hoehn[3], Anthony C. Bruce[1], Bijan K. Dey[4], Alexander M. Guendel[1,4], Daniel N. Tavakol[1], Ira M. Herman[5], Shayn M. Peirce[1,4], and Paul A. Yates[1,4]

[1]Department of Biomedical Engineering, University of Virginia
[2]Department of Pathology, University of Virginia
[3]Department of Pharmacology, University of Virginia
[4]Department of Ophthalmology, University of Virginia
[5]Department of Developmental, Molecular and Chemical Biology, Tufts University

The text included in this chapter has been published:
Cronk S and Kelly-Goss M (co-first author), Mendel T, Hoehn K, Ray H, Bruce A, Dey B, Guendel A, Tavakol D, Herman I, Peirce S, Yates P. Adipose-derived stem cells from diabetic mice show impaired vascular stabilization in a murine model of diabetic retinopathy. Stem Cells Translational Medicine, 2015.

Abstract

Diabetic retinopathy is characterized by progressive vascular drop-out with subsequent vision loss. We have recently shown that an intra-vitreal injection of adipose-derived stem cells (ASCs) can stabilize the retinal microvasculature, enabling repair and regeneration of damaged capillary beds in vivo (ref). Because an understanding of ASC status from healthy vs. diseased donors will be important as autologous cellular therapies are developed for unmet clinical needs, we took advantage of the hyperglycemic Akimba mouse as a pre-clinical in vivo model of diabetic retinopathy in an effort aimed at evaluating therapeutic efficacy of adipose-derived stem cells (mASCs) derived from either healthy, non-diabetic or diabetic mice. To these ends, Akimba mice received intra-vitreal injections of medias conditioned (conditioned media, CM) by mASCs or mASCs, themselves, subsequent to development of substantial retinal capillary drop-out. mASCs from healthy mice were more effective than diabetic mASCs in protecting the diabetic retina from further vascular drop-out. Engrafted ASCs were found to preferentially associate with the retinal vasculature. CM was unable to recapitulate the vasoprotection seen with injected ASCs. *In vitro* diabetic ASCs showed decreased proliferation and increased apoptosis compared to healthy mASCs. Diabetic ASCs also secreted less vasoprotective factors than healthy mASCs, as determined by high-throughput ELISA. Our findings suggest that diabetic ASCs are functionally impaired compared to healthy ASCs and support the utility of an allogeneic injection of ASCs versus autologous or conditioned media approaches in the treatment of diabetic retinopathy.

Introduction

The therapeutic potential of adipose-derived stem cells (ASCs) has been demonstrated with success in several applications, including myocardial infarction, diabetic wound healing, and neurodegenerative disorders [549-551]. Studies comparing the efficacy of ASCs from diabetic and non-diabetic sources have focused on their application in diabetic ulcers [552] and hindlimb ischemia Koci, et al. [553]. Both of these studies found that mASCs derived from diabetic sources have impaired treatment efficacy relative to their non-diabetic counterparts. Stem cells from different sources, such as bone marrow (BMSCs), have also shown functional impairment when derived from diabetic mice in the treatment of cardiovascular disease [551,554].

We have recently shown that intra-vitreal injection of ASCs stabilizes the retinal microvasculature and encourages regeneration of damaged capillary beds in several mouse models of retinal vasculopathy [74]. ASCs are desirable due to their relative ease of harvest from accessible fat depots, as well as their potential for allogeneic or even autologous treatment [555]. However, only a few studies have examined whether ASCs obtained from diabetic donors are negatively impacted by the disease; in turn, negative outcomes here would have implications for the feasibility of autologous cell-based therapies [556]. To date, no studies have assessed the functional impact of diabetes on ASCs for the treatment of diabetic retinopathy.

Diabetes profoundly impacts the microvasculature in nearly every tissue. Diabetic retinopathy results in retinal capillary drop-out, vessel leakage, and pathological neovascularization, leading to severe and irreversible vision loss. Current surgical and pharmacologic treatments are only effective at managing complications of diabetic retinopathy, but do not repair existing damage [72]. Laser photocoagulation is the current treatment standard for proliferative diabetic retinopathy, and operates on the principle of cauterizing hypoxic retinal

tissue [557]. While effective at stemming the progression of retinopathy, this procedure damages peripheral and night vision, often requires repeated treatments, and only prevents visual deterioration in half of cases [72,557,558]. Anti-VEGF therapy has been increasingly used alone or in combination with laser therapy, with improvements in vision loss due to diabetic macular edema [559]. However, anti-VEGF therapy requires frequent intra-vitreal injections for several years with potential complications, and does not reverse the underlying pathology [72]. A lasting, non-destructive treatment for diabetic retinopathy is clearly needed.

Using the Akimba mouse model of diabetic retinopathy, we have probed the differences in treatment efficacy and function of mASCs derived from healthy versus diabetic mice. The Akimba is a cross between the hyperglycemic Akita mouse, which carries a dominant negative mutation in its insulin-2 gene, and the Kimba mouse, which transiently overexpresses human VEGF in retinal photoreceptor cells [560,561]. The combination of these modifications creates a mouse whose retina exhibits hallmarks of proliferative diabetic retinopathy in humans with retinal edema, aberrant neovascularization, and progressive vascular drop-out over time [561].

The primary goal of this study was to determine whether mASCs from healthy, non-diabetic mice are more effective than diabetic mASCs from Akimba mice in preventing progressive vascular damage and drop-out in the diabetic retina. We also sought to investigate potential functional differences between healthy and diabetic mASCs, both *in vivo* with respect to their abilities to associate with and affect the retinal vasculature, and *in vitro* with respect to their proliferative capacities, apoptosis rates, metabolic functions, and abilities to secrete soluble factors that promote vascular stability. We were subsequently interested in determining whether a single intra-vitreal injection of healthy or diabetic ASC-conditioned media was equivalent to injecting either healthy or diabetic hASCs in terms of preventing vascular drop-out in the diseased Akimba

retina. Our functional analysis of healthy versus diabetic mASCs in an established *in vivo* model of retinal vascular damage may have implications for the future ocular use of autologous ASCs from diabetic patients. By evaluating different mechanisms and cellular behaviors in both healthy and diabetic mASCs, our study contributes to understanding how ASCs might confer a vasoprotective effect in settings of progressive vascular damage and suggests strategies for enhancing their therapeutic capabilities.

Methods

mASC Harvest and Culture

Isolation of the stromal vascular fraction from the epididymal fat pad and culture of mASCs was performed as detailed in Zuk et al 2001 [555]. Briefly, fat pads were harvested from nine-week old Akimba ($Ins2^{Akita}VEGF^{+/-}$) mice and non-diabetic Kimba ($VEGF^{+/-}$) littermates, then digested in collagenase-containing digestion buffer (Sigma, St. Louis, MO) for one hour at 37°C. The resulting mixture was filtered through 200-μm mesh (Corning, Corning, NY) to exclude any undigested tissue. The filtrate was centrifuged, and the pellet was resuspended in phosphoate buffered saline (PBS) and incubated with red blood cell lysis buffer (Sigma, St. Louis, MO) for five minutes at room temperature. The cell suspension was then sterile-filtered through 40-μm mesh and plated on sterile culture plates (Corning, Corning, NY). Cells harvested from Akimba mice are referred to as "diabetic mASCs", while cells harvested from Kimba mice are referred to as "healthy mASCs". All mice were maintained on a C57BL/6 background. The Kimba hVEGF transgene is expressed only in retinal photoreceptors from postnatal day 9 to postnatal day 28 [562], thus we assumed that mASCs procured from fat pads harvested from Kimba mice at nine weeks are unlikely to be affected by the short-term hVEGF pulse in the retina that terminated five weeks prior to mASC harvest. mASCs were maintained at 37°C and 5% CO_2, and cultured and passaged as previously reported[74]. Briefly, growth media consisted of 10% fetal bovine serum (Hyclone, Logan, UT) and 1% penicillin/streptomycin (Fisher Scientific, Waltham MA) in Dulbecco's Modified Eagle Medium (DMEM-F12) with added glutamate and sodium bicarbonate (Life Technologies). Cells were passaged at roughly 80% confluence, and culture media was changed every other day.

Vital Labeling mASCs for Intra-vitreal Injection

All animal studies were approved by the University of Virginia's Animal Care and Use Committee. Presence of the Akita genotype was detected by RT-PCR [561] and hyperglycemia was confirmed by taking blood glucose measurements at five weeks of age using a OneTouch UltraMini blood glucose meter (LifeScan, Milpitas CA). At passage 4 (P4), mASCs were fluorescently labeled with Vybrant DiI Cell-Labeling Solution (Life Technologies, Grand Island, NY) as per manufacturer's instructions, and re-suspended in PBS at the appropriate concentration determined by hemocytometer. Each cell injection consisted of 10,000 mASCs suspended in 1.5 microliters of PBS. Control vehicle injections consisted of 1.5 microliters of PBS. Cells were re-suspended by pipette immediately before injection to minimize cell clumping. Five week-old, male Akimba mice were anesthetized with ketamine/xylazine injected intraperitoneally, and proparacaine was applied topically to the eyes just prior to injection. mASCs were injected through the pars plana into the vitreous using a 33-gauge Hamilton syringe. A total of twelve Akimba mice were injected in this manner, with mASCs injected into one eye (with six randomized mice receiving healthy mASCs and six mice receiving diabetic mASCs) and PBS control injected into the other eye.

Retinal Whole-Mounting and Immunostaining

Treated mice were maintained in a controlled vivarium for four weeks post-injection before harvesting retinae. At the harvest time point, mice were euthanized with carbon dioxide, followed immediately by cardiac perfusion-fixation by cutting the right atrium and injecting the left ventricle with 10 mL of 4% paraformaldehyde (PFA). Intact eyes were then removed and fixed by submersion in 4% PFA for 10 minutes. After rinsing the eyes with PBS, retinae were isolated and whole-mounted on gel-coated slides. Retinae were then permeabilized with 1 mg/mL

digitonin (MP Biomedical, Solon, OH) for 1 hour, stained with 1:100 IB4 lectin AlexaFluor-647 (Life Technologies, Carlsbad, CA) to visualize blood vessels, and counterstained with 1:500 DAPI (Sigma, St. Louis, MO) to visualize cell nuclei.

Imaging & Image Analysis

10x, 20x, and 60x image stacks were taken of retinal whole mounts on a Nikon Ti Eclipse confocal laser scanning microscope. 10x stacks were flattened and tiled into whole-retina montages using ImageJ. Vessel length density was measured by a blinded observer in six random representative fields of view (FOV) (10x magnification) in each retina by manually tracing and measuring the length of all vessels within the FOV using Image J. This number was normalized to the total tissue area in each FOV by dividing the total vessel length by the total tissue area within the FOV. In the same 10x images, the number of vessel branch points were counted and similarly normalized by the total tissue area within the FOV. The normalized vascular length density (vessel length/tissue area) and the normalized number of branch points (branch points/tissue area) were averaged across all six FOVs so that each retina was described by an average vascular length density and an average number of branch points (n=6 FOVs per retina). For both the vascular length density and the number of branch points, we calculated the percent change between the mASC-injected retina and contralateral PBS-injected retina in the same mouse. DiI-labeled mASCs were counted in three representative 20x image stacks per retina by a blinded observer. Each FOV was taken at the same distance from the optic nerve.

Monte Carlo Simulation

A Monte Carlo simulation was created in MATLAB to determine the distribution of randomly placed mASCs that would be expected to be associated with the retinal vasculature by chance. The simulation used binary images of fluorescent retinal vasculature micrographs (20X magnification) to generate a matrix of coordinates for the retinal vasculature. For each micrograph, a random matrix of mASC coordinates was generated. Identical retinal vasculature coordinates and mASC coordinates were counted to determine the probability of mASCs randomly contacting retinal vasculature after random distribution. The simulation was looped 1000 times for more accurate probability calculations. Utilizing Delaunay triangulation, the simulation also created a histogram to visualize the probability distribution of the distance of randomly simulated mASCs from retinal vasculature. These simulated predicted distributions and associations with the retinal vasculature were then compared with the actual observed association of mASCs with the retinal vasculature. This allowed us to determine if mASCs were associated with the retinal vasculature at a rate greater than that expected by chance.

Acquisition of mASC Conditioned Media and Angiogenesis Secretome Analysis

Healthy, wildtype mASCs and diabetic mASCs were raised to passage 4 in 10% FBS, as specified above, and they were plated at densities to ensure approximately equivalent cell numbers in order to collect cell conditioned media from equal sized passage 4 populations. The media was removed from culture plates, and plates were then washed with PBS twice. Defined media lacking serum was then added to mASC culture plates for 24 hours as cells incubated at 37°C. ASC conditioned media samples were collected for analysis from four age-matched populations each of healthy Kimba and diabetic Akimba mASCs, taken from mice of equal age. These fresh media samples were run on a Mouse Proteome Profiler Angiogenesis Array (RnD Systems ARY015),

which tested for 53 factors. X-ray film captured chemiluminescence from each dot, which was proportional to the amount of factor bound. Relative expression levels were obtained from densitometry analysis (ImageJ) of x-ray film spots. Raw intensity values were normalized to blot area, cell number, the positive control value, and then the background value was subtracted from the normalized intensity.

mASC Conditioned Media Injections in Akimba Mice

Male, five-week old Akimba mice were anesthetized with ketamine/xylazine injected intraperitoneally and proparacaine applied topically to the eyes just prior to injection. Cell conditioned media (CM) was obtained from healthy and diabetic mASCs according to the procedure described in the main Methods section. Cell CM was concentrated so that the concentration of the cell secretome was equal to that produced by the number of ASCs injected in other experiments (10,000 ASCs / 1.5 microliters) using an Amicon Ultra-15 Centrifugal Filter (EMD-Millipore, Germany). 1.5 microliters of media conditioned by diabetic mASCs was injected into the left eye, while CM from healthy mASCs was injected into the right. Injections went through the pars plana, into the vitreous using a 33-gauge Hamilton syringe (n=6 Akimba mice). Four weeks post-injection, mice were anesthetized and euthanized as described in the main Methods section, and retaine were removed, immunostained, and imaged according to the procedures described in the main Methods section.

Cell Proliferation & Apoptosis Assays

mASCs from three 9-week old healthy Kimba and three 9-week old diabetic Akimba animals were plated on glass coverslips in 12-well dishes at a density of 4000 cells/cm^2 and allowed to adhere

for 24 hours (Cold Spring Harbor proceedings). Three coverslips were cultured per animal. To measure cell proliferation in each population of mASCs, mASCs were incubated with 5-ethynyl-2'-deoxyuridine (EdU) for 12 hours, then stained following the manufacturer's instructions. To measure apoptosis, the terminal deoxynucleotidyl transferase dUTP nick end labeling (TUNEL) method was used. Fluorescence intensity from both EdU and TUNEL assays was measured for each coverslip using confocal microscopy, taking image stacks with a 3-micron spacing and measuring total fluorescence intensity for each coverslip in ImageJ.

Measurements of oxygen consumption and mitochondrial function

Oxygen consumption rate (OCR) was measured using a Seahorse XF-24 Flux Analyzer (Seahorse Biosciences, Billerica, MA), as previously described 1. mASCs were seeded in a Seahorse 24-well tissue culture plate at a density of 3.0x104 cells/well in normal growth media for 24 hours prior to the assay. On the day of the assay the media was changed to unbuffered DMEM and equilibrated at 37°C. Oligomycin (2 μM), FCCP (1 μM), and Rotenone and Antimycin A (1 μM and 10 μM) were injected sequentially during the assay as indicated. Each OCR measurement represents the average of a 3 minute reading every 10 min, with 3 min of mixing and 4 min of wait time per cycle. 3-4 wells were used for each experimental group.

Statistical Analyses

The vascular length density and branch point analysis in PBS-injected vs. ASC-injected retinae were statistically analyzed using a Mann-Whitney Rank Sum test (reported in Figure 2). The statistical difference between the average ratios of ASCs residing in perivascular locations relative to the total number of ASCs in the retina in healthy versus diabetic ASC-injected retinae was

assessed using a Wilcoxon Signed-Rank test (reported in Figure 3). The *in vitro* cell proliferation and apoptosis mASC experiments were statistically analyzed using a Student's t-test (reported in Figure 5). The *in vitro* angiocrine secretome data was statistically assessed by comparing healthy ASC secretome levels to diabetic ASC secretome levels for each factor using a Mann-Whitney Rank Sum test (reported in Figure 6). Statistical tests were performed in SigmaStat (Systat Software Inc, San Jose, CA), with statistical significance asserted as $p \leq 0.05$.

Results

Incorporation of injected mASCs into the retina

10,000 DiI-labeled, P4 mASCs derived from either healthy or diabetic mice were injected in 1.5 microliters of PBS into the vitreous of five-week old male Akimba mice. 1.5 microliters of PBS was injected into the contralateral eye as vehicle control. Four weeks post-injection of cells, retinae were harvested demonstrating DiI-positive cells that had engrafted into the retina and had DAPI+ nuclei, some of which were associated with the retinal vasculature residing in perivascular locations (Figure 6.1). The number of mASCs that incorporated into the retina per 1,250 mm^2 FOV did not significantly differ between retinae injected with healthy and diabetic mASCs (6.77 healthy mASCs/FOV, 6.73 diabetic mASCs/FOV).

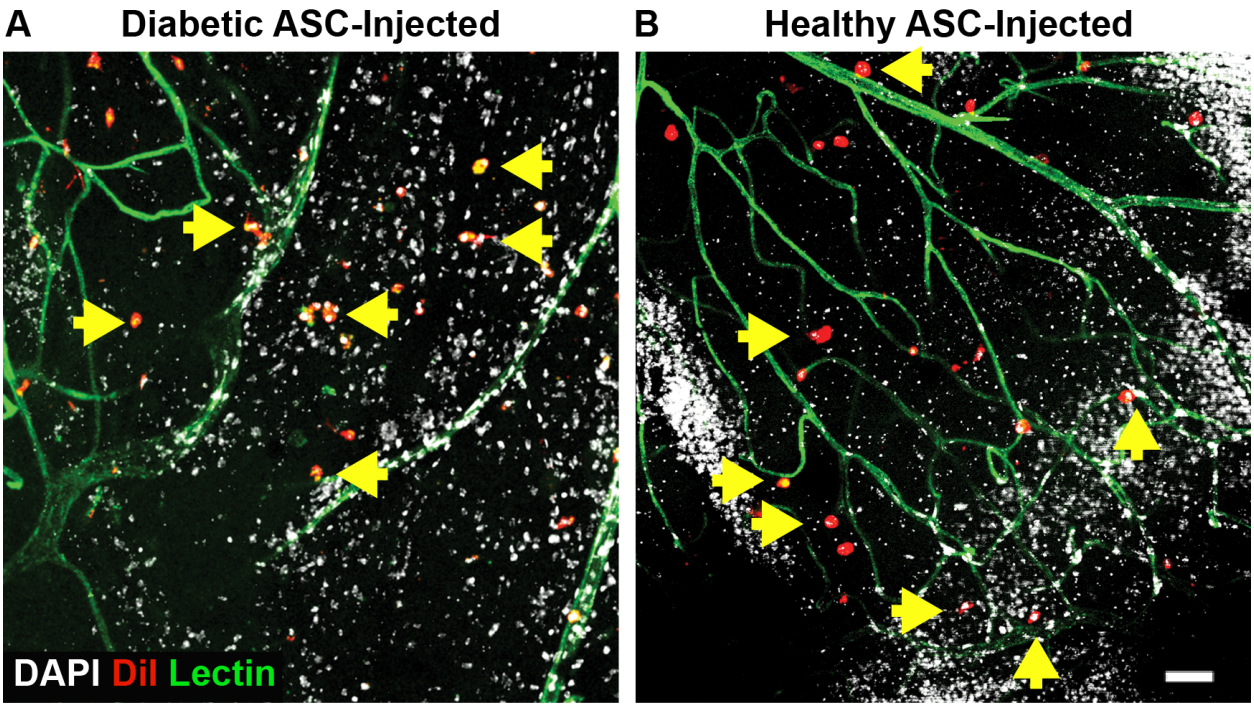

Figure 6.1 Injected ASCs incorporate into the retina and some reside in perivascular locations along the vasculature (green; IB4 lectin staining).

(**A**) Healthy ASC-treated and (**B**) diabetic ASC-treated retinae had similar numbers of engrafted DiI+ mASCs (red). DAPI staining (grey) confirmed intact nuclei of the DiI+ ASCs one month after treatment (yellow arrows). Cells are found in both the interstitial space and along IB4 lectin stained vessels (green). The scale in (A) and (B) are the same, and the scale bar = 50 micrometers.

Protection against vascular drop-out

The Akimba retina demonstrates several hallmarks of proliferative diabetic retinopathy seen in humans, including retinal thinning, retinal edema, aberrant neovascularization, retinal capillary drop-out, and nonperfusion [561]. When healthy mASCs were injected, the average vascular density of the superficial vascular plexus in the Akimba retinae (n=6) was significantly increased by 10.3% compared the contralateral PBS-injected retinae (p=0.015) (Figure 6.2A). However, when diabetic mASCs were injected, the average vascular density was decreased by 5.7% compared to the contralateral PBS-injected retinae, but this decrease was not statistically significant (n=6, p=0.82) (Figure 6.2C). Similarly, there were 20.2% more branch points in the retinal vasculature in eyes injected with healthy mASCs relative to the number of branch points in the contralateral PBS-injected controls (p=0.029) (Figure 6.2B). Finally, there were 13.8% fewer branch points in the retinal vasculature of eyes that were injected with diabetic mASCs relative to the number of branch points in the contralateral PBS-injected controls (p=0.71) (Figure 6.2D). No differences were seen in the development of subretinal neovascularization in either healthy or diabetic ASC injected eyes as compared to PBS-injected controls.

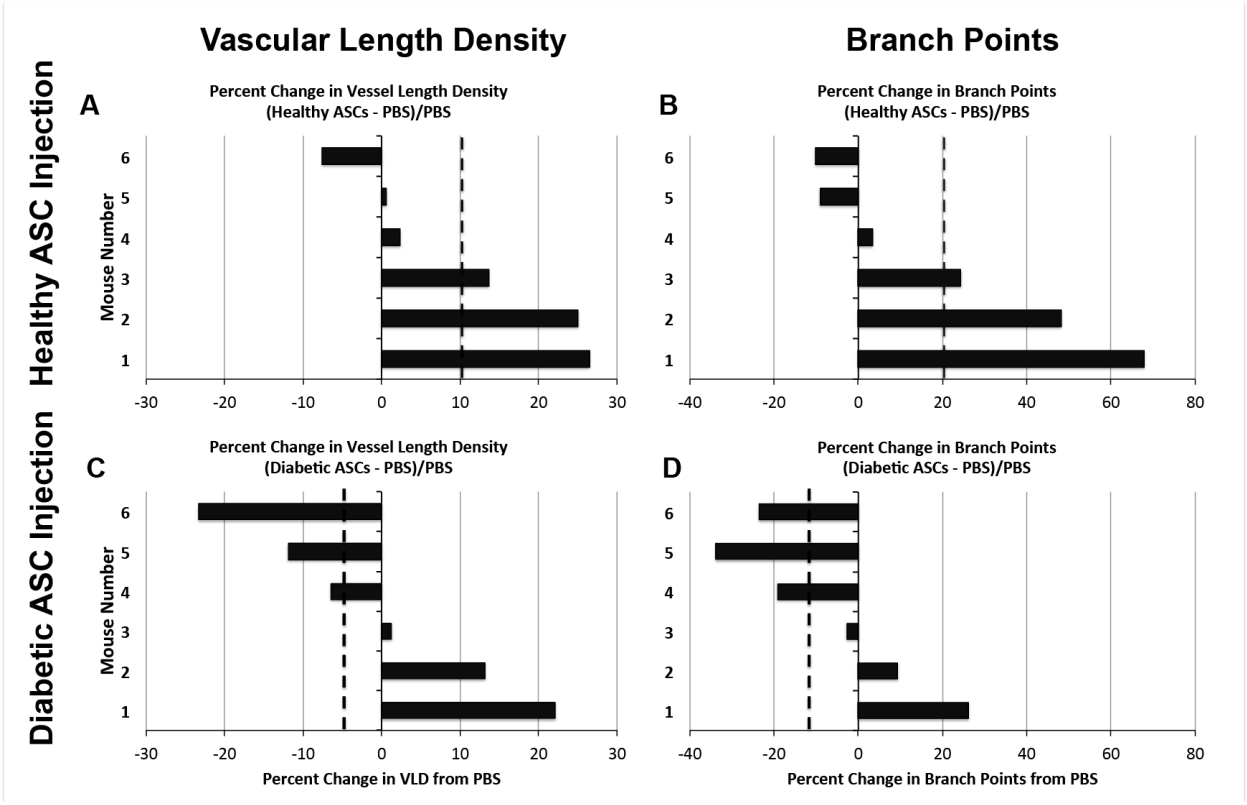

Figure 6.2 Treatment with healthy vs. diabetic mASCs have differential effects on the Akimba mouse retinal microvasculature.

The percent difference in vascular length density for each mouse between ASC-injected retinae and contralateral PBS-injected retinae showed a significant ($p=0.015$; Mann-Whitney Rank Sum test) increase in healthy ASC-injected retinae (A: 10.28% increase), yet no significant change in diabetic ASC-injected retinae (C: 5.71% decrease) relative to contralateral PBS-injected retinae ($p=0.82$; Mann-Whitney Rank Sum test). Healthy ASC-injected retinae also showed a statistically significant ($p=0.029$; Mann-Whitney Rank Sum test) increase in vessel branch points (B: 20.17% increase) relative to PBS-injected retinae, while diabetic ASC-injected retinae had no significant change in branch points compared to PBS-injected retinae (D: 13.77% decrease) ($p=0.71$; Mann-

Whitney Rank Sum test). Dashed line indicates mean percent change between ASC-injected and PBS-injected contralateral control eye.

Incorporation of injected mASCs into perivascular locations

We and others have previously shown that when ASCs are injected into different tissues *in vivo* [11,563-565], including the retina [74], they exhibit pericyte-like behaviors and archetypical pericyte-like morphology. In these previously published studies, injected ASCs have been observed to reside in perivascular locations, enwrap capillaries, and modulate vascular length density in settings of injury and disease. In our study, approximately 60% of injected healthy mASCs were observed in perivascular locations (Figure 6.3), whereas a significantly smaller percentage of diabetic mASCs were observed in perivascular locations (n=16 healthy, n=19 diabetic, $p<0.05$). To determine whether the injected mASCs preferentially resided in perivascular positions, or were localized there by chance, we carried out a Monte Carlo simulation on each 20x FOV. This stochastic simulation provided an estimate of the number of cells for each given field that one would expect to find in contact with a vessel by chance alone based on the observed vascular density and a random distribution of mASCs (Figure 6.4). A larger number of data points were found on the upper left side of the diagonal for both healthy and diabetic mASCs, indicating that the number of mASCs found in contact with the retinal vasculature was greater than what was expected due to chance alone for both healthy and diabetic mASCs. However, a slightly greater number of healthy cell-treated points were found above the line (62%) than diabetic cell-treated points (57%), suggesting a marginally higher preference of healthy cells for perivascular incorporation.

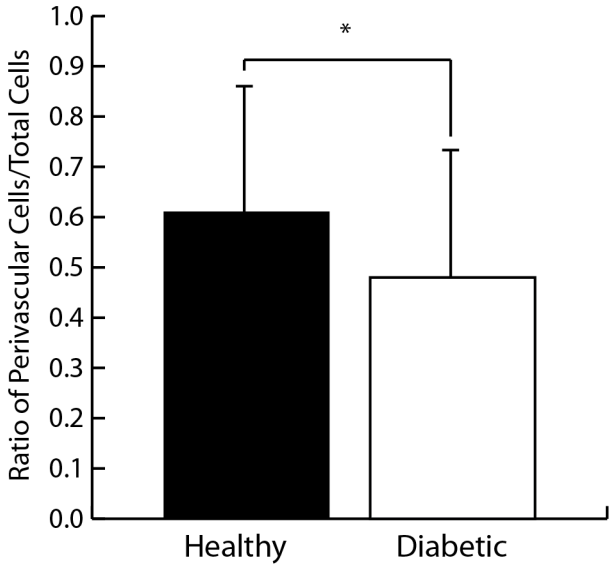

Figure 6.3 Injected healthy mASCs that have engrafted into the retina assume perivascular positions more often than diabetic mASCs.

Engrafted mASCs occupying perivascular and non-perivascular positions were counted in representative 20x confocal image stacks of whole mount Akimba retina. The average ratio of perivascular cells to total engrafted cells in each field is shown for both healthy and diabetic mASCs. n = 16 fields (healthy), n = 19 fields (diabetic), *$p < 0.05$, Wilcoxon Signed Rank test.

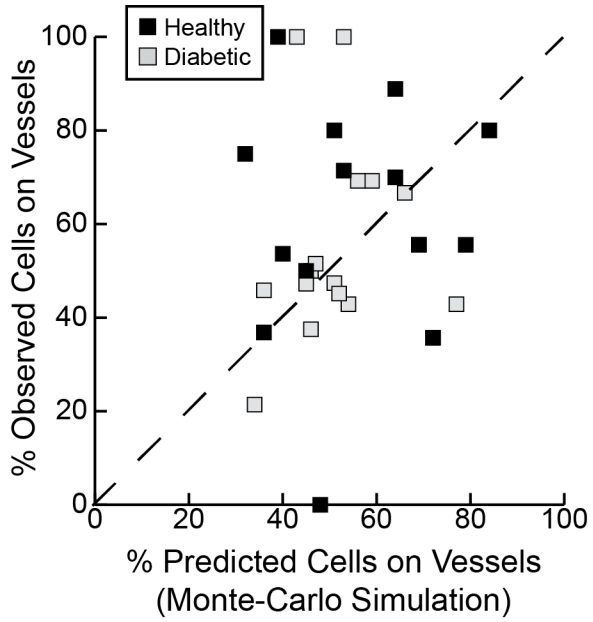

Figure 6.4: Stochastic analysis of mASC spatial distribution in the retina reveals a preference of mASCs to incorporate near retinal vessels.

Each analyzed 20x confocal image of the retinal whole mount is represented as a dot, with the model-predicted percentage of perivascular cells for each image on the x-axis, and the percentage actually observed on the y-axis. At the dashed line (y = x), the observed percentage of perivascular cells is exactly what would be expected due to chance. Above this line, a greater number of perivascular cells were observed than expected by chance, and below the line, fewer were observed than expected by chance, with overall both diabetic and healthy mASCs observed in greater frequency on vessels than would be predicted from a random distribution.

Healthy and diabetic mASC viability and apoptosis

Relative rates of proliferation and apoptosis between healthy and diabetic mASCs were quantified *in vitro* using P4 cultured mASCs. Proliferation frequencies were measured using an EdU-incorporation assay (Life Technologies, Inc.). Diabetic mASC proliferation activity was 77±5% that of healthy mASCs (Figure 6.5A). Diabetic mASC apoptosis was 121±3% that of healthy mASCs, as determined by a TUNEL assay (Figure 6.5B) (n=3 healthy and 3 diabetic animals with 3 cell plates per animal; ±SEM; $p<0.05$).

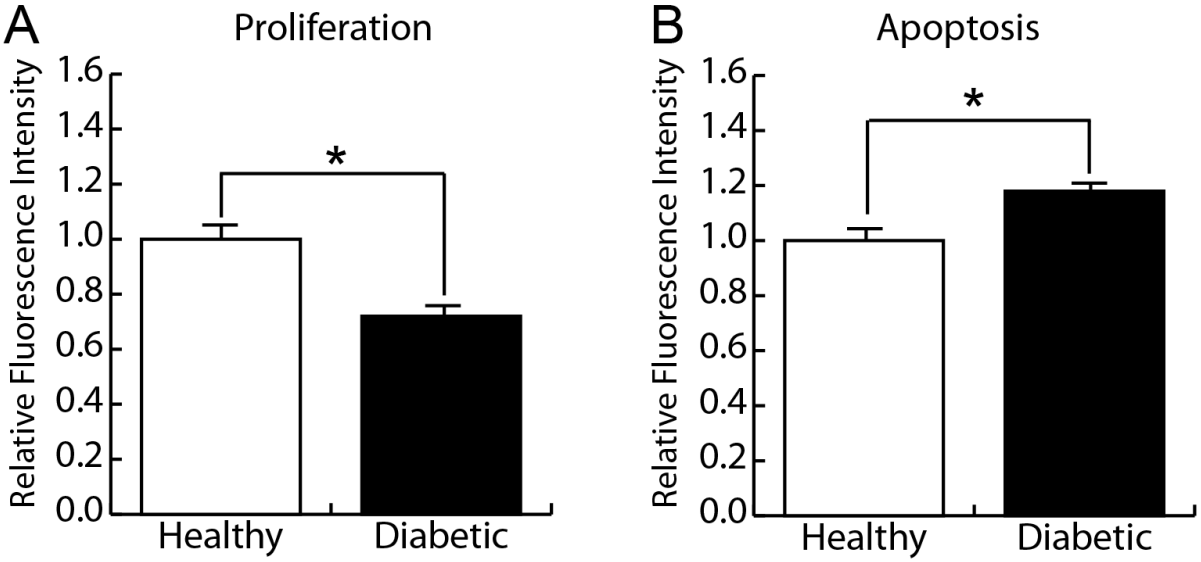

Figure 6.5 Healthy mASCs exhibit higher rates of proliferation and lower rates of apoptosis than diabetic mASCs.

(**A**). Relative number of mASCs in S phase determined by EdU incorporation assay. (**B**). mASCs undergoing apoptosis determined by TUNEL assay. mASCs from 3 healthy and 3 diabetic animals were used for each condition, with three cell plates per animal. Values were normalized to the healthy value in each case. *$p < 0.001$, Student's t-test.

Healthy and diabetic mASC cellular bioenergetics

An analysis of the bioenergetic profiles of healthy mASCs and diabetic mASCs was then performed using the Seahorse instrument to determine whether differences in cellular metabolism may account for their differing treatment efficacy and function *in vivo*. Specifically, mitochondrial bioenergetics in whole cells was evaluated by measuring oxygen consumption over time following the sequential addition of the ATP synthase inhibitor oligomycin, the mitochondrial uncoupler FCCP, and the complexes I and III inhibitors rotenone and Antimycin A[566]. These data revealed that diabetic and non-diabetic mASCs had comparable rates of basal cellular respiration, ATP-dependent respiration, spare respiratory capacity, uncoupled respiration, non-mitochondrial respiration, and extracellular acidification (Figure 6.6).

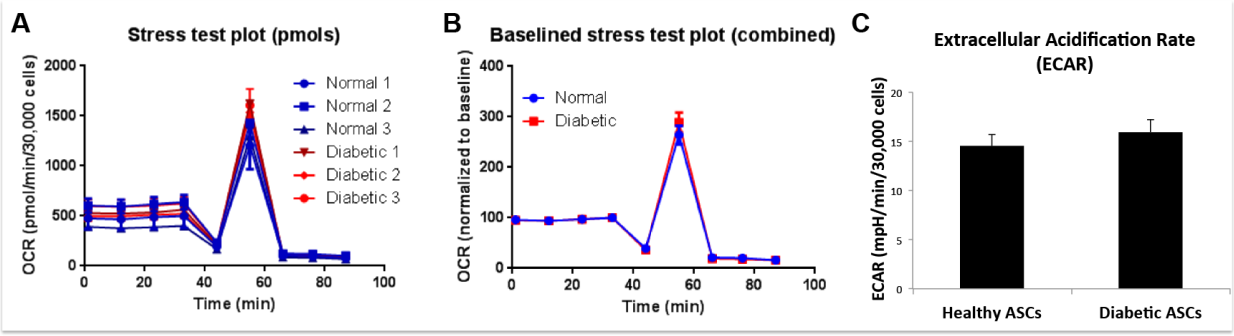

Figure 6.6 Healthy and diabetic mASCs show no difference in metabolic activity.

Healthy and diabetic mASCs were isolated from three diabetic mice and three healthy mice, passaged to P4, and subjected to mitochondrial stress tests on the Seahorse XF Bioanalyzer. Individual profiles (**A**) and combined profiles (**B**) show no difference in baseline cellular respiration, spare respiratory capacity, ATP-linked respiration, uncoupled respiration, or non-mitochondrial respiration. (**C**) Likewise, extracellular acidification rate (ECAR, mpH/min/30,000 cells) analysis showed no difference between healthy and diabetic cell activity.

Angiogenesis factor secretome of healthy and diabetic mASCs

Levels of angiogenic factors secreted by ASCs were measured by analyzing conditioned media samples that collected from P4 healthy and diabetic mASCs (n=4 independent samples per group, each group was analyzed in duplicate, and each sample was obtained from ASCs sourced from a different mouse) using high-throughput ELISA. Each sample was run on a separate array under identical conditions, which enabled us to calculate a relative abundance of each angiogenesis factor by comparing arrays after normalizing to the number of cells that produced the sample. Four angiogenic factors were secreted at significantly higher levels by healthy mASCs than diabetic mASCs, namely IGFBP-3, MCP-1, osteopontin, and SDF-1 ($n=4$, $p<0.01$) (Figure 6.7).

To determine if the angiogenesis factor secretomes of the healthy and diabetic mASCs were capable of affecting the retinal vasculature in the Akimba disease model, healthy mASC conditioned media (CM) was injected into one eye and diabetic mASC CM was injected into the contralateral eye in five-week old Akimba mice (n=6 mice; all mASCs cultured in high glucose, under standard culture conditions). Four weeks later, retinae were harvested and lectin labeling of blood vessels revealed that a single injection of CM did not protect retinal vessels against drop-out in the Akimba model to the same extent that a single injection of healthy or diabetic mASCs did, regardless of ASC origin (Figure 6.8).

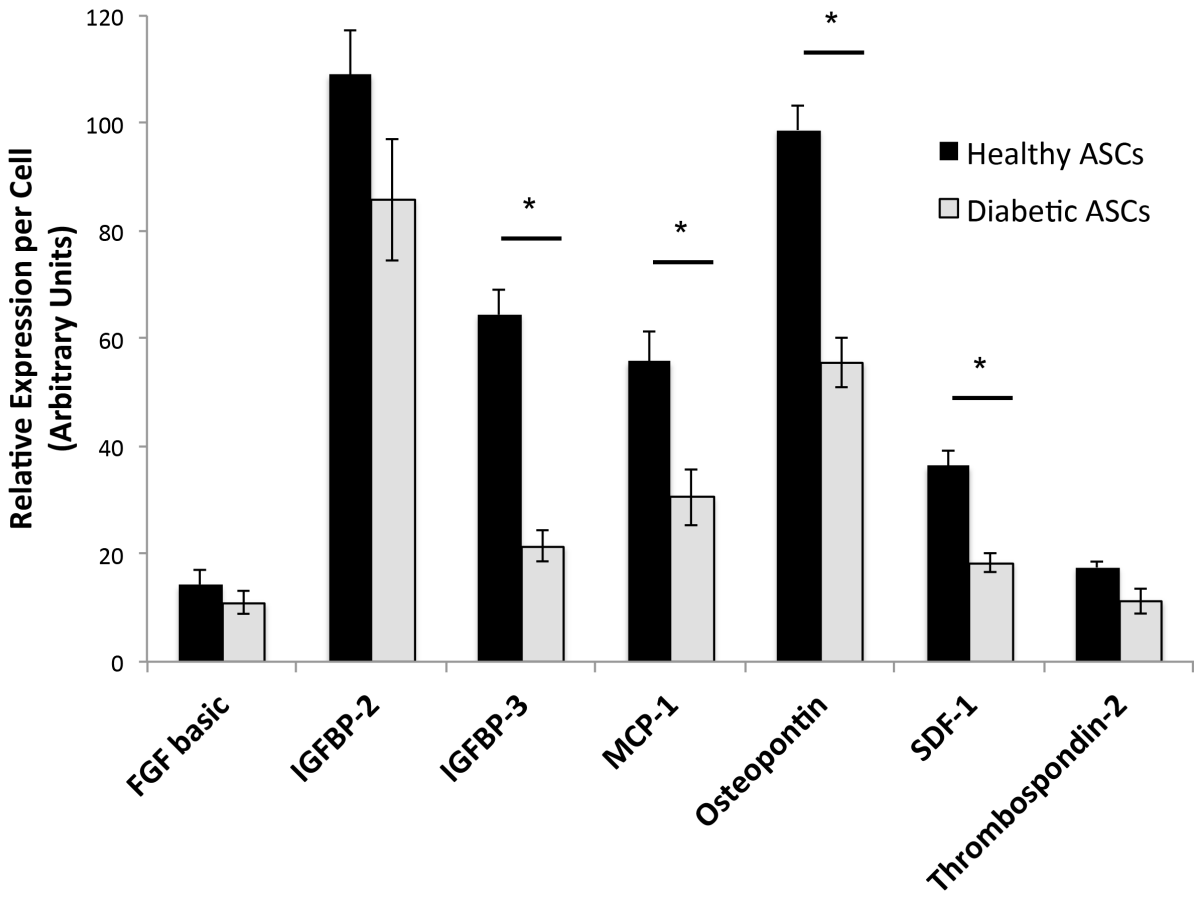

Figure 6.7 Diabetic mASCs secrete lower levels of four factors that have been shown to promote vascular stability.

Relative expression levels of secreted angiogenesis factors by healthy versus diabetic mASCs were obtained using high-throughput ELISA arrays. mASCs were isolated from "healthy" Kimba (black bars) and "diabetic" Akimba (gray bars) mice and maintained to passage 4. Samples consisted of conditioned media obtained by incubating cells immediately after passage in fresh, serum-free media, and collecting media after 24 hours. Relative expression levels were obtained from densitometry analysis (ImageJ) of x-ray film spots. Raw intensity values were normalized to blot area, cell number, the positive control value, and then the background value was subtracted from the normalized intensity. n = 4 mASC populations from 4 mice per group, *$p < 0.01$ Mann-Whitney rank sum test, value are presented as mean +/- SEM.

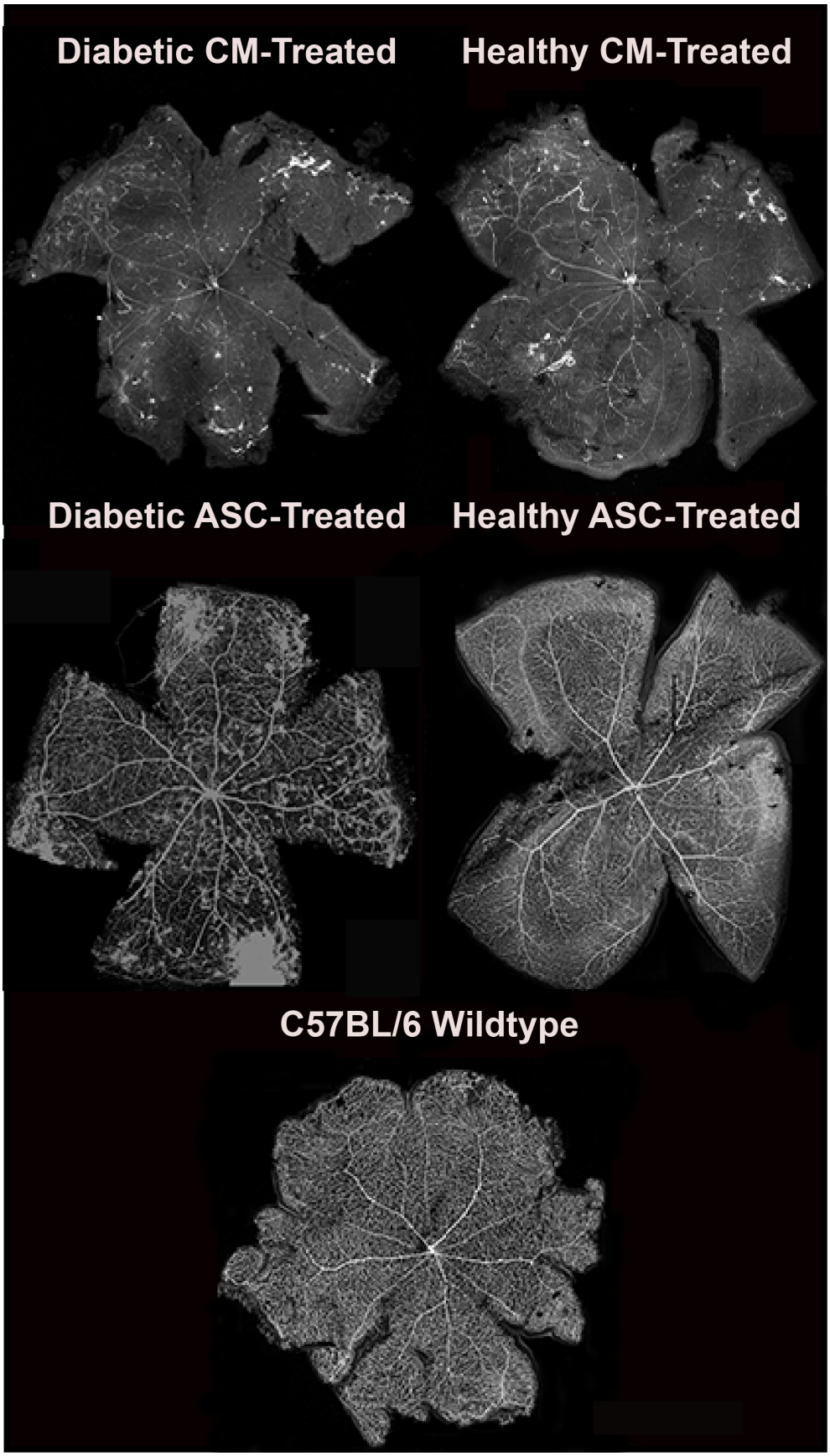
Diabetic CM-Treated
Healthy CM-Treated
Diabetic ASC-Treated
Healthy ASC-Treated
C57BL/6 Wildtype

Figure 6.8 Neither healthy nor diabetic cell conditioned media is sufficient for protecting or restoring retinal vasculature in the Akimba mouse model.

Retinal whole-mounts from mice treated with either diabetic or healthy conditioned media demonstrate significant avascular area and loss of capillaries. ASC-treated or conditioned media (CM)-treated five week-old Akimba mice received a single intra-vitreal injection, and retinae were harvested for analysis 4 weeks later. WIldtype shows vascular pattern in an 8 week-old untreated C57Bl/6 control. All mice were perfused with lectin to visualize the retinal vasculature. Whole mount images were taken at 10x magnification and stitched together as a montage.

Discussion

ASC therapy holds promise for many debilitating and increasingly common vascular disorders due to their stabilizing effects on the microvasculature. This has been attributed to the ability of ASCs and other stem cells to release vasoprotective cytokines and to differentiate into vascular and vascular support cells, such as pericytes [11,73,567]. Furthermore, isolation of ASCs has several advantages over other cell types due to the relative abundance of adipose tissue and relatively painless extraction procedure [568]. The fact that ASCs can be rapidly isolated at high enough quantities for treatment without culture and expansion holds great implications for autologous treatment options. Thus, it is important to assess whether or to what extent ASCs isolated from a diabetic source have compromised treatment efficacy.

In this study, we have demonstrated that intraocularly injected mASCs harvested from diabetic mice have an impaired ability to protect retinal vasculature against progressive pathological vessel drop-out as compared to ASCs harvested from non-diabetic mice. In addition to highlighting the effect of diabetes on mASCs treatment efficacy *in vivo*, this experiment corroborated our group's previous findings that healthy ASCs can both protect and accelerate regeneration of damaged retinal microvasculature [74]. In an effort to explain the observed decreased treatment efficacy when using ASCs from diabetic sources, we carried out an analysis of mASC incorporation *in vivo*, and an *in vitro* functional analysis. We found that mASCs from diabetic sources were less likely to reside in perivascular locations along vessels in the retina compared to mASCs derived from healthy sources. When cultured *in vitro*, mASCs from diabetic donors underwent decreased proliferation and increased apoptosis, in accordance with other studies that have compared diabetic to healthy ASCs [552,569]. However, a statistically similar number of diabetic ASCs and healthy ASCs engrafted in the retina one month after injection, underscoring the fact

that cells growing in well-controlled culture conditions can behave quite differently than cells injected *in vivo*, especially if pathological conditions are present [570]. Hence, we cannot rule out the possibility that the diabetic and non-diabetic ASCs that engraft into the retina may have similar proliferation rates and it is also possible that the engraftment process either normalizes proliferation rates between diabetic and non-diabetic ASCs (i.e. by slowing down non-diabetic ASC proliferation or speeding up diabetic ASC proliferation) or selects for a subpopulation of ASCs with a certain proliferation capacity. Analysis of mASC bioenergetics revealed no differences between healthy and diabetic mASCs, but analysis of their secretome profiles differed with respect to four factors that have been implicated in vascular stability, as discussed in more detail below.

The mechanisms by which mASCs protect the retinal vasculature and the underlying the failure of diabetic mASCs to perform this function as well as non-diabetic mASCs remain unclear. Pericytes belong to the vascular smooth muscle cell lineage [571], and are known to communicate with endothelial cells through paracrine, juxtacrine, and direct cell-cell contact. ASCs have been found to have many similarities with pericytes, such as expressing pericyte surface markers, taking up a perivascular location, and stabilizing endothelial networks [563-565,572]. An absence of pericytes, such as in the pathogenesis of diabetic retinopathy, leads to loss of endothelial cells, dysfunction of endothelial cell junctions and abnormal vessel morphology [573]. MSCs are thought to be closely connected with perivascular cells [574,575], and ASCs have been shown to originate from perivascular MSCs which reside in great numbers in adipose tissue [573]. This would suggest that ASCs might exert their vascular-stabilizing effects in the retina by effectively substituting for decreased native pericyte activity either through replacing their paracrine functions or directly taking up retinal perivascular positions, as we have observed in this and our prior study.

Several studies have found that the regenerative effects of mesenchymal stem cells (MSCs) are at least in part due to the release of paracrine factors [576-578], which act on the microvasculature by facilitating endothelial progenitor cell homing and restructuring vascular networks [575]. A comparison of diabetic and healthy embryonic stem cell function using a hindlimb ischemia model also determined that the loss of function and treatment efficacy was due to lower angiogenic factor secretion by diabetic ESCs [579]. Consistent with these prior studies we find that mASCs from diabetic mice secrete a milieu of growth factors and chemokines *in vitro* that differ markedly from that secreted by ASCs harvested from non-diabetic mice. In particular, mASCs from diabetic sources secreted lower levels of known retinal vasoprotective and neuro-protective factors including IGFBP-3, MCP-1, osteopontin, and SDF-1 [580-583]. Each of these factors has been associated with increased stability and preservation of the vasculature in retina and other tissues. Notably, secretome differences persist whether the mASCs are raised in high or physiologic glucose, except for osteopontin, which under physiologic glucose conditions has similar levels in diabetic and non-diabetic mASCs (data not shown). For all of the studies we report here, we cultured mASCs in conventional (high) glucose conditions because mASCs were subsequently injected into the chronic hyperglycemic environment of the Akimba eye and remained there for the duration of the month prior to harvest.

While we observed vasoprotective effects of mASCs on the superficial vasculature, importantly we do not find increases in aberrant neovascularization, which characteristically develops in the outer nuclear layer in the Akimba mouse [561]. The primary vasoprotective effect of mASCs on the superficial retinal vasculature may be secondary to decreased inflammation, or a rebalancing between pro-angiogenic and anti-angiogenic factors in the Akimba retina. Both mechanisms have been demonstrated to control vascular stability during development and vascular

network formation, and appear to be characteristic of ASC function [11,74,563-565]. The current results suggest that diabetic mASCs are less effective at restoring stability to the highly unstable Akimba retinal vasculature, though whether this is due to reduced sensing of versus response to the microenvironment associated with this progressive retinopathy remains unclear.

Surprisingly, we were unable to recapitulate the vasoprotective effects of injected healthy mASCs through use of concentrated media conditioned by these cells. This runs counter to previous studies that found ASC conditioned media was neuro-protective against light induced retinal toxicity [584]. The reason for this discrepancy remains unclear, but could be explained by the fact that in Tsuruma et al. the conditioned media injection was performed prior to retinal insult, retinal neural cells rather than the vasculature were assessed, and an earlier time point (five days) than what was evaluated in our study (one month) was assessed. It is possible that the levels of growth factors and cytokines that can be achieved with injection of concentrated conditioned media are sub-threshold compared to that achieved with direct ASC injection, or that ASCs are responding to the microenvironment of the Akimba retina in a manner markedly different than they do in culture. It is also possible that direct injection of ASCs has more anti-inflammatory effects than injection of conditioned media does on the retina, which would be expected to improve retinal vascular protection [585]. Regardless, our present findings would argue that direct ASC injection into the eye, including autologous diabetic ASCs, may have higher therapeutic potential than injection of derivative cell conditioned products for the treatment of diabetic retinopathy.

It is interesting to note that while diabetic mASCs showed decreased secretion of these vasoprotective factors, diminished ability to home to and reside in perivascular locations, and an inability to protect the retinal vasculature from drop-out, impairments were not universally seen in all aspects of cell function. Specifically, metabolic capacity and mitochondrial function were

identical in healthy and diabetic cells, under both oxidative respiration and glycolysis conditions, suggesting diabetes-associated hyperglycemia had no lasting effect on these particular cellular functions (Supplementary Figure 1). While others have reported significant hyperglycemia-induced changes in metabolism in other cell types such as bovine retinal pericytes, these studies were performed using high-glucose media [586]. The fact that we saw no metabolic differences after culturing cells to passage 4 indicates that these differences were likely transient, in contrast to changes in the secretome, which was persistent.

Recent evidence implicates epigenetic modification as a driving force in diabetic microvascular complications, which are thought to lead to dysregulation of oxidant and pro-inflammatory factors, and promote vascular inflammation [587-589]. MSCs are well known for their anti-inflammatory role [590], and have been hypothesized to transition between multiple states in response to local cues during infection and wound healing [591]. The mechanism of epigenetic modifications in MSCs or ASCs in response to hyperglycemia is as of yet unknown, but it is possible that these modifications cause similar pro-inflammatory changes in ASCs, and are responsible for the observed differences in cell survival and cytokine secretion.

The observed therapeutic differences in mASCs isolated from healthy and diabetic sources, as well as their cell conditioned media, have implications for the use and study of stem cells beyond the model disease in this study. Cell conditioned media, at least for our model system, appears to lack the full complement of regenerative factors needed to protect the retinal vasculature. Based on the fact that diabetic mASCs are impaired in their regenerative ability to the point that their use did not elicit a predictable and positive response *in vivo*, an autologous approach to ASC therapy in diabetic patients requires careful consideration of the need to correct for these differences. The apparent dysfunction of diabetic perivascular ASCs in the fat may be reflective of the known

dysfunction of retinal pericytes in the diabetic retina [592]. Furthermore, the greater levels of vasoprotective factor secretion in healthy mASCs and concomitant increase in retinal microvascular regeneration supports the notion that allogeneic approaches may ultimately be more effective for treating diabetic retinopathy.

Conclusion

In summary, we have shown that ASCs taken from diabetic sources have an impaired ability to stabilize the microvasculature in diabetic retinopathy, and that use of autologously-derived ASCs from diabetic patients may not be as effective in protecting against vascular drop-out in the retina. Furthermore, hyperglycemia causes distinct changes in ASC function, but only to certain aspects related to regulation of inflammation and vasoprotection. To improve ASC therapy for diabetic retinopathy as well as other diabetic complications, it is critical to better understand their mechanism of action *in vivo*. Future work may focus on describing the means by which ASCs migrate towards and incorporate into the retina and their activity *in vivo*, as well as the mode of diabetes-induced changes in ASC function.

CHAPTER 7

DISCUSSION AND FUTURE DIRECTIONS

Synthesis

The body of work presented in this thesis is motivated by the incredible diversity of endothelial and perivascular cells, as well as the potential for diabetes to undermine the therapeutic capability of perivascular mesenchymal stem cells. So long as the microvasculature remains elusive to therapy, there exists a need for biomedical engineers to develop new tools with which to study the vasculature, and within those tools, the ability to consider the cellular mechanics and environment, in addition to the physiology. Previous studies were limited to either single terminal time-point histological analyses, high-resolution imaging systems (typically in non-mammalian organisms), or low-resolution assessments of vessel perfusion. Here, I leveraged pre-existing microscopy systems to conduct novel imaging of angiogenesis and vascular remodeling in the murine cornea; further, this imaging method enabled quantitative assessment of vascular hierarchy, vessel phenotype, blood flow velocity, vessel permeability, and cellular migration.

Through this technique, I observed heterogeneous endothelial Tie2 expression, which was manipulated by changes in microvascular hemodynamics. Additionally, I observed that the pluripotent stem cell gene Oct4 is required for stable angiogenesis, including pericyte and endothelial migration. While pericyte "steminess" is believed to contribute to their wide heterogeneity, pericyte stem cell character had been predominantly explored *ex vivo*. We used the first pericyte-specific knockout of a gene to demonstrate (1) pluripotent Oct4 is not somatically silenced in perivascular cells and is required for angiogenesis, and (2) the loss of a gene exclusively in pericytes compromises endothelial behavior during adult angiogenesis. Finally, previous studies leveraged adipose-derived stem cells for potential therapeutic use in the diabetic retina, demonstrating that ASCs injected into the retina may assume a perivascular location and morphology, concurrent with the protection of vascular drop out. Yet, these studies were

predominantly conducted with healthy ASCs being injected into diabetic organisms. Given the known heterogeneity of pericytes, the active role of stem cell gene Oct4 in pericytes, and the ability for aberrant perivascular signaling to impede healthy endothelial function, I conducted analysis on the different angiogenic capability and therapeutic potential of healthy versus diabetic ASCs. In all these studies provide a deeper understanding for microvascular heterogeneity, in both health and disease. In addition, they provide new tools with which to study angiogenesis and microvascular remodeling, and, ideally, the basis for more robust therapies aimed at harnessing the microvasculature.

Contributions

Creation of a novel intravital imaging technique

In this dissertation, I developed an intravital imaging technique (Chapter 3) in order to analyze cellular behavior during angiogenesis. When imaging the corneal neovascularization, I was interested in quantifying the vascular network architecture, vessel hierarchy via sO_2, blood flow velocity, as well as protein expression, and cell population at a single-cell resolution, serially over time. Previous studies were unable to capture the complete scope of the vasculature, presented here. As microvascular remodeling is highly dynamic and heterogeneous, I hope this new approach will open the door to novel microvascular studies. Further, this technique is compatible with any fluorescently-labeled mouse, including gene-knockout mice, lineage tracing, and constitutive expression. Thus, it may be applied to any physiologic study in the cornea, including angiogenesis, lymphangiogenesis, and wound healing. Even more, independent of PAM, the intravital confocal analysis may be applied to serial imaging of nerve or epithelial growth and immune cell behavior.

Assessment of Tie2 heterogeneity in the living microvasculature

This work demonstrated the dynamic expression of Tie2 along capillaries during hemodynamic remodeling. While previous studies had addressed Tie2 remodeling *in vitro,* or after a single hemorrhagic chock, no study had putatively shown that Tie2 is heterogeneous and dynamic in the adult vasculature. Further, previous studies had posited that Tie2 is expressed early in the angiogenic vasculature. However, my initial findings demonstrated that Tie2 expression is indeed a marker of endothelial maturity and would not be compatible for early-angiogenic or vascular sprouting studies. Further, Tie2 is a widely-used promoter for genetic knockout studies; considering this data, I would caution against the use of Tie2, as it may not capture all endothelial cells. Finally, there currently exist a number of clinical trials analyzing a small molecule, VE-PTP,

and its therapeutic benefit from constitutively expressing Tie2 along the retinal and kidney microvasculature to prevent hemorrhagic events. The evidence presented here serves as a cautionary tale for systemic circulation of such a molecule, as the vasculature may require down-regulation of Tie2 in order to undergo physiologic angiogenesis, say during wound healing. It is my hope that the method outlined above could be married with studies on VE-PTP to ensure prolonged Tie2 up-regulation is not detrimental to physiologic neovascular growth.

Formation of an in vivo murine model of microvascular hemodynamic remodeling in the cornea

At the time of this dissertation, I had not observed any technique in the cornea that was intended to modulate microvascular hemodynamics. In order to study the endothelial phenotypic response to changes in blood flow, I adopted a study that had recently been published as a small clinical trial in ophthalmology. One fairly common complication in the eye is the growth of excessive tissue on top of and across the cornea, termed a pterygium. Sometimes, these growths become vascularized and obstruct patient vision. In one study, a clinician ligated the neovessels of a tissue growth, in tandem with anti-VEGF therapy, to prevent corneal neovascularization. This inspired the technique I developed, in which a thermal cautery knife was used to ligate a single vessel. This approach allows for observable hemodynamic remodeling, without compromising global tissue oxygenation.

Separation of vascular beds in PAM for quantitative analysis of functionality

Upon the start of my collaboration with the Hu lab, there existed imaging processing techniques capable of isolating different tissue beds. Yet, upon discussion with one of the post-docs with whom I worked most closely, Bo Ning, I realized they had not yet developed the MATLAB code to analyze capillary segments from different tissue beds. Therefore, I developed a protocol that permitted the analysis (and subsequent image generation) of either the corneal or the iris blood

vessels, rather than both of them combined. Previously, it was difficult for a novice to the field of PAM, such as myself, to determine which vessels were within the cornea or iris later for analysis of single vascular segments. With this addition, I was certain that the vessels I analyzed were within the tissue layer I imaged with the intravital confocal microscopy. Finally, this technique permitted higher-fidelity layovers of the confocal and photoacoustic images.

Pericyte-specific genetic knockout study of adult angiogenesis

In this thesis (Chapter 5), we presented the first perivascular cell-specific genetic knockout study of adult angiogenesis. Previous studies had indeed assessed the use of global genetic knockout, endothelial-specific knockouts, and pericyte-gene knockouts during development. All of these studies have contributed invaluable information of the role of pericytes in vascular biology. However, no study had previously demonstrated either the effect of losing gene expression exclusively in a subset of perivascular cells (including a large subset of pericytes), or the subsequent response during angiogenesis. Through this, we uniquely determined that the loss of Oct4, specifically in perivascular cells, was a detriment in overall vascular health, including vessel leakiness, as well as endothelial migration and expansion into the cornea.

Oct4 is not somatically silenced in microvascular pericytes

Previous work by my collaborators were able to demonstrate, for the first time, that pluripotent Oct4 is not silenced in all somatic cells, but rather, played a role in smooth muscle cell investment into atherosclerotic plaques. Inspired by their work, this dissertation was the first to demonstrate the pericytes not only have a multipotent capacity *in vitro*, they are actively using pluripotent genetic pathways during angiogenesis in the adult. This conclusion opens the door to future studies in pericyte multipotency *in vivo*, and underscores their plasticity observed in the

vasculature. Consequential to this data, future studies will be able to explore the underpinning genetic mechanisms of pericyte plasticity and the consequential heterogeneity.

Assessment of pericyte migration and location in vascular networks over time

As discussed in the introduction, there exists a growing and active computational modeling field. In this study, I provided two data-rich quantifications that will be able to inform future computational studies. First, previous studies have conducted rigorous analysis of computational fluid dynamics on the vasculature. I hope that the data presented in Chapter 2 will further inform the cellular phenotype predictions made by these models. Second, within our own lab, there exists agent-based modeling of sprouting angiogenesis that are newly considering pericyte biology. The data presented in Chapter 5 present a rigorous quantification of pericyte quantity and location throughout angiogenesis, with and without Oct4 gene expression. I hope this data is useful to my peers as they seek quantitative assessment of pericyte investment into neovascular beds over time.

Comparison of angiogenic potential of healthy versus diabetic stem cells

Adipose-derived stem cells are an exciting potential therapy for the microvascular complications caused by diabetes. While previous studies indicated that ASCs from a diabetic source have decrease proliferative and wound-healing capabilities, I was specifically interested in how diabetes effects their angiogenic output. Here, we analyzed over 50 factors important in angiogenesis and demonstrated that diabetic ASCs have a decreased angiogenic secretome. Further, while not discussed in depth in this dissertation, we demonstrated that ASCs culture in a "diabetic" high glucose environment – which is the generally-accepted culture condition – have a far lower angiogenic potential than those cultured in a "healthy," low glucose environment. Through this, we uncovered a potential avenue of study to optimize ASC culture conditions to prime them for a robust angiogenic response before their use in treatment.

Extended Applications

No science is truly complete. Each of the studies discussed above brought forth countless follow-up questions and hypotheses, waiting to be tested. Here, I will discuss a few of the exciting future directions that have been inspired from this work.

Role of shear stress versus static stretch in endothelial Tie2 expression

Prior work has demonstrated that the re-distribution of blood flow is sufficient to cause a change in circumferential stretch, in addition to our reported change in shear stress. Upon reviewing the literature, I was unable to find any discussion on the role of static stretch in Tie2 expression. Thus, in collaboration with my colleagues at the Hienrich Hiene University in Düsseldorf, Germany, I leveraged *in vitro* methods to test the response of endothelial cells to both static stretch and shear stress (Figure 7.1). For brevity, the following figure includes both experimental design and data considerations. Through this study, we have preliminarily observed that stretch is not sufficient to cause a change in the presence of phosphorylated Tie2 on HUVECs yet changes in shear stress was sufficient in a time-dependent manner. This result is consistent both with our observations reported in Chapter 2, as well as those made regarding shear stress in the literature. Without static stretch as a confounding variable, further studies may be done to uncover the mechanism behind endothelial cell responses to shear stress, and how those relate to Tie2 phenotypic expression.

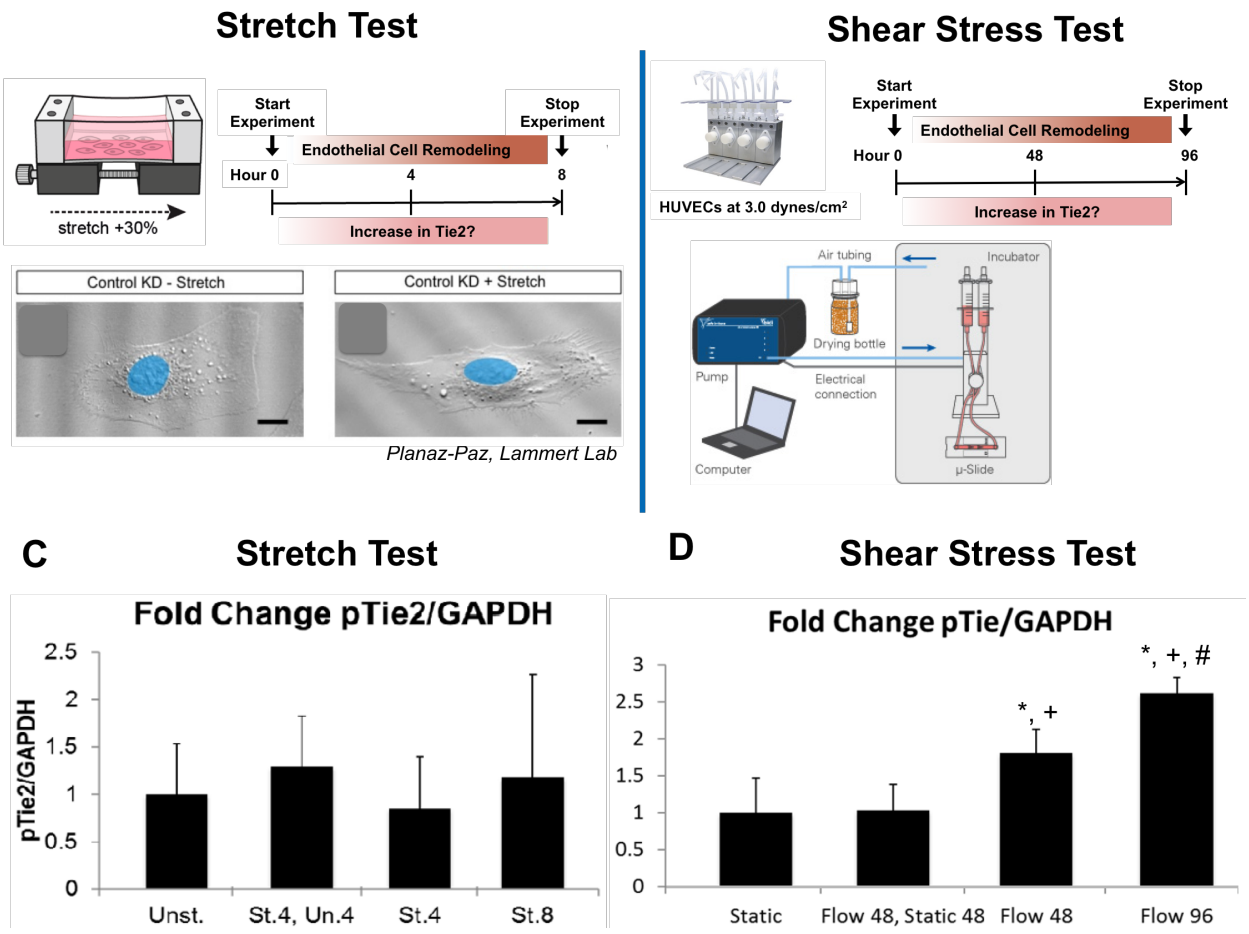

Figure 7. 1 Mechanical stimulation of HUVECs by stretch or shear stress

The change in stretch was not sufficient to induce a change of Tie2 expression. Increased low shear stress for 48 and 96 hours was sufficient to cause a significant increase in the expression of Tie2. $n = 4$, $p < 0.05$, compared to [*] static; [+] flow 48 hours, static 48 hours; [#] flow 48 hours.

Role of Oct4 in the endothelial vasculature

Currently, my ongoing collaboration with the Owens lab continues to grow. Recently, they repeated their studies analyzing the role of Oct4 in the progression of atherosclerotic plaques. However, rather than studying the loss of Oct4 in pericytes, they have conducted very preliminary experiments in which they knock out Oct4 exclusively in the endothelium in a model of murine atherosclerosis. Surprisingly, preliminary data seem to indicate that the endothelium-specific knockout leads to a very similar phenotype as the perivascular cell knock-out. Consequently, exciting new experiments are being conducted to observe whether a loss of Oct4 in the endothelium leads to aberrant angiogenesis. Herein would exist the first evidence that Oct4 is not somatically silenced in endothelial cells. Further, this result could elucidate some of the underpinning mechanism behind endothelial-to-mesenchymal transition in fibrotic disease[593].

Role of Klf4 in perivascular cells during angiogenesis

In Chapter 5, we uncovered that a loss of Oct4 in pericytes leads to increased vascular leakiness by Day 3 post-stimulus. When these studies were repeated at Day 0, before any stimulus, we did not observe a statistically significant increase in vascular leak, but we did observe a slight increase in the knockout. Concurrently, the Owens lab had ongoing studies in the role of another pluripotent gene, Klf4, in perivascular biology. They observed that the loss of Klf4 in pericytes lead to the creation of gaps along the small arterioles and capillaries. This has inspired a new collaboration, examining whether perivascular Klf4 is required for vessel patency during both baseline and angiogenic conditions.

Fate of Myh11-lineage pericytes at the onset of angiogenesis.

One of the major unresolved questions within the Oct4-knock out study is the fate of the Myh11-lineage tracing cells between the onset of angiogenesis and Day 3. In both the wild type

and the knockout, there is a significant decrease in pericyte population, indicating the loss of hundreds of cells. Therefore, there exist a number of studies that could be leveraged to answer both the fate of these cells, and the identity of the perivascular population that replaces them.

First, there exists a strong effort to capture the potential apoptosis of these cells by isolating corneas at multiple time points after angiogenic stimulus for TUNEL staining. Additionally, we have conducted pilot studies injecting Clodronate liposomes into the subconjunctival tissue of the mouse. These liposomes deplete macrophages within a tissue, thus reducing their ability to phagocytose cells within the cornea. Upon doing so, we have observed increased Myh11-lineage populations within the cornea, and even a greater extension of the neovasculature into the cornea. These studies merit follow-up as they may indicate that Myh11-lineage cells are being cleared, and create an explanation for their dramatic population decrease.

Next, in addition to the Myh11-lineage tracing mouse model that was leveraged in Chapter 5, we also have a mouse bred to the Myh11-lineage tracing mouse to an NG2 constitutive reporter mouse. Through this, we have observed that there exists a large NG2-positive, Myh11-lineage-negative population of pericytes that extend along the vasculature. This indicates that even in the wild type, there may be selective subpopulations of perivascular cells (or cells of another origin) that are homing to neovessels. Further, our initial observations seem to indicate that Myh11-lineage cells may have preferential migration to small venules. By using PAM to uncover vessel identity along the microvascular hierarchy, future studies could identify is there is a preference for the vessel type to which Myh11-lineage cells are migrating. Indeed, there exists many fundamental questions on the origin of pericytes, as well as their requisite signaling for migration and investment, in neovascular networks.

Clinical applications of intravital imaging approach.

In addition to answering important questions on basic vascular biology, the methods presented in this thesis are being used to forge new clinical collaborations. First, in collaboration with Dr. Shruti Aggarwal in the Department of Ophthalmology, we are testing the efficacy in a novel therapeutic VEGF-C trap in preventing corneal lymphangiogenesis. In her surface ocular diseases clinic, patients suffer from the complications of increased lymphangiogenesis, most commonly after corneal transplant or during aniridia associated keratopathy. Here, we will leverage a proposed drug dosing technique in our murine corneal angiogenesis assay in an exciting pre-clinical experiment.

Second, in collaboration with the Departments of Electrical and Computer Engineering and Transplant Surgery, we are using the cornea micropocket assay and intravital imaging techniques to test the ability of pancreatic islets sorted with a novel microfluidic device to connect to a patient's vasculature. One major limiting factor in pancreatic islet transplant success is their ability to connect with the host microvasculature to permit islet oxygenation and nutrient delivery, as well as delivery of the islet insulin. We have conducted preliminary studies demonstrating that both sorted and unsorted, "pristine" islets are perfusion competent and able to interact with the host vasculature (Figure 7.2). Now, there exists multiple potential studies testing the efficacy of these implanted islets at protecting their host from hyperglycemia.

Finally, these studies have opened the door to opportunities with the new Center for Biomanufacturing. Already, we have conducted exiting studies using a contact lens to deliver ASCs to angiogenic vessels in the mouse eye (Figure 7.3). Now, new studies are using the cornea assay in order to test the physiologic relevance and efficacy of new biomanufactured, 3D-printed

constructs. Indeed, the cornea is proving to be a highly usable model system for testing construct biocomptability.

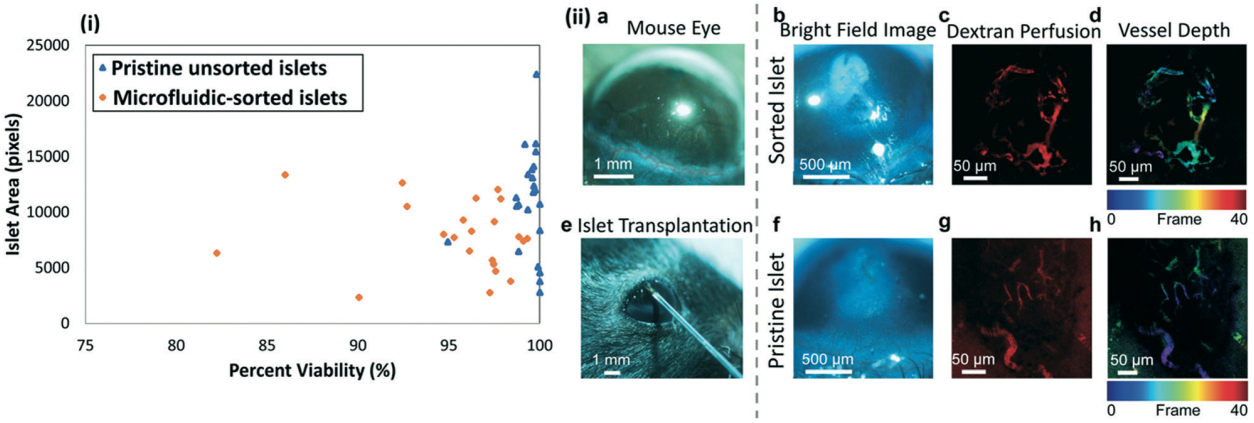

Figure 7.2 Intravital image of implanted pancreatic islets sorted with a novel microfluidic device. (**i**) Percent viability of pristine (unsorted) islets versus microfluidic-sorted islets based on % pixels with 2-fold intensity above background (non-viable tissue) after PI staining; (**ii**) islet vascularization based on angiogenesis assay. (**A, E**) Sorted and pristine pancreatic islets were placed into the mouse cornea using the corneal micropocket assay, (**B, F**) where they remained viable for at least seven days. (**C, D, G,H**) Both sorted and pristine islets incorporated their vasculature into the nearby capillary network, as indicated by (**C,G**) capillaries labelled with the endothelial cell marker CD31, and (**D,H**) were observed going from the limbus vessels (red-orange) into the pancreatic islet (blue-cyan) in the corneal epithelium 28 days after transplantation with the respective islet.

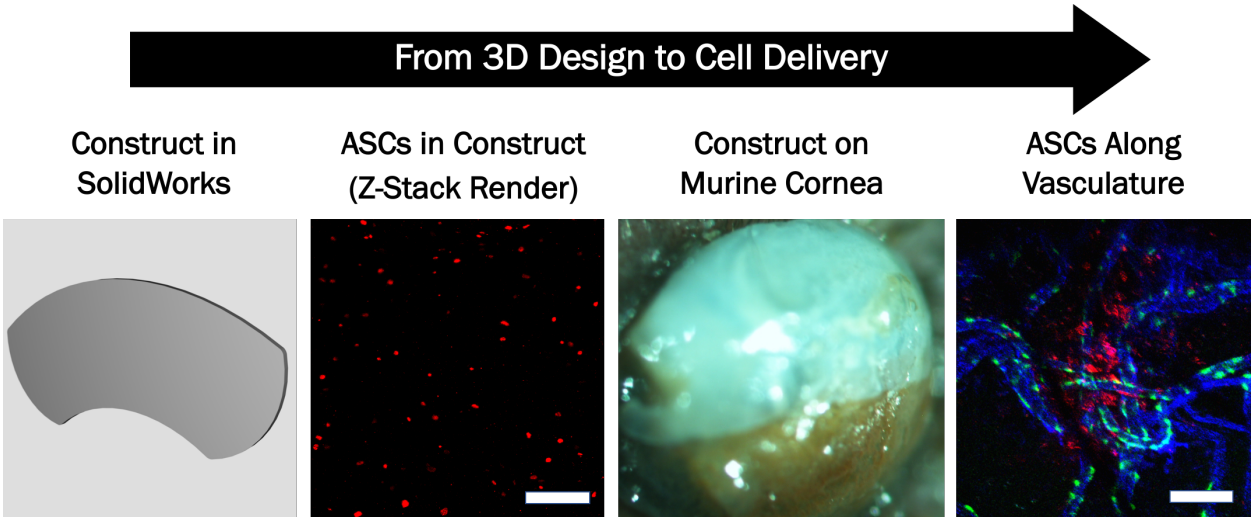

Figure 7.3 Pipeline for biomanufactured construct design and validation in the mouse cornea.

Constructs designed in SolidWorks were used to inform a RegenHu Bioprinter and print ASCs throughout a contact lens (left panels). Intravital imaging was completed 7 days after transplantation. Here we observed ASCs successfully associated with the native vasculature (right panels). Red indicates DiI-Labeled ASCs, blue indicates perfused lectin, and green are Myh11-lineage Scale bar = 0.1 mm

Existing Limitations

While there has been great progress in vascular biology, angiogenic therapeutics, and stem cell therapeutics, there exists a number of limitations within the field. Indeed, both negative findings and major technical hurdles limit the extent to which we can both treat and study the microvasculature. Here, I will briefly consider some of these challenges.

Perhaps the greatest challenge we face in targeting the microvasculature is understanding the multi-faceted identity of the pericyte. Without a universal genetic marker for pericytes, conventional mouse models are unable to leverage fluorescent reporter, lineage tracing, or genetic knockout approaches to their full potential. As discussed in Chapter 4, no genetic mouse model is yet able to capture every pericyte, nor does any current genetic mouse model uniquely isolate pericytes. Even Myh11, often used in this dissertation, captures only a subset of pericytes, and also is expressed by larger smooth muscle cells. Further, given the innate heterogeneity of pericytes, understanding the frequency and type of transcriptional changes they undergo at baseline – or in response to disease – presents a monumental technical challenge. While dual lineage tracing permits fluorescent reporting of a single change in cell expression (e.g., upon the transcript of a gene of interest, a lineage-tracing fluorescent marker for another gene expresses TdTomato, red, instead of the original eGFP, green), more robust methods are required to better grasp the multiplicity of pericyte gene expression patterns during both health and disease. Finally, if the ultimate goal is to either recruit or repel a specific subset of pericytes, targeting them during treatment is yet unfeasible Indeed, the organotypicity of pericytes, as well as their varied subsets along a vessel, underscore the need for targeted or localized therapies. Combined, the highly plastic and heterogeneous nature of pericytes provide technical challenges we cannot yet overcome.

Further, treatments aimed at modulating angiogenesis face a bevy of obstacles. To date, both pro- and anti-angiogenic therapies have limited clinical success. Pro-angiogenic treatments often stimulate the creation of disorganized, leaky vessels that lead to edema[545,594]. In the VIVA trial, 178 patients received placebo, low dose rhVEGF, or high dose rhVEGF. At the end of the trial, neither of the treatment groups saw an improvement in cardiac perfusion[544]. This is consistent with preclinical porcine data that showed no new vessel growth after VEGF treatment[595]. I posit the underpinning mechanism of failure is the inattention to the recruitment of pericytes. While there exists a limited number of therapies delivering a dual antagonist of both endothelial (VEGF) and perivascular (PDGF) cells, they, too, result in edema; pre-clinical data for one such trial includes of images of limbal vessels stripped of their supportive pericytes[596]. Conversely, anti-angiogenic therapies are widely used in the clinic. Intravitral injection of anti-VEGF treatments (e.g., aflibercept, bevacizumab, and ranibizumab), is the most widely-used drug therapy for proliferative diabetic retinopathy[72]. While these treatments are viewed as a therapeutic success, they only serve to delay vision-compromising laser coagulation, typically only for 6-24 months[597]. Indeed, the current fate of therapies aimed at angiogenesis remain uncertain. While there has been marginal success, a greater understanding of pericyte migration to angiogenic endothelium and subsequent vascular stabilization is required.

Lastly, stem cell therapeutics remain highly controversial, with a large population of clinical trials failing, despite significant financial and patient investment. A recent review of cell therapy for heart disease underscored the 17 years of struggle to find an FDA-approved treatment using stem cell therapy for heart failure[598]. Citing numerous failures, including the PreSERVE-AMI trial demonstrating no improvement in 161 patients with acute myocardial infarction, the authors ask for other alternatives[599]. However, it seems the "cat has been let out of the bag" for stem cell

therapy. Horrifyingly, a recent analysis identified nearly 600 direct-to-patient businesses marketing stem cell interventions[600], just for cardiac repair alone. Likewise, in ophthalmology, private businesses are using stem cell interventions. One such instance includes the autologous use of ASCs in three women with macular degeneration, which lead to the complete loss of their vision[601]. This trial underscores a major challenge: stem cells isolated for therapy are considered to be a homogeneous population. However, given their innate heterogeneity and highly plastic nature, little is known regarding what cell phenotypes exist in a given bolus for treatment. Further, current treatments are largely autologous. Yet, as discussed in Chapter 6, these patients often have a number of co-morbidities, including diabetes and metabolic syndrome, which dramatically impacts the therapeutic potential of the cells. Thus, it is important to determine how to select for therapeutically-capable cells, either from an autologous or donor source. Finally, pre-clinical trials on the use of stem cells in stroke demonstrate two sources of risk: tumor formation at site of injection and collection of stem cells in the lung[602,603]. Indeed, these challenges may be too great to overcome. While solutions exist, such as cell-mimicking microparticles and the use of bioactive components (i.e., mRNA-filled exosomes), they too are far from being clinically relevant. Thus, further studies on stem cell reaction to pathologic conditions, as well as how to better select and prime cells for injection, are required for clinical success.

Final Remarks

The field of biomedical engineering is diverse. At its core, though, exists the desire to use engineering principles and design to better biomedical outcomes. The microvasculature, with all its mysteries, embodies considerations in biomechanics and biochemical signaling. Further still, its deep complexities demand increasingly refined and informative imaging approaches, and in light of the data collected from those, invites the fields of multiscale modeling to sift through and clarify our findings. In this thesis, I was inspired by the diverse opportunities afforded by the study biomedical engineering to approach the questions provided by the plastic, heterogeneous microvasculature.

In this dissertation, I used a novel intravital imaging approach to analyze the heterogeneity of endothelial and perivascular populations. Further, from this imaging approach, I considered the role of biomechanics in phenotypic presentations of cellular maturity and stability. These considerations revealed new relationships between shear stress and the endothelium in a living vascular network. Additionally, inspired by what I observed in the microscope, I wrote a review of the role of mechanosensing in vascular development, homeostasis, and disease, also presented in this dissertation.

Employing the imaging approach again, I sought to study the role of plasticity in perivascular biology. Through this, I presented new substantial evidence on the role of stem cell gene signaling in the adult microvasculature. In turn, I presented considerations for the effect of diabetes on the angiogenic potential of stem cells isolated to replace this pericyte population. These considerations are especially relevant to studies in tissue engineering, such as the Biomanufacturing Center within our department, when seeking to therapeutically isolate or replace pericyte populations.

In a narrow sense, I hope these studies present greater understanding of the microvasculature and its heterogeneities. Even further, I hope that my efforts to develop new tools and new mechanistic insights will help unravel the incredible complexity of vascular disease. And, finally, I hope that these studies are viewed in their greater context. In the incredible scope of human health, and the innumerable ways it finds to fail, I hope the work here is considered a small, but useful, step forward.

REFERENCES

1. Carmeliet, P. Angiogenesis in life, disease and medicine. *Nature* **438**, 932-936 (2005).
2. Aird, W.C. Phenotypic heterogeneity of the endothelium: I. Structure, function, and mechanisms. *Circ Res* **100**, 158-173 (2007).
3. Ballermann, B.J., Dardik, A., Eng, E. & Liu, A. Shear stress and the endothelium. *Kidney Int Suppl* **67**, S100-108 (1998).
4. Yang, B. & Rizzo, V. Shear Stress Activates eNOS at the Endothelial Apical Surface Through beta1 Containing Integrins and Caveolae. *Cell Mol Bioeng* **6**, 346-354 (2013).
5. White, C.R. & Frangos, J.A. The shear stress of it all: the cell membrane and mechanochemical transduction. *Philos Trans R Soc Lond B Biol Sci* **362**, 1459-1467 (2007).
6. Vozzi, F., Bianchi, F., Ahluwalia, A. & Domenici, C. Hydrostatic pressure and shear stress affect endothelin-1 and nitric oxide release by endothelial cells in bioreactors. *Biotechnol J* **9**, 146-154 (2014).
7. Urner, S., Kelly-Goss, M., Peirce, S.M. & Lammert, E. Mechanotransduction in Blood and Lymphatic Vascular Development and Disease. *Adv Pharmacol* **81**, 155-208 (2018).
8. Mazzoni, J., Cutforth, T. & Agalliu, D. Dissecting the Role of Smooth Muscle Cells versus Pericytes in Regulating Cerebral Blood Flow Using In Vivo Optical Imaging. *Neuron* **87**, 4-6 (2015).
9. Hall, C.N.*, et al.* Capillary pericytes regulate cerebral blood flow in health and disease. *Nature* **508**, 55-60 (2014).
10. Fernandez-Klett, F. & Priller, J. Diverse functions of pericytes in cerebral blood flow regulation and ischemia. *J Cereb Blood Flow Metab* **35**, 883-887 (2015).
11. Kelly-Goss, M.R., Sweat, R.S., Stapor, P.C., Peirce, S.M. & Murfee, W.L. Targeting pericytes for angiogenic therapies. *Microcirculation* **21**, 345-357 (2014).
12. Carmeliet, P. Mechanisms of angiogenesis and arteriogenesis. *Nature medicine* **6**, 389-395 (2000).
13. Risau, W. Mechanisms of angiogenesis. *Nature* **386**, 671-674 (1997).
14. Drake, C.J. & Fleming, P.A. Vasculogenesis in the day 6.5 to 9.5 mouse embryo. *Blood* **95**, 1671-1679 (2000).
15. Asahara, T.*, et al.* Tie2 receptor ligands, angiopoietin-1 and angiopoietin-2, modulate VEGF-induced postnatal neovascularization. *Circulation research* **83**, 233-240 (1998).
16. Cai, W. & Schaper, W. Mechanisms of arteriogenesis. *Acta Biochim Biophys Sin (Shanghai)* **40**, 681-692 (2008).
17. Eichmann, A.*, et al.* Vascular development: from precursor cells to branched arterial and venous networks. *The International journal of developmental biology* **49**, 259-267 (2005).
18. Gerhardt, H. & Betsholtz, C. Endothelial-pericyte interactions in angiogenesis. *Cell and tissue research* **314**, 15-23 (2003).

19. Bazmara, H.*, et al.* Blood flow and endothelial cell phenotype regulation during sprouting angiogenesis. *Medical & biological engineering & computing* **54**, 547-558 (2016).
20. Makanya, A.N., Hlushchuk, R. & Djonov, V.G. Intussusceptive angiogenesis and its role in vascular morphogenesis, patterning, and remodeling. *Angiogenesis* **12**, 113-123 (2009).
21. Florey. The endothelial cell. *Br Med J* **2**, 487-490 (1966).
22. Tan, P.E., Yu, P.K., Cringle, S.J., Morgan, W.H. & Yu, D.Y. Regional heterogeneity of endothelial cells in the porcine vortex vein system. *Microvasc Res* **89**, 70-79 (2013).
23. Aird, W.C. Endothelial cell heterogeneity. *Cold Spring Harb Perspect Med* **2**, a006429 (2012).
24. dela Paz, N.G. & D'Amore, P.A. Arterial versus venous endothelial cells. *Cell Tissue Res* **335**, 5-16 (2009).
25. Simionescu, M., Simionescu, N. & Palade, G.E. Segmental differentiations of cell junctions in the vascular endothelium. Arteries and veins. *J Cell Biol* **68**, 705-723 (1976).
26. Molema, G. & Aird, W.C. Vascular heterogeneity in the kidney. *Semin Nephrol* **32**, 145-155 (2012).
27. Wisse, E. An electron microscopic study of the fenestrated endothelial lining of rat liver sinusoids. *J Ultrastruct Res* **31**, 125-150 (1970).
28. Lacorre, D.A.*, et al.* Plasticity of endothelial cells: rapid dedifferentiation of freshly isolated high endothelial venule endothelial cells outside the lymphoid tissue microenvironment. *Blood* **103**, 4164-4172 (2004).
29. Nolan, D.J.*, et al.* Molecular signatures of tissue-specific microvascular endothelial cell heterogeneity in organ maintenance and regeneration. *Dev Cell* **26**, 204-219 (2013).
30. Regan, E.R. & Aird, W.C. Dynamical systems approach to endothelial heterogeneity. *Circ Res* **111**, 110-130 (2012).
31. Chi, J.T.*, et al.* Endothelial cell diversity revealed by global expression profiling. *Proc Natl Acad Sci U S A* **100**, 10623-10628 (2003).
32. Walpole, J., Mac Gabhann, F., Peirce, S.M. & Chappell, J.C. Agent-based computational model of retinal angiogenesis simulates microvascular network morphology as a function of pericyte coverage. *Microcirculation* **24**(2017).
33. Walpole, J.*, et al.* Agent-based model of angiogenesis simulates capillary sprout initiation in multicellular networks. *Integr Biol (Camb)* **7**, 987-997 (2015).
34. Aparicio, P.*, et al.* Modelling the influence of endothelial heterogeneity on the progression of arterial disease: application to abdominal aortic aneurysm evolution. *Int J Numer Method Biomed Eng* **30**, 563-586 (2014).
35. Kelly-Goss, M.R., Sweat, R.S., Stapor, P.C., Peirce, S.M. & Murfee, W.L. Targeting pericytes for angiogenic therapies. *Microcirculation (New York, N.Y.: 1994)* **21**, 345-357 (2014).
36. Crisan, M.*, et al.* A perivascular origin for mesenchymal stem cells in multiple human organs. *Cell stem cell* **3**, 301-313 (2008).
37. He, L.*, et al.* Analysis of the brain mural cell transcriptome. *Sci Rep* **6**, 35108 (2016).
38. Vanlandewijck, M.*, et al.* A molecular atlas of cell types and zonation in the brain vasculature. *Nature* **554**, 475-480 (2018).

39. Alliot, F., Rutin, J., Leenen, P.J. & Pessac, B. Pericytes and periendothelial cells of brain parenchyma vessels co-express aminopeptidase N, aminopeptidase A, and nestin. *J Neurosci Res* **58**, 367-378 (1999).
40. Jager, M., Weber, P. & Wolf, S. Immunohistochemical localization of 5-oxo-L-prolinase, an enzyme of the gamma-glutamyl cycle, in porcine brain microvessels. *FEBS Lett* **445**, 215-217 (1999).
41. Knittel, T.*, et al.* Expression and regulation of cell adhesion molecules by hepatic stellate cells (HSC) of rat liver: involvement of HSC in recruitment of inflammatory cells during hepatic tissue repair. *Am J Pathol* **154**, 153-167 (1999).
42. Sims, D.E. Diversity within pericytes. *Clin Exp Pharmacol Physiol* **27**, 842-846 (2000).
43. Li, X.F.*, et al.* Angiogenic growth factor messenger ribonucleic acids in uterine natural killer cells. *J Clin Endocrinol Metab* **86**, 1823-1834 (2001).
44. Fernandez, P.M. & Rickles, F.R. Tissue factor and angiogenesis in cancer. *Curr Opin Hematol* **9**, 401-406 (2002).
45. Folkman, J. Tumor angiogenesis: therapeutic implications. *N Engl J Med* **285**, 1182-1186 (1971).
46. Bergers, G., Song, S., Meyer-Morse, N., Bergsland, E. & Hanahan, D. Benefits of targeting both pericytes and endothelial cells in the tumor vasculature with kinase inhibitors. *J Clin Invest* **111**, 1287-1295 (2003).
47. Song, S., Ewald, A.J., Stallcup, W., Werb, Z. & Bergers, G. PDGFRbeta+ perivascular progenitor cells in tumours regulate pericyte differentiation and vascular survival. *Nat Cell Biol* **7**, 870-879 (2005).
48. Orimo, A.*, et al.* Stromal fibroblasts present in invasive human breast carcinomas promote tumor growth and angiogenesis through elevated SDF-1/CXCL12 secretion. *Cell* **121**, 335-348 (2005).
49. De Palma, M.*, et al.* Tie2 identifies a hematopoietic lineage of proangiogenic monocytes required for tumor vessel formation and a mesenchymal population of pericyte progenitors. *Cancer Cell* **8**, 211-226 (2005).
50. Jain, R.K. Normalization of tumor vasculature: an emerging concept in antiangiogenic therapy. *Science* **307**, 58-62 (2005).
51. Ye, W. The Complexity of Translating Anti-angiogenesis Therapy from Basic Science to the Clinic. *Dev Cell* **37**, 114-125 (2016).
52. Nagy, J.A., Chang, S.H., Shih, S.C., Dvorak, A.M. & Dvorak, H.F. Heterogeneity of the tumor vasculature. *Semin Thromb Hemost* **36**, 321-331 (2010).
53. Denekamp, J. & Hobson, B. Endothelial-cell proliferation in experimental tumours. *Br J Cancer* **46**, 711-720 (1982).
54. Morikawa, S.*, et al.* Abnormalities in pericytes on blood vessels and endothelial sprouts in tumors. *Am J Pathol* **160**, 985-1000 (2002).
55. Hida, K., Ohga, N., Akiyama, K., Maishi, N. & Hida, Y. Heterogeneity of tumor endothelial cells. *Cancer Sci* **104**, 1391-1395 (2013).
56. Fukumura, D., Yuan, F., Monsky, W.L., Chen, Y. & Jain, R.K. Effect of host microenvironment on the microcirculation of human colon adenocarcinoma. *Am J Pathol* **151**, 679-688 (1997).
57. Roberts, W.G.*, et al.* Host microvasculature influence on tumor vascular morphology and endothelial gene expression. *Am J Pathol* **153**, 1239-1248 (1998).

58. Calabrese, C.*, et al.* A perivascular niche for brain tumor stem cells. *Cancer Cell* **11**, 69-82 (2007).
59. Cheng, L.*, et al.* Glioblastoma stem cells generate vascular pericytes to support vessel function and tumor growth. *Cell* **153**, 139-152 (2013).
60. Boscolo, E., Mulliken, J.B. & Bischoff, J. Pericytes from infantile hemangioma display proangiogenic properties and dysregulated angiopoietin-1. *Arterioscler Thromb Vasc Biol* **33**, 501-509 (2013).
61. Ribeiro, A.L. & Okamoto, O.K. Combined effects of pericytes in the tumor microenvironment. *Stem Cells Int* **2015**, 868475 (2015).
62. Bergers, G. & Hanahan, D. Modes of resistance to anti-angiogenic therapy. *Nat Rev Cancer* **8**, 592-603 (2008).
63. Cogan, D.G. & Kuwabara, T. The mural cell in perspective. *Archives of Ophthalmology* **78**, 133-139 (1967).
64. Kuwabara, T. & Cogan, D.G. Retinal vascular patterns. VI. Mural cells of the retinal capillaries. *Arch Ophthalmol* **69**, 492-502 (1963).
65. vom Hagen, F.*, et al.* Early loss of arteriolar smooth muscle cells: more than just a pericyte loss in diabetic retinopathy. *Exp Clin Endocrinol Diabetes* **113**, 573-576 (2005).
66. Enge, M.*, et al.* Endothelium-specific platelet-derived growth factor-B ablation mimics diabetic retinopathy. *EMBO J* **21**, 4307-4316 (2002).
67. Arboleda-Velasquez, J.F., Valdez, C.N., Marko, C.K. & D'Amore, P.A. From pathobiology to the targeting of pericytes for the treatment of diabetic retinopathy. *Curr Diab Rep* **15**, 573 (2015).
68. Chuang, P.Y., Yu, Q., Fang, W., Uribarri, J. & He, J.C. Advanced glycation endproducts induce podocyte apoptosis by activation of the FOXO4 transcription factor. *Kidney Int* **72**, 965-976 (2007).
69. Kobayashi, T. & Puro, D.G. Loss of insulin-mediated vasoprotection: early effect of diabetes on pericyte-containing microvessels of the retina. *Invest Ophthalmol Vis Sci* **48**, 2350-2355 (2007).
70. Spinetti, G., Kraenkel, N., Emanueli, C. & Madeddu, P. Diabetes and vessel wall remodelling: from mechanistic insights to regenerative therapies. *Cardiovasc Res* **78**, 265-273 (2008).
71. Stewart, M.W. Treatment of diabetic retinopathy: Recent advances and unresolved challenges. *World J Diabetes* **7**, 333-341 (2016).
72. Heng, L.Z.*, et al.* Diabetic retinopathy: pathogenesis, clinical grading, management and future developments. *Diabet Med* **30**, 640-650 (2013).
73. Ebrahimian, T.G.*, et al.* Cell therapy based on adipose tissue-derived stromal cells promotes physiological and pathological wound healing. *Arterioscler Thromb Vasc Biol* **29**, 503-510 (2009).
74. Mendel, T.A.*, et al.* Pericytes derived from adipose-derived stem cells protect against retinal vasculopathy. *PloS one* **8**, e65691 (2013).
75. Amos, P.J.*, et al.* IFATS collection: The role of human adipose-derived stromal cells in inflammatory microvascular remodeling and evidence of a perivascular phenotype. *Stem cells (Dayton, Ohio)* **26**, 2682-2690 (2008).
76. Irvin, M.W., Zijlstra, A., Wikswo, J.P. & Pozzi, A. Techniques and assays for the study of angiogenesis. *Exp Biol Med (Maywood)* **239**, 1476-1488 (2014).

77. Nesmith, J.E., Chappell, J.C., Cluceru, J.G. & Bautch, V.L. Blood vessel anastomosis is spatially regulated by Flt1 during angiogenesis. *Development* **144**, 889-896 (2017).
78. Liu, X. & Sun, J. Potential proinflammatory effects of hydroxyapatite nanoparticles on endothelial cells in a monocyte-endothelial cell coculture model. *Int J Nanomedicine* **9**, 1261-1273 (2014).
79. Eckermann, C.W., Lehle, K., Schmid, S.A., Wheatley, D.N. & Kunz-Schughart, L.A. Characterization and modulation of fibroblast/endothelial cell co-cultures for the in vitro preformation of three-dimensional tubular networks. *Cell Biol Int* **35**, 1097-1110 (2011).
80. Liu, Y., Li, H., Yan, S., Wei, J. & Li, X. Hepatocyte cocultures with endothelial cells and fibroblasts on micropatterned fibrous mats to promote liver-specific functions and capillary formation capabilities. *Biomacromolecules* **15**, 1044-1054 (2014).
81. Katyshev, V. & Dore-Duffy, P. Pericyte coculture models to study astrocyte, pericyte, and endothelial cell interactions. *Methods Mol Biol* **814**, 467-481 (2012).
82. van der Meer, A.D., Orlova, V.V., ten Dijke, P., van den Berg, A. & Mummery, C.L. Three-dimensional co-cultures of human endothelial cells and embryonic stem cell-derived pericytes inside a microfluidic device. *Lab Chip* **13**, 3562-3568 (2013).
83. Durham, J.T., Surks, H.K., Dulmovits, B.M. & Herman, I.M. Pericyte contractility controls endothelial cell cycle progression and sprouting: insights into angiogenic switch mechanics. *Am J Physiol Cell Physiol* **307**, C878-892 (2014).
84. Bowers, S.L., Meng, C.X., Davis, M.T. & Davis, G.E. Investigating human vascular tube morphogenesis and maturation using endothelial cell-pericyte co-cultures and a doxycycline-inducible genetic system in 3D extracellular matrices. *Methods Mol Biol* **1189**, 171-189 (2015).
85. Sasaki, N., Bos, C., Escoffre, J.M., Storm, G. & Moonen, C. Development of a tumor tissue-mimicking model with endothelial cell layer and collagen gel for evaluating drug penetration. *Int J Pharm* **482**, 118-122 (2015).
86. Gough, W.*, et al.* A quantitative, facile, and high-throughput image-based cell migration method is a robust alternative to the scratch assay. *J Biomol Screen* **16**, 155-163 (2011).
87. Sheets, A.R., Durham, J.T. & Herman, I.M. Quantitative Imaging-Based Examination of Pericytes Controlling Endothelial Growth Dynamics and Angiogenesis. *Methods Mol Biol* **1430**, 221-229 (2016).
88. Jonkman, J.E.*, et al.* An introduction to the wound healing assay using live-cell microscopy. *Cell Adh Migr* **8**, 440-451 (2014).
89. Yue, P.Y., Leung, E.P., Mak, N.K. & Wong, R.N. A simplified method for quantifying cell migration/wound healing in 96-well plates. *J Biomol Screen* **15**, 427-433 (2010).
90. Hebeiss, I., Truckenmuller, R., Giselbrecht, S. & Schepers, U. Novel three-dimensional Boyden chamber system for studying transendothelial transport. *Lab Chip* **12**, 829-834 (2012).
91. Aplin, A.C. & Nicosia, R.F. The rat aortic ring model of angiogenesis. *Methods Mol Biol* **1214**, 255-264 (2015).
92. Baker, M.*, et al.* Use of the mouse aortic ring assay to study angiogenesis. *Nat Protoc* **7**, 89-104 (2011).

93. Sweat, R.S., Sloas, D.C. & Murfee, W.L. VEGF-C induces lymphangiogenesis and angiogenesis in the rat mesentery culture model. *Microcirculation* **21**, 532-540 (2014).
94. Azimi, M.S.*, et al.* An ex vivo model for anti-angiogenic drug testing on intact microvascular networks. *PLoS One* **10**, e0119227 (2015).
95. Planas-Paz, L. & Lammert, E. Mechanosensing in developing lymphatic vessels. *Adv Anat Embryol Cell Biol* **214**, 23-40 (2014).
96. Zeiger, A.S.*, et al.* Static mechanical strain induces capillary endothelial cell cycle re-entry and sprouting. *Phys Biol* **13**, 046006 (2016).
97. Conway, D.E.*, et al.* Fluid shear stress on endothelial cells modulates mechanical tension across VE-cadherin and PECAM-1. *Curr Biol* **23**, 1024-1030 (2013).
98. Walshe, T.E., Ferguson, G., Connell, P., O'Brien, C. & Cahill, P.A. Pulsatile flow increases the expression of eNOS, ET-1, and prostacyclin in a novel in vitro coculture model of the retinal vasculature. *Invest Ophthalmol Vis Sci* **46**, 375-382 (2005).
99. Wang, C., Baker, B.M., Chen, C.S. & Schwartz, M.A. Endothelial cell sensing of flow direction. *Arterioscler Thromb Vasc Biol* **33**, 2130-2136 (2013).
100. Hwang, J.*, et al.* Pulsatile versus oscillatory shear stress regulates NADPH oxidase subunit expression: implication for native LDL oxidation. *Circ Res* **93**, 1225-1232 (2003).
101. Zheng, C.*, et al.* Quantitative study of the dynamic tumor-endothelial cell interactions through an integrated microfluidic coculture system. *Anal Chem* **84**, 2088-2093 (2012).
102. Ghalichi, F. & Deng, X. Turbulence detection in a stenosed artery bifurcation by numerical simulation of pulsatile blood flow using the low-Reynolds number turbulence model. *Biorheology* **40**, 637-654 (2003).
103. Yeon, J.H., Ryu, H.R., Chung, M., Hu, Q.P. & Jeon, N.L. In vitro formation and characterization of a perfusable three-dimensional tubular capillary network in microfluidic devices. *Lab Chip* **12**, 2815-2822 (2012).
104. Yeh, C.H., Tsai, S.H., Wu, L.W. & Lin, Y.C. Using a co-culture microsystem for cell migration under fluid shear stress. *Lab Chip* **11**, 2583-2590 (2011).
105. Moya, M.L., Hsu, Y.H., Lee, A.P., Hughes, C.C. & George, S.C. In vitro perfused human capillary networks. *Tissue Eng Part C Methods* **19**, 730-737 (2013).
106. Baker, B.M., Trappmann, B., Stapleton, S.C., Toro, E. & Chen, C.S. Microfluidics embedded within extracellular matrix to define vascular architectures and pattern diffusive gradients. *Lab Chip* **13**, 3246-3252 (2013).
107. Brooks, P.C., Montgomery, A.M. & Cheresh, D.A. Use of the 10-day-old chick embryo model for studying angiogenesis. *Methods Mol Biol* **129**, 257-269 (1999).
108. Chavez, M.N., Aedo, G., Fierro, F.A., Allende, M.L. & Egana, J.T. Zebrafish as an Emerging Model Organism to Study Angiogenesis in Development and Regeneration. *Front Physiol* **7**, 56 (2016).
109. Chappell, J.C.*, et al.* Flt-1 (VEGFR-1) coordinates discrete stages of blood vessel formation. *Cardiovascular research* **111**, 84-93 (2016).
110. Nicoli, S. & Presta, M. The zebrafish/tumor xenograft angiogenesis assay. *Nat Protoc* **2**, 2918-2923 (2007).

111. Hlushchuk, R., *et al.* Zebrafish Caudal Fin Angiogenesis Assay-Advanced Quantitative Assessment Including 3-Way Correlative Microscopy. *PLoS One* **11**, e0149281 (2016).
112. Norrby, K. In vivo models of angiogenesis. *J Cell Mol Med* **10**, 588-612 (2006).
113. Kelly-Goss, M.R., Sweat, R.S., Azimi, M.S. & Murfee, W.L. Vascular islands during microvascular regression and regrowth in adult networks. *Frontiers in physiology* **4**, 108 (2013).
114. Kelly-Goss, M.R., *et al.* Cell proliferation along vascular islands during microvascular network growth. *BMC Physiol* **12**, 7 (2012).
115. Elia, R., *et al.* Stimulation of in vivo angiogenesis by in situ crosslinked, dual growth factor-loaded, glycosaminoglycan hydrogels. *Biomaterials* **31**, 4630-4638 (2010).
116. Shepard, J.A., *et al.* Hydrogel macroporosity and the prolongation of transgene expression and the enhancement of angiogenesis. *Biomaterials* **33**, 7412-7421 (2012).
117. Kastellorizios, M., Papadimitrakopoulos, F. & Burgess, D.J. Multiple tissue response modifiers to promote angiogenesis and prevent the foreign body reaction around subcutaneous implants. *J Control Release* **214**, 103-111 (2015).
118. Mammoto, T. & Mammoto, A. Implantation of fibrin gel on mouse lung to study lung-specific angiogenesis. *J Vis Exp* (2014).
119. Sun, W., *et al.* Co-culture of outgrowth endothelial cells with human mesenchymal stem cells in silk fibroin hydrogels promotes angiogenesis. *Biomed Mater* **11**, 035009 (2016).
120. Peirce, S.M., Price, R.J. & Skalak, T.C. Spatial and temporal control of angiogenesis and arterialization using focal applications of VEGF164 and Ang-1. *Am J Physiol Heart Circ Physiol* **286**, H918-925 (2004).
121. Rogers, M.S., Birsner, A.E. & D'Amato, R.J. The mouse cornea micropocket angiogenesis assay. *Nature protocols* **2**, 2545-2550 (2007).
122. Morbidelli, L. & Ziche, M. The Rabbit Corneal Pocket Assay. *Methods Mol Biol* **1430**, 299-310 (2016).
123. Figueroa-Ortiz, L.C., Martin Rodriguez, O., Garcia-Ben, A. & Garcia-Campos, J. Neovascular growth in an experimental alkali corneal burn model. *Archivos de la Sociedad Espanola de Oftalmologia* **89**, 303-307 (2014).
124. Giacomini, C., Ferrari, G., Bignami, F. & Rama, P. Alkali burn versus suture-induced corneal neovascularization in C57BL/6 mice: an overview of two common animal models of corneal neovascularization. *Exp Eye Res* **121**, 1-4 (2014).
125. Klotz, O., Park, J.K., Pleyer, U., Hartmann, C. & Baatz, H. Inhibition of corneal neovascularization by alpha(v)-integrin antagonists in the rat. *Graefes Arch Clin Exp Ophthalmol* **238**, 88-93 (2000).
126. Keeling, A.N., *et al.* Clinical correlates of size and number of collateral vessels in peripheral artery disease. *Vasc Med* **17**, 223-230 (2012).
127. Amin, P., *et al.* Evaluating peripheral arterial disease with unenhanced quiescent-interval single-shot MR angiography at 3 T. *AJR Am J Roentgenol* **202**, 886-893 (2014).
128. Rush, R.B. & Rush, S.W. Predictability of Recalcitrance in Neovascular Age-Related Macular Degeneration With Indocyanine Green Angiography. *Asia Pac J Ophthalmol (Phila)* **4**, 187-190 (2015).

129. Rush, R.B., Rush, S.W., Aragon, A.V., 2nd & Ysasaga, J.E. Predictability of Recurrent Exudation and Subretinal Hemorrhaging in Neovascular Age-Related Macular Degeneration With Indocyanine Green Angiography. *Ophthalmic Surg Lasers Imaging Retina* **46**, 718-723 (2015).
130. Louveau, A.*, et al.* Structural and functional features of central nervous system lymphatic vessels. *Nature* **523**, 337-341 (2015).
131. Aspelund, A.*, et al.* A dural lymphatic vascular system that drains brain interstitial fluid and macromolecules. *J Exp Med* **212**, 991-999 (2015).
132. Gimbrone, M.A., Jr.*, et al.* Special communicationthe critical role of mechanical forces in blood vessel development, physiology and pathology. *J Vasc Surg* **29**, 1104-1151 (1999).
133. Culver, J.C. & Dickinson, M.E. The effects of hemodynamic force on embryonic development. *Microcirculation* **17**, 164-178 (2010).
134. Granados-Riveron, J.T. & Brook, J.D. The impact of mechanical forces in heart morphogenesis. *Circ Cardiovasc Genet* **5**, 132-142 (2012).
135. Lindsey, S.E., Butcher, J.T. & Yalcin, H.C. Mechanical regulation of cardiac development. *Front Physiol* **5**, 318 (2014).
136. Fernandez-Sanchez, M.E., Brunet, T., Roper, J.C. & Farge, E. Mechanotransduction's impact on animal development, evolution, and tumorigenesis. *Annu Rev Cell Dev Biol* **31**, 373-397 (2015).
137. Haack, T. & Abdelilah-Seyfried, S. The force within: endocardial development, mechanotransduction and signalling during cardiac morphogenesis. *Development* **143**, 373-386 (2016).
138. Avraamides, C.J., Garmy-Susini, B. & Varner, J.A. Integrins in angiogenesis and lymphangiogenesis. *Nat Rev Cancer* **8**, 604-617 (2008).
139. Neufeld, S., Planas-Paz, L. & Lammert, E. Blood and lymphatic vascular tube formation in mouse. *Semin Cell Dev Biol* **31**, 115-123 (2014).
140. Koch, S., Tugues, S., Li, X., Gualandi, L. & Claesson-Welsh, L. Signal transduction by vascular endothelial growth factor receptors. *Biochem J* **437**, 169-183 (2011).
141. Thoma, R. Studies on histogenesis and histomechanics of the vascular system. *Cardiovascular System Histology* **IV**, 91 (1893).
142. Hahn, C. & Schwartz, M.A. Mechanotransduction in vascular physiology and atherogenesis. *Nat Rev Mol Cell Biol* **10**, 53-62 (2009).
143. Baeyens, N.*, et al.* Vascular remodeling is governed by a VEGFR3-dependent fluid shear stress set point. *Elife* **4**(2015).
144. Langille, R.M. & Hall, B.K. Developmental processes, developmental sequences and early vertebrate phylogeny. *Biol Rev Camb Philos Soc* **64**, 73-91 (1989).
145. Langille, B.L. & O'Donnell, F. Reductions in arterial diameter produced by chronic decreases in blood flow are endothelium-dependent. *Science* **231**, 405-407 (1986).
146. Roman, B.L. & Pekkan, K. Mechanotransduction in embryonic vascular development. *Biomech Model Mechanobiol* **11**, 1149-1168 (2012).
147. Aung, K.Z., Pereira, B.P., Tan, P.H., Han, H.C. & Nathan, S.S. Interstitial fluid pressure as an alternate regulator of angiogenesis independent of hypoxia driven HIF-1alpha in solid tumors. *J Orthop Res* **30**, 2038-2045 (2012).
148. Boucher, Y., Leunig, M. & Jain, R.K. Tumor angiogenesis and interstitial hypertension. *Cancer Res* **56**, 4264-4266 (1996).

149. Reed, R.K. & Rubin, K. Transcapillary exchange: role and importance of the interstitial fluid pressure and the extracellular matrix. *Cardiovasc Res* **87**, 211-217 (2010).
150. Ledoux, J., Gee, D.M. & Leblanc, N. Increased peripheral resistance in heart failure: new evidence suggests an alteration in vascular smooth muscle function. *British journal of pharmacology* **139**, 1245-1248 (2003).
151. Raven, P.B. & Chapleau, M.W. Blood pressure regulation XI: overview and future research directions. *European journal of applied physiology* **114**, 579-586 (2014).
152. Ketsawatsomkron, P. & Sigmund, C.D. Molecular mechanisms regulating vascular tone by peroxisome proliferator activated receptor gamma. *Current opinion in nephrology and hypertension* **24**, 123-130 (2015).
153. Forstermann, U. & Sessa, W.C. Nitric oxide synthases: regulation and function. *European heart journal* **33**, 829-837, 837a-837d (2012).
154. Singh, A., Sventek, P., Lariviere, R., Thibault, G. & Schiffrin, E.L. Inducible nitric oxide synthase in vascular smooth muscle cells from prehypertensive spontaneously hypertensive rats. *American journal of hypertension* **9**, 867-877 (1996).
155. Durante, W., Johnson, F.K. & Johnson, R.A. Arginase: a critical regulator of nitric oxide synthesis and vascular function. *Clinical and experimental pharmacology & physiology* **34**, 906-911 (2007).
156. Chiu, J.J. & Chien, S. Effects of disturbed flow on vascular endothelium: pathophysiological basis and clinical perspectives. *Physiological Reviews* **91**, 327-387 (2011).
157. Li, M., Tan, Y., Stenmark, K.R. & Tan, W. High Pulsatility Flow Induces Acute Endothelial Inflammation through Overpolarizing Cells to Activate NF-kappaB. *Cardiovascular engineering and technology* **4**, 26-38 (2013).
158. Fung, Y.C. & Liu, S.Q. Elementary mechanics of the endothelium of blood vessels. *J Biomech Eng* **115**, 1-12 (1993).
159. Tzima, E.*, et al.* A mechanosensory complex that mediates the endothelial cell response to fluid shear stress. *Nature* **437**, 426-431 (2005).
160. Tzima, E., del Pozo, M.A., Shattil, S.J., Chien, S. & Schwartz, M.A. Activation of integrins in endothelial cells by fluid shear stress mediates Rho-dependent cytoskeletal alignment. *EMBO J* **20**, 4639-4647 (2001).
161. Coon, B.G.*, et al.* Intramembrane binding of VE-cadherin to VEGFR2 and VEGFR3 assembles the endothelial mechanosensory complex. *J Cell Biol* **208**, 975-986 (2015).
162. Chen, K.D.*, et al.* Mechanotransduction in response to shear stress. Roles of receptor tyrosine kinases, integrins, and Shc. *J Biol Chem* **274**, 18393-18400 (1999).
163. Jin, Z.G.*, et al.* Ligand-independent activation of vascular endothelial growth factor receptor 2 by fluid shear stress regulates activation of endothelial nitric oxide synthase. *Circ Res* **93**, 354-363 (2003).
164. Shay-Salit, A.*, et al.* VEGF receptor 2 and the adherens junction as a mechanical transducer in vascular endothelial cells. *Proc Natl Acad Sci U S A* **99**, 9462-9467 (2002).
165. Abu Taha, A., Taha, M., Seebach, J. & Schnittler, H.J. ARP2/3-mediated junction-associated lamellipodia control VE-cadherin-based cell junction dynamics and maintain monolayer integrity. *Mol Biol Cell* **25**, 245-256 (2014).

166. Liu, Y., Sweet, D.T., Irani-Tehrani, M., Maeda, N. & Tzima, E. Shc coordinates signals from intercellular junctions and integrins to regulate flow-induced inflammation. *J Cell Biol* **182**, 185-196 (2008).
167. van der Meer, A.D.*, et al.* Shear stress induces a transient and VEGFR-2-dependent decrease in the motion of injected particles in endothelial cells. *Biorheology* **47**, 179-192 (2010).
168. Liu, Z.*, et al.* Mechanical tugging force regulates the size of cell-cell junctions. *Proc Natl Acad Sci U S A* **107**, 9944-9949 (2010).
169. Oldenburg, J. & de Rooij, J. Mechanical control of the endothelial barrier. *Cell Tissue Res* **355**, 545-555 (2014).
170. Gulino-Debrac, D. Mechanotransduction at the basis of endothelial barrier function. *Tissue Barriers* **1**, e24180 (2013).
171. Timmerman, I.*, et al.* A local VE-cadherin and Trio-based signaling complex stabilizes endothelial junctions through Rac1. *J Cell Sci* **128**, 3041-3054 (2015).
172. Huveneers, S.*, et al.* Vinculin associates with endothelial VE-cadherin junctions to control force-dependent remodeling. *J Cell Biol* **196**, 641-652 (2012).
173. Fraccaroli, A.*, et al.* Visualization of endothelial actin cytoskeleton in the mouse retina. *PLoS One* **7**, e47488 (2012).
174. Sauteur, L.*, et al.* Cdh5/VE-cadherin promotes endothelial cell interface elongation via cortical actin polymerization during angiogenic sprouting. *Cell Rep* **9**, 504-513 (2014).
175. Orsenigo, F.*, et al.* Phosphorylation of VE-cadherin is modulated by haemodynamic forces and contributes to the regulation of vascular permeability in vivo. *Nat Commun* **3**, 1208 (2012).
176. Schulte, D.*, et al.* Stabilizing the VE-cadherin-catenin complex blocks leukocyte extravasation and vascular permeability. *EMBO J* **30**, 4157-4170 (2011).
177. van Geemen, D.*, et al.* F-actin-anchored focal adhesions distinguish endothelial phenotypes of human arteries and veins. *Arterioscler Thromb Vasc Biol* **34**, 2059-2067 (2014).
178. Dorland, Y.L. & Huveneers, S. Cell-cell junctional mechanotransduction in endothelial remodeling. *Cell Mol Life Sci* **74**, 279-292 (2017).
179. Chachisvilis, M., Zhang, Y.L. & Frangos, J.A. G protein-coupled receptors sense fluid shear stress in endothelial cells. *Proc Natl Acad Sci U S A* **103**, 15463-15468 (2006).
180. Hsieh, H.J., Li, N.Q. & Frangos, J.A. Shear-induced platelet-derived growth factor gene expression in human endothelial cells is mediated by protein kinase C. *J Cell Physiol* **150**, 552-558 (1992).
181. Gudi, S.*, et al.* Rapid activation of Ras by fluid flow is mediated by Galpha(q) and Gbetagamma subunits of heterotrimeric G proteins in human endothelial cells. *Arterioscler Thromb Vasc Biol* **23**, 994-1000 (2003).
182. Davies, P.F. Flow-mediated endothelial mechanotransduction. *Physiol Rev* **75**, 519-560 (1995).
183. Arcangeli, A.*, et al.* Integrin-mediated neurite outgrowth in neuroblastoma cells depends on the activation of potassium channels. *J Cell Biol* **122**, 1131-1143 (1993).
184. Jones, T.J.*, et al.* Primary cilia regulates the directional migration and barrier integrity of endothelial cells through the modulation of hsp27 dependent actin cytoskeletal organization. *J Cell Physiol* **227**, 70-76 (2012).

185. Praetorius, H.A. & Spring, K.R. Removal of the MDCK cell primary cilium abolishes flow sensing. *J Membr Biol* **191**, 69-76 (2003).
186. Donnelly, E., Ascenzi, M.G. & Farnum, C. Primary cilia are highly oriented with respect to collagen direction and long axis of extensor tendon. *J Orthop Res* **28**, 77-82 (2010).
187. Praetorius, H.A., Praetorius, J., Nielsen, S., Frokiaer, J. & Spring, K.R. Beta1-integrins in the primary cilium of MDCK cells potentiate fibronectin-induced Ca2+ signaling. *Am J Physiol Renal Physiol* **287**, F969-978 (2004).
188. Praetorius, H.A. & Spring, K.R. Bending the MDCK cell primary cilium increases intracellular calcium. *J Membr Biol* **184**, 71-79 (2001).
189. Nauli, S.M.*, et al.* Non-motile primary cilia as fluid shear stress mechanosensors. *Methods Enzymol* **525**, 1-20 (2013).
190. AbouAlaiwi, W.A.*, et al.* Ciliary polycystin-2 is a mechanosensitive calcium channel involved in nitric oxide signaling cascades. *Circ Res* **104**, 860-869 (2009).
191. Nauli, S.M.*, et al.* Endothelial cilia are fluid shear sensors that regulate calcium signaling and nitric oxide production through polycystin-1. *Circulation* **117**, 1161-1171 (2008).
192. Shihata, W.A., Michell, D.L., Andrews, K.L. & Chin-Dusting, J.P. Caveolae: A Role in Endothelial Inflammation and Mechanotransduction? *Front Physiol* **7**, 628 (2016).
193. Drab, M.*, et al.* Loss of caveolae, vascular dysfunction, and pulmonary defects in caveolin-1 gene-disrupted mice. *Science* **293**, 2449-2452 (2001).
194. Razani, B.*, et al.* Caveolin-1-deficient mice are lean, resistant to diet-induced obesity, and show hypertriglyceridemia with adipocyte abnormalities. *J Biol Chem* **277**, 8635-8647 (2002).
195. Razani, B.*, et al.* Caveolin-1 null mice are viable but show evidence of hyperproliferative and vascular abnormalities. *J Biol Chem* **276**, 38121-38138 (2001).
196. Yu, J.*, et al.* Direct evidence for the role of caveolin-1 and caveolae in mechanotransduction and remodeling of blood vessels. *J Clin Invest* **116**, 1284-1291 (2006).
197. Zhao, Y.Y.*, et al.* Persistent eNOS activation secondary to caveolin-1 deficiency induces pulmonary hypertension in mice and humans through PKG nitration. *J Clin Invest* **119**, 2009-2018 (2009).
198. Jalali, S.*, et al.* Integrin-mediated mechanotransduction requires its dynamic interaction with specific extracellular matrix (ECM) ligands. *Proc Natl Acad Sci U S A* **98**, 1042-1046 (2001).
199. Wilson, E., Sudhir, K. & Ives, H.E. Mechanical strain of rat vascular smooth muscle cells is sensed by specific extracellular matrix/integrin interactions. *J Clin Invest* **96**, 2364-2372 (1995).
200. Thodeti, C.K.*, et al.* TRPV4 channels mediate cyclic strain-induced endothelial cell reorientation through integrin-to-integrin signaling. *Circ Res* **104**, 1123-1130 (2009).
201. Otey, C.A., Pavalko, F.M. & Burridge, K. An interaction between alpha-actinin and the beta 1 integrin subunit in vitro. *J Cell Biol* **111**, 721-729 (1990).

202. Luu, N.T., Glen, K.E., Egginton, S., Rainger, G.E. & Nash, G.B. Integrin-substrate interactions underlying shear-induced inhibition of the inflammatory response of endothelial cells. *Thromb Haemost* **109**, 298-308 (2013).
203. Zaragoza, C., Marquez, S. & Saura, M. Endothelial mechanosensors of shear stress as regulators of atherogenesis. *Curr Opin Lipidol* **23**, 446-452 (2012).
204. Shyy, J.Y. & Chien, S. Role of integrins in endothelial mechanosensing of shear stress. *Circ Res* **91**, 769-775 (2002).
205. Bhullar, I.S.*, et al.* Fluid shear stress activation of IkappaB kinase is integrin-dependent. *J Biol Chem* **273**, 30544-30549 (1998).
206. Muller, J.M., Chilian, W.M. & Davis, M.J. Integrin signaling transduces shear stress--dependent vasodilation of coronary arterioles. *Circ Res* **80**, 320-326 (1997).
207. Loftus, J.C. & Liddington, R.C. New insights into integrin-ligand interaction. *J Clin Invest* **100**, S77-81 (1997).
208. Humphries, M.J. & Newham, P. The structure of cell-adhesion molecules. *Trends Cell Biol* **8**, 78-83 (1998).
209. Spofford, C.M. & Chilian, W.M. The elastin-laminin receptor functions as a mechanotransducer in vascular smooth muscle. *Am J Physiol Heart Circ Physiol* **280**, H1354-1360 (2001).
210. Chung, T.W.*, et al.* Growth of human endothelial cells on different concentrations of Gly-Arg-Gly-Asp grafted chitosan surface. *Artif Organs* **27**, 155-161 (2003).
211. Yeh, Y.T.*, et al.* Matrix stiffness regulates endothelial cell proliferation through septin 9. *PLoS One* **7**, e46889 (2012).
212. Lu, X. & Kassab, G.S. Integrins mediate mechanical compression-induced endothelium-dependent vasodilation through endothelial nitric oxide pathway. *J Gen Physiol* **146**, 221-232 (2015).
213. Li, S., Huang, N.F. & Hsu, S. Mechanotransduction in endothelial cell migration. *J Cell Biochem* **96**, 1110-1126 (2005).
214. Shi, Z.D. & Tarbell, J.M. Fluid flow mechanotransduction in vascular smooth muscle cells and fibroblasts. *Ann Biomed Eng* **39**, 1608-1619 (2011).
215. Clyman, R.I., Mauray, F. & Kramer, R.H. Beta 1 and beta 3 integrins have different roles in the adhesion and migration of vascular smooth muscle cells on extracellular matrix. *Exp Cell Res* **200**, 272-284 (1992).
216. Parsons, J.T. & Parsons, S.J. Src family protein tyrosine kinases: cooperating with growth factor and adhesion signaling pathways. *Curr Opin Cell Biol* **9**, 187-192 (1997).
217. Schlaepfer, D.D., Jones, K.C. & Hunter, T. Multiple Grb2-mediated integrin-stimulated signaling pathways to ERK2/mitogen-activated protein kinase: summation of both c-Src- and focal adhesion kinase-initiated tyrosine phosphorylation events. *Mol Cell Biol* **18**, 2571-2585 (1998).
218. Schwartz, M.A. Integrins and extracellular matrix in mechanotransduction. *Cold Spring Harb Perspect Biol* **2**, a005066 (2010).
219. Wary, K.K., Mainiero, F., Isakoff, S.J., Marcantonio, E.E. & Giancotti, F.G. The adaptor protein Shc couples a class of integrins to the control of cell cycle progression. *Cell* **87**, 733-743 (1996).

220. Reitsma, S., Slaaf, D.W., Vink, H., van Zandvoort, M.A. & oude Egbrink, M.G. The endothelial glycocalyx: composition, functions, and visualization. *Pflugers Arch* **454**, 345-359 (2007).
221. Weinbaum, S., Tarbell, J.M. & Damiano, E.R. The structure and function of the endothelial glycocalyx layer. *Annu Rev Biomed Eng* **9**, 121-167 (2007).
222. Thi, M.M., Tarbell, J.M., Weinbaum, S. & Spray, D.C. The role of the glycocalyx in reorganization of the actin cytoskeleton under fluid shear stress: a "bumper-car" model. *Proc Natl Acad Sci U S A* **101**, 16483-16488 (2004).
223. Pahakis, M.Y., Kosky, J.R., Dull, R.O. & Tarbell, J.M. The role of endothelial glycocalyx components in mechanotransduction of fluid shear stress. *Biochem Biophys Res Commun* **355**, 228-233 (2007).
224. Florian, J.A*., et al.* Heparan sulfate proteoglycan is a mechanosensor on endothelial cells. *Circ Res* **93**, e136-142 (2003).
225. Zeng, Y. & Tarbell, J.M. The adaptive remodeling of endothelial glycocalyx in response to fluid shear stress. *PLoS One* **9**, e86249 (2014).
226. Yen, W*., et al.* Endothelial surface glycocalyx can regulate flow-induced nitric oxide production in microvessels in vivo. *PLoS One* **10**, e0117133 (2015).
227. Mochizuki, S*., et al.* Role of hyaluronic acid glycosaminoglycans in shear-induced endothelium-derived nitric oxide release. *Am J Physiol Heart Circ Physiol* **285**, H722-726 (2003).
228. Gautam, M., Gojova, A. & Barakat, A.I. Flow-activated ion channels in vascular endothelium. *Cell Biochem Biophys* **46**, 277-284 (2006).
229. Hoger, J.H., Ilyin, V.I., Forsyth, S. & Hoger, A. Shear stress regulates the endothelial Kir2.1 ion channel. *Proc Natl Acad Sci U S A* **99**, 7780-7785 (2002).
230. Barakat, A.I., Lieu, D.K. & Gojova, A. Secrets of the code: do vascular endothelial cells use ion channels to decipher complex flow signals? *Biomaterials* **27**, 671-678 (2006).
231. Ando, J. & Yamamoto, K. Flow detection and calcium signalling in vascular endothelial cells. *Cardiovasc Res* **99**, 260-268 (2013).
232. Lieu, D.K., Pappone, P.A. & Barakat, A.I. Differential membrane potential and ion current responses to different types of shear stress in vascular endothelial cells. *Am J Physiol Cell Physiol* **286**, C1367-1375 (2004).
233. Gautam, M., Shen, Y., Thirkill, T.L., Douglas, G.C. & Barakat, A.I. Flow-activated chloride channels in vascular endothelium. Shear stress sensitivity, desensitization dynamics, and physiological implications. *J Biol Chem* **281**, 36492-36500 (2006).
234. O'Neil, R.G. & Heller, S. The mechanosensitive nature of TRPV channels. *Pflugers Arch* **451**, 193-203 (2005).
235. Sackin, H. Stretch-activated ion channels. *Kidney Int* **48**, 1134-1147 (1995).
236. Birukov, K.G*., et al.* Stretch affects phenotype and proliferation of vascular smooth muscle cells. *Molecular and cellular biochemistry* **144**, 131-139 (1995).
237. Helmke, B.P., Goldman, R.D. & Davies, P.F. Rapid displacement of vimentin intermediate filaments in living endothelial cells exposed to flow. *Circ Res* **86**, 745-752 (2000).
238. Helmke, B.P., Thakker, D.B., Goldman, R.D. & Davies, P.F. Spatiotemporal analysis of flow-induced intermediate filament displacement in living endothelial cells. *Biophys J* **80**, 184-194 (2001).

239. Osborn, E.A., Rabodzey, A., Dewey, C.F., Jr. & Hartwig, J.H. Endothelial actin cytoskeleton remodeling during mechanostimulation with fluid shear stress. *Am J Physiol Cell Physiol* **290**, C444-452 (2006).
240. Slee, J.B. & Lowe-Krentz, L.J. Actin realignment and cofilin regulation are essential for barrier integrity during shear stress. *J Cell Biochem* **114**, 782-795 (2013).
241. Deguchi, S., Maeda, K., Ohashi, T. & Sato, M. Flow-induced hardening of endothelial nucleus as an intracellular stress-bearing organelle. *J Biomech* **38**, 1751-1759 (2005).
242. Tkachenko, E.*, et al.* The nucleus of endothelial cell as a sensor of blood flow direction. *Biol Open* **2**, 1007-1012 (2013).
243. Barakat, A.I., Leaver, E.V., Pappone, P.A. & Davies, P.F. A flow-activated chloride-selective membrane current in vascular endothelial cells. *Circulation research* **85**, 820-828 (1999).
244. Olesen, S.P., Clapham, D.E. & Davies, P.F. Haemodynamic shear stress activates a K+ current in vascular endothelial cells. *Nature* **331**, 168-170 (1988).
245. Hoger, J.H., Ilyin, V.I., Forsyth, S. & Hoger, A. Shear stress regulates the endothelial Kir2.1 ion channel. *Proceedings of the National Academy of Sciences of the United States of America* **99**, 7780-7785 (2002).
246. Osawa, M., Masuda, M., Harada, N., Lopes, R.B. & Fujiwara, K. Tyrosine phosphorylation of platelet endothelial cell adhesion molecule-1 (PECAM-1, CD31) in mechanically stimulated vascular endothelial cells. *European journal of cell biology* **72**, 229-237 (1997).
247. Andrews, A.M., Jaron, D., Buerk, D.G., Kirby, P.L. & Barbee, K.A. Direct, real-time measurement of shear stress-induced nitric oxide produced from endothelial cells in vitro. *Nitric oxide : biology and chemistry* **23**, 335-342 (2010).
248. Jin, Z.G.*, et al.* Ligand-independent activation of vascular endothelial growth factor receptor 2 by fluid shear stress regulates activation of endothelial nitric oxide synthase. *Circulation research* **93**, 354-363 (2003).
249. Jalali, S.*, et al.* Shear stress activates p60src-Ras-MAPK signaling pathways in vascular endothelial cells. *Arteriosclerosis, Thrombosis, and Vascular Biology* **18**, 227-234 (1998).
250. Berk, B.C., Corson, M.A., Peterson, T.E. & Tseng, H. Protein kinases as mediators of fluid shear stress stimulated signal transduction in endothelial cells: a hypothesis for calcium-dependent and calcium-independent events activated by flow. *Journal of Biomechanics* **28**, 1439-1450 (1995).
251. Wojciak-Stothard, B. & Ridley, A.J. Shear stress-induced endothelial cell polarization is mediated by Rho and Rac but not Cdc42 or PI 3-kinases. *The Journal of cell biology* **161**, 429-439 (2003).
252. Li, S.*, et al.* Distinct roles for the small GTPases Cdc42 and Rho in endothelial responses to shear stress. *The Journal of clinical investigation* **103**, 1141-1150 (1999).
253. Hay, D.C.*, et al.* Activation of NF-kappaB nuclear transcription factor by flow in human endothelial cells. *Biochimica et biophysica acta* **1642**, 33-44 (2003).
254. Orr, A.W., Hahn, C., Blackman, B.R. & Schwartz, M.A. p21-activated kinase signaling regulates oxidant-dependent NF-kappa B activation by flow. *Circulation research* **103**, 671-679 (2008).

255. Hahn, C., Wang, C., Orr, A.W., Coon, B.G. & Schwartz, M.A. JNK2 promotes endothelial cell alignment under flow. *PloS one* **6**, e24338 (2011).
256. Tzima, E., del Pozo, M.A., Shattil, S.J., Chien, S. & Schwartz, M.A. Activation of integrins in endothelial cells by fluid shear stress mediates Rho-dependent cytoskeletal alignment. *The EMBO journal* **20**, 4639-4647 (2001).
257. Mott, R.E. & Helmke, B.P. Mapping the dynamics of shear stress-induced structural changes in endothelial cells. *American journal of physiology.Cell physiology* **293**, C1616-1626 (2007).
258. Davies, P.F., Robotewskyj, A. & Griem, M.L. Quantitative studies of endothelial cell adhesion. Directional remodeling of focal adhesion sites in response to flow forces. *The Journal of clinical investigation* **93**, 2031-2038 (1994).
259. Obi, S.*, et al.* Fluid shear stress induces differentiation of circulating phenotype endothelial progenitor cells. *American journal of physiology.Cell physiology* **303**, C595-606 (2012).
260. Zhang, J.*, et al.* Angiopoietin-1/Tie2 signal augments basal Notch signal controlling vascular quiescence by inducing delta-like 4 expression through AKT-mediated activation of beta-catenin. *J Biol Chem* **286**, 8055-8066 (2011).
261. Augustin, H.G., Koh, G.Y., Thurston, G. & Alitalo, K. Control of vascular morphogenesis and homeostasis through the angiopoietin-Tie system. *Nat Rev Mol Cell Biol* **10**, 165-177 (2009).
262. Aird, W.C. Phenotypic heterogeneity of the endothelium: II. Representative vascular beds. *Circulation research* **100**, 174-190 (2007).
263. Goettsch, W.*, et al.* Flow-dependent regulation of angiopoietin-2. *Journal of cellular physiology* **214**, 491-503 (2008).
264. Kurniati, N.F.*, et al.* The flow dependency of Tie2 expression in endotoxemia. *Intensive care medicine* **39**, 1262-1271 (2013).
265. Osawa, M., Masuda, M., Kusano, K. & Fujiwara, K. Evidence for a role of platelet endothelial cell adhesion molecule-1 in endothelial cell mechanosignal transduction: is it a mechanoresponsive molecule? *The Journal of cell biology* **158**, 773-785 (2002).
266. Collins, C.*, et al.* Localized tensional forces on PECAM-1 elicit a global mechanotransduction response via the integrin-RhoA pathway. *Current biology : CB* **22**, 2087-2094 (2012).
267. Dusserre, N.*, et al.* PECAM-1 interacts with nitric oxide synthase in human endothelial cells: implication for flow-induced nitric oxide synthase activation. *Arteriosclerosis, Thrombosis, and Vascular Biology* **24**, 1796-1802 (2004).
268. Uhl, J.F. & Gillot, C. Anatomy of the veno-muscular pumps of the lower limb. *Phlebology* **30**, 180-193 (2015).
269. Bazigou, E. & Makinen, T. Flow control in our vessels: vascular valves make sure there is no way back. *Cell Mol Life Sci* **70**, 1055-1066 (2013).
270. Geng, X.*, et al.* Multiple mouse models of primary lymphedema exhibit distinct defects in lymphovenous valve development. *Dev Biol* **409**, 218-233 (2016).
271. Munger, S.J.*, et al.* Segregated Foxc2, NFATc1 and Connexin expression at normal developing venous valves, and Connexin-specific differences in the valve phenotypes of Cx37, Cx43, and Cx47 knockout mice. *Dev Biol* **412**, 173-190 (2016).

272. Bazigou, E.*, et al.* Genes regulating lymphangiogenesis control venous valve formation and maintenance in mice. *J Clin Invest* **121**, 2984-2992 (2011).
273. Lurie, F., Kistner, R.L., Eklof, B. & Kessler, D. Mechanism of venous valve closure and role of the valve in circulation: a new concept. *Journal of vascular surgery* **38**, 955-961 (2003).
274. Atta, H.M. Varicose veins: role of mechanotransduction of venous hypertension. *International journal of vascular medicine* **2012**, 538627 (2012).
275. Itoh, H., Nelson, P.R., Mureebe, L., Horowitz, A. & Kent, K.C. The role of integrins in saphenous vein vascular smooth muscle cell migration. *Journal of vascular surgery* **25**, 1061-1069 (1997).
276. Meng, X., Mavromatis, K. & Galis, Z.S. Mechanical stretching of human saphenous vein grafts induces expression and activation of matrix-degrading enzymes associated with vascular tissue injury and repair. *Experimental and molecular pathology* **66**, 227-237 (1999).
277. Udan, R.S., Culver, J.C. & Dickinson, M.E. Understanding vascular development. *Wiley interdisciplinary reviews.Developmental biology* **2**, 327-346 (2013).
278. Strilic, B., Kucera, T. & Lammert, E. Formation of cardiovascular tubes in invertebrates and vertebrates. *Cell Mol Life Sci* **67**, 3209-3218 (2010).
279. Udan, R.S., Vadakkan, T.J. & Dickinson, M.E. Dynamic responses of endothelial cells to changes in blood flow during vascular remodeling of the mouse yolk sac. *Development (Cambridge, England)* **140**, 4041-4050 (2013).
280. Lenard, A.*, et al.* Endothelial cell self-fusion during vascular pruning. *PLoS Biol* **13**, e1002126 (2015).
281. Pelster, B. & Burggren, W.W. Disruption of hemoglobin oxygen transport does not impact oxygen-dependent physiological processes in developing embryos of zebra fish (Danio rerio). *Circulation research* **79**, 358-362 (1996).
282. Lucitti, J.L.*, et al.* Vascular remodeling of the mouse yolk sac requires hemodynamic force. *Development (Cambridge, England)* **134**, 3317-3326 (2007).
283. Chen, C.Y.*, et al.* Analysis of early embryonic great-vessel microcirculation in zebrafish using high-speed confocal muPIV. *Biorheology* **48**, 305-321 (2011).
284. Corti, P.*, et al.* Interaction between alk1 and blood flow in the development of arteriovenous malformations. *Development (Cambridge, England)* **138**, 1573-1582 (2011).
285. Yoshisue, H.*, et al.* Large scale isolation of non-uniform shear stress-responsive genes from cultured human endothelial cells through the preparation of a subtracted cDNA library. *Atherosclerosis* **162**, 323-334 (2002).
286. Bautch, V.L. Endoglin moves and shapes endothelial cells. *Nat Cell Biol* **19**, 593-595 (2017).
287. Sugden, W.W.*, et al.* Endoglin controls blood vessel diameter through endothelial cell shape changes in response to haemodynamic cues. *Nat Cell Biol* **19**, 653-665 (2017).
288. Buschmann, I.*, et al.* Pulsatile shear and Gja5 modulate arterial identity and remodeling events during flow-driven arteriogenesis. *Development (Cambridge, England)* **137**, 2187-2196 (2010).
289. Gray, C.*, et al.* Ischemia is not required for arteriogenesis in zebrafish embryos. *Arteriosclerosis, Thrombosis, and Vascular Biology* **27**, 2135-2141 (2007).

290. Weinstein, B.M., Stemple, D.L., Driever, W. & Fishman, M.C. Gridlock, a localized heritable vascular patterning defect in the zebrafish. *Nature medicine* **1**, 1143-1147 (1995).
291. Banjo, T.*, et al.* Haemodynamically dependent valvulogenesis of zebrafish heart is mediated by flow-dependent expression of miR-21. *Nature communications* **4**, 1978 (2013).
292. Dekker, R.J.*, et al.* KLF2 provokes a gene expression pattern that establishes functional quiescent differentiation of the endothelium. *Blood* **107**, 4354-4363 (2006).
293. Dekker, R.J.*, et al.* Prolonged fluid shear stress induces a distinct set of endothelial cell genes, most specifically lung Kruppel-like factor (KLF2). *Blood* **100**, 1689-1698 (2002).
294. Dekker, R.J.*, et al.* Endothelial KLF2 links local arterial shear stress levels to the expression of vascular tone-regulating genes. *The American journal of pathology* **167**, 609-618 (2005).
295. Dietrich, A.C., Lombardo, V.A., Veerkamp, J., Priller, F. & Abdelilah-Seyfried, S. Blood flow and Bmp signaling control endocardial chamber morphogenesis. *Developmental cell* **30**, 367-377 (2014).
296. Heckel, E.*, et al.* Oscillatory Flow Modulates Mechanosensitive klf2a Expression through trpv4 and trpp2 during Heart Valve Development. *Current biology : CB* **25**, 1354-1361 (2015).
297. Lee, J.S.*, et al.* Klf2 is an essential regulator of vascular hemodynamic forces in vivo. *Developmental cell* **11**, 845-857 (2006).
298. Parmar, K.M.*, et al.* Integration of flow-dependent endothelial phenotypes by Kruppel-like factor 2. *The Journal of clinical investigation* **116**, 49-58 (2006).
299. Cavalli, A.*, et al.* Decreased blood pressure response in mice deficient of the alpha1b-adrenergic receptor. *Proceedings of the National Academy of Sciences of the United States of America* **94**, 11589-11594 (1997).
300. Harris, I.S. & Black, B.L. Development of the endocardium. *Pediatric cardiology* **31**, 391-399 (2010).
301. Van der Heiden, K.*, et al.* Monocilia on chicken embryonic endocardium in low shear stress areas. *Dev Dyn* **235**, 19-28 (2006).
302. Vermot, J.*, et al.* Reversing blood flows act through klf2a to ensure normal valvulogenesis in the developing heart. *PLoS biology* **7**, e1000246 (2009).
303. Vermot, J.*, et al.* Reversing blood flows act through klf2a to ensure normal valvulogenesis in the developing heart. *PLoS Biol* **7**, e1000246 (2009).
304. Moorman, A., Webb, S., Brown, N.A., Lamers, W. & Anderson, R.H. Development of the heart: (1) formation of the cardiac chambers and arterial trunks. *Heart (British Cardiac Society)* **89**, 806-814 (2003).
305. Samsa, L.A., Yang, B. & Liu, J. Embryonic cardiac chamber maturation: Trabeculation, conduction, and cardiomyocyte proliferation. *American journal of medical genetics.Part C, Seminars in medical genetics* **163C**, 157-168 (2013).
306. McCormick, M.E. & Tzima, E. Pulling on my heartstrings: mechanotransduction in cardiac development and function. *Current opinion in hematology* **23**, 235-242 (2016).

307. Barquera, S.*, et al.* Global Overview of the Epidemiology of Atherosclerotic Cardiovascular Disease. *Archives of Medical Research* **46**, 328-338 (2015).
308. Caro, C.G., Fitz-Gerald, J.M. & Schroter, R.C. Atheroma and arterial wall shear. Observation, correlation and proposal of a shear dependent mass transfer mechanism for atherogenesis. *Proceedings of the Royal Society of London.Series B, Biological sciences* **177**, 109-159 (1971).
309. Caro, C.G., Fitz-Gerald, J.M. & Schroter, R.C. Arterial wall shear and distribution of early atheroma in man. *Nature* **223**, 1159-1160 (1969).
310. Cheng, C.*, et al.* Atherosclerotic lesion size and vulnerability are determined by patterns of fluid shear stress. *Circulation* **113**, 2744-2753 (2006).
311. Nam, D.*, et al.* Partial carotid ligation is a model of acutely induced disturbed flow, leading to rapid endothelial dysfunction and atherosclerosis. *American journal of physiology.Heart and circulatory physiology* **297**, H1535-1543 (2009).
312. SenBanerjee, S.*, et al.* KLF2 Is a novel transcriptional regulator of endothelial proinflammatory activation. *The Journal of experimental medicine* **199**, 1305-1315 (2004).
313. Cheng, C.*, et al.* Shear stress affects the intracellular distribution of eNOS: direct demonstration by a novel in vivo technique. *Blood* **106**, 3691-3698 (2005).
314. Dunn, J.*, et al.* Flow-dependent epigenetic DNA methylation regulates endothelial gene expression and atherosclerosis. *The Journal of clinical investigation* **124**, 3187-3199 (2014).
315. Wang, K.C.*, et al.* Flow-dependent YAP/TAZ activities regulate endothelial phenotypes and atherosclerosis. *Proceedings of the National Academy of Sciences of the United States of America* **113**, 11525-11530 (2016).
316. Wang, L.*, et al.* Integrin-YAP/TAZ-JNK cascade mediates atheroprotective effect of unidirectional shear flow. *Nature* (2016).
317. Chistiakov, D.A., Sobenin, I.A. & Orekhov, A.N. Vascular extracellular matrix in atherosclerosis. *Cardiology in review* **21**, 270-288 (2013).
318. Plenz, G.A., Deng, M.C., Robenek, H. & Volker, W. Vascular collagens: spotlight on the role of type VIII collagen in atherogenesis. *Atherosclerosis* **166**, 1-11 (2003).
319. Babaev, V.R.*, et al.* Absence of regulated splicing of fibronectin EDA exon reduces atherosclerosis in mice. *Atherosclerosis* **197**, 534-540 (2008).
320. Tan, M.H.*, et al.* Deletion of the alternatively spliced fibronectin EIIIA domain in mice reduces atherosclerosis. *Blood* **104**, 11-18 (2004).
321. Chen, Z., Givens, C., Reader, J.S. & Tzima, E. Haemodynamics Regulate Fibronectin Assembly via PECAM. *Scientific reports* **7**, 41223 (2017).
322. Gupta, V. & Grande-Allen, K.J. Effects of static and cyclic loading in regulating extracellular matrix synthesis by cardiovascular cells. *Cardiovascular research* **72**, 375-383 (2006).
323. Kim, B.S., Nikolovski, J., Bonadio, J. & Mooney, D.J. Cyclic mechanical strain regulates the development of engineered smooth muscle tissue. *Nature biotechnology* **17**, 979-983 (1999).
324. Leung, D.Y., Glagov, S. & Mathews, M.B. Cyclic stretching stimulates synthesis of matrix components by arterial smooth muscle cells in vitro. *Science (New York, N.Y.)* **191**, 475-477 (1976).

325. O'Callaghan, C.J. & Williams, B. Mechanical strain-induced extracellular matrix production by human vascular smooth muscle cells: role of TGF-beta(1). *Hypertension (Dallas, Tex.: 1979)* **36**, 319-324 (2000).
326. Li, Q., Muragaki, Y., Hatamura, I., Ueno, H. & Ooshima, A. Stretch-induced collagen synthesis in cultured smooth muscle cells from rabbit aortic media and a possible involvement of angiotensin II and transforming growth factor-beta. *Journal of vascular research* **35**, 93-103 (1998).
327. Sumpio, B.E., Banes, A.J., Link, W.G. & Johnson, G., Jr. Enhanced collagen production by smooth muscle cells during repetitive mechanical stretching. *Archives of surgery (Chicago, Ill.: 1960)* **123**, 1233-1236 (1988).
328. Lee, R.T.*, et al.* Mechanical strain induces specific changes in the synthesis and organization of proteoglycans by vascular smooth muscle cells. *The Journal of biological chemistry* **276**, 13847-13851 (2001).
329. Peirce, S.M., Mac Gabhann, F. & Bautch, V.L. Integration of experimental and computational approaches to sprouting angiogenesis. *Current opinion in hematology* **19**, 184-191 (2012).
330. Baeyens, N.*, et al.* Vascular remodeling is governed by a VEGFR3-dependent fluid shear stress set point. *eLife* **4**, 10.7554/eLife.04645 (2015).
331. Saharinen, P.*, et al.* Angiopoietins assemble distinct Tie2 signalling complexes in endothelial cell-cell and cell-matrix contacts. *Nature cell biology* **10**, 527-537 (2008).
332. Liu, D.*, et al.* Tie2/TEK modulates the interaction of glioma and brain tumor stem cells with endothelial cells and promotes an invasive phenotype. *Oncotarget* **1**, 700-709 (2010).
333. Erber, R.*, et al.* Combined inhibition of VEGF and PDGF signaling enforces tumor vessel regression by interfering with pericyte-mediated endothelial cell survival mechanisms. *FASEB journal : official publication of the Federation of American Societies for Experimental Biology* **18**, 338-340 (2004).
334. Fuxe, J.*, et al.* Pericyte requirement for anti-leak action of angiopoietin-1 and vascular remodeling in sustained inflammation. *The American journal of pathology* **178**, 2897-2909 (2011).
335. Peirce, S.M., Price, R.J. & Skalak, T.C. Spatial and temporal control of angiogenesis and arterialization using focal applications of VEGF164 and Ang-1. *American journal of physiology.Heart and circulatory physiology* **286**, H918-925 (2004).
336. Dai, G.*, et al.* Distinct endothelial phenotypes evoked by arterial waveforms derived from atherosclerosis-susceptible and -resistant regions of human vasculature. *Proceedings of the National Academy of Sciences of the United States of America* **101**, 14871-14876 (2004).
337. Nagel, T., Resnick, N., Dewey, C.F., Jr. & Gimbrone, M.A., Jr. Vascular endothelial cells respond to spatial gradients in fluid shear stress by enhanced activation of transcription factors. *Arteriosclerosis, Thrombosis, and Vascular Biology* **19**, 1825-1834 (1999).
338. Davies, P.F. Hemodynamic shear stress and the endothelium in cardiovascular pathophysiology. *Nature clinical practice.Cardiovascular medicine* **6**, 16-26 (2009).
339. Davies, P.F., Civelek, M., Fang, Y. & Fleming, I. The atherosusceptible endothelium: endothelial phenotypes in complex haemodynamic shear stress regions in vivo. *Cardiovascular research* **99**, 315-327 (2013).

340. Simmers, M.B., Pryor, A.W. & Blackman, B.R. Arterial shear stress regulates endothelial cell-directed migration, polarity, and morphology in confluent monolayers. *American journal of physiology.Heart and circulatory physiology* **293**, H1937-1946 (2007).
341. Bailey, A.M., Lawrence, M.B., Shang, H., Katz, A.J. & Peirce, S.M. Agent-based model of therapeutic adipose-derived stromal cell trafficking during ischemia predicts ability to roll on P-selectin. *PLoS computational biology* **5**, e1000294 (2009).
342. Bauer, A.L., Jackson, T.L. & Jiang, Y. A cell-based model exhibiting branching and anastomosis during tumor-induced angiogenesis. *Biophysical journal* **92**, 3105-3121 (2007).
343. Bauer, A.L., Jackson, T.L. & Jiang, Y. Topography of extracellular matrix mediates vascular morphogenesis and migration speeds in angiogenesis. *PLoS computational biology* **5**, e1000445 (2009).
344. Campochiaro, P.A.*, et al.* Enhanced Benefit in Diabetic Macular Edema from AKB-9778 Tie2 Activation Combined with Vascular Endothelial Growth Factor Suppression. *Ophthalmology* **123**, 1722-1730 (2016).
345. Campochiaro, P.A. & Peters, K.G. Targeting Tie2 for Treatment of Diabetic Retinopathy and Diabetic Macular Edema. *Current diabetes reports* **16**, 126 (2016).
346. Campochiaro, P.A.*, et al.* Treatment of diabetic macular edema with an inhibitor of vascular endothelial-protein tyrosine phosphatase that activates Tie2. *Ophthalmology* **122**, 545-554 (2015).
347. Schofield, J.W., Gaffney, E.A., Gatenby, R.A. & Maini, P.K. Tumour angiogenesis: the gap between theory and experiments. *Journal of theoretical biology* **274**, 97-102 (2011).
348. Folkman, J. Proceedings: Tumor angiogenesis factor. *Cancer research* **34**, 2109-2113 (1974).
349. Birsner, A.E., Benny, O. & D'Amato, R.J. The corneal micropocket assay: a model of angiogenesis in the mouse eye. *Journal of visualized experiments : JoVE* **(90). doi**, 10.3791/51375 (2014).
350. Speier, S.*, et al.* Noninvasive in vivo imaging of pancreatic islet cell biology. *Nature medicine* **14**, 574-578 (2008).
351. Espandar, L.*, et al.* Adipose-derived stem cells on hyaluronic acid-derived scaffold: a new horizon in bioengineered cornea. *Archives of ophthalmology (Chicago, Ill.: 1960)* **130**, 202-208 (2012).
352. Poche, R.A., Saik, J.E., West, J.L. & Dickinson, M.E. The mouse cornea as a transplantation site for live imaging of engineered tissue constructs. *Cold Spring Harbor protocols* **2010**, pdb.prot5416 (2010).
353. Nakasato, H., Uemoto, R. & Mizuki, N. Treatment of pterygium by ligation and bevacizumab injection. *Cornea* **31**, 1339-1341 (2012).
354. Kang, G.J.*, et al.* Intravital Imaging Reveals Dynamics of Lymphangiogenesis and Valvulogenesis. *Scientific reports* **6**, 19459 (2016).
355. Liu, W.*, et al.* Corneal Neovascularization Imaging by Optical-Resolution Photoacoustic Microscopy. *Photoacoustics* **2**, 81-86 (2014).
356. Nakasato, S., Uemoto, R. & Mizuki, N. Thermocautery for inferior conjunctivochalasis. *Cornea* **31**, 514-519 (2012).

357. Jakobsson, L.*, et al.* Endothelial cells dynamically compete for the tip cell position during angiogenic sprouting. *Nature cell biology* **12**, 943-953 (2010).
358. Suvarnamani, C., Halperin, E.C., Proia, A.D. & Klintworth, G.K. The effects of total lymphoid irradiation upon corneal vascularization in the rat following chemical cautery. *Radiation research* **117**, 259-272 (1989).
359. Di Girolamo, N.*, et al.* Tracing the fate of limbal epithelial progenitor cells in the murine cornea. *Stem cells (Dayton, Ohio)* **33**, 157-169 (2015).
360. Ning, B.*, et al.* Simultaneous photoacoustic microscopy of microvascular anatomy, oxygen saturation, and blood flow. *Optics Letters* **40**, 910-913 (2015).
361. Ning, B.*, et al.* Ultrasound-aided Multi-parametric Photoacoustic Microscopy of the Mouse Brain. *Scientific reports* **5**, 18775 (2015).
362. Chen, S.L., Xie, Z., Carson, P.L., Wang, X. & Guo, L.J. In vivo flow speed measurement of capillaries by photoacoustic correlation spectroscopy. *Optics Letters* **36**, 4017-4019 (2011).
363. Unekawa, M.*, et al.* RBC velocities in single capillaries of mouse and rat brains are the same, despite 10-fold difference in body size. *Brain research* **1320**, 69-73 (2010).
364. Ren, S.*, et al.* Selection of housekeeping genes for use in quantitative reverse transcription PCR assays on the murine cornea. *Molecular vision* **16**, 1076-1086 (2010).
365. Schmittgen, T.D. & Livak, K.J. Analyzing real-time PCR data by the comparative C(T) method. *Nature protocols* **3**, 1101-1108 (2008).
366. Peixoto, A., Monteiro, M., Rocha, B. & Veiga-Fernandes, H. Quantification of multiple gene expression in individual cells. *Genome research* **14**, 1938-1947 (2004).
367. Long, D.S., Smith, M.L., Pries, A.R., Ley, K. & Damiano, E.R. Microviscometry reveals reduced blood viscosity and altered shear rate and shear stress profiles in microvessels after hemodilution. *Proceedings of the National Academy of Sciences of the United States of America* **101**, 10060-10065 (2004).
368. Taylor, A.C., Murfee, W.L. & Peirce, S.M. EphB4 expression along adult rat microvascular networks: EphB4 is more than a venous specific marker. *Microcirculation (New York, N.Y.: 1994)* **14**, 253-267 (2007).
369. Dasa, S.S.*, et al.* Development of target-specific liposomes for delivering small molecule drugs after reperfused myocardial infarction. *Journal of controlled release : official journal of the Controlled Release Society* **220**, 556-567 (2015).
370. Jampol, L.M.*, et al.* Anti-Vascular Endothelial Growth Factor Comparative Effectiveness Trial for Diabetic Macular Edema: Additional Efficacy Post Hoc Analyses of a Randomized Clinical Trial. *JAMA ophthalmology* (2016).
371. Bosetti, F.*, et al.* "Small Blood Vessels: Big Health Problems?": Scientific Recommendations of the National Institutes of Health Workshop. *Journal of the American Heart Association* **5**, e004389 (2016).
372. Baeyens, N., Bandyopadhyay, C., Coon, B.G., Yun, S. & Schwartz, M.A. Endothelial fluid shear stress sensing in vascular health and disease. *The Journal of clinical investigation* **126**, 821-828 (2016).
373. Hu, S., Maslov, K. & Wang, L.V. Second-generation optical-resolution photoacoustic microscopy with improved sensitivity and speed. *Optics Letters* **36**, 1134-1136 (2011).

374. Werner, D.*, et al.* Accelerated reperfusion of poorly perfused retinal areas in central retinal artery occlusion and branch retinal artery occlusion after a short treatment with enhanced external counterpulsation. *Retina (Philadelphia, Pa.)* **24**, 541-547 (2004).
375. Opremcak, E., Rehmar, A.J., Ridenour, C.D., Borkowski, L.M. & Kelley, J.K. Restoration of retinal blood flow via translumenal Nd:YAG embolysis/embolectomy (TYL/E) for central and branch retinal artery occlusion. *Retina (Philadelphia, Pa.)* **28**, 226-235 (2008).
376. Chappell, J.C., Taylor, S.M., Ferrara, N. & Bautch, V.L. Local guidance of emerging vessel sprouts requires soluble Flt-1. *Developmental cell* **17**, 377-386 (2009).
377. Sato, Y.*, et al.* Dynamic analysis of vascular morphogenesis using transgenic quail embryos. *PloS one* **5**, e12674 (2010).
378. Lawson, N.D. & Weinstein, B.M. In vivo imaging of embryonic vascular development using transgenic zebrafish. *Developmental biology* **248**, 307-318 (2002).
379. Jung, H.M.*, et al.* Imaging blood vessels and lymphatic vessels in the zebrafish. *Methods in cell biology* **133**, 69-103 (2016).
380. Yu, J.A., Castranova, D., Pham, V.N. & Weinstein, B.M. Single-cell analysis of endothelial morphogenesis in vivo. *Development (Cambridge, England)* **142**, 2951-2961 (2015).
381. Sriram, K., Intaglietta, M. & Tartakovsky, D.M. Non-Newtonian flow of blood in arterioles: consequences for wall shear stress measurements. *Microcirculation (New York, N.Y.: 1994)* **21**, 628-639 (2014).
382. Avari, H., Savory, E. & Rogers, K.A. An In Vitro Hemodynamic Flow System to Study the Effects of Quantified Shear Stresses on Endothelial Cells. *Cardiovascular engineering and technology* **7**, 44-57 (2016).
383. Arakelyan, L., Vainstein, V. & Agur, Z. A computer algorithm describing the process of vessel formation and maturation, and its use for predicting the effects of anti-angiogenic and anti-maturation therapy on vascular tumor growth. *Angiogenesis* **5**, 203-214 (2002).
384. Logsdon, E.A., Finley, S.D., Popel, A.S. & Mac Gabhann, F. A systems biology view of blood vessel growth and remodelling. *Journal of Cellular and Molecular Medicine* **18**, 1491-1508 (2014).
385. Witmer, A.N., van Blijswijk, B.C., van Noorden, C.J., Vrensen, G.F. & Schlingemann, R.O. In vivo angiogenic phenotype of endothelial cells and pericytes induced by vascular endothelial growth factor-A. *The journal of histochemistry and cytochemistry : official journal of the Histochemistry Society* **52**, 39-52 (2004).
386. Xiang, W.*, et al.* Dynamic remodeling of arteriolar collaterals after acute occlusion in chick chorioallantoic membrane. *Microcirculation (New York, N.Y.: 1994)* **24**, 10.1111/micc.12351 (2017).
387. Walpole, J.*, et al.* Agent-based model of angiogenesis simulates capillary sprout initiation in multicellular networks. *Integrative biology : quantitative biosciences from nano to macro* **7**, 987-997 (2015).
388. Bazmara, H.*, et al.* The Vital Role of Blood Flow-Induced Proliferation and Migration in Capillary Network Formation in a Multiscale Model of Angiogenesis. *PloS one* **10**, e0128878 (2015).

389. Soboleski, M.R., Oaks, J. & Halford, W.P. Green fluorescent protein is a quantitative reporter of gene expression in individual eukaryotic cells. *FASEB journal : official publication of the Federation of American Societies for Experimental Biology* **19**, 440-442 (2005).
390. Saharinen, P. & Alitalo, K. The yin, the yang, and the angiopoietin-1. *The Journal of clinical investigation* **121**, 2157-2159 (2011).
391. Wong, A.L.*, et al.* Tie2 expression and phosphorylation in angiogenic and quiescent adult tissues. *Circulation research* **81**, 567-574 (1997).
392. Reginato, S., Gianni-Barrera, R. & Banfi, A. Taming of the wild vessel: promoting vessel stabilization for safe therapeutic angiogenesis. *Biochemical Society transactions* **39**, 1654-1658 (2011).
393. Hamaguchi, I.*, et al.* Loss of Tie2 receptor compromises embryonic stem cell-derived endothelial but not hematopoietic cell survival. *Blood* **107**, 1207-1213 (2006).
394. Anghelina, M., Moldovan, L. & Moldovan, N.I. Preferential activity of Tie2 promoter in arteriolar endothelium. *Journal of Cellular and Molecular Medicine* **9**, 113-121 (2005).
395. Hirschi, K.K. & D'Amore, P.A. Pericytes in the microvasculature. *Cardiovascular research* **32**, 687-698 (1996).
396. Edelman, D.A., Jiang, Y., Tyburski, J., Wilson, R.F. & Steffes, C. Pericytes and their role in microvasculature homeostasis. *The Journal of surgical research* **135**, 305-311 (2006).
397. Andreeva, E.R., Pugach, I.M., Gordon, D. & Orekhov, A.N. Continuous subendothelial network formed by pericyte-like cells in human vascular bed. *Tissue & cell* **30**, 127-135 (1998).
398. Hellstrom, M.*, et al.* Lack of pericytes leads to endothelial hyperplasia and abnormal vascular morphogenesis. *The Journal of cell biology* **153**, 543-553 (2001).
399. Hirschi, K.K., Rohovsky, S.A., Beck, L.H., Smith, S.R. & D'Amore, P.A. Endothelial cells modulate the proliferation of mural cell precursors via platelet-derived growth factor-BB and heterotypic cell contact. *Circulation research* **84**, 298-305 (1999).
400. Leveen, P.*, et al.* Mice deficient for PDGF B show renal, cardiovascular, and hematological abnormalities. *Genes & development* **8**, 1875-1887 (1994).
401. Stapor, P.C., Azimi, M.S., Ahsan, T. & Murfee, W.L. An angiogenesis model for investigating multicellular interactions across intact microvascular networks. *American journal of physiology.Heart and circulatory physiology* **304**, H235-245 (2013).
402. Kutcher, M.E. & Herman, I.M. The pericyte: cellular regulator of microvascular blood flow. *Microvascular research* **77**, 235-246 (2009).
403. Kutcher, M.E., Kolyada, A.Y., Surks, H.K. & Herman, I.M. Pericyte Rho GTPase mediates both pericyte contractile phenotype and capillary endothelial growth state. *The American journal of pathology* **171**, 693-701 (2007).
404. Lee, S.*, et al.* Pericyte actomyosin-mediated contraction at the cell-material interface can modulate the microvascular niche. *Journal of physics.Condensed matter : an Institute of Physics journal* **22**, 194115 (2010).
405. Peppiatt, C.M., Howarth, C., Mobbs, P. & Attwell, D. Bidirectional control of CNS capillary diameter by pericytes. *Nature* **443**, 700-704 (2006).

406. Franco, M., Roswall, P., Cortez, E., Hanahan, D. & Pietras, K. Pericytes promote endothelial cell survival through induction of autocrine VEGF-A signaling and Bcl-w expression. *Blood* **118**, 2906-2917 (2011).
407. Durham, J.T. & Herman, I.M. Microvascular modifications in diabetic retinopathy. *Current diabetes reports* **11**, 253-264 (2011).
408. Van Gieson, E.J., Murfee, W.L., Skalak, T.C. & Price, R.J. Enhanced smooth muscle cell coverage of microvessels exposed to increased hemodynamic stresses in vivo. *Circulation research* **92**, 929-936 (2003).
409. Yoshida, T. & Owens, G.K. Molecular determinants of vascular smooth muscle cell diversity. *Circulation research* **96**, 280-291 (2005).
410. Egginton, S., Hudlicka, O., Brown, M.D., Graciotti, L. & Granata, A.L. In vivo pericyte-endothelial cell interaction during angiogenesis in adult cardiac and skeletal muscle. *Microvascular research* **51**, 213-228 (1996).
411. Ayres-Sander, C.E.*, et al.* Transendothelial migration enables subsequent transmigration of neutrophils through underlying pericytes. *PloS one* **8**, e60025 (2013).
412. Torsney, E. & Xu, Q. Resident vascular progenitor cells. *Journal of Molecular and Cellular Cardiology* **50**, 304-311 (2011).
413. Rehman, J.*, et al.* Secretion of angiogenic and antiapoptotic factors by human adipose stromal cells. *Circulation* **109**, 1292-1298 (2004).
414. Taylor, A.C., Seltz, L.M., Yates, P.A. & Peirce, S.M. Chronic whole-body hypoxia induces intussusceptive angiogenesis and microvascular remodeling in the mouse retina. *Microvascular research* **79**, 93-101 (2010).
415. Ashton, N. & de Oliveira, F. Nomenclature of pericytes. Intramural and extramural. *The British journal of ophthalmology* **50**, 119-123 (1966).
416. Hellerbrand, C. Hepatic stellate cells--the pericytes in the liver. *Pflugers Archiv : European journal of physiology* **465**, 775-778 (2013).
417. Sasaki, M.*, et al.* Mesenchymal stem cells are recruited into wounded skin and contribute to wound repair by transdifferentiation into multiple skin cell type. *Journal of immunology (Baltimore, Md.: 1950)* **180**, 2581-2587 (2008).
418. Pinzani, M. Hepatic stellate (ITO) cells: expanding roles for a liver-specific pericyte. *Journal of hepatology* **22**, 700-706 (1995).
419. Bergers, G. & Song, S. The role of pericytes in blood-vessel formation and maintenance. *Neuro-oncology* **7**, 452-464 (2005).
420. Armulik, A., Genove, G. & Betsholtz, C. Pericytes: developmental, physiological, and pathological perspectives, problems, and promises. *Developmental cell* **21**, 193-215 (2011).
421. Benjamin, L.E., Hemo, I. & Keshet, E. A plasticity window for blood vessel remodelling is defined by pericyte coverage of the preformed endothelial network and is regulated by PDGF-B and VEGF. *Development (Cambridge, England)* **125**, 1591-1598 (1998).
422. Ponce, A.M. & Price, R.J. Angiogenic stimulus determines the positioning of pericytes within capillary sprouts in vivo. *Microvascular research* **65**, 45-48 (2003).
423. Ozerdem, U., Grako, K.A., Dahlin-Huppe, K., Monosov, E. & Stallcup, W.B. NG2 proteoglycan is expressed exclusively by mural cells during vascular

morphogenesis. *Developmental dynamics : an official publication of the American Association of Anatomists* **222**, 218-227 (2001).
424. Folkman, J. & D'Amore, P.A. Blood vessel formation: what is its molecular basis? *Cell* **87**, 1153-1155 (1996).
425. Hellstrom, M., Kalen, M., Lindahl, P., Abramsson, A. & Betsholtz, C. Role of PDGF-B and PDGFR-beta in recruitment of vascular smooth muscle cells and pericytes during embryonic blood vessel formation in the mouse. *Development (Cambridge, England)* **126**, 3047-3055 (1999).
426. Nehls, V., Denzer, K. & Drenckhahn, D. Pericyte involvement in capillary sprouting during angiogenesis in situ. *Cell and tissue research* **270**, 469-474 (1992).
427. Nehls, V. & Drenckhahn, D. Heterogeneity of microvascular pericytes for smooth muscle type alpha-actin. *The Journal of cell biology* **113**, 147-154 (1991).
428. Ren, S. & Duffield, J.S. Pericytes in kidney fibrosis. *Current opinion in nephrology and hypertension* **22**, 471-480 (2013).
429. Schrimpf, C. & Duffield, J.S. Mechanisms of fibrosis: the role of the pericyte. *Current opinion in nephrology and hypertension* **20**, 297-305 (2011).
430. Lai, C.H. & Kuo, K.H. The critical component to establish in vitro BBB model: Pericyte. *Brain research.Brain research reviews* **50**, 258-265 (2005).
431. Iijima, T. & Zhang, J.Q. Three-dimensional wall structure and the innervation of dental pulp blood vessels. *Microscopy research and technique* **56**, 32-41 (2002).
432. Murfee, W.L., Skalak, T.C. & Peirce, S.M. Differential arterial/venous expression of NG2 proteoglycan in perivascular cells along microvessels: identifying a venule-specific phenotype. *Microcirculation (New York, N.Y.: 1994)* **12**, 151-160 (2005).
433. Tavazoie, M.*, et al.* A specialized vascular niche for adult neural stem cells. *Cell stem cell* **3**, 279-288 (2008).
434. Price, R.J., Owens, G.K. & Skalak, T.C. Immunohistochemical identification of arteriolar development using markers of smooth muscle differentiation. Evidence that capillary arterialization proceeds from terminal arterioles. *Circulation research* **75**, 520-527 (1994).
435. Weinstein, B.M. Vessels and nerves: marching to the same tune. *Cell* **120**, 299-302 (2005).
436. Rhodin, J.A. & Fujita, H. Capillary growth in the mesentery of normal young rats. Intravital video and electron microscope analyses. *Journal of submicroscopic cytology and pathology* **21**, 1-34 (1989).
437. Humphreys, B.D.*, et al.* Fate tracing reveals the pericyte and not epithelial origin of myofibroblasts in kidney fibrosis. *The American journal of pathology* **176**, 85-97 (2010).
438. Ozerdem, U., Monosov, E. & Stallcup, W.B. NG2 proteoglycan expression by pericytes in pathological microvasculature. *Microvascular research* **63**, 129-134 (2002).
439. Murfee, W.L., Rehorn, M.R., Peirce, S.M. & Skalak, T.C. Perivascular cells along venules upregulate NG2 expression during microvascular remodeling. *Microcirculation (New York, N.Y.: 1994)* **13**, 261-273 (2006).
440. Shi, S. & Gronthos, S. Perivascular niche of postnatal mesenchymal stem cells in human bone marrow and dental pulp. *Journal of bone and mineral research : the official journal of the American Society for Bone and Mineral Research* **18**, 696-704 (2003).

441. Chekenya, M. & Immervoll, H. NG2/HMP proteoglycan as a cancer therapeutic target. *Methods in molecular biology (Clifton, N.J.)* **361**, 93-117 (2007).
442. Dore-Duffy, P., Katychev, A., Wang, X. & Van Buren, E. CNS microvascular pericytes exhibit multipotential stem cell activity. *Journal of cerebral blood flow and metabolism : official journal of the International Society of Cerebral Blood Flow and Metabolism* **26**, 613-624 (2006).
443. Stallcup, W.B. The NG2 proteoglycan: past insights and future prospects. *Journal of neurocytology* **31**, 423-435 (2002).
444. Katsetos, C.D.*, et al.* Class III beta-tubulin and gamma-tubulin are co-expressed and form complexes in human glioblastoma cells. *Neurochemical research* **32**, 1387-1398 (2007).
445. Gan, P.P.*, et al.* Microtubule dynamics, mitotic arrest, and apoptosis: drug-induced differential effects of betaIII-tubulin. *Molecular cancer therapeutics* **9**, 1339-1348 (2010).
446. Kavallaris, M. Microtubules and resistance to tubulin-binding agents. *Nature reviews.Cancer* **10**, 194-204 (2010).
447. Bertani, N., Malatesta, P., Volpi, G., Sonego, P. & Perris, R. Neurogenic potential of human mesenchymal stem cells revisited: analysis by immunostaining, time-lapse video and microarray. *Journal of cell science* **118**, 3925-3936 (2005).
448. Foudah, D.*, et al.* Human mesenchymal stem cells express neuronal markers after osteogenic and adipogenic differentiation. *Cellular & Molecular Biology Letters* **18**, 163-186 (2013).
449. Au, P., Tam, J., Fukumura, D. & Jain, R.K. Bone marrow-derived mesenchymal stem cells facilitate engineering of long-lasting functional vasculature. *Blood* **111**, 4551-4558 (2008).
450. Eichmann, A., Le Noble, F., Autiero, M. & Carmeliet, P. Guidance of vascular and neural network formation. *Current opinion in neurobiology* **15**, 108-115 (2005).
451. Eichmann, A., Makinen, T. & Alitalo, K. Neural guidance molecules regulate vascular remodeling and vessel navigation. *Genes & development* **19**, 1013-1021 (2005).
452. Vojtassak, J.*, et al.* Autologous biograft and mesenchymal stem cells in treatment of the diabetic foot. *Neuro endocrinology letters* **27 Suppl 2**, 134-137 (2006).
453. Sacchetti, B.*, et al.* Self-renewing osteoprogenitors in bone marrow sinusoids can organize a hematopoietic microenvironment. *Cell* **131**, 324-336 (2007).
454. Paul, G.*, et al.* The adult human brain harbors multipotent perivascular mesenchymal stem cells. *PloS one* **7**, e35577 (2012).
455. Katare, R.*, et al.* Boosting the pentose phosphate pathway restores cardiac progenitor cell availability in diabetes. *Cardiovascular research* **97**, 55-65 (2013).
456. Chen, W.C.*, et al.* Cellular kinetics of perivascular MSC precursors. *Stem cells international* **2013**, 983059 (2013).
457. Dominici, M.*, et al.* Minimal criteria for defining multipotent mesenchymal stromal cells. The International Society for Cellular Therapy position statement. *Cytotherapy* **8**, 315-317 (2006).
458. Lin, G.*, et al.* Defining stem and progenitor cells within adipose tissue. *Stem cells and development* **17**, 1053-1063 (2008).
459. Rojas, A., Chang, F.C., Lin, S.L. & Duffield, J.S. The role played by perivascular cells in kidney interstitial injury. *Clinical nephrology* **77**, 400-408 (2012).

460. Shepro, D. & Morel, N.M. Pericyte physiology. *FASEB journal : official publication of the Federation of American Societies for Experimental Biology* **7**, 1031-1038 (1993).
461. Stark, K.*, et al.* Capillary and arteriolar pericytes attract innate leukocytes exiting through venules and 'instruct' them with pattern-recognition and motility programs. *Nature immunology* **14**, 41-51 (2013).
462. Stratman, A.N., Malotte, K.M., Mahan, R.D., Davis, M.J. & Davis, G.E. Pericyte recruitment during vasculogenic tube assembly stimulates endothelial basement membrane matrix formation. *Blood* **114**, 5091-5101 (2009).
463. Cossu, G. & Bianco, P. Mesoangioblasts--vascular progenitors for extravascular mesodermal tissues. *Current opinion in genetics & development* **13**, 537-542 (2003).
464. Galli, D.*, et al.* Mesoangioblasts, vessel-associated multipotent stem cells, repair the infarcted heart by multiple cellular mechanisms: a comparison with bone marrow progenitors, fibroblasts, and endothelial cells. *Arteriosclerosis, Thrombosis, and Vascular Biology* **25**, 692-697 (2005).
465. Tang, W.*, et al.* White fat progenitor cells reside in the adipose vasculature. *Science (New York, N.Y.)* **322**, 583-586 (2008).
466. Corselli, M., Chen, C.W., Crisan, M., Lazzari, L. & Peault, B. Perivascular ancestors of adult multipotent stem cells. *Arteriosclerosis, Thrombosis, and Vascular Biology* **30**, 1104-1109 (2010).
467. Corselli, M.*, et al.* Identification of perivascular mesenchymal stromal/stem cells by flow cytometry. *Cytometry.Part A : the journal of the International Society for Analytical Cytology* **83**, 714-720 (2013).
468. You, W.K., Yotsumoto, F., Sakimura, K., Adams, R.H. & Stallcup, W.B. NG2 proteoglycan promotes tumor vascularization via integrin-dependent effects on pericyte function. *Angiogenesis* **17**, 61-76 (2014).
469. Park, T.S.*, et al.* Placental perivascular cells for human muscle regeneration. *Stem cells and development* **20**, 451-463 (2011).
470. Montemurro, T.*, et al.* Differentiation and migration properties of human foetal umbilical cord perivascular cells: potential for lung repair. *Journal of Cellular and Molecular Medicine* **15**, 796-808 (2011).
471. Yoshimura, K.*, et al.* Characterization of freshly isolated and cultured cells derived from the fatty and fluid portions of liposuction aspirates. *Journal of cellular physiology* **208**, 64-76 (2006).
472. Carvalho, M.M., Teixeira, F.G., Reis, R.L., Sousa, N. & Salgado, A.J. Mesenchymal stem cells in the umbilical cord: phenotypic characterization, secretome and applications in central nervous system regenerative medicine. *Current stem cell research & therapy* **6**, 221-228 (2011).
473. Tigges, U., Komatsu, M. & Stallcup, W.B. Adventitial pericyte progenitor/mesenchymal stem cells participate in the restenotic response to arterial injury. *Journal of vascular research* **50**, 134-144 (2013).
474. von Tell, D., Armulik, A. & Betsholtz, C. Pericytes and vascular stability. *Experimental cell research* **312**, 623-629 (2006).
475. Zebardast, N., Lickorish, D. & Davies, J.E. Human umbilical cord perivascular cells (HUCPVC): A mesenchymal cell source for dermal wound healing. *Organogenesis* **6**, 197-203 (2010).

476. Zheng, B.*, et al.* Prospective identification of myogenic endothelial cells in human skeletal muscle. *Nature biotechnology* **25**, 1025-1034 (2007).
477. Zimmerlin, L., Donnenberg, V.S. & Donnenberg, A.D. Rare event detection and analysis in flow cytometry: bone marrow mesenchymal stem cells, breast cancer stem/progenitor cells in malignant effusions, and pericytes in disaggregated adipose tissue. *Methods in molecular biology (Clifton, N.J.)* **699**, 251-273 (2011).
478. Zimmerlin, L., Donnenberg, V.S. & Donnenberg, A.D. Pericytes: a universal adult tissue stem cell? *Cytometry.Part A : the journal of the International Society for Analytical Cytology* **81**, 12-14 (2012).
479. Yamanishi, H., Fujiwara, S. & Soma, T. Perivascular localization of dermal stem cells in human scalp. *Experimental dermatology* **21**, 78-80 (2012).
480. Meury, T., Verrier, S. & Alini, M. Human endothelial cells inhibit BMSC differentiation into mature osteoblasts in vitro by interfering with osterix expression. *Journal of cellular biochemistry* **98**, 992-1006 (2006).
481. Lee, M.J.*, et al.* Macrophages regulate smooth muscle differentiation of mesenchymal stem cells via a prostaglandin F(2)alpha-mediated paracrine mechanism. *Arteriosclerosis, Thrombosis, and Vascular Biology* **32**, 2733-2740 (2012).
482. Murphy, C.M., Matsiko, A., Haugh, M.G., Gleeson, J.P. & O'Brien, F.J. Mesenchymal stem cell fate is regulated by the composition and mechanical properties of collagen-glycosaminoglycan scaffolds. *Journal of the mechanical behavior of biomedical materials* **11**, 53-62 (2012).
483. Kloxin, A.M., Benton, J.A. & Anseth, K.S. In situ elasticity modulation with dynamic substrates to direct cell phenotype. *Biomaterials* **31**, 1-8 (2010).
484. Koike, N.*, et al.* Tissue engineering: creation of long-lasting blood vessels. *Nature* **428**, 138-139 (2004).
485. Sandvig, A., Berry, M., Barrett, L.B., Butt, A. & Logan, A. Myelin-, reactive glia-, and scar-derived CNS axon growth inhibitors: expression, receptor signaling, and correlation with axon regeneration. *Glia* **46**, 225-251 (2004).
486. Ozerdem, U. & Stallcup, W.B. Early contribution of pericytes to angiogenic sprouting and tube formation. *Angiogenesis* **6**, 241-249 (2003).
487. Jung, K.H.*, et al.* Multipotent PDGFRbeta-expressing cells in the circulation of stroke patients. *Neurobiology of disease* **41**, 489-497 (2011).
488. Amos, P.J.*, et al.* Functional binding of human adipose-derived stromal cells: effects of extraction method and hypoxia pretreatment. *Annals of Plastic Surgery* **60**, 437-444 (2008).
489. Katare, R.*, et al.* Transplantation of human pericyte progenitor cells improves the repair of infarcted heart through activation of an angiogenic program involving micro-RNA-132. *Circulation research* **109**, 894-906 (2011).
490. Kim, J.W., Lee, J.H., Lyoo, Y.S., Jung, D.I. & Park, H.M. The effects of topical mesenchymal stem cell transplantation in canine experimental cutaneous wounds. *Veterinary dermatology* **24**, 242-e253 (2013).
491. Amos, P.J.*, et al.* Human adipose-derived stromal cells accelerate diabetic wound healing: impact of cell formulation and delivery. *Tissue engineering.Part A* **16**, 1595-1606 (2010).
492. Potente, M., Gerhardt, H. & Carmeliet, P. Basic and therapeutic aspects of angiogenesis. *Cell* **146**, 873-887 (2011).

493. Carmeliet, P. & Jain, R.K. Molecular mechanisms and clinical applications of angiogenesis. *Nature* **473**, 298-307 (2011).
494. Abramsson, A.*, et al.* Analysis of mural cell recruitment to tumor vessels. *Circulation* **105**, 112-117 (2002).
495. Armulik, A., Abramsson, A. & Betsholtz, C. Endothelial/pericyte interactions. *Circ Res* **97**, 512-523 (2005).
496. Gaengel, K., Genove, G., Armulik, A. & Betsholtz, C. Endothelial-mural cell signaling in vascular development and angiogenesis. *Arteriosclerosis, Thrombosis, and Vascular Biology* **29**, 630-638 (2009).
497. Stapor, P.C., Sweat, R.S., Dashti, D.C., Betancourt, A.M. & Murfee, W.L. Pericyte dynamics during angiogenesis: new insights from new identities. *Journal of vascular research* **51**, 163-174 (2014).
498. Suri, C.*, et al.* Requisite role of angiopoietin-1, a ligand for the TIE2 receptor, during embryonic angiogenesis. *Cell* **87**, 1171-1180 (1996).
499. Seki, T., Yun, J. & Oh, S.P. Arterial endothelium-specific activin receptor-like kinase 1 expression suggests its role in arterialization and vascular remodeling. *Circ Res* **93**, 682-689 (2003).
500. Larsson, J.*, et al.* Abnormal angiogenesis but intact hematopoietic potential in TGF-beta type I receptor-deficient mice. *EMBO J* **20**, 1663-1673 (2001).
501. Domenga, V.*, et al.* Notch3 is required for arterial identity and maturation of vascular smooth muscle cells. *Genes Dev* **18**, 2730-2735 (2004).
502. Mizugishi, K.*, et al.* Essential role for sphingosine kinases in neural and vascular development. *Mol Cell Biol* **25**, 11113-11121 (2005).
503. Lindahl, P., Johansson, B.R., Leveen, P. & Betsholtz, C. Pericyte loss and microaneurysm formation in PDGF-B-deficient mice. *Science (New York, N.Y.)* **277**, 242-245 (1997).
504. Armulik, A.*, et al.* Pericytes regulate the blood-brain barrier. *Nature* **468**, 557-561 (2010).
505. Bjarnegard, M.*, et al.* Endothelium-specific ablation of PDGFB leads to pericyte loss and glomerular, cardiac and placental abnormalities. *Development* **131**, 1847-1857 (2004).
506. Limbourg, A.*, et al.* Evaluation of postnatal arteriogenesis and angiogenesis in a mouse model of hind-limb ischemia. *Nature protocols* **4**, 1737-1746 (2009).
507. Limbourg, F.P.*, et al.* Essential role of endothelial Notch1 in angiogenesis. *Circulation* **111**, 1826-1832 (2005).
508. High, F.A.*, et al.* Endothelial expression of the Notch ligand Jagged1 is required for vascular smooth muscle development. *Proc Natl Acad Sci U S A* **105**, 1955-1959 (2008).
509. Shen, T.L.*, et al.* Conditional knockout of focal adhesion kinase in endothelial cells reveals its role in angiogenesis and vascular development in late embryogenesis. *J Cell Biol* **169**, 941-952 (2005).
510. Franco, C.A.*, et al.* SRF selectively controls tip cell invasive behavior in angiogenesis. *Development* **140**, 2321-2333 (2013).
511. Rama, N.*, et al.* Slit2 signaling through Robo1 and Robo2 is required for retinal neovascularization. *Nat Med* **21**, 483-491 (2015).

512. Foo, S.S., *et al.* Ephrin-B2 controls cell motility and adhesion during blood-vessel-wall assembly. *Cell* **124**, 161-173 (2006).
513. Chen, J., *et al.* CD146 coordinates brain endothelial cell-pericyte communication for blood-brain barrier development. *Proc Natl Acad Sci U S A* **114**, E7622-E7631 (2017).
514. Eilken, H.M., *et al.* Pericytes regulate VEGF-induced endothelial sprouting through VEGFR1. *Nat Commun* **8**, 1574 (2017).
515. Cherepanova, O.A., *et al.* Loss of Oct4 in SMC results in major changes in atherosclerotic lesion size and composition. *Nat.Med.* (2016).
516. Kelly-Goss, M.R., *et al.* Combined in vivo photoacoustic and confocal imaging of neovascularization reveals dynamic and heterogenous Tie2 expression in endothelial cells. *In Review.*
517. Kelly-Goss, M.R., *et al.* Dynamic, heterogeneous endothelial Tie2 expression and capillary blood flow during microvascular remodeling. *Sci Rep* **7**, 9049 (2017).
518. Kisucka, J., *et al.* Platelets and platelet adhesion support angiogenesis while preventing excessive hemorrhage. *Proc Natl Acad Sci U S A* **103**, 855-860 (2006).
519. Mac Gabhann, F. & Peirce, S.M. Collateral capillary arterialization following arteriolar ligation in murine skeletal muscle. *Microcirculation (New York, N.Y.: 1994)* **17**, 333-347 (2010).
520. Gomez, D., Shankman, L.S., Nguyen, A.T. & Owens, G.K. Detection of histone modifications at specific gene loci in single cells in histological sections. *Nat Methods* **10**, 171-177 (2013).
521. Murgai, M., *et al.* KLF4-dependent perivascular cell plasticity mediates pre-metastatic niche formation and metastasis. *Nat Med* **23**, 1176-1190 (2017).
522. Hazarika, S., *et al.* MicroRNA-93 controls perfusion recovery after hindlimb ischemia by modulating expression of multiple genes in the cell cycle pathway. *Circulation* **127**, 1818-1828 (2013).
523. Zhang, B., *et al.* Repulsive axon guidance molecule Slit3 is a novel angiogenic factor. *Blood* **114**, 4300-4309 (2009).
524. Zhang, B., *et al.* Heparan sulfate deficiency disrupts developmental angiogenesis and causes congenital diaphragmatic hernia. *J Clin Invest* **124**, 209-221 (2014).
525. Paul, J.D., *et al.* SLIT3-ROBO4 activation promotes vascular network formation in human engineered tissue and angiogenesis in vivo. *J Mol Cell Cardiol* **64**, 124-131 (2013).
526. Ypsilanti, A.R., Zagar, Y. & Chedotal, A. Moving away from the midline: new developments for Slit and Robo. *Development* **137**, 1939-1952 (2010).
527. Wang, B., *et al.* Induction of tumor angiogenesis by Slit-Robo signaling and inhibition of cancer growth by blocking Robo activity. *Cancer Cell* **4**, 19-29 (2003).
528. Liu, D., *et al.* Neuronal chemorepellent Slit2 inhibits vascular smooth muscle cell migration by suppressing small GTPase Rac1 activation. *Circ Res* **98**, 480-489 (2006).
529. Guijarro-Munoz, I., *et al.* The axonal repellent Slit2 inhibits pericyte migration: potential implications in angiogenesis. *Exp Cell Res* **318**, 371-378 (2012).
530. Bell, R.D., *et al.* Pericytes control key neurovascular functions and neuronal phenotype in the adult brain and during brain aging. *Neuron* **68**, 409-427 (2010).

531. Orlidge, A. & D'Amore, P.A. Inhibition of capillary endothelial cell growth by pericytes and smooth muscle cells. *J Cell Biol* **105**, 1455-1462 (1987).
532. Stratman, A.N., Malotte, K.M., Mahan, R.D., Davis, M.J. & Davis, G.E. Pericyte recruitment during vasculogenic tube assembly stimulates endothelial basement membrane matrix formation. *Blood* **114**, 5091-5101 (2009).
533. Lengner, C.J.*, et al.* Oct4 expression is not required for mouse somatic stem cell self-renewal. *Cell Stem Cell* **1**, 403-415 (2007).
534. Loh, Y.H.*, et al.* The Oct4 and Nanog transcription network regulates pluripotency in mouse embryonic stem cells. *Nat Genet* **38**, 431-440 (2006).
535. Guo, Y., Mantel, C., Hromas, R.A. & Broxmeyer, H.E. Oct-4 is critical for survival/antiapoptosis of murine embryonic stem cells subjected to stress: effects associated with Stat3/survivin. *Stem Cells* **26**, 30-34 (2008).
536. Chen, T., Du, J. & Lu, G. Cell growth arrest and apoptosis induced by Oct4 or Nanog knockdown in mouse embryonic stem cells: a possible role of Trp53. *Mol Biol Rep* **39**, 1855-1861 (2012).
537. Jones, C.A.*, et al.* Robo4 stabilizes the vascular network by inhibiting pathologic angiogenesis and endothelial hyperpermeability. *Nat Med* **14**, 448-453 (2008).
538. Li, G.J.*, et al.* Slit2 suppresses endothelial cell proliferation and migration by inhibiting the VEGF-Notch signaling pathway. *Mol Med Rep* **15**, 1981-1988 (2017).
539. Mukovozov, I.*, et al.* The Neurorepellent Slit2 Inhibits Postadhesion Stabilization of Monocytes Tethered to Vascular Endothelial Cells. *J Immunol* **195**, 3334-3344 (2015).
540. Tanno, T.*, et al.* Slit3 regulates cell motility through Rac/Cdc42 activation in lipopolysaccharide-stimulated macrophages. *FEBS Lett* **581**, 1022-1026 (2007).
541. Geutskens, S.B., Hordijk, P.L. & van Hennik, P.B. The chemorepellent Slit3 promotes monocyte migration. *J Immunol* **185**, 7691-7698 (2010).
542. Schwend, T., Lwigale, P.Y. & Conrad, G.W. Nerve repulsion by the lens and cornea during cornea innervation is dependent on Robo-Slit signaling and diminishes with neuron age. *Dev Biol* **363**, 115-127 (2012).
543. Marlow, R.*, et al.* Vascular Robo4 restricts proangiogenic VEGF signaling in breast. *Proc Natl Acad Sci U S A* **107**, 10520-10525 (2010).
544. Henry, T.D.*, et al.* The VIVA trial: Vascular endothelial growth factor in Ischemia for Vascular Angiogenesis. *Circulation* **107**, 1359-1365 (2003).
545. Rajagopalan, S.*, et al.* Regional angiogenesis with vascular endothelial growth factor in peripheral arterial disease: a phase II randomized, double-blind, controlled study of adenoviral delivery of vascular endothelial growth factor 121 in patients with disabling intermittent claudication. *Circulation* **108**, 1933-1938 (2003).
546. Belch, J.*, et al.* Effect of fibroblast growth factor NV1FGF on amputation and death: a randomised placebo-controlled trial of gene therapy in critical limb ischaemia. *Lancet* **377**, 1929-1937 (2011).
547. Annex, B.H. & Simons, M. Growth factor-induced therapeutic angiogenesis in the heart: protein therapy. *Cardiovasc Res* **65**, 649-655 (2005).
548. Cao, R.*, et al.* Angiogenic synergism, vascular stability and improvement of hind-limb ischemia by a combination of PDGF-BB and FGF-2. *Nat Med* **9**, 604-613 (2003).

549. Leu, S.*, et al.* Adipose-derived mesenchymal stem cells markedly attenuate brain infarct size and improve neurological function in rats. *Journal of translational medicine* **8**, 63 (2010).
550. Zografou, A.*, et al.* Autologous transplantation of adipose-derived stem cells enhances skin graft survival and wound healing in diabetic rats. *Annals of plastic surgery* **71**, 225-232 (2013).
551. Fadini, G.P. & Avogaro, A. Diabetes impairs mobilization of stem cells for the treatment of cardiovascular disease: a meta-regression analysis. *International journal of cardiology* **168**, 892-897 (2013).
552. Cianfarani, F.*, et al.* Diabetes impairs adipose tissue-derived stem cell function and efficiency in promoting wound healing. *Wound repair and regeneration : official publication of the Wound Healing Society [and] the European Tissue Repair Society* **21**, 545-553 (2013).
553. Koci, Z.*, et al.* Characterization of human adipose tissue-derived stromal cells isolated from diabetic patient's distal limbs with critical ischemia. *Cell biochemistry and function* **32**, 597-604 (2014).
554. Tamarat, R.*, et al.* Impairment in ischemia-induced neovascularization in diabetes: bone marrow mononuclear cell dysfunction and therapeutic potential of placenta growth factor treatment. *The American journal of pathology* **164**, 457-466 (2004).
555. Zuk, P.A.*, et al.* Multilineage cells from human adipose tissue: implications for cell-based therapies. *Tissue engineering* **7**, 211-228 (2001).
556. Keats, E.C. & Khan, Z.A. Vascular stem cells in diabetic complications: evidence for a role in the pathogenesis and the therapeutic promise. *Cardiovascular diabetology* **11**, 37 (2012).
557. Gardner, T.W., Antonetti, D.A., Barber, A.J., LaNoue, K.F. & Nakamura, M. New insights into the pathophysiology of diabetic retinopathy: potential cell-specific therapeutic targets. *Diabetes technology & therapeutics* **2**, 601-608 (2000).
558. Hammes, H.P.*, et al.* Pericytes and the pathogenesis of diabetic retinopathy. *Diabetes* **51**, 3107-3112 (2002).
559. Nguyen, Q.D.*, et al.* Ranibizumab for diabetic macular edema: results from 2 phase III randomized trials: RISE and RIDE. *Ophthalmology* **119**, 789-801 (2012).
560. Han, Z., Guo, J., Conley, S.M. & Naash, M.I. Retinal angiogenesis in the Ins2(Akita) mouse model of diabetic retinopathy. *Investigative ophthalmology & visual science* **54**, 574-584 (2013).
561. Rakoczy, E.P.*, et al.* Characterization of a mouse model of hyperglycemia and retinal neovascularization. *The American journal of pathology* **177**, 2659-2670 (2010).
562. van Eeden, P.E.*, et al.* Early vascular and neuronal changes in a VEGF transgenic mouse model of retinal neovascularization. *Investigative ophthalmology & visual science* **47**, 4638-4645 (2006).
563. Amos, P.J.*, et al.* Human adipose-derived stromal cells accelerate diabetic wound healing: impact of cell formulation and delivery. *Tissue engineering. Part A* **16**, 1595-1606 (2010).
564. Amos, P.J.*, et al.* Hypoxic culture and in vivo inflammatory environments affect the assumption of pericyte characteristics by human adipose and bone marrow progenitor cells. *American journal of physiology. Cell physiology* **301**, C1378-1388 (2011).

565. Amos, P.J., *et al.* IFATS collection: The role of human adipose-derived stromal cells in inflammatory microvascular remodeling and evidence of a perivascular phenotype. *Stem Cells* **26**, 2682-2690 (2008).
566. Kenwood, B.M., *et al.* Identification of a novel mitochondrial uncoupler that does not depolarize the plasma membrane. *Molecular Metabolism*.
567. Takakura, N., *et al.* A role for hematopoietic stem cells in promoting angiogenesis. *Cell* **102**, 199-209 (2000).
568. Mizuno, H. Adipose-derived stem cells for tissue repair and regeneration: ten years of research and a literature review. *Journal of Nippon Medical School = Nippon Ika Daigaku zasshi* **76**, 56-66 (2009).
569. Shin, L. & Peterson, D.A. Impaired therapeutic capacity of autologous stem cells in a model of type 2 diabetes. *Stem cells translational medicine* **1**, 125-135 (2012).
570. Salamon, A., Adam, S., Rychly, J. & Peters, K. Long-term tumor necrosis factor treatment induces NFkappaB activation and proliferation, but not osteoblastic differentiation of adipose tissue-derived mesenchymal stem cells in vitro. *The international journal of biochemistry & cell biology* **54**, 149-162 (2014).
571. Winkler, E.A., Bell, R.D. & Zlokovic, B.V. Central nervous system pericytes in health and disease. *Nature neuroscience* **14**, 1398-1405 (2011).
572. Traktuev, D.O., *et al.* A population of multipotent CD34-positive adipose stromal cells share pericyte and mesenchymal surface markers, reside in a periendothelial location, and stabilize endothelial networks. *Circulation research* **102**, 77-85 (2008).
573. Cai, X., Lin, Y., Hauschka, P.V. & Grottkau, B.E. Adipose stem cells originate from perivascular cells. *Biology of the cell / under the auspices of the European Cell Biology Organization* **103**, 435-447 (2011).
574. Feng, J., Mantesso, A. & Sharpe, P.T. Perivascular cells as mesenchymal stem cells. *Expert opinion on biological therapy* **10**, 1441-1451 (2010).
575. Melero-Martin, J.M., *et al.* Engineering robust and functional vascular networks in vivo with human adult and cord blood-derived progenitor cells. *Circulation research* **103**, 194-202 (2008).
576. Chen, L., Tredget, E.E., Wu, P.Y. & Wu, Y. Paracrine factors of mesenchymal stem cells recruit macrophages and endothelial lineage cells and enhance wound healing. *PloS one* **3**, e1886 (2008).
577. Wu, Y., Chen, L., Scott, P.G. & Tredget, E.E. Mesenchymal stem cells enhance wound healing through differentiation and angiogenesis. *Stem cells (Dayton, Ohio)* **25**, 2648-2659 (2007).
578. Falanga, V., *et al.* Autologous bone marrow-derived cultured mesenchymal stem cells delivered in a fibrin spray accelerate healing in murine and human cutaneous wounds. *Tissue engineering* **13**, 1299-1312 (2007).
579. Ho, J.C., *et al.* Reversal of endothelial progenitor cell dysfunction in patients with type 2 diabetes using a conditioned medium of human embryonic stem cell-derived endothelial cells. *Diabetes/metabolism research and reviews* **28**, 462-473 (2012).
580. Zhang, Q., *et al.* IGFBP-3 and TNF-alpha regulate retinal endothelial cell apoptosis. *Investigative ophthalmology & visual science* **54**, 5376-5384 (2013).
581. Jiang, Y., Zhang, Q. & Steinle, J.J. Intravitreal injection of IGFBP-3 restores normal insulin signaling in diabetic rat retina. *PloS one* **9**, e93788 (2014).

582. Rowe, G.C., *et al.* PGC-1alpha induces SPP1 to activate macrophages and orchestrate functional angiogenesis in skeletal muscle. *Circulation research* **115**, 504-517 (2014).
583. Song, N., *et al.* Overexpression of platelet-derived growth factor-BB increases tumor pericyte content via stromal-derived factor-1alpha/CXCR4 axis. *Cancer research* **69**, 6057-6064 (2009).
584. Tsuruma, K., *et al.* Progranulin, a major secreted protein of mouse adipose-derived stem cells, inhibits light-induced retinal degeneration. *Stem cells translational medicine* **3**, 42-53 (2014).
585. Zhang, S., *et al.* Comparison of the therapeutic effects of human and mouse adipose-derived stem cells in a murine model of lipopolysaccharide-induced acute lung injury. *Stem cell research & therapy* **4**, 13 (2013).
586. Trudeau, K., Molina, A.J. & Roy, S. High glucose induces mitochondrial morphology and metabolic changes in retinal pericytes. *Investigative ophthalmology & visual science* **52**, 8657-8664 (2011).
587. Cooper, M.E. & El-Osta, A. Epigenetics: mechanisms and implications for diabetic complications. *Circulation research* **107**, 1403-1413 (2010).
588. Ling, C. & Groop, L. Epigenetics: a molecular link between environmental factors and type 2 diabetes. *Diabetes* **58**, 2718-2725 (2009).
589. Paneni, F., Costantino, S., Volpe, M., Luscher, T.F. & Cosentino, F. Epigenetic signatures and vascular risk in type 2 diabetes: a clinical perspective. *Atherosclerosis* **230**, 191-197 (2013).
590. Prockop, D.J. & Oh, J.Y. Mesenchymal stem/stromal cells (MSCs): role as guardians of inflammation. *Molecular therapy : the journal of the American Society of Gene Therapy* **20**, 14-20 (2012).
591. Anton, K., Banerjee, D. & Glod, J. Macrophage-associated mesenchymal stem cells assume an activated, migratory, pro-inflammatory phenotype with increased IL-6 and CXCL10 secretion. *PloS one* **7**, e35036 (2012).
592. Lutty, G.A. Effects of diabetes on the eye. *Investigative ophthalmology & visual science* **54**, ORSF81-87 (2013).
593. Piera-Velazquez, S., Mendoza, F.A. & Jimenez, S.A. Endothelial to Mesenchymal Transition (EndoMT) in the Pathogenesis of Human Fibrotic Diseases. *J Clin Med* **5**(2016).
594. Robich, M.P., Chu, L.M., Oyamada, S., Sodha, N.R. & Sellke, F.W. Myocardial therapeutic angiogenesis: a review of the state of development and future obstacles. *Expert Rev Cardiovasc Ther* **9**, 1469-1479 (2011).
595. Voisine, P., *et al.* Inhibition of the cardiac angiogenic response to exogenous vascular endothelial growth factor. *Surgery* **136**, 407-415 (2004).
596. Jaffe, G.J., *et al.* Dual Antagonism of PDGF and VEGF in Neovascular Age-Related Macular Degeneration: A Phase IIb, Multicenter, Randomized Controlled Trial. *Ophthalmology* **124**, 224-234 (2017).
597. Arevalo, J.F., *et al.* Intravitreal Bevacizumab (Avastin) for Diabetic Retinopathy: The 2010 GLADAOF Lecture. *J Ophthalmol* **2011**, 584238 (2011).
598. Tang, J.N., *et al.* Concise Review: Is Cardiac Cell Therapy Dead? Embarrassing Trial Outcomes and New Directions for the Future. *Stem Cells Transl Med* **7**, 354-359 (2018).

599. A futile cycle in cell therapy. *Nat Biotechnol* **35**, 291 (2017).
600. Goff, Z.D., Kichura, A.B., Chibnall, J.T. & Hauptman, P.J. A Survey of Unregulated Direct-to-Consumer Treatment Centers Providing Stem Cells for Patients With Heart Failure. *JAMA Intern Med* **177**, 1387-1388 (2017).
601. Kuriyan, A.E.*, et al.* Vision Loss after Intravitreal Injection of Autologous "Stem Cells" for AMD. *N Engl J Med* **376**, 1047-1053 (2017).
602. Pendharkar, A.V.*, et al.* Biodistribution of neural stem cells after intravascular therapy for hypoxic-ischemia. *Stroke* **41**, 2064-2070 (2010).
603. Kawai, H.*, et al.* Tridermal tumorigenesis of induced pluripotent stem cells transplanted in ischemic brain. *J Cereb Blood Flow Metab* **30**, 1487-1493 (2010).